haute école neuchâtel berne jura
arc conservation restauration neuchâtel
Laboratory of Microbiology
Certifié ISO 9001

New ecological and sustainable solution for protecting architectural metals using an ecologically friendly biological treatment

Final Report, 30 April 2018

Université de Neuchâtel

Hes·so
Haute Ecole Spécialisée de Suisse occidentale

Table of content

Information on the project

Project duration

The project started on March the 1st, 2015 and lasted for 3 years, until April the 30th, 2018.

Project content

The different activities of the project will allow the development of an efficient, durable and non-toxic treatment for metal surfaces by the use of natural and harmless microorganisms creating a stabilizing and aesthetic *biopatina*. Indeed, the *biopatina* process based on *s*elected fungal strains will be used for different applications on architectural metals based on copper, iron, zinc and aluminum alloys. The aims of the treatment are:

- Stabilization of corrosion on outdoor metal surfaces;
- Pre-patination of different architectural metal elements, such as roofs, gutters and vertical sheets;
- Chromatic integration of repairs.

The application of the biopatina process on different types of alloys will result in the formation of a homogeneous patina providing the treated surfaces with a naturally aged appearance while inhibiting corrosion.

Project valorisation

In terms of the diffusion of the results of the project to the public, the scientific team involved in the project has already presented part of the results obtained as scientific publications, or as oral and poster communications in conferences, both in the domain of metal conservation, as well as in biotechnology.

Publications

W.M. Kooli, L. Comensoli, J. Maillard, M. Albini, A. Gelb, P. Junier* & E. Joseph. (2018). Bacterial iron reduction and biogenic mineral formation for the stabilisation of corroded iron objects. *Scientific reports*, 8(1), 764.

P. Junier, E. Joseph. (2017). Microbial biotechnology approaches to mitigating the deterioration of construction and heritage materials. *Microbial biotechnology*, 10(5), 1145-1148. *1 citation*

L. Comensoli, J. Maillard, M. Albini, F. Sandoz, P. Junier, E. Joseph. (2017). Use of bacteria to stabilize archaeological iron. *Applied and Environmental Microbiology*, 83:e03478-16.

E. Joseph, S. Bindschedler, M. Albini, L. Comensoli, W. Kooli, L. Mathys (2017). Chapter 35 Microorganisms for Safeguarding Cultural Heritage. In The Fungal Community: Its Organization and Role in the Ecosystem, Fourth Edition (pp. 509-518). CRC Press.

L. Comensoli, S. Bindschedler, P. Junier, E. Joseph (2017). Iron and Fungal Physiology: A Review of Biotechnological Opportunities. In S. Sariaslani, & G. M. Gadd (Eds.), Advances in Applied Microbiology, volume 98, chapter 2 (pp. 31–60).

S. Bindschedler, T.Q.T. Vu Bouquet, D. Job, **E. joseph**, P. Junier* (2017). Fungal ricovery of gold from e-waste. In S. Sariaslani, & G. M. Gadd (Eds.), Advances in Applied Microbiology, volume 99, chapter 2 (pp. 53-81).

M. Albini, C. Chiavari, E. Bernardi, C. Martini, L. Mathys, P. Letardi, P. Junier, E. Joseph. Evaluation of the influence of alloying elements on the performances of a biological treatment. In *METAL 2016 Interim Meeting of the ICOM-CC Metal Working Group Conference Proceedings. New Delhi, India, 26th-30th September 2016*. R.

Mehon, C. Chemello, A. Pandya (Eds.), IGNCA and International Council of Museums, 2017; ISBN 9789290124184, 306-313.

M. Albini, C. Chiavari, E. Bernardi, C. Martini, L. Mathys, E. Joseph (2017). *Evaluation of the performances of a biological treatment on tin-enriched bronze.* Environmental Science and Pollution Research, 24(3), 2150-2159.

M. Albini, L. Comensoli, L. Brambilla, E. Domon Beuret, W. Kooli, L. Mathys, P. Letardi, E. Joseph (2016). Innovative biological approaches for metal conservation. Materials and Corrosion, 67: 200–206.

E. Joseph, P. Junier, M. Albini, P. Letardi, E. Domon Beuret, L. Brambilla, L. Mathys, C. Cevey, R. Bertholon. *Biologically induced patina for metal built heritage*. In Metalli in architettura. Atti del 31° convegno scienza e beni culturali, Bressanone, Italy, 30th June- 3rd July 2015. G. Biscontin, G. Driussi (Eds.), ARCADIA ricerche srl: Marghera, 2015; ISBN 9788895409191, 273-282.

Conference communications

P. Letardi, M. Albini, E. Joseph. EIS measurements for treatments testing: the case of a bio-based method applied on outdoor bronze statues in Switzerland. *69th Annual International Society of Electrochemistry Meeting*, Bologna, Italy. September 2-7 2018. (Poster)

F. Sandoz, L. Mathys, P. junier, E. Joseph. Nuit de la Science, Tout un art ?, Genève, 7-8 Juillet 2018 : http://institutions.ville-geneve.ch/fr/mhn/votre-visite/site-du-musee-dhistoire-des-sciences/evenements/nuit-de-la-science/. (Poster et démostration).

E. Joseph. M. Albelda W. Kooli, L. Mathys, M. Monachon, J. Schröter, P. Junier. Stabilization of endangered heritage objects: Call a microbial plumber!. *ECB 2018, 18th European Congress On Biotechnology, July 1-4 2018.* (Oral presentation+ chairman session biotechnology environmental)
N. Gutknecht, L. Mathys, E. Joseph. Stabilisation of archaeological copper alloys objects from chlorides-induced active corrosion with the use of a bio-based passivation treatment, 8th Student Colloquium (StuCo) 2018 in Dresden 23trd - 24th June 2018. (Oral presentation)

E. Joseph. Microbes for archaeological iron artefacts. *Journées des Restaurateurs en Archéologie 2017*, Nancy, France. October 12-13 2017. (Oral presentation)

L. Comensoli, S. Bindschedler, P. Junier and E. Joseph. The role of fungi in the geochemical cycle of iron. *Zürich mycology meeting 2017*, Switzerland, Zürich, January 22 2017. (Oral presentation)

M. Albini, L. Comensoli, W. Kooli, L. Mahys, E.Joseph. Biotechnology for art safeguarding, *CUSO Symposium in biotechnologies for the preservation of art and built heritage*, Switzerland, Neuchâtel, March 24 2017. (Oral presentation)

M. Albini, C. Chiavari, E. Bernardi, C. Martini, L. Mathys, P. Letardi, P. Junier and E. Joseph. Evaluation of the influence of alloying elements on the performances of a biological treatment. METAL 2016 Interim Meeting of the ICOM-CC Metal Working Group Conference Proceedings, New Delhi, India, 26th to 30th September 2016. (Oral presentation)

M. Albini, L. Mathys-Paganuzzi, J. Schröter, P. Junier and E. Joseph. Biological treatment for the conservation of copper-based alloys. New strategies for the conservation of metallic cultural heritage, Paris, France, 11th – 12th April 2016. (Oral presentation)

M. Albini, P. Letardi, L. Mathys, P. Junier, E. Joseph. Biopatina treatment for the stabilization of contemporary bronze artworks. International Workshop Green conservation of cultural heritage, Rome, Italy, 27th-28th October 2015. (Oral presentation)

L. Comensoli, J. Maillard, P. Junier, E. Joseph. Can bacteria and fungi be used to preserve archaeological iron objects? International Workshop Green Conservation of Cultural Heritage, Rome, Italy, 27th-28th October 2015. (Oral presentation)

M. Albini, E. Joseph. Comparison between biologically-induced copper oxalates and benzotriazole for the stabilization of copper chlorides. Journées des Restaurateurs en Archéologie 2015, Nantes, France, 8th-9th October 2015. (Oral presentation)

L. Comensoli, J. Maillard, P. Junier and E. Joseph. Can microbes be used to preserve archaeological iron objects? 6th Swiss Microbial Ecology Meeting, Ascona, Switzerland, 10th-12th September 2015. (Short oral presentation)

M. Albini, P. Letardi, L. Mathys, P. Junier, E. Joseph. Biopatina treatment for the stabilization of contemporary bronze artworks. 6th Swiss Microbial Ecology Meeting, Ascona, Switzerland, 10th-12th September 2015. (Poster)

M. Albini, C. Chiavari, E. Bernardi, C. Martini, L. Mathys, E. Joseph. Evaluation of the performances of a biological treatment on tin-enriched bronze. EUROANALYSIS 2015, 18th European Conference on Analytical Chemistry, Bordeaux, France, 6th-10th September 2015. (Oral presentation)

E. Joseph, P. Junier, M. Albin, P. Letardi, E. Domon Beuret, L. Brambilla, L. Mathys, C. Cevey, R. Bertholon. Biologically induced patina for metal built heritage. 31° convegno scienza e beni culturali, Bressanone, Italy, June 30 – July 3 2015. (Oral presentation).

L. Comensoli, J. Maillard, P. Junier and E. Joseph. Can we exploit bacteria to preserve archaeological iron objects? 6th Congress of European Microbiologists, Maastricht, The Netherlands, 7th-11th June 2015. (Oral presentation)

E. Joseph. Microorganisms for safeguarding built heritage. 73rd Annual Meeting of the Swiss Society for Microbiology, Lugano, Switzerland, 28th-29th May 2015. (Invited speaker)

M. Albini, P. Letardi, L. Mathys, P. Junier, E. Joseph. Biopatina treatment for the stabilization of contemporary bronze artworks. 73nd Annual Assembly of the Swiss Society for Microbiology (SSM), Lugano, Switzerland, 28th-29th May 2015. (Poster)

L. Comensoli, J. Maillard, P. Junier, E. Joseph. Can bacteria and fungi be used to preserve archaeological iron objects? 73rd Annual Meeting of the Swiss Society for Microbiology, Lugano, Switzerland, 28th-29th May 2015. (Poster)

Work progress and achievements during the period

The main scientific and technical objective of the project is the application of a biotechnological solution on metal architectural parts made of copper, iron, zinc and aluminum alloys for the preservation of built heritage. The different research activities of the project would allow standardizing the newly developed biological processes with the aim to create protective *biopatinas* on architectural metals. Particular attention was be devoted to the efficiency, compatibility and impact on color of the innovative treatment to overcome the problems associated with the treatments in use nowadays. The activities were be divided in the following tasks:

Task 1. Definition of new treatments and procedures

1-a. Selection of naturally aged and bare metal samples *(see previous reports for details)*

Different metal alloys were chosen as metal substrates according to their use in architecture (Table **1**).

Table 1- Selected metals and their use in architecture

Alloy	Use in architecture (external structures)
(Anodized) aluminum	Roofing, flashing, gutters, downspouts, wall panels, spandrels, decorative features (entrances, window spandrels..)
Copper	In Switzerland [1] : roofing (edger, dormers, chimneys, domes, architectural ornaments,..)
Tin	« Tinplates » (sheet-iron coated with tin), ornamental windows and door lintels
Zinc	Roofing (has been replaced progressively by lead and copper), gutters cladding, roof seam , chimneys..
Iron and steel (galvanized or painted)	Roofing, cladding (galvanized) Decorative ironwork in balconies, railings fences and gates (wrought and painted)
Weathering steel	Cladding, bridges

In accordance to this state of the art, metal samples of different alloys were prepared. For tin, either pure tin coupons or tin-enriched bronze coupons were prepared. Three tin coupons of approximately 4 cm^2 were cut directly from a pure tin foil (FINOTIN 0.10mm, Original FINO GmbH, Germany). Bronze coupons of 2.5x1.0x0.5 cm^3 were cut from sand cast alloy. The alloy corresponds to a quaternary bronze (UNS C83600, 85Cu/Sn5/Zn5/Pb5) generally used for artistic casting. Its composition, determined by Glow Discharge Optical Emission Spectroscopy (GDOES), resulted to be 90.3 Cu, 5.7 Sn, 3.3 Pb, 0.3 Zn, 0.4 Ni (% wt). The surface was polished by abrasive papers up to 1000 grit, cleaned with acetone and rinsed with deionized water. Three bronze coupons were prepared in total: two of them (G85dx and G85sx) were used for the biological treatment and one (G85) was left untreated in order to be used as reference. For the other alloy-patina systems, $15^{-1}6$

[1] http://copperalliance.fr/les-produits-et-applications/architecture/la-couverture-cuivre

coupons (5X5 or 6x6 cm) were produced using metal sheets. The surface finish chosen for the bare metals was a brushed (satin) finish as mirror-polished surfaces. Although these do not represent architectural metal parts, it is important to have homogenous reproducible surfaces that can be compared before and after treatment and from one series to another. The soft bare metals like tin and aluminum that were more difficult to handle were abraded manually with grinding paper (1913 Siawat© granulometry 1000 and 1200, SIA). Harder metals like copper, steel and zinc were prepared by a company in Neuchâtel (Gravadhoc). These coupons were also abraded with grinding paper but machine processed. All bare metal coupons were washed in ethanol and acetone and dried in air. In all cases, regular parallel grinding marks were obtained (Figure **1**).

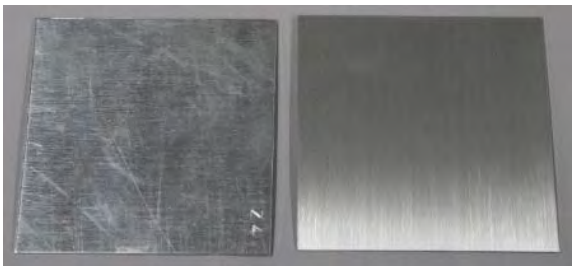

Figure 1- Example of a zinc coupon before (left) and after machine processed grinding (right)

Except for tin-enriched bronze coupons characterized by mean of GDOES, the composition of each alloy was analyzed using a Niton™ Thermoscientific XL3t GOLDD+ XRF Analyzer in a static modus (analyze time 45-45-90 sec., « general metals » option). Data collection and post-run processing were carried out using the Thermo Scientific™ Niton Data Transfer (NDT™) software (Table 2).

Table 2 - Composition of the selected alloys

Alloy	Acronym	Size (mm)	composition	Norm, reference
Aluminum	A	60X60X5	0,2% Fe ; 98,7% Al ; 1% Mg	Niton database : Al-3004[2] Given by manufacturer : Eloxal® quality : EN AW-AlMg1 / EN AW-5005
Anodized Aluminum	AA	60X60X5	95,5 % Al ; 3 % Mg ; 0,5% Fe ; 0,2% Ni	Niton database : AlMg3_5754 Given by manufacturer : EN 12373, DIN 3.3315 (butler finish)
copper	C	60X60X8	99,9% Cu	--
steel	S	60X60X8	99,6% Fe ; 0,2% Mn	laminated TAF DKP
tin	T	60X60X8	Sn 98,9%	-
Ancient zinc (corroded)	ZA	60X60X8	97% Zn ; 1% Pb	--
steel (corroded)	IMN	50X50X8	99% Fe ; Mn 0.34% ; Si 0,3% ; 0.2% S	--
Weathering steel (corroded)	CS	50X50X10	98% Fe ; 1% Cr ; 0.4% Mn ; 0.3% Cu ; 0,2% Si ; 0.2 % Ni	Composition indicates Corten-A type[3]

[2] 3004 aluminum alloy is an alloy in the wrought aluminum-manganese family (3000 or 3xxx series). It is a general-purpose alloy with moderate strength, good workability, and good corrosion resistance. It is commonly rolled and extruded, but typically not forged. As a wrought alloy, it is not used in casting (https//en.wikipedia.org/wiki/3004_aluminium alloy)

[3]Document : ThyssenKrupp, tôles d'acier Cor-Ten, gamme de produits

Some of the selected alloys were already naturally-aged or were previously exposed to outdoor conditions to obtain a corrosion layer:

The ancient zinc alloy (ZA) used in the construction of organs aged for over 80 years in humid indoor conditions to form a homogenous grey patina.

An iron alloy (IMN) was exposed to a marine atmosphere (rich in chlorine) for a period of 12 months (in Brest, France) Orientation and position were selected according to ISO 9223 standard: the samples were placed facing south exposed skyward in the position of 45 degrees from horizontal level.

The bare weathering steel was prepared by grinding (granulometry 600 and 1000) and was degreased with ethanol before its outdoor exposure for a period of 7 months. The coupons were exposed to an urban environment on the roof of the building of the Sciences Faculty of the University of Neuchâtel. Orientation and position were selected according to ISO 9223 standard: the samples were placed facing south exposed skyward in the position of 45 degrees from horizontal level (Figure 2).

After exposure, the corroded samples were washed in demineralized water to remove a maximum of free salts, than dried in ethanol and acetone.

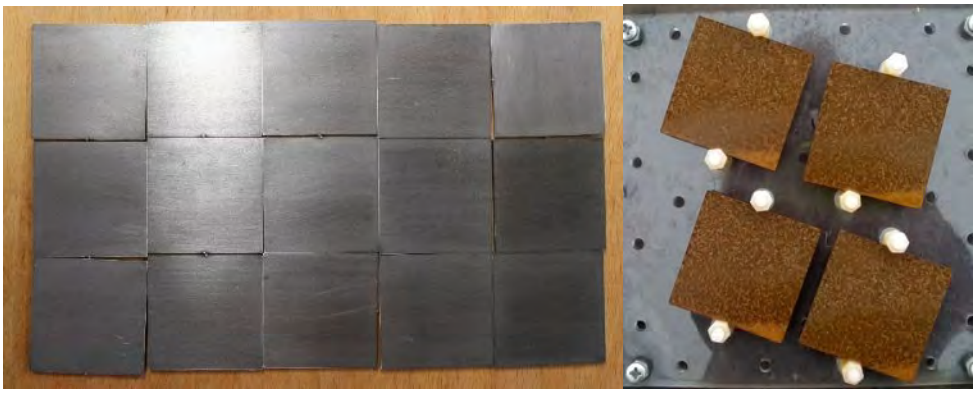

Figure 2 - Bare coupons of weathering steel after grinding (left) and after 7 months exposure (right).

1-b. Individuation of the best fungal strains *(see previous reports for details)*

The selection of individual fungal strains focused initially on the analysis of three elements: zinc, aluminum and tin alloys. However, results for two additional elements (copper and iron) were also obtained and reported here.

Based on the overall results, the four strains able to grow in media containing aluminum, zinc and tin (*Acremonium* sp., *B. bassiana*, *B. caledonica* and *C. sinensis*) were used for additional experiments with mineral powders. Moreover the experiments to ascertain the nature of the aggregates obtained were performed. Further investigation has to be performed in order to determine the homogeneity and the quantity of aggregates produced by each strain. Indeed we encountered some difficulties to separate the formed aggregates from the culture media used. **Regarding iron, either the formation of iron aggregates in the form of crystals or as iron-containing EPS could be exploited for the protection of architectural surfaces made of iron or its alloys.**

1-c. Laboratory studies on chemical processes involved *(see previous reports for details)*

The mechanisms involved in the assimilation of metal ions and production of insoluble and stable *biopatinas* have been investigated. In order to understand the mechanisms involved in the production of metal oxalates by *Beauveria bassiana* different experiments were conducted (Figure 3).

First the production of oxalic acid and other organic acids was ascertained. The High-performance liquid chromatography (HPLC) analyzes confirmed that ***B. Bassiana*** **produced mainly oxalic acid**. Oxalic acid was observed in all media at a retention time between 14, and 15.1 minutes. A second peak was detected at a retention time of 26 minutes in the control at day 0 and day 1 and in MC (copper oxide amended) cultures from day 0 to day 7. The nature of this peak was not identified among the external standards used and further investigation will be conducted for its identification.

Second, we evaluated if the production of oxalic acid was continued or if there is the presence of an optimum during fungal growth. The peak of oxalic acid production is after 5 days. The highest concentrations of oxalic acid in malt-agar medium were recorded at day 5 (0.11 ± 0.03 g.L^{-1}) and at day 28 (0.13 ± 0.09 g.L^{-1}), (Figure 3). The use of amended media allowed to evaluate the production of oxalic acid as defensive mechanism against toxic copper. It appeared that the copper content initially inhibited fungal growth depending on the solubility of the product used. The higher the solubility of the copper source the more the degree of growth inhibition. The amount of oxalic acid produced by the fungus was counterintuitive with respect to the toxicity of the copper source. Furthermore, **the production of oxalic acid was not linear overtime but proceeded by a sequence of incremental steps**. This is probably due to a cyclic reaction between the formation of copper oxalates and the dissolution of further solid copper phases due to medium acidification. Also, it seemed that the strain used for this study may be able to degrade copper oxalates previously formed in order to use them as carbon source. In order to confirm this hypothesis, further investigation in this direction needs to be performed. Finally, the use of *B. bassiana* for the transformation of copper corrosion products into copper oxalates seemed appropriate due to the **high production of oxalic acid when in contact with the most common copper corrosion product, namely copper oxide**. The same mechanism could be translated to further alloys.

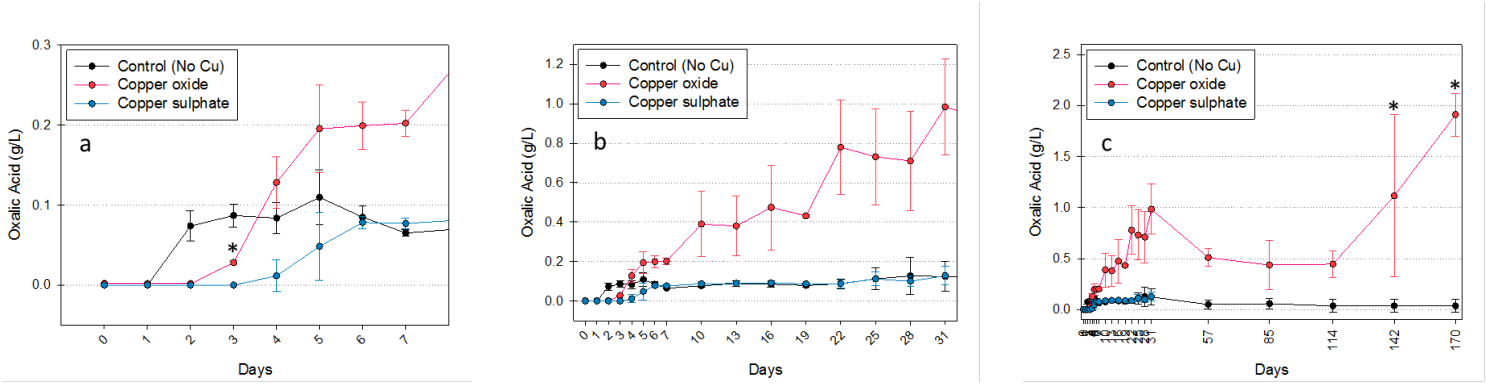

Figure 3 –Plots of the oxalic acid concentration in control (black), copper oxide (red) and copper sulphate (blue) amended culture media during the first seven (a), thirty-one (b) and hundred-seventy (c) days. The asterisks indicate the sets where one outlier was excluded from the calculation of the mean.

Finally we confirmed that **the use of oxalic acid for the production of metal oxalates is not recommended due to lack of control of the layer formed.** It appears that the use of pure chemical is far too aggressive in respect to conservation ethics. With a lower concentration of 0.001 M, a color change towards blue tonality is perceivable (Figure 4).

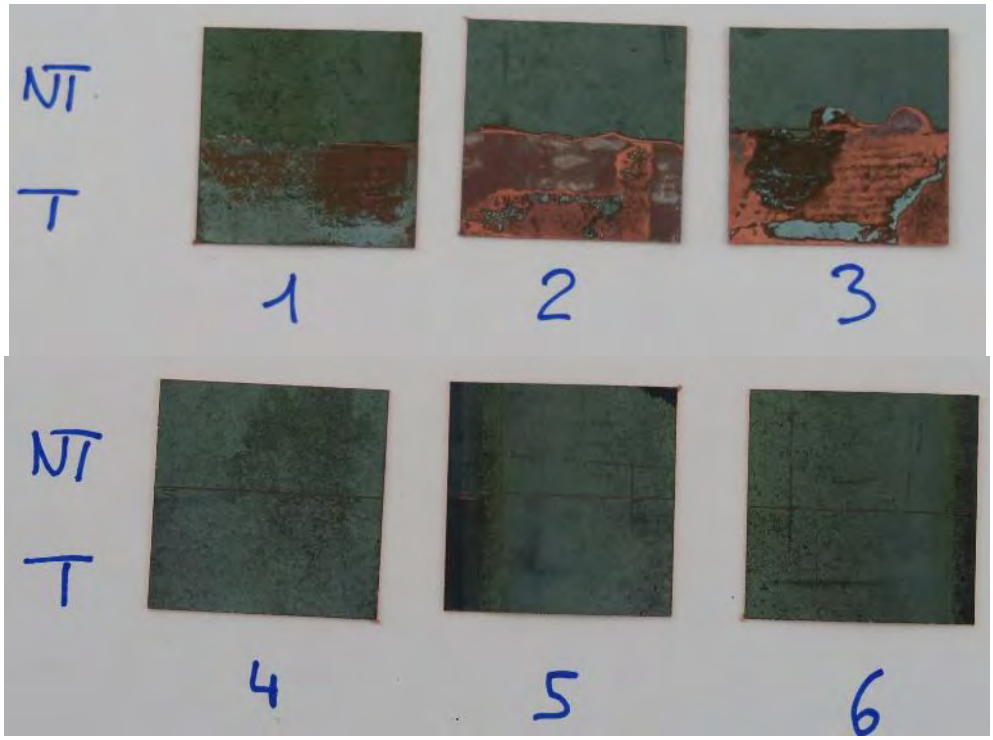

Figure 4 –Corroded copper coupons treated with oxalic acid at 0.1M during 2h (1), 4h (2) and 8h (3) and at the same concentration measured after 5 days of fungal growth (0.001M) during 2h (4), 4h (5) and 8h (6). NT: untreated area; T: treated areas.

1-d. Definition of application protocols

We selected the fungal strain of B*eauveria bassiana* as model candidate. It was decided according to these results to proceed tests with bare coupons of the different alloys studied (Table 3). On all substrates, the application protocol based on a jelly delivery system developed on copper alloys seems to be ideal also for further alloys.

Table 3 – Summary table of the biopassivation treatment applied to the different selected alloys.

Alloy	Photographs of treated (left) and untreated areas (right).	Alloy	Photographs of treated (left) and untreated areas (right).
Aluminum	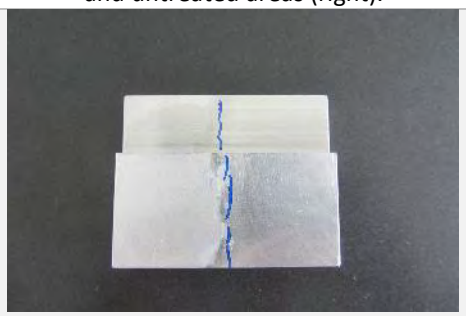	**Brass** (**c**opper-zinc alloy)	
Tin	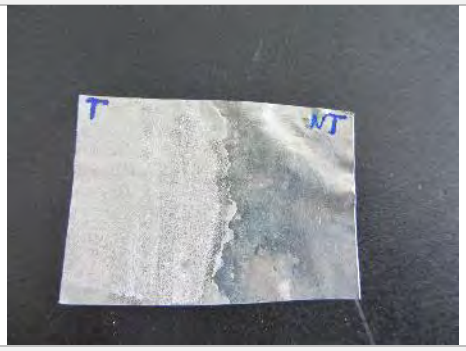	**Bronze** (copper-tin alloy)	
Steel		Stainless steel	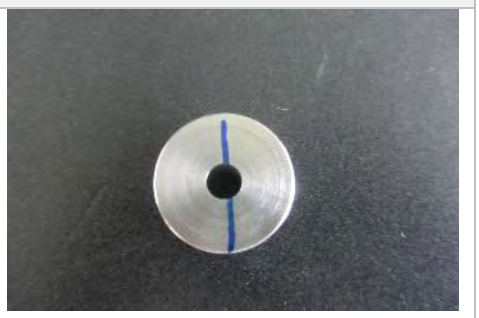
Ancient zinc (corroded)	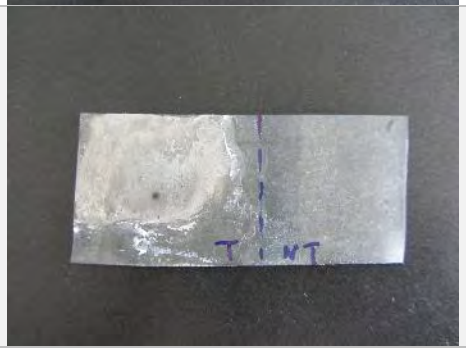		

Based on the promising results presented on bronze substrates in the previous report, further experiments were carried out in order to ascertain the protectiveness of the biological treatment on real artifacts. In particular, the wrestler group exposed in Lucerne, Switzerland where both sheltered and unsheltered areas are presented was treated through biopassivation (Figure 5). In situ measurements campaign should be performed in order to confirm the color change observed after treatment. However the results indicated clearly the formation of both copper and tin oxalates as observed on artificially tin-enriched coupons and presented in the previous report.

Figure 5 – Wrestler group exposed in Lucerne, before (left) and after (right) biopassivation treatment. Tests performed under the supervision of the conservator-restorer Wolf Meyer zu Bargholz.

Task 2. Selection and characterization of metal architectural parts to be used as case studies

2-a. Identification of metal architectural parts

The cultural affairs service of the Canton of Neuchâtel (Office du patrimoine et de l'archéologie du canton de Neuchâtel OPAN in charge of the maintenance of outdoor monuments) as well as the architecture office 0815 in Biel were contacted.
The aim was to identify metal architectural parts in the vicinity and possible test locations.
Potential test elements were located in the pre-industrial historical site the Gor de Vauseyon situated northwest from Neuchâtel (Different associations are in charge of the care and preservation of the historic elements), in Boveresse, in the center of Neuchâtel and in Biel. The elements are summarized in the following Table 4. It was decided to focus on galvanized iron as laboratory tests conducted on iron and zinc coupons were promising (see paragraph above).
Tests with biopassivation were performed on two historical buildings:

1. the absinthe dryer in Boveresse
2. architectural parts of the Farelhaus in Biel.

Surface characterization was also performed on the bandstand and Gossliwheel (see Appendix 1 and 2), although no treatments were performed yet.

picture	Location	Identification (metal parts)
	Gor du Vauseyon	bandstand, painted iron
	Gor du Vauseyon	Gossliwil wheel, painted iron
	absinthe dryer, Boveresse	Building covered with galvanized iron sheets
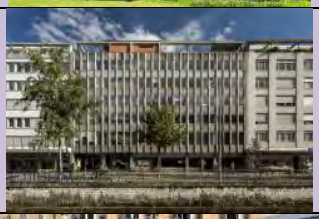	Farelhaus, Biel	Curtain walls (aluminium), bench on the rooftop (galvanized iron alloy)
	Neuchâtel, place Pury	stand, Roof elements (copper alloy?)

Table 4- historical monuments with architectural metal parts, selected case studies

2-b. Non- and micro-destructive characterization of surfaces

2.b.1. Case studies (galvanized iron alloy)

2-b.1.1. Absinthe dryer, Boveresse

The absinthe dryer is located Route de Môtiers 1a, in Boveresse and is part of the regional cultural heritage. Built in 1893, this dryer harvested and dried wormwood plants from growers throughout the region. The ban on absinthe throughout Switzerland marks the end of its agricultural activities. Since then, the dryer has been attached to the regional museum. It currently houses an exhibition on the cultivation and drying of wormwood plants.

It is a wooden building which a large part of the external facade has been covered by metal sheets made of galvanized iron. At first glance, it is possible to observe substantially different surface conditions on these sheets depending on their orientation.

Figure 6- General view of the western side with heavily corroded metal sheets

Figure 7- detailed view of the damaged metal sheets and the painted panel

The facade (with the entrance to the dryer) on the western side has a very heterogeneous surface conditions. The whole facade is covered with metal sheets, but the elements on the middle part of the building are more heavily corroded than on the rest of the building (Figure 6). These sheets corroded strongly, revealing red-brown rust spots. There's a metal panel above the main entrance with the inscription *BUCHER*. On this panel the remains of an orange paint can be seen. The same paint could also be present in the form of residues on the metal sheets (Figure 7).
The presence of sheets in better condition on the lateral parts could be related to a replacement of the sheets.
One metal sheet located on the backside of the northern side of the building was chosen for the tests (Figures 8-9). Another zone on the frontside of the building was initially selected for some tests with biopatina. Unfortunately, the setting didn't withstand the storm. For this reason, test results aren't available for this zone (see location and preliminary characterization in appendix 3)

Figure 8- general view of the east-side

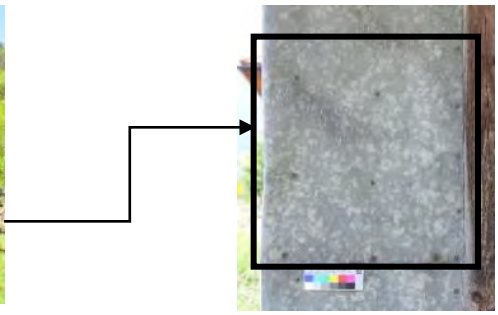

Figure 9- localization of the test sheet (north-side)

The facade is covered with rolled ferrous alloy sheets that have been fastened by nailing. The zinc coating acts as a protection against corrosion (sacrificial protective coating for carbon steel or low alloy steel parts).
Elemental analysis by X-ray fluorescence spectroscopy (XRF) was performed in situ on both facades (Table 5) to identify the substrates and metal coatings[4].
A magnet test confirmed the presence of a ferrous substrate in all cases (even the less degraded sheets).

The systematic presence of tin and antimony may be related to the actual composition of zinc. Indeed these two elements can be included during the galvanizing process.

[4] These were performed using a Niton ™ Thermoscientific XL3t instrument GOLDD + XRF Analyzer.

Northern side Sound zinc coating		**Zn**	Pb, Fe, S, Cl, P, Si	Sn

Table 5 - elementary analysis of a galvanized iron sheet

2-b.1.2. Farelhaus, Biel

The Farelhaus is located in the center of the city of Biel (Quai du Haut 12, 2502 Bienne). It's the youth work of the architect Max Schlup and an important witness of the architecture of the late fifties. This building is listed as a cantonal heritage. In the 50s, the architect Max Schlup from Biel executes the Farelhaus for the reformed parish of Biel. The project is characterized, among other things, by its not-to-be-missed facade but also by the choice of materials used and the spaces layout. The construction includes curtain-walls. The elements are made both of aluminum and anodized aluminum (Figure 10).
A bench covered with galvanized iron sheets was also located on the rooftop (Figure 11). Another zone, located on the roofledge (aluminium alloy) was initially selected for some tests with biopatina. Unfortunately, the setting didn't withstand the storm. For this reason, test results aren't available for this zone (see location and preliminary characterization in appendix 4).

Figure 10- General view of the eastern front of the Farelhaus and its curtainwalls (© W. Gassmann AG/SA 2017)

Figure 11- General view of the bench located on the north east side

The surface of the bench located on the rooftop on the northern side of the building was assessed. It is covered by a zinc coated iron sheet (Figures 12-13).

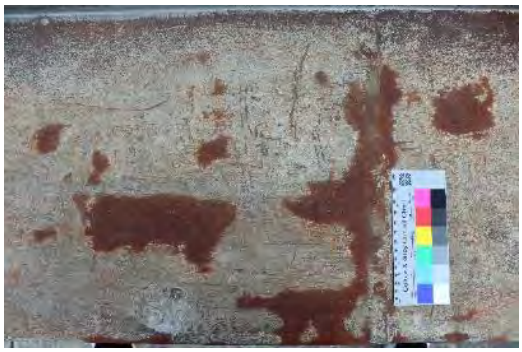

Figure 12- General view of the bench located on the north east side and localization of the test zone

Figure 13- Detailed view of the test zone

Traces of chlorine were always detected as well other elements like phosphor, sulfur and this could be linked to atmospheric pollution.
The top of the bench is made of a galvanized iron sheet (Table 6). The zinc coating was applied as a protection against corrosion. The standard electrode potential of zinc in comparison with the standard electrode potential of iron or steel justifies its use as a coating in outdoor conditions, working as a sacrificial element. Pb was only detected on the test area of the bench. It can indicate the presence of a former coating containing Pb (anti-corrosive paint?). Lead can also more likely be part of the zinc coating (as well as tin) [5].

Localisation of the analyzed spot		Major elements >10 % at	Minor elements	Trace elements (<0.1 % at)
Galvanized steel bench	 **Zone 1** Scratched zinc coating	**Zn, Fe**	Sn, Pb, Ca, Cu, Co, Cr, Ti, K	Mn, Cl
	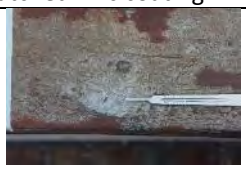 **Zone 2** Sound zinc coating	**Zn, Al**	Fe, Pb, Sn, Si, P, S, Co, Ca	Cl, Cu, Ti
	 **Zone 3** Corroded zone	**Fe**	Zn, Sn, Pb, Ca, Cu, Co, Mn, Cr, Ti, K, Al, Si, P, Cl, S	Cl
	 **Zone 4** Zinc coating stained by ferrous corrosion products	**Zn, Al**	Fe, Sn, Si, Ca, Pb, Co, S, P, K, Ti	Cu, Cl, Cr, Mn

Table 6 - Major, minor and trace elements detected during XRF analysis on bench

[5] Lead can be used during the galvanization process for several reasons: dissolving lead in the melt zinc has influence on the fluidity of the zinc and will help dross particles (zinc-iron alloy particles formed during coating) to sink to the bottom - floating dross particles would cause roughness on the material galvanized. The lead layer on the bottom of the kettle will prevent dross particles to be stuck to the kettle's bottom and allow their easier removal. In fact, lead is heavier than the zinc-iron dross particles and will not alloy with dross or zinc.

2.b.2. Samples

2.b.2.1 Methodology

In parallel the coupons prepared in task 1 were used as demonstration samples and exposed on the roof of the Sciences faculty from the University of Neuchâtel.

In order to assess and characterize possible changes in surface appearances, color and morphology and composition before and after biopatina treatments, several visual and analytical methods were performed on the samples. The methods are summarized/listed in the following Table 7:

Alloy Acronym	**Visual assessment**				coating thickness	colorimetry	**composition**			
	Photos scan	microscopy	SEM (SE)	interferometry			SEM-EDX	XRF	FTIR	Raman spectroscopy
A										
AA										
Z										
ZA										
S										
IMN										
CS										
T										
C										

Table 7- Assessment and characterization methods performed on the metal samples before biopatina treatment.

Visual documentation of samples

For the visual characterization of all samples, a scanner CanoScan 8800F was used and a Kodak® color and grey control chart. A resolution of 600 dpi was applied and the white balance set on a white paper (Figure **14**). Each sample was also recorded with a digital camera CANON EOS 500 and a 60 mm lens. Standard conditions were set by using a light box (mini Studio 60 x 60 cm, 2 fluorescents lights 35 w 5500°K from Kaiser®). Each picture was taken with a color and grey control Kodak® chart (Figure 14). White balance was performed later on for each alloy series with Photoshop® using the grey control chart.

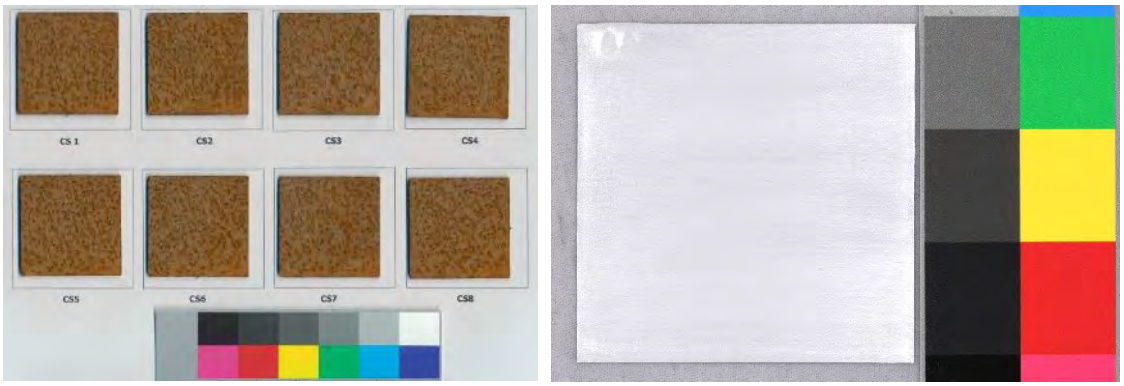

Figure 14 - Scanned image of the weathering steel samples (left) and picture of an aluminum coupon (right).

Optical microscopy (Olympus micro LC) was carried out on all samples. Four zones (A_B_C_D) were assessed for each coupon with help of a perforated paper mask (the diameter of each zone is 5 mm). Grinding marks were positioned horizontally to the lens and visualized under three different magnifications: 46X, 96X and 145X (Figures 15-16).

Figure 15 - Aluminium sample A1 zone A, magnification 46X, 96X and 145X (from left to right).

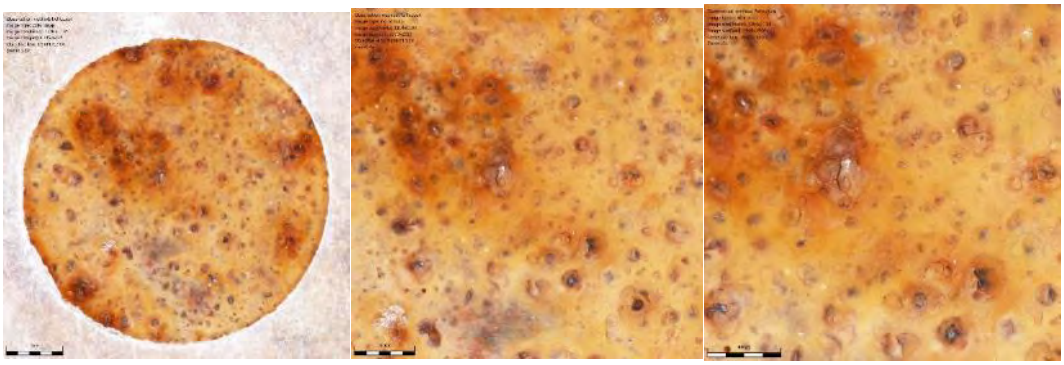

Figure 16 - Weathering steel sample CS 1 zone A magnification 46X, 96X and 145X (from left to right).

Interferometry

Interferometry was carried out on anodized aluminium to get additional information and characterize surface rugosity. Imaging was carried out with a Contour GT-K 3D Optical Microscope (Figure 17).

Zone localization (A_B_C) was done with the same procedure as for SEM. 3D-imaging shows the brush finish as well as a higher rugosity on certain zones.

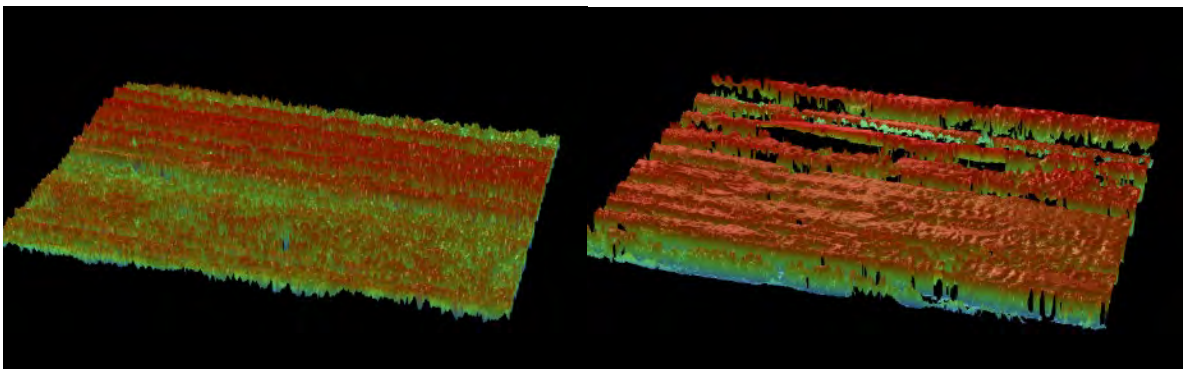

Figure 17 - Two different zones on one anodized aluminum sample (AA2 zone A 50X / AA2 zone C 50X)

SEM-EDS

Scanning Electron Microscopy (SEM) studies were performed with a Philips XL30 system at acceleration voltages of 10^{-1}5 kV and equipped with secondary and backscattered electrons detector. This system was coupled with an Oxford Instruments Energy Dispersive Spectroscopy (EDS) microprobe. In order to assess surface morphology on anodized aluminium 30kV was applied for imaging as the superficial oxide layer is non-conductive. Two samples for each alloy series were non-destructively analyzed by Scanning Electron Microscope and Energy Dispersive X-ray spectroscopy without any kind of preparation, just positioning them into the microscope chamber. In order to characterize the non-conductive oxide layer on the anodized aluminum, environmental scanning electron microscopy had to be performed. Secondary electron images were collected in order to characterize the surface morphology (Figure 18) and the elemental composition was obtained recording EDS spectra. Three zones (A_B_C) for each coupon were examined (a total of 6 zones for each alloy). In the case of bare metals the sample was always positioned with horizontal marks on the image. The zones were visualized with a magnification 250X at least one time, magnification 650X was performed on all 6 spots and magnification 1500X was carried out on at least three spots. EDS spectra were provided at magnification 250X and magnification 650X.

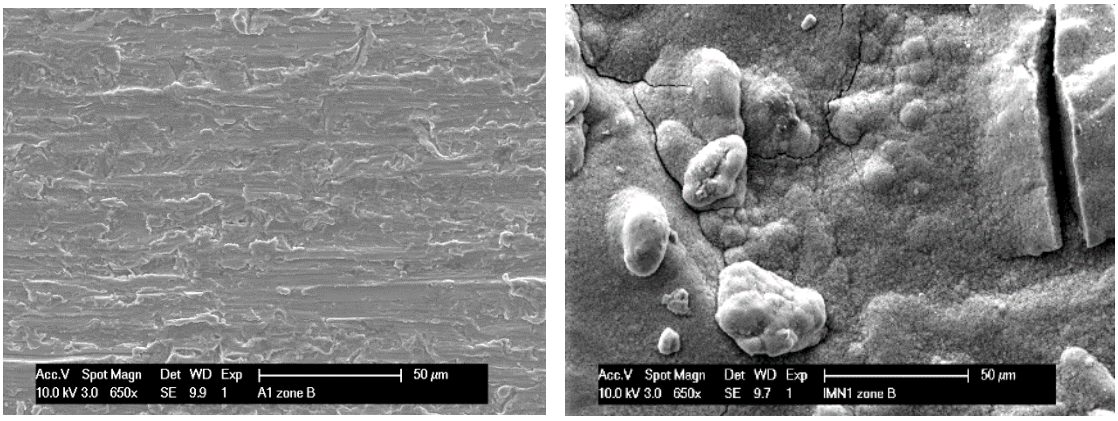

Figure 18 - Secondary electron image of an aluminum sample (left) and a corroded iron sample, magnification 650X (right).

On bare soft metals (like tin and aluminum), a slight contamination by grinding residues[6] could be detected by EDS. This is taken into account for data interpretation (Figure 19).

[6] grinding papers were analyzed by X-Ray microFluorescence: The abrasive particles from the grinding paper contain aluminium, iron, titanium and silicium.

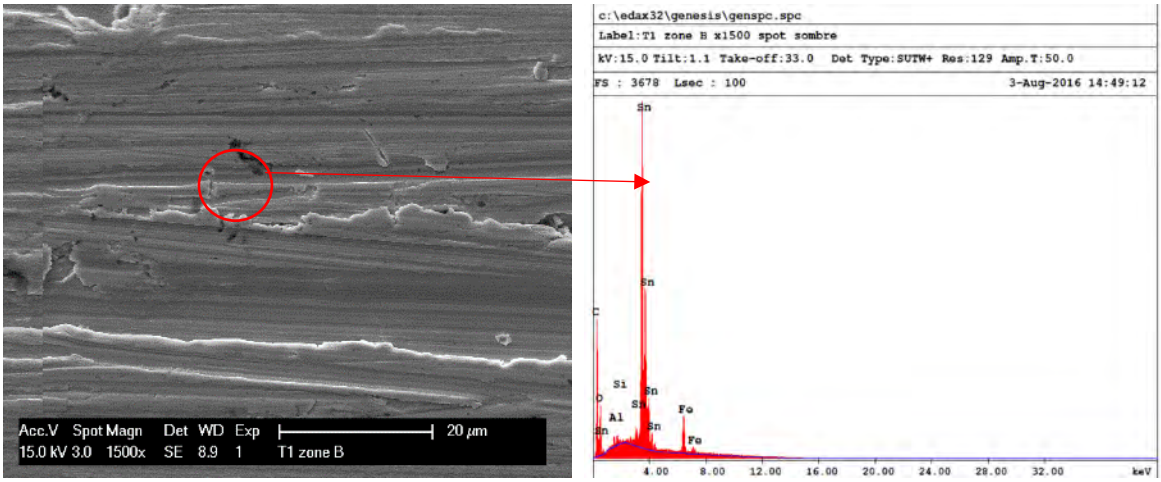

Figure 19 - Secondary electron image of a tin sample with a grinding residue indicated by a red circle (left) and corresponding EDS spectrum of the residue where the presence of Si, Al and Fe is observed (right).

Comparison of EDS spectra of bare aluminum and anodized aluminum, indicates that the anodizing process was probably done by sulfuric acid. The oxide layer contains besides a characteristic high oxygen rate and a certain amount of sulfur (Figure 20).

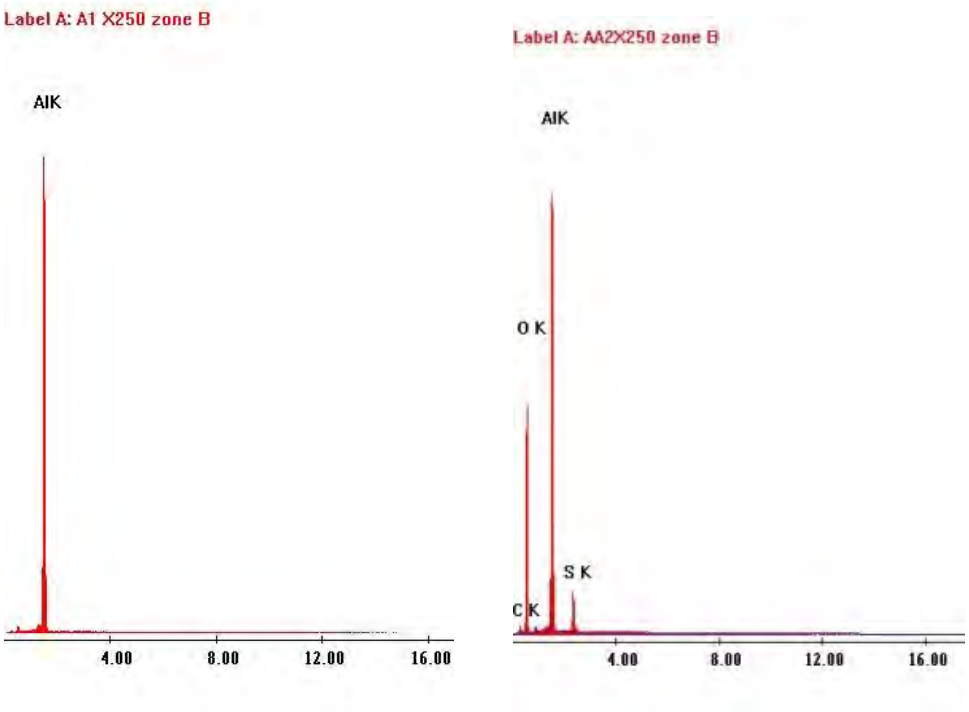

Figure 20 - EDS spectra of bare aluminum (left) and anodized aluminium (right).

Thickness measurements

Measurements were performed with a Phynix Surface Pro S gauge (and a dual FN 1.5 probe) on the corroded metal samples as well as on the anodized aluminium sample to assess the thickness of the surface layers. The measurements on ferrous substrates are based on magnetic induction[7] and the measurements non-ferrous substrates are based on the eddy current principle[8].

Standard Works calibration was applied (flat surfaces larger than 35 mm X35 mm) with a precision of +/-3 µm. Five measurements were carried out on each sample on the following areas:

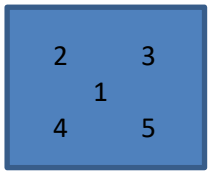

Two samples of each series were measured: corten steel (CS), corroded iron (IMN), ancient zinc (ZA) and anodized aluminium (AA), see Table 8.

alloy	Mean value (10 measurements)	Standard deviation
Corrosion layer ancient zinc (ZA)	0.2 µm (limit of detection)	2.5
Corrosion layer marine iron (IMN)	88.1 µm	15.2
Corrosion layer corten steel (CS)	27.5 µm	6.9
Anodized layer aluminium (AA)	5.4 µm	1.3

Table 8- thickness measurements performed on corroded and anodized layers

Colorimetric measurements

Measurements of the colorimetric coordinates in the CIE L*a*b* space were performed in order to evaluate the chromatic variation of the patinas present on the different coupons.

[7] According to following norms: DIN EN ISO 2808 et 2178; DIN 50 982; ASTM B499 / ASTM B499, ISO 19840

[8] DIN EN ISO 2808; DIN EN ISO 2360; ASTM D1400

Colorimetric measurements were carried out using a spectrophotometer Minolta CM-2300d portable spectrophotometer with a D65 illuminant, a 10º observer and specular component excluded (SCE), using CIELab 1976 color space. On each sample, before and after treatment and/or ageing, three measurements were carried out at three different points using a paper mask (zones A-B-C) and the mean value calculated as well as the standard deviation.

$$\Delta E^*_{ab} = \sqrt{(L^*_2 - L^*_1)^2 + (a^*_2 - a^*_1)^2 + (b^*_2 - b^*_1)^2}$$

In this system, the value ~2.3 corresponds to a JND (just noticeable difference)[9].

The graphs below show the colorimetric values for all alloys (Figure 21). Each point represents the averaged value of the measurements recorded on one type of test alloy (Specular component included SCI). The values show that the standard deviations are very low for the bare metals. This proves a good reproducibility for each test series. The standard deviations are significantly higher for the corroded metals, which is expectedly due to the heterogeneous appearance and composition of corrosion products.

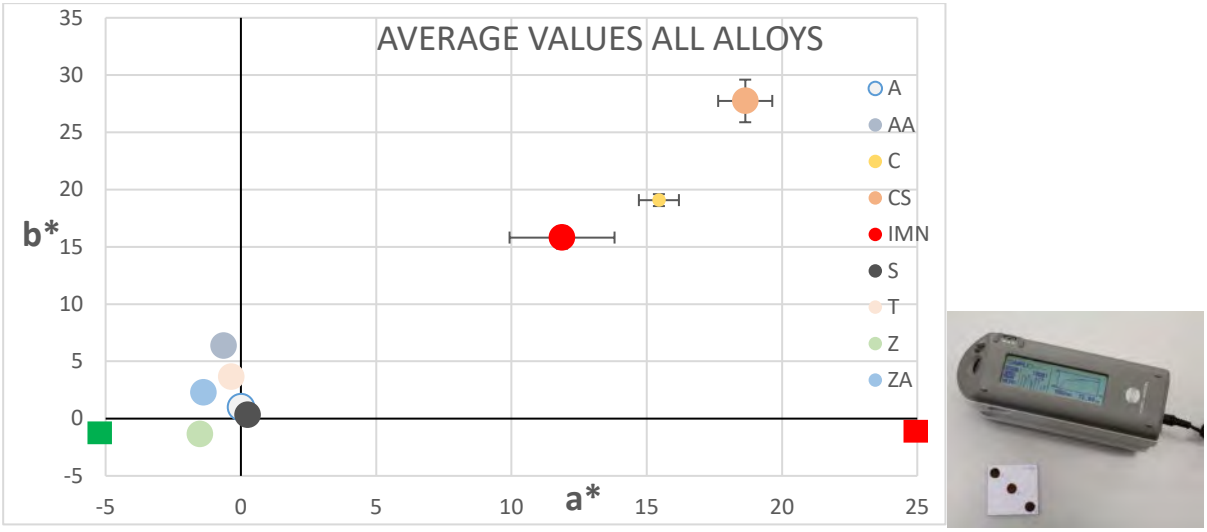

Figure 21 - Average values of colorimetric measurements performed on different alloys with enclosed image of the measurement setting used.

FTIR spectroscopy

The zinc patina of the naturally aged alloy was analyzed by FTIR spectroscopy without preparation, just positioning the samples onto a diamond Attenuated Total Reflectance (ATR) crystal plate and using the same paper mask as for microscopy (Figure 22). ATR spectra were acquired in the range of 4000 - 650 cm^{-1} on an iS5 Thermo Scientific spectrometer connected to an iDTM5 ATR accessory. A total of 64 scans were recorded with a resolution of 4 cm^{-1} and the resulting interferogram averaged. Data collection and post-run processing were carried out using the Thermo Scientific Omnic™ software. The analysis was performed on one spot for each coupon of the ZA series (zone A of the paper mask). Data interpretation is still in progress.

[9] https://en.wikipedia.org/wiki/Color_difference

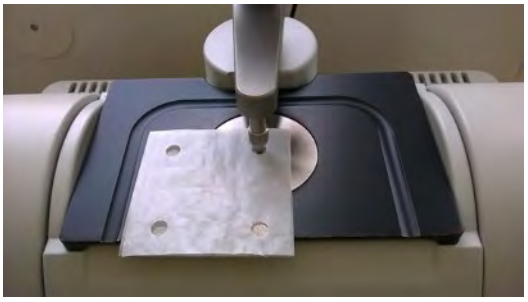

Figure 22- Analysis of zone A of an ancient zinc sample using a paper mask.

Raman spectroscopy

Raman spectroscopy was used to characterize the iron alloy samples applying the following parameters: green laser: 532 nm, Spectrum range between 2000-50 cm^{-1}. Most acquisitions were done with Magnification X50; filter D2; hole 1000; slit 100; grading = 600; acquisition time 20X5. Data collection and post-run processing were carried out with Horiba Yobin Yvon- Lab Spec. Before and after treatment, analysis was performed at least on 5 five different zones following this schema:

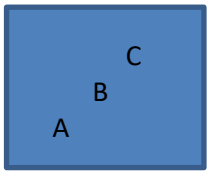

After exposure, analysis was performed on the following zones of the samples:

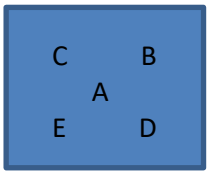

2.b.2.1 Sample preparation and exposure

For each series three samples were selected and for each alloy one non treated series was also exposed to natural ageing (Figure 23).

	bare metal				
reference	C15	Z1	S1	A8	AA3
	C10	Z3	S4	A10	AA4
	C6	Z4	S7	A3	AA16
biopatina	C9	Z5	S16	A2	AA9
	C3	Z6	S2	A5	AA7
	C1	Z15	S9	A4	AA15

A

Naturally corroded metal			
CA1	ZA1	CS1	IMN6
CA2	ZA4	CS4	IMN3
CA4	ZA8	CS12	IMN1
CA3	ZA3	CS2	IMN2
CA5	ZA5	CS3	IMN4
CA6	ZA13	CS11	IMN7

C

	Naturally corroded metal		Bare metal
Cleaned and coated	CS6	IMN10	S6
	CS10	IMN11	S8
	CS15	IMN12	S10

B

Naturally corroded metal		
Cleaned and biopatina	CS9	IMN8
	CS7	IMN9
	CS8	IMN13

D

Figure 23- general view of the test samples and the applied treatments

Test series with preliminary cleaning and comparative conservation treatments

As surface preparation and the morphology of corrosion products located in the upper layers can play an important role in the efficiency of surface passivation, preliminary cleaning was carried out on additional series (Table 9, Figure 24). In order to compare the efficiency and the type of surface modification with biopatina, additional sample series were also produced with bare steel samples (S), Corten steel (CS) and the strongly corroded steel (IMN). The goal was to assess the effect of biopatina in comparison to traditional conservation treatments (Figures 25-27). The corroded samples were cleaned to remove the superficial and less adherent corrosion products before applying biopatina or barrier coatings which are traditionally used for the conservation of metals in outdoor conditions. Cleaning was performed by sandblasting at a constant distance and pressure to obtain a homogenous finish (Figure 24). The bare steel samples needed only to be degreased before applying the barrier coating. The conservation coatings are a microcrystalline wax on the corroded samples (Figure 27) and a polyurethane varnish on the bare steel samples. These treatments are representative of the actual conservation practices. Although it seems to be in some way a contradiction in itself to coat a weathering steel, this has often been done in hands-on conservation to overcome corrosion problems[10]. In conservation practice, protective organic coatings (such as microcrystalline waxes, acrylic, polyurethane resins) are often applied to weathering steel to extend its lifetime. Prior to protection cleaning is carried out to remove old protective systems or superficial corrosion products. Microcristalline waxes, especially Cosmoloid 80H® are

[10] Decker P. et al, To coat or not to coat? The maintenance of Cor-Ten® sculptures. In. Materials and corrosion, Volume 59, Issue 3, March 2008, Pages 239–247

widely used in the conservation of outdoor monuments[11]. In the case of a bare steel, a thick and resistant transparent coating is needed to keep an esthetical surface finish.

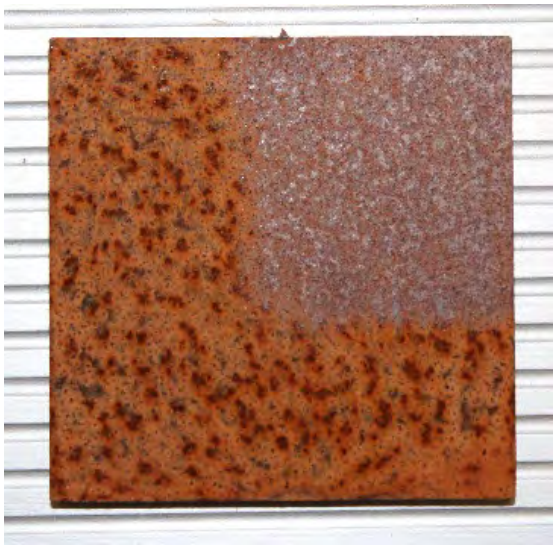

Figure 24 - cleaning test by abrasive airblasting on a corten steel sample

Figure 25- preparing the microcrystalline wax solution by heating

Figure 26 - preliminary heating of the corroded samples before wax coating

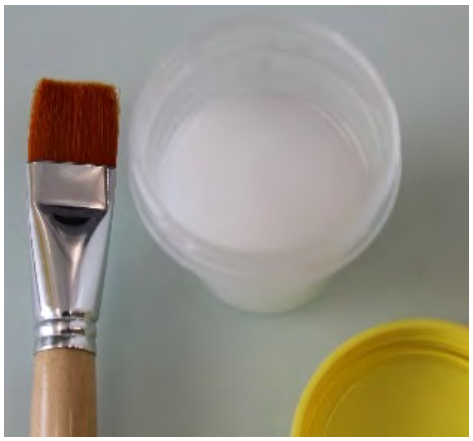

Figure 27- solution and brush used for the wax application

CS series	IMN series	S series
Low pressure cleaning with apricot kernel powder (Ø 200 µm) Debit=2, pressure= 2 bar, distance: 2-3 cm. the nozzle was removed to get a larger cleaning spot	Low pressure cleaning with glass microbeads Debit=2, pressure= 1.5 bar, distance: 2-3 cm. The nozzle was removed to get a larger cleaning spot	Degreasing of the surface with acetone and a paper tissue

[11] Texier A., et al les cires microcristallines dans la protection de la statuaire en cuivre et alliages de cuivre exposée en extérieur ; Sansonetti A., et al, a multi-analytical approach for the conservation of the brera napoleon by antonio canova. In : Métal à ciel ouvert, La sculpture métallique d'extérieur du XIXe siècle au début du XXe siècle, 15es journées d'étude de la SFIIC – 4 & 5 décembre 2014, Paris, ICOMOS France - LRMH

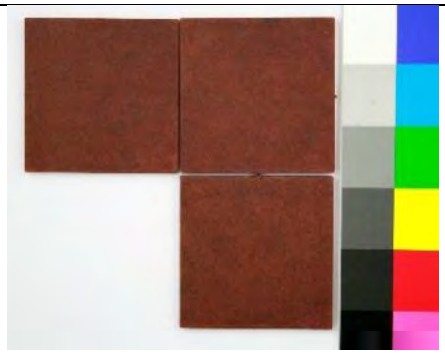 General view of a CS series after cleaning	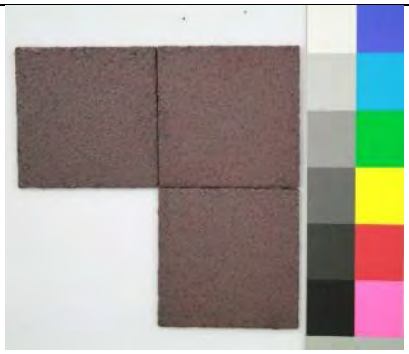 General view of a IMN series after cleaning	
- Rinsing with ethanol applied on the tilted sample - Heating of the sample at 70-75°C for half an hour in an oven - Coating with Cosmoloid 80H® 7% m/m diluted in Shellsol T® applied on the center of the sample with a 0.9 ml pipette, then blended in with a brush - Heating at 80°C for a better penetration of the wax into the porosities.		-Application of a transparent two-component polyurethane (Autocolor® Sikkens) varnish by airbrush

Table 9- preliminary cleaning and reference conservation treatments performed on CS, IMN and S series

Outdoor exposure of the samples

In order to evaluate the treatments efficiency and durability, all samples were exposed to an urban environment on the roof of the building of the Sciences Faculty of the University of Neuchâtel. The exposure started june 26 and was stopped December 19, 2018. Orientation and position were selected according to ISO 9223 standard: the samples were placed facing south exposed skyward in the position of 45 degrees from the horizontal (Figure 28). They were mounted in order to obtain an even distribution of the different alloys and surface treatments on the rack (Figure 29). The treatments' behavior was assessed after 1 month, 3 months and 6 months of exposure. The non-destructive assessment on site was done by photographic documentation, digital microscopy and thickness measurements.

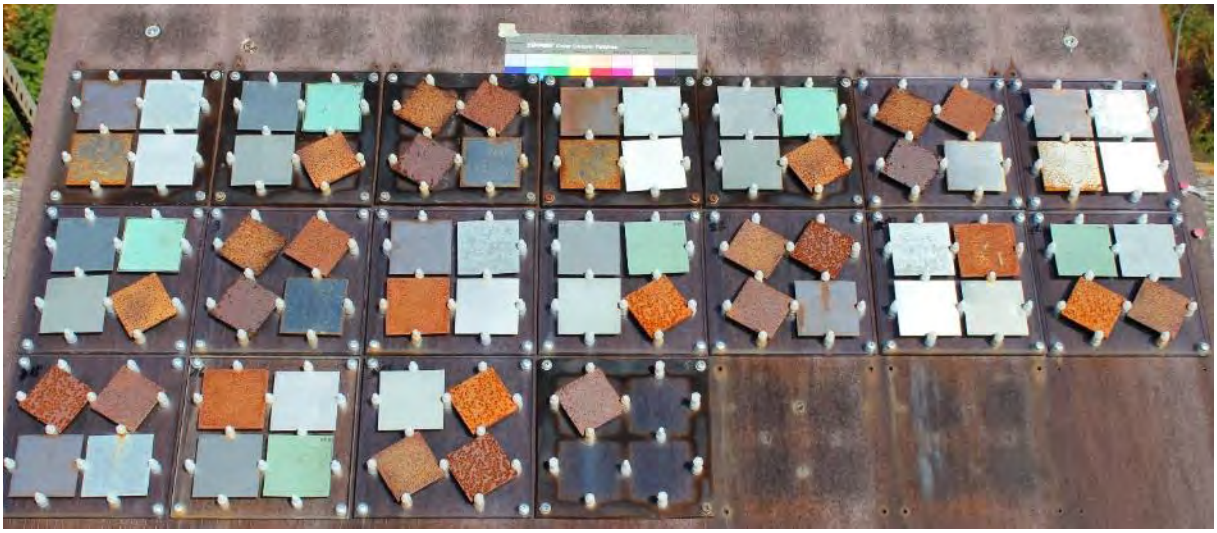

Figure 28- Exposure site for weathering of treated samples, Sciences Faculty roof in Neuchâtel (October 2018)

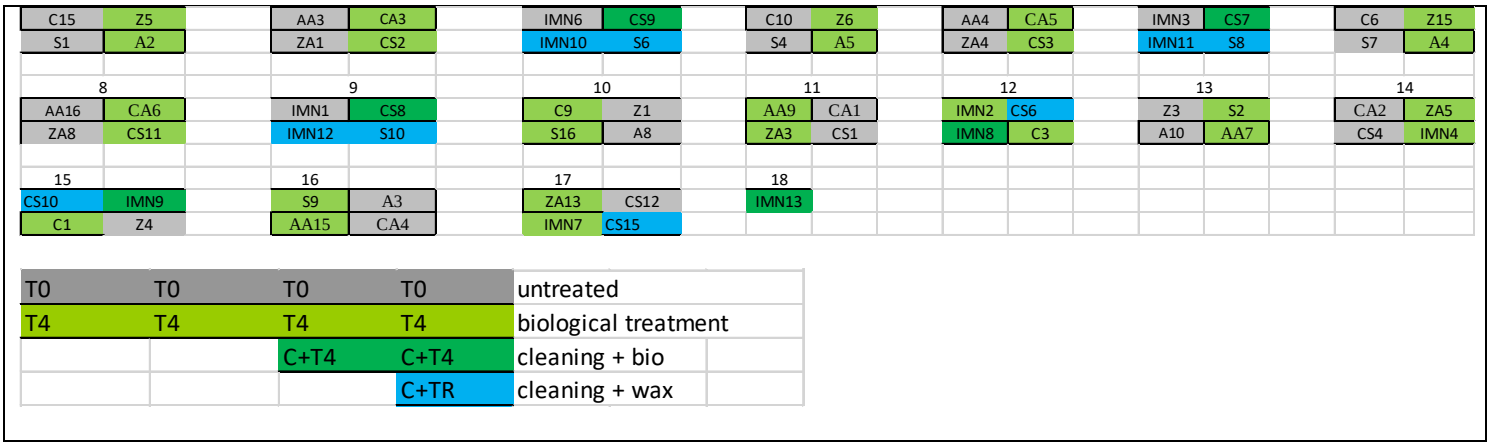

Figure 29- Exposure plan for the samples

Task 3. Application of treatments and evaluation of their performance, efficiency and durability

3-a. Application of the biopatina gel to the case studies

The treatments were performed in June 2017 (Table 10). In both cases (absinthe dryer and Farelhaus), the test surface was degreased with a non-woven textile impregnated with acetone to achieve a good compatibility of the metal with the aqueous biopatina gel and eliminate a maximum of loose particles (dust, less adherent corrosion products). The test zone was delimitated using an adhesive tape. The surface was decontaminated using an ethanol spray. The biopatina gel was applied homogenously with a spatula to obtain a regular gel thickness of a few mm. Then, the test zone was successively covered by a wet gauze, bubble pack and a solar film to avoid strong heating and drying of the underlying gel (Figures 30-34). After treatment the gel was removed first of all mechanically and then with water, before using a nylon brush to eliminate all residues.

Location	Treatment time
Absinthe dryer, Boveresse	5 days / june 13-19 2017
Farelhaus, Biel	7 days / june 12-21 2017

Table 10 - length of performed treatments

Figure 30 - application of the biopatina gel on the northern side of the absinthe dryer

Figure 31 - treatment in progress

Figure 32- Surface decontamination before the biopatina gel application

Figure 33- After application of the biopatina gel and before surface protection of the bench located on the north east side

Figure 34- Setting during biopatina treatment

3-b. Non- and micro-destructive characterization of treated surfaces

3-b.1. Case studies

3-b.1.1 Methods

The test zones were assessed before and after biopatina treatment by the following methods:

Visual evaluation
The surface morphology and appearance were recorded by photography and digital microscopy (Dinolite®).

Thickness measurements were performed by magnetic induction (Phynix® apparatus with a FN 1.5 probe) to evaluate the presence and thickness of a non-magnetic layer (such as zinc) on a ferromagnetic support (In this case the substrate in the form of a ferrous sheet). A total of 5 measurements were performed randomly on both test areas before and after treatment.

Colorimetric measurements were made with a portable spectrophotometer having a wavelength range of 360 nm to 740 nm (with a D65 / 10 ° illuminant and in specular reflection mode excluded). A standard white and zero calibration was performed beforehand.
The principle of colorimetric measurements is based on the location of color points in a mathematical space. This allows the evaluation of color differences by measuring the geometric distance that separates color points in the system. In the International Commission on Color system, CIE 1976, the total color difference (ΔE *) integrates the difference of three independent variables: in rectangular coordinates L *, a *, b * with the difference in clarity on the L * axis expressed by ΔL *; the red-green color difference on the axis a * expressed by Δa *; and finally the yellow-blue color difference on the b * axis expressed in Δb *.
The diameter of the measurement zone is 8 mm. The test areas were characterized by three successive measurements before and after treatment. The average of the obtained values was exploited to evaluate the possible modifications of appearance of the surface.

Fourier transform infrared spectroscopy was also performed on a sample taken after biopatina treatment on the absinthe dryer. The powder sample was placed directly under the objective of the infrared microscope and analyzed in attenuated total reflection mode (ATR). The spectrum was acquired in a range of 4000-700 cm^{-1} using a Thermo Scientific Nicolet iN10MX microscope connected to an ATR accessory equipped with a germanium crystal. A total of 16 scans with a resolution of 4 cm^{-1} was conducted. The interpretation of the data obtained was performed using Thermo Scientific OmnicTM software.

3-b.1.2. Results

3-b.1.2.1. Absinthe dryer

visual evaluation and digital optical microscopy
Two test zones for the measurements were defined (Figure 35). After removing the outer cover (sunshade) and before removing the gauze covering the gel, it was noticed that the latter began to dry in an irregular manner (Figure 36). The contrast between lighter and darker areas before treatment seems significantly greater after treatment (Figures 37-39). Visual evaluation by light microscopy shows that a lighter layer has formed over the entire treated surface (Table 11).

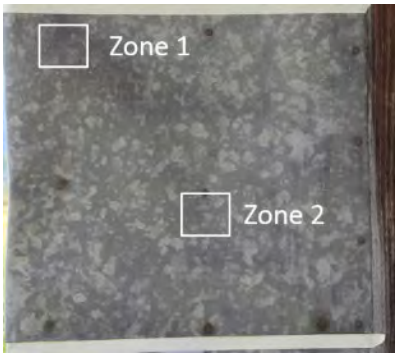

Figure 35- localization of the test zones on the northern side of the building

Figure 36- end of the treatment, before gel removal

Figure 37- end of the treatment, after gel removal

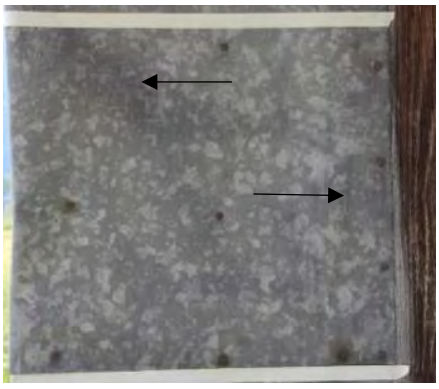

Figure 38- test zone before treatment

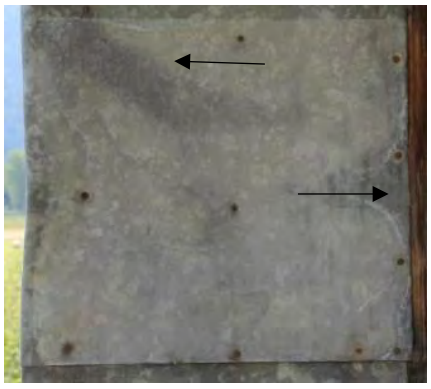

Figure 39 - test zone after biopatina treatment

Evaluation of the layer thickness before and after treatment

Since the zinc coating appears to be only slightly oxidized before treatment, the values obtained indicate a zinc coating thickness between 75 and 102 µm on the characterized zones. A significant variation of about 18 µm of the average thickness after treatment is only found in zone 2. This indicates that a passivation layer has actually formed after the application of the biopatina gel. This layer is very thin on zone 1 (limit of detection) and thicker on zone 2.

Test zone	zone	Before treatment		After treatment	
		Microphotographie (magnification X50)	Average thickness	Microphotographie (magnification X50)	Average thickness
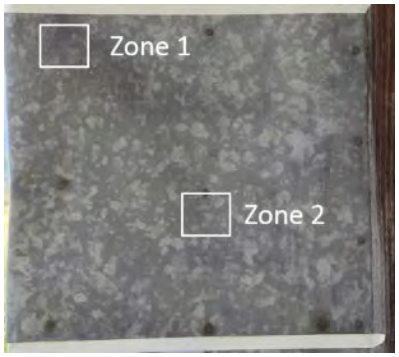 Localization of the test areas on the northern side	1		92.6 µm	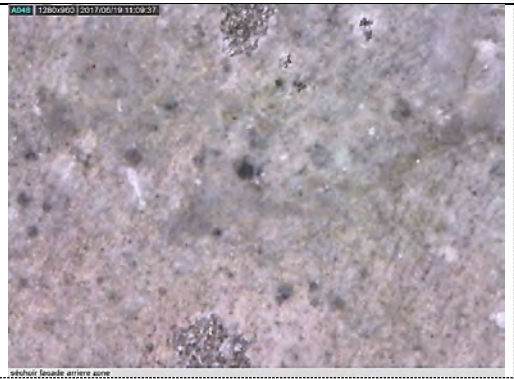	90.00 µm
	2		102.1 µm	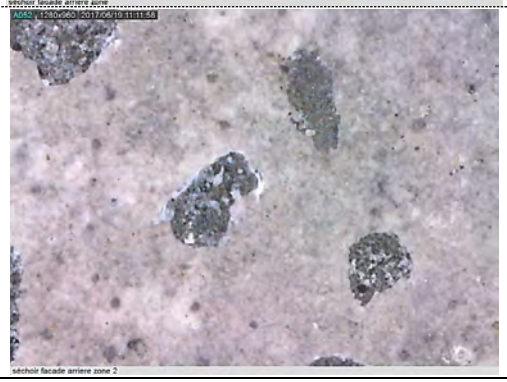	120.1 µm

Table 11- Visual evaluation of the test zone on the northern side before and after biopatina treatment

Colorimetric measurements

The total color difference ΔE * is respectively 2 (zone 1) and 2.78 (zone 2) before and after treatment, which shows a modification of the slightly noticeable appearance. Moreover, the L * values before and after treatment on the axis of clarity show that a slight lightening of the surface takes place (see appendix 3)

FTIR analysis

Given the small thickness of the layer formed during the treatment, it was taken only in an area where a larger whitish rim of corrosion products had formed (Figure 40). Unlike copper alloys, passivation by the formation of metal oxalates does not occur by the application of biopatina on zinc. In contrast, a characteristic peak of hydrozincite $Zn5(OH)_6 (CO3)_2$ was detected at 1393 cm^{-1} (see Appendix 3: Case study absinthe dryer, Boveresse). It is an insoluble light grey zinc carbonate and therefore protective. This species seems to be mainly present.

Figure 40- detailed view of the sampled area before gel removal (left) and sample location (right)

3-b.1.2.2. Farelhaus

The test zone located on the bench was evaluated after treatment.
The test area on the bench was evaluated before and after biopatina to assess the effect and the performance of the treatment. Comparative measurements were carried out on the following zones (Figure 41).

Figure 41- Localization of the measured areas on the bench

General visual evaluation and digital microscopy

A global darker appearance of the surface can be observed after treatment on the test area (Figure 42). This is due do the extraction of less adherent corrosion products that results in the darkening of all visible iron spots (located in the damaged zinc coating areas), Figurex 43-46. The development of less soluble and stable products is confirmed by the FTIR analysis on a sample of corrosion products after treatment (Appendix 4: Case study Farelhaus, Biel). This was also confirmed by the observations using digital microscopy (Table 12). A visible modification on the zinc parts wasn't noticed.
More local phenomena were also observed: a darker fringe in a strongly damaged and corroded area (lacuna in the zinc coating, a few cm large, zone 3 (Figure 46) as well as whitish traces in the same area, which didn't disappear despite several rinsing stages (Figure 46).
In the less damaged areas a slight cleaning effect was observed on the zinc coating. This effect is due to the action of the oxalic acid (a complexing agent which is contained in the biological biopatina treatment).

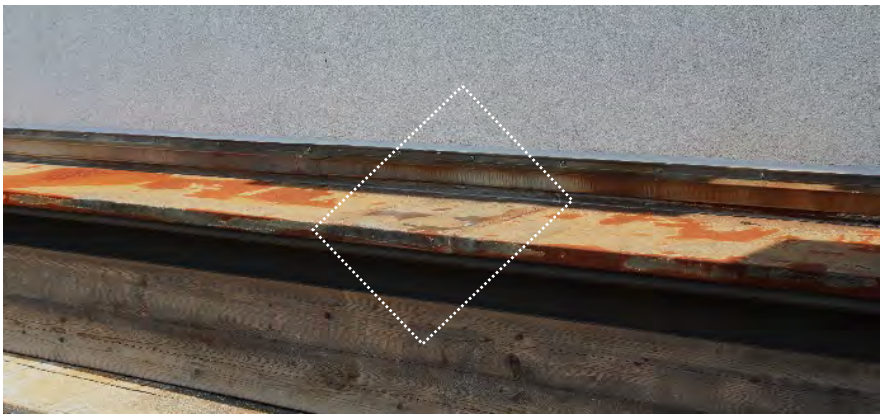

Figure 42- After biopatina treatment

a)  b) 

Figure 43 - General view of the test area, a) before and b) after treatment

a)  b) 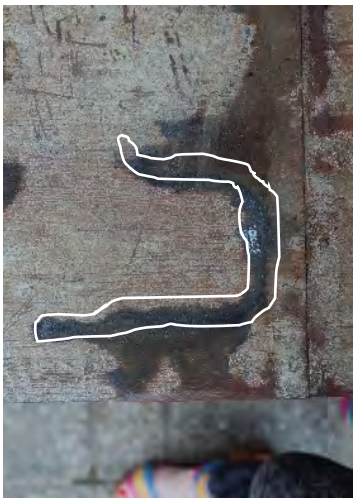

Figure 44- Detailed view of zone 1, a) before and b) after treatment

a)  b) 

Figure 45 - Detailed view of zone 4, a) before and b) after treatment

a)  b) 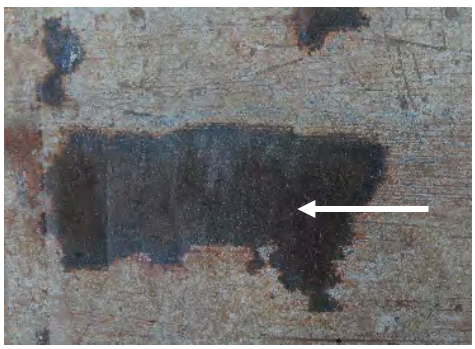

Figure 46- Detailed view of zone 3, a) before and b) after treatment

Thickness measurements before and after biopatina treatment

The average thickness decreases slightly after treatment on all test zones (Table 12). This is due to the dissolution and repassivation of the powdery ferrous corrosion products during the biopatina treatment (associated with a modification of their volume).

Evaluated zones	Zone	Before treatment (magnification X50)	After treatment (Magnification X50)	Layer thickness
	1	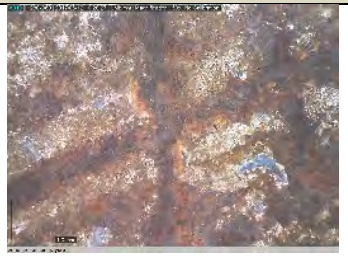		53.1→55.6 µm
	2	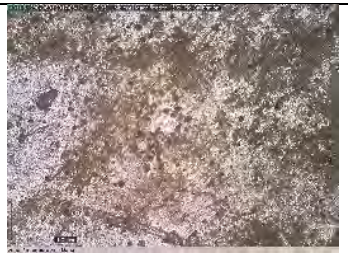		106→86.4 µm
	3			104.7→72.8 µm
	4		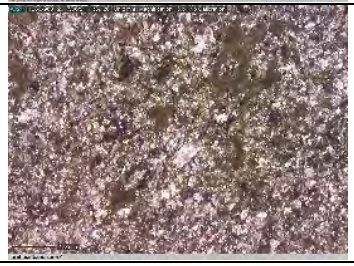	116.3→103.1 µm

Table 12- Visual evaluation and thickness measurements on the test zones on the bench (northern side) before and after biopatina treatment

Colorimetric measurements

The average value of ΔE* on the test zones before and after biopatina treatment can differ strongly depending on the selected zone. Different studies[12] have proposed different ΔE* values that have a JND (just noticeable difference). The JND values are generally defined between 1 - 2.3. From this point of view a very noticeable difference can only be observed on the damaged strongly corroded zone 3 and a less noticeable difference on zone 2 which corresponds to a very metallic zinc zone alternating with small darker iron spots (Table 13).

As already mentioned, the strongest chromatic difference was noticed for the corroded iron spots which get darker with the treatment (see Appendix 3: Case study absinthe dryer, Boveresse) and tend on the a* and b* axis toward blue and green.

Zone	Color difference Δ E before and after treatment
1	1.56
2	4.71
3	10.5
4	2.65

Table 13 - color difference before and after biopatina treatment (ΔE)

CONCLUSIONS

First of all, these tests showed that some practical aspects need to be improved. In fact, complementary test zones on the Farelhaus and the absinthe dryer couldn't be exploited as in both cases the test setting didn't resist to extreme weather conditions. Removal of the gel protection by strong wind occurred and there's the risk of drying out the gel if the temperatures are high. These on-site tests have demonstrated that the application process and the device for implementing the treatment are perfectible.

Nevertheless the results obtained on the preserved test zones with a biopatine gel show encouraging first results in application on zinc surfaces. In both cases, the change of the surface appearance by the treatment is small and the overall aesthetic appearance satisfactory. On the well preserved zinc coating of the absinthe dryer, the presence of hydrozincite, which is a zinc-passivating corrosion product was identified after treatment.

The very degraded zinc coating on the bench of the Farelhaus, characterized by strong iron corrosion showed the strongest modification in appearance after treatment. In general, all visible iron rich zones reacted during treatment and got darker. A visible modification of the intact zinc spots wasn't noticed. In terms of conservation, the presence of darker iron spots could indicate the presence of more chemically stable (less soluble) and dense corrosion products. This would imply a benefic action of the biopatina treatment by development of passivating compounds. This hypothesis has to be verified by complementary non-invasive characterization of the corrosion in-situ. A regular monitoring of the test zone of the bench on the north east side would also be necessary to confirm these observations and study the long-term performance of the biopatina treatment.

[12] M. Melgosa, J. J. Quesada, and E. Hita, Uniformity of some recent color metrics tested with an accurate color-difference tolerance dataset. In. Applied Optics, Vol. 33, Issue 34, 1994, pp. 8069-8077 ; Mokrzycki W.S., Tatol M. Colour difference _E - A survey, Preprint submitted to Machine Graphic & Vision, 08:10:2012

3-b.2. Samples: Results

3-b.2.1. Non ferrous metals

3-b.2.1.1. Bare zinc alloy (Z series)

After treatment

The biopatina treatment induced the development of a heterogeneous white-grey corrosion product layer. This layer is about 4 µm thick. Microscopic observation shows that poorly adherent white corrosion products also formed (Table 14). The average colorimetric values indicate that the surface tends to get darker with the treatment. A slight decrease in lightness (Figure 47) and an evolution on the blue-yellow axe towards yellow (Figure 48) can be observed after biopatina treatment. This difference is visible[13] (delta E = 13.65).

FTIR analysis shows that zinc oxalates are present on the surface after biopatina treatment. Characteristic peaks are observed at 1622, 1362 and 819 cm^{-1} (Figure 49).

After 6-months exposure

Outdoor exposure induces on the biopatina treated samples the development of microscopic dark spots which alternate with poorly adherent white corrosion products (table 14).

In contrast, the reference series without biopatina treatment is covered after a 6-months exposure with a very heterogeneous corrosion layer, which seems to be adherent. Larger darker spots are visible all over the surface. Exposure induces for all samples – treated and untreated- a movement on the yellow-blue axe (towards yellow), Figure 47. Colorimetric measurements also show that all samples get darker, Figure 48. The overall Delta E is more important before and after 6-months exposure for the untreated samples in comparison to the biopatina treated samples (28.61 / 21.87).

The thickness of the corrosion layer formed after exposure is similar for both treated and untreated samples (Table 15). FTIR analysis indicates that there is a predominance of hydrozincite on the untreated reference samples with strong bands at 1495 cm^{-1}, corresponding to the asymmetric stretching vibrations of the carbonate ion. Other modes attributable to carbonate are present at 1040 cm^{-1} (the symmetric stretch), 830 cm^{-1} and probably 691 cm^{-1}. On the biopatina treated samples, zinc oxalates are still detected with characteristic peaks at 1623 and 1362 cm^{-1}, but alternate with hydrozincite (Figure 50).

After exposure the thickness layer between the treated and untreated samples has been leveled out (table 15). SEM imaging (SE) shows that on biopatina treated samples the corrosion layer is more voluminous and masks sometimes completely the surface marks.

[13] Generally spoken, a well-trained eye can detect a color difference of delta E=2

Bare zinc (Z)	Before 6 months exposure	After treatment	After 6 months exposure
T0 Reference	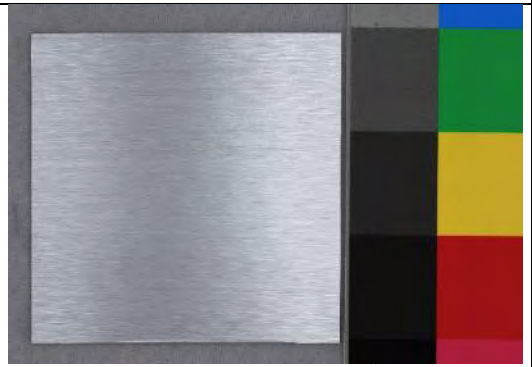 Sample Z1, General view	----------	 Sample Z1, General view
	 Sample Z1, zone B, X96	----------	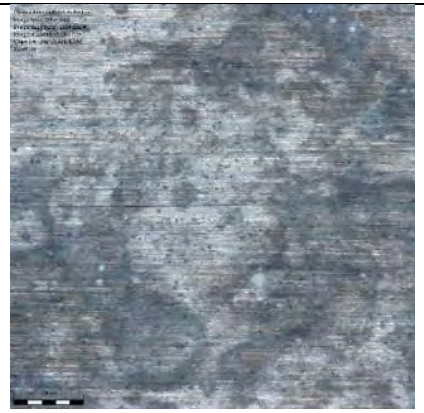 Sample Z1, zone B, X96

	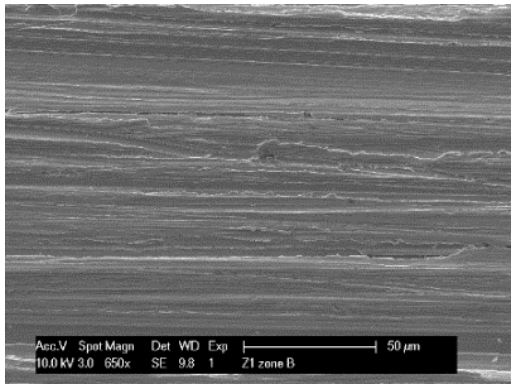 Sample Z1 zone B, x650 (SE)	----------	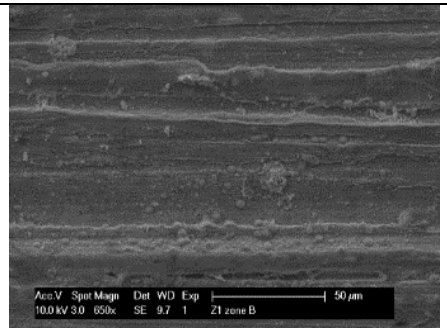 Sample Z1 zone B, x650 (SE) 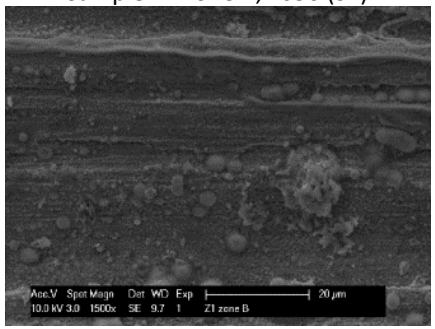 Sample Z1 zone B, x1500 (SE)
T4 biopatina	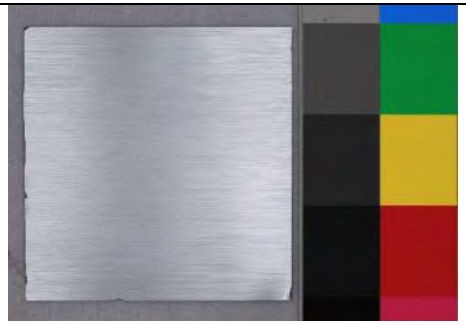 Sample Z5, general view	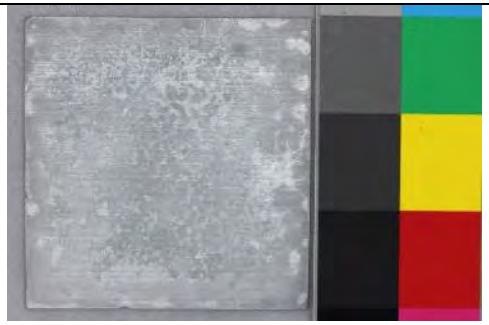 Sample Z5, general view	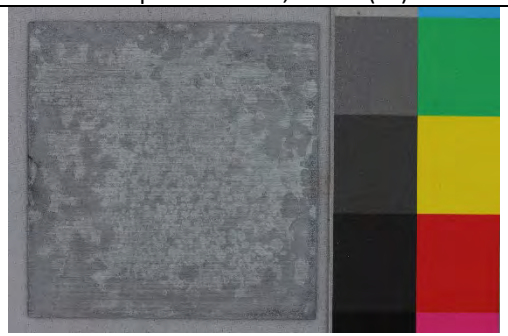 Sample Z5, general view

	 Sample Z5, zone B, x96	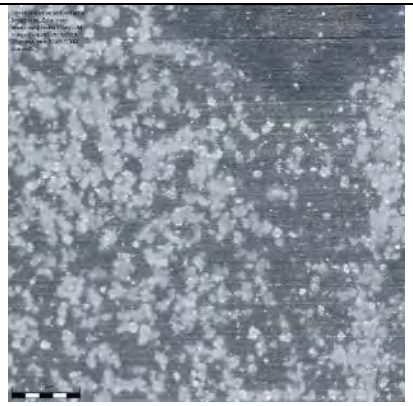 Sample Z5,zone B, x96	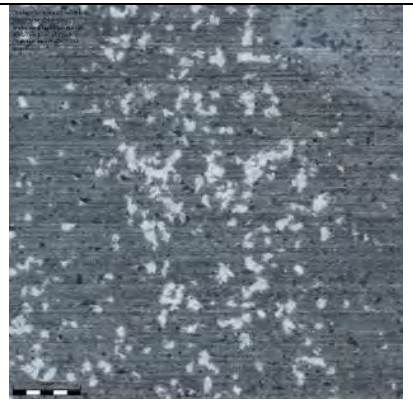 Sample Z5, zone B, x96
	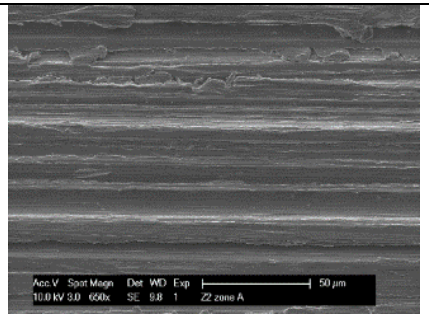 Sample Z2 zone B, x650 (SE)	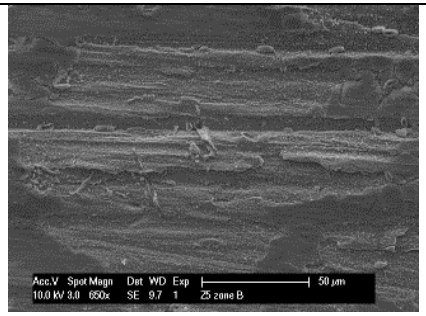 Sample Z5 zone B, x650 (SE)	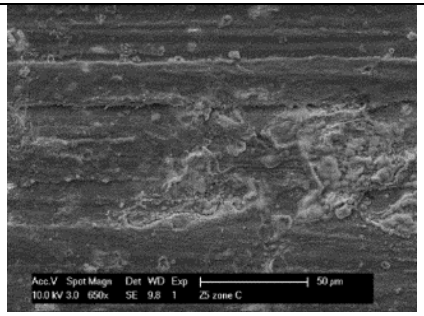 Sample Z5 zone B, x650 (SE)
	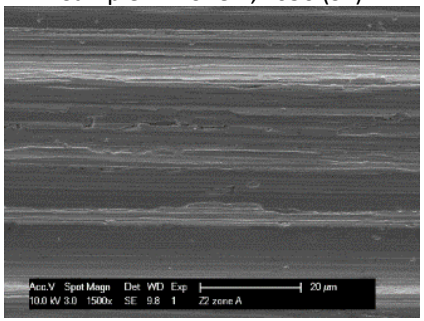 Sample Z2 zone B, x1500 (SE)	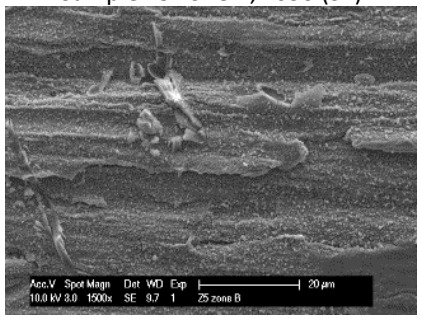 Sample Z5 zone B, x1500 (SE)	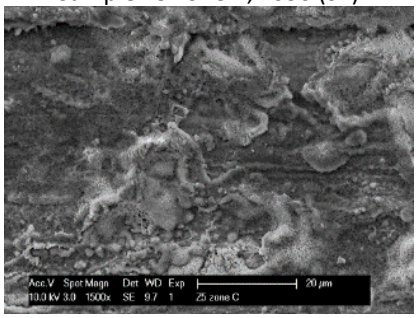 Sample Z5 zone B, x1500 (SE)

Table 14- Results of the visual examination on the bare zinc samples (Z)

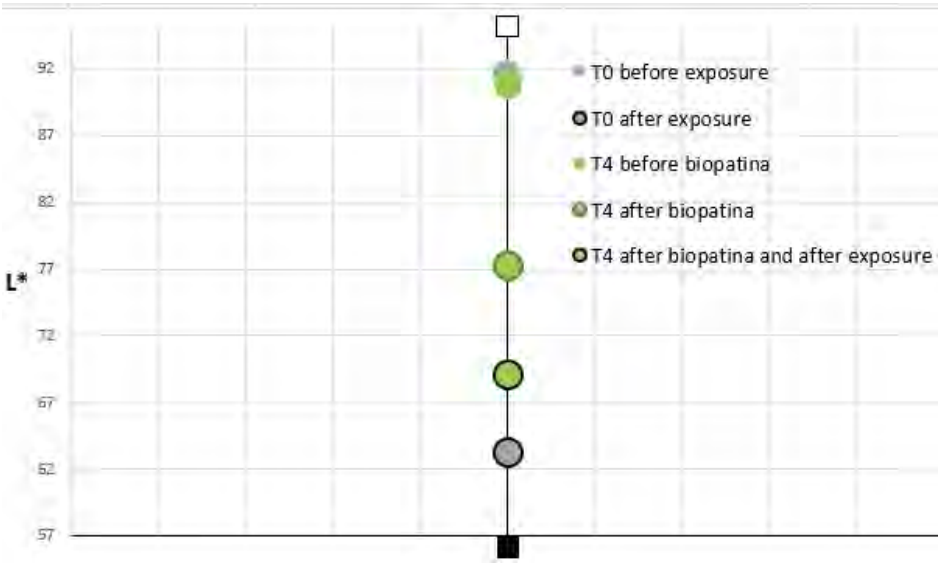

Figure 47- colorimetric measurements L* performed on bare zinc samples (Z)

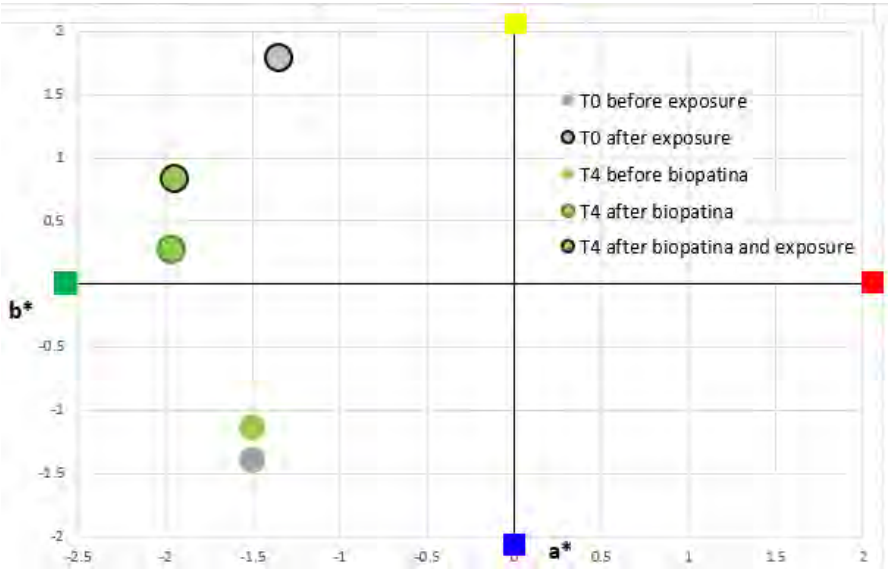

Figure 48- colorimetric measurements a*B* performed on bare zinc samples (Z)

Z	Before exposure	After treatment	After 1 month	After 3 months	After 6 months
T0 (reference)	na	----------	5.47	6.27	6.53
T4	na	4.05	11.7	10.23	5.17

Table 15- average thickness of the corrosion layer in µm on the bare zinc samples (Z)

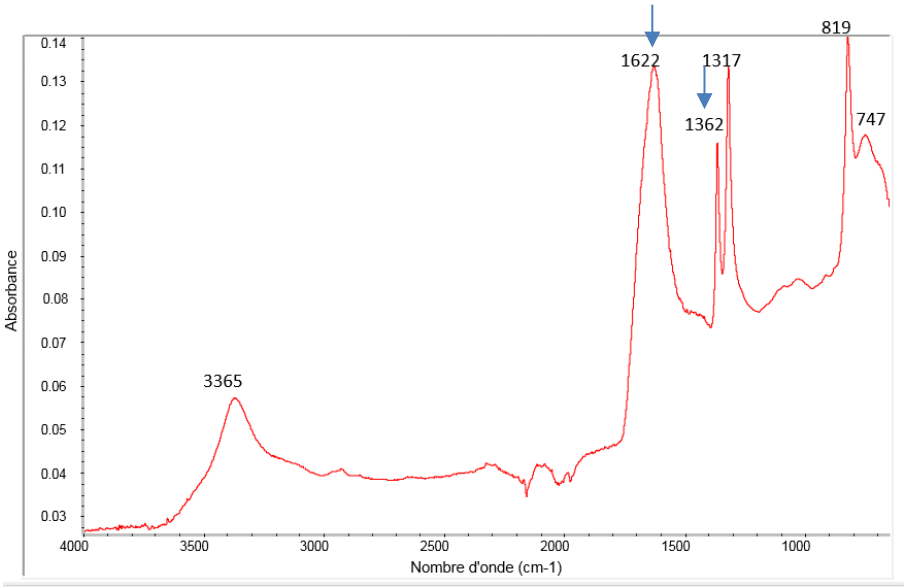

Figure 49- T4 after treatment (sample Z5), ATR- FTIR spectrum

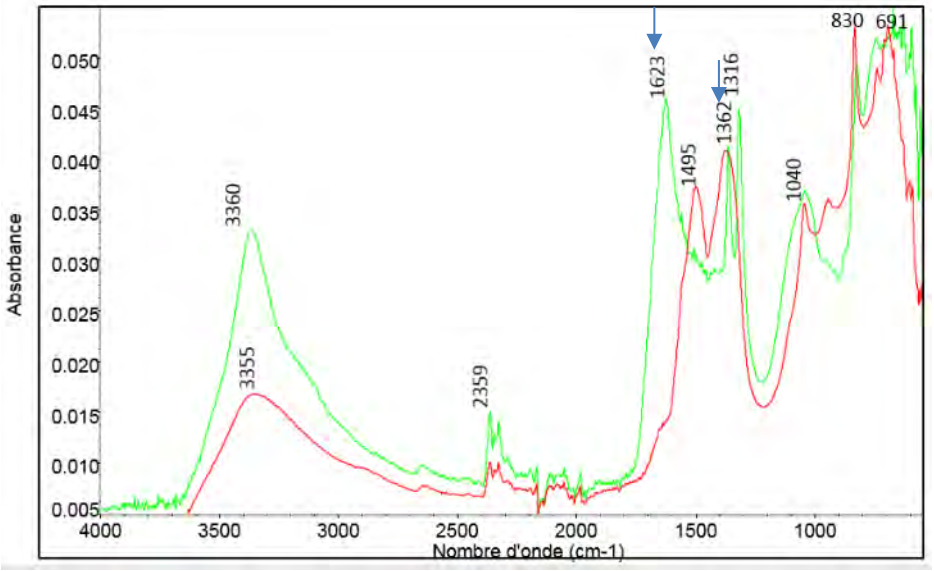

Figure 50- after 6 months exposure: T4 (Z15) in green/ T0 (Z1) in red, ATR- FTIR spectra

3-b.2.1.2. Naturally corroded zinc alloy (ZA series)

Biopatina treatment

The biopatina treatment induces the development of a heterogeneous white-grey corrosion product layer. The overall thickness of this layer is slightly higher than the natural intact corrosion layer on the untreated samples. Microscopic observation shows that white corrosion products which seem poorly adherent develop on the surface. This layer is discontinuous, a lot of porosities can be seen. SEM imaging shows the development of specific corrosion products and crystallizations (table 16, which can be observed at magnification X1500). Before treatment the samples show characteristic peaks attributable to carbonate of hydrozincite at 1495/1575, 1378/1384, 1040/1036, 830/826 cm^{-1} (Figures 53-54) The peak at 692/670 cm^{-1} might arise from hydroxide deformations.

The biopatina treatment induces clearly the formation of zinc oxalates, characteristic peaks are detected by FTIR analysis at 1622 and 1362 cm^{-1} (Figure 55).

After 6-months exposure

The samples treated with biopatina formed a homogenous patina, which is slightly less dark than on the untreated exposed samples. The average colorimetric values confirm that the surface gets darker without a biopatina treatment (Figure 52). At a microscopic scale the untreated samples show a very similar corrosion product morphology to their state before exposure (Table 16).

In the case of samples treated with biopatina, the superficial whitish corrosion layer which formed during the treatment, tends to get off. This could explain the more homogenous and darker appearance after the 6-month exposure. The same surface morphology could not be observed by SEM after treatment. This observation could confirm that a part of the corrosion layer was modified or disappeared with exposure.

Exposure induces for all samples – treated and untreated- a movement on the yellow-blue axe, but in different directions. In fact untreated samples tend to evolve towards yellow, as treated samples go to blue (Figure 51). Delta E is more important before and after 6-months exposure for the treated samples (2.83 /9.54).

The thickness of the corrosion layer formed after exposure is slightly higher for the treated samples after exposure (Table 17).

The spectra obtained on treated and untreated samples after 6 months exposure are different. The untreated samples show a predominance of hydrozincite on the surface: characteristic peaks attributable to carbonate of hydrozincite are identified at 1495, 1353, 828 cm^{-1} (Figure 56).

Zinc oxalates are still present on the biopatina treated samples (with characteristic peaks at 1622 and 1362 cm^{-1}), but they are associated to or alternate with hydrozincite (characteristic peaks at 1495, 829 cm^{-1}), Figures 57-58.

ZA	Before 6 months exposure	After treatment	After 6 months exposure
T0 **Reference** **Before /after exposure**	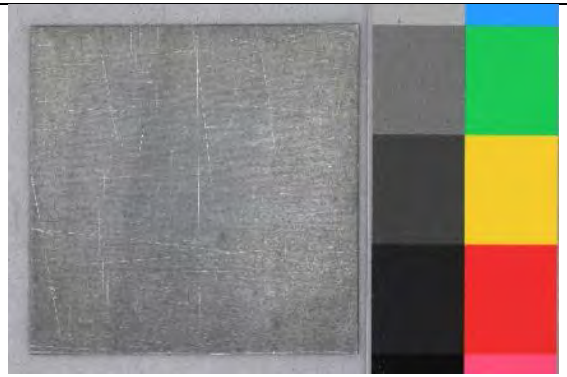 Sample ZA1, general view	----------	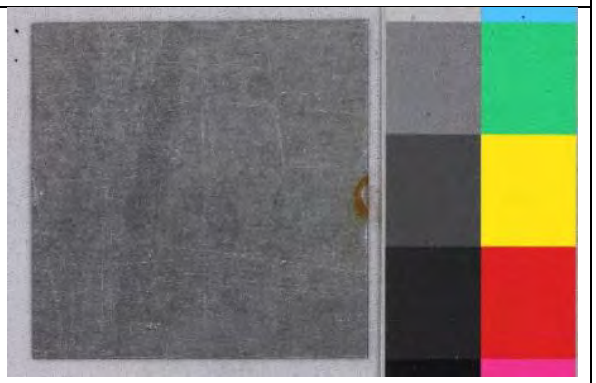 Sample ZA1, general view
	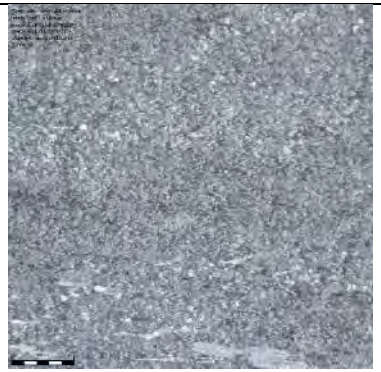 Sample ZA1, zone B, x96	----------	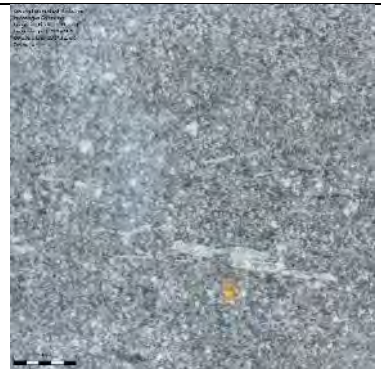 Sample ZA1, zone B, x96

	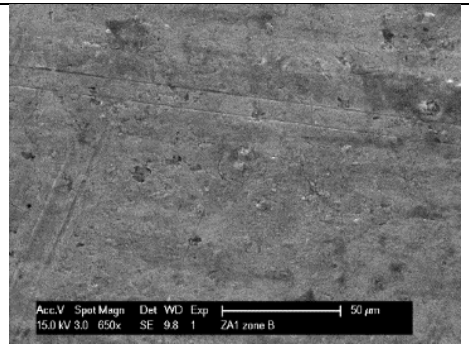 Sample ZA1, zone B, x650 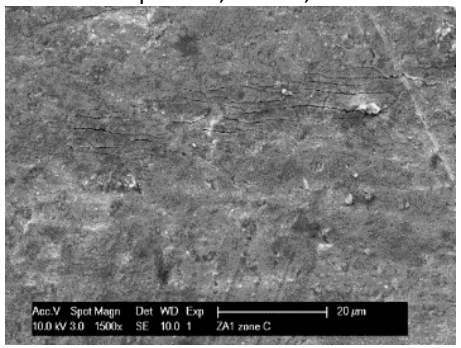 Sample ZA1, zone B, x1500	----------	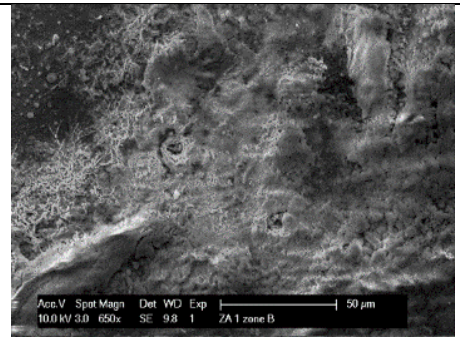 Sample ZA1, zone B, x650 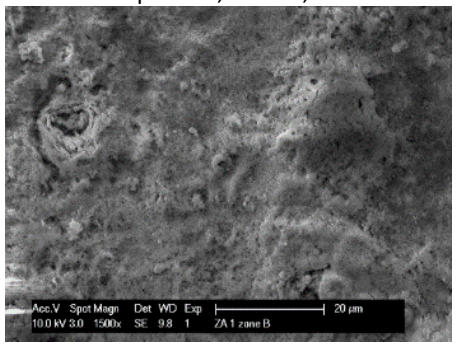 Sample ZA1, zone B, x1500
T4 **biopatina**	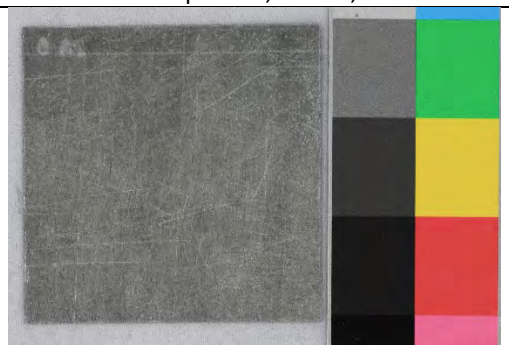 Sample ZA5, general view	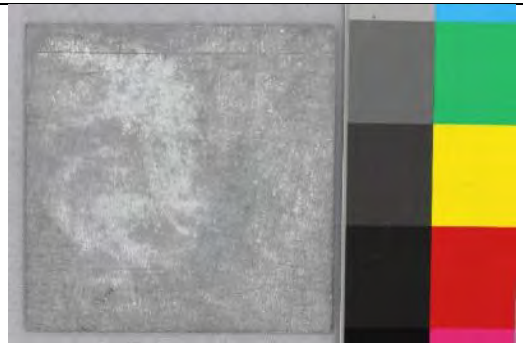 Sample ZA5, general view	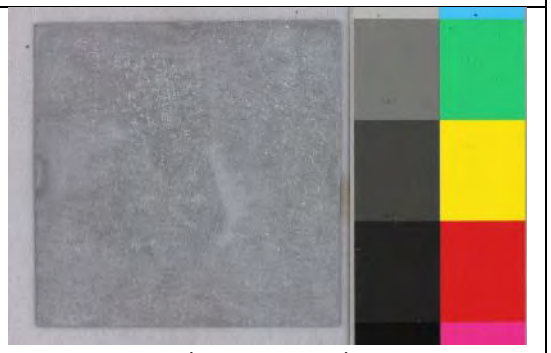 Sample ZA5, general view

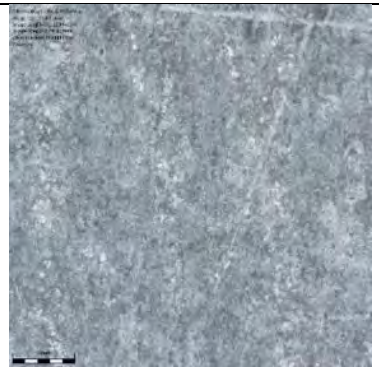

Sample ZA5, zone B, x96

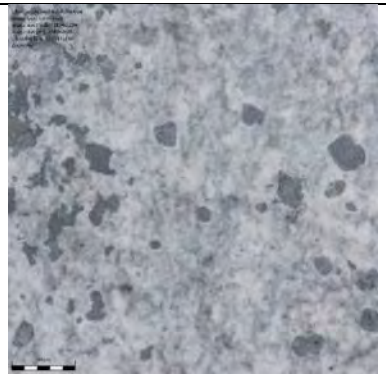

Sample ZA5, zone B, x96

Sample ZA5, zone B, x96

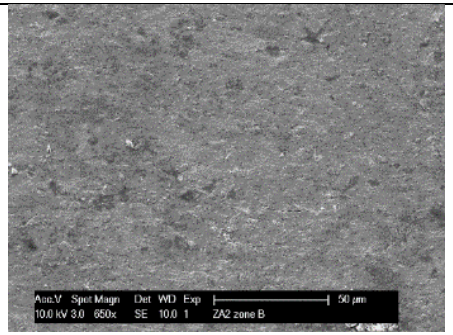

Sample ZA2, zone B, x650 (SE)

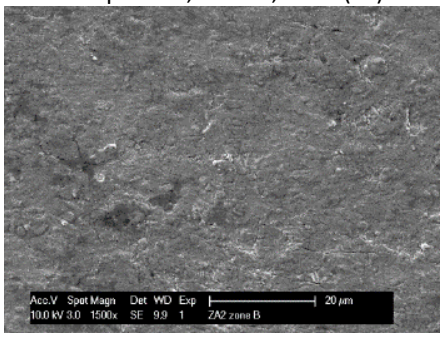

Sample ZA2, zone B, x1500 (SE)

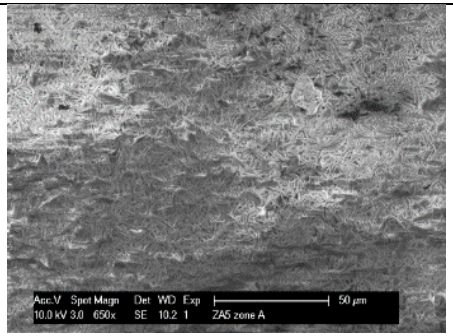

Sample ZA5, zone A, x650 (SE)

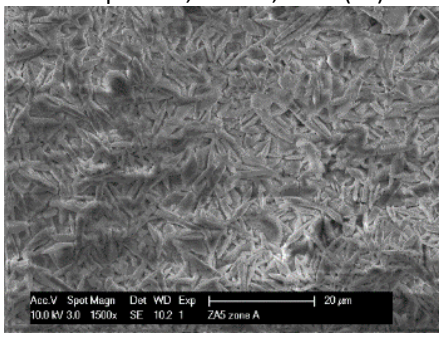

Sample ZA2, zone A, x1500 (SE)

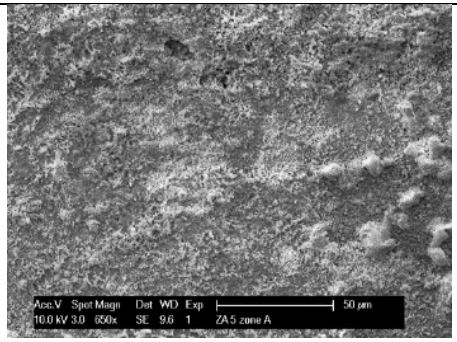

Sample ZA5, zone A, x650 (SE)

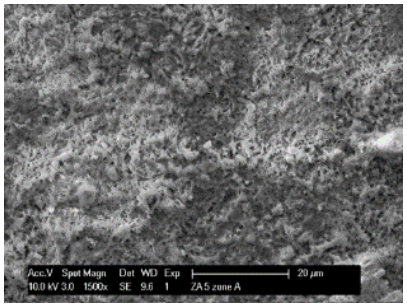

Sample ZA2, zone A, x1500 (SE)

Table 16– Results of the visual examination on the ancient zinc samples (ZA)

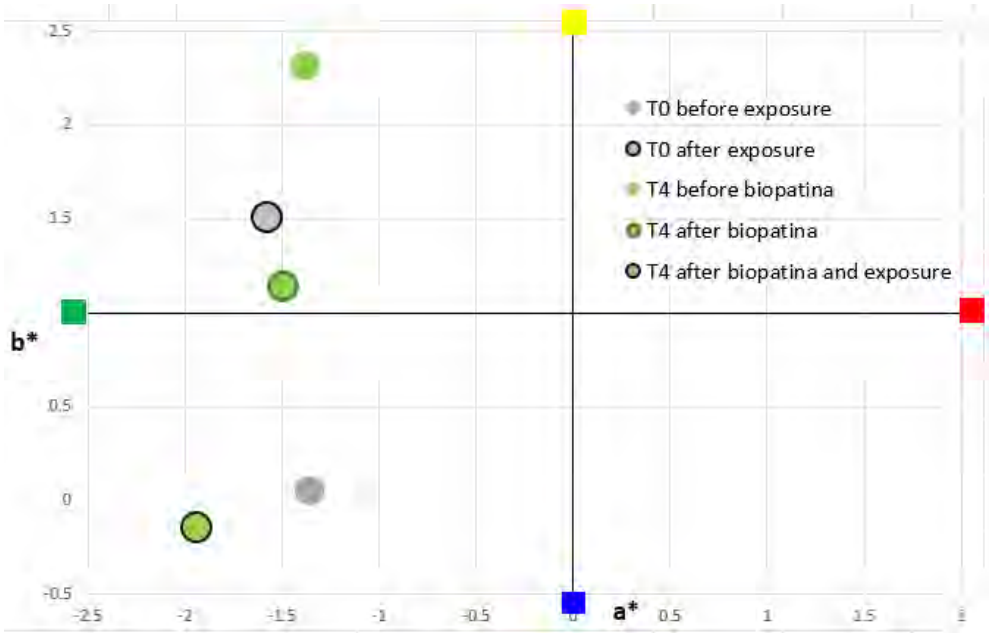

Figure 51- colorimetric measurements performed on ancient zinc samples (ZA)

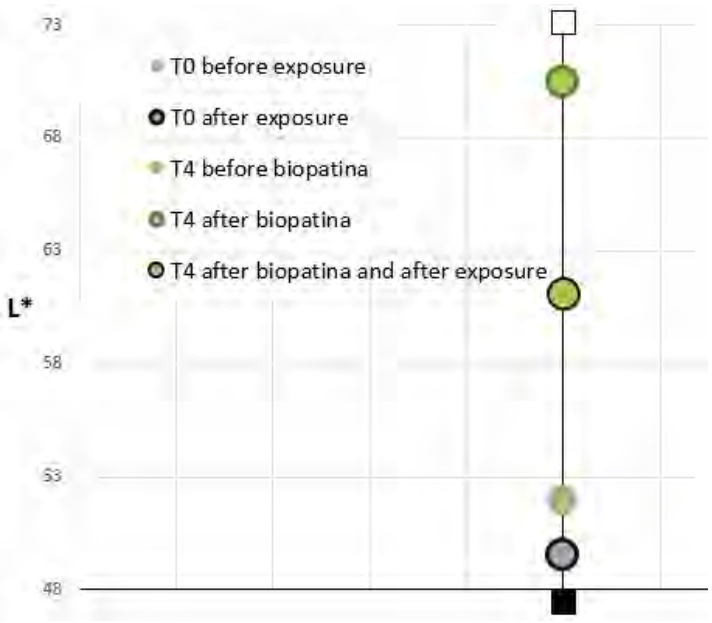

Figure 52- colorimetric measurements performed on ancient zinc samples (ZA)

ZA	Before exposure	After treatment	After 1 month	After 3 months	After 6 months
T0 (reference)	0.6	----------	4.77	5.1	3.9
T4	0.6	7.05	7.87	8.3	5.73

Table 17 - average thickness of the corrosion layer in µm on the ancient zinc samples (ZA)

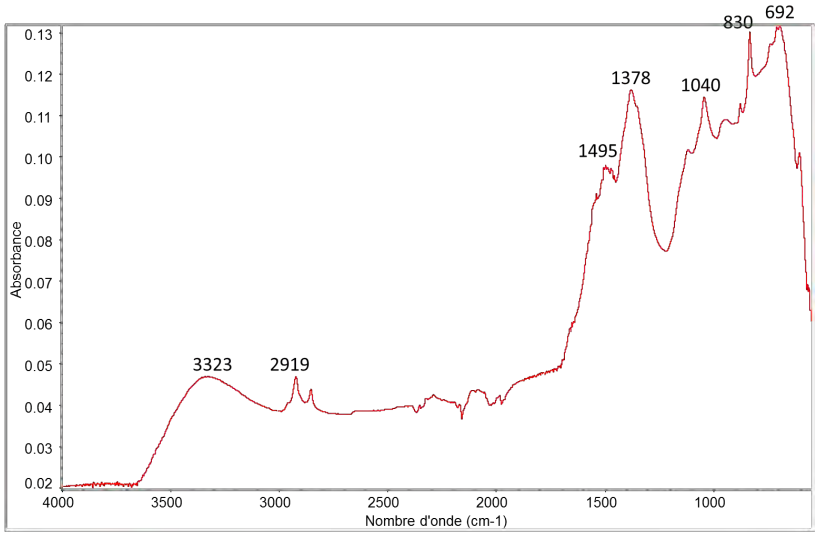

Figure 53- T4 before treatment (sample ZA12), ATR- FTIR spectrum

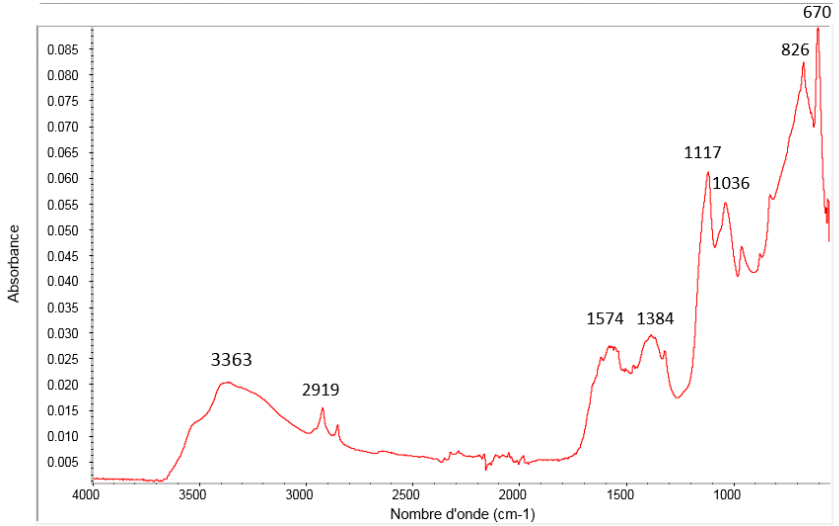

Figure 54- T4 before treatment (sample ZA5), ATR- FTIR spectrum

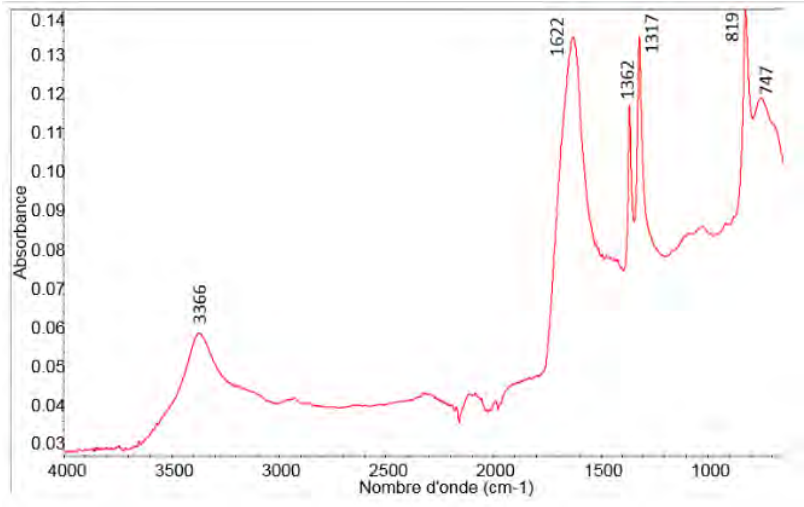

Figure 55- T4 after treatment and before exposure (ZA5), ATR- FTIR spectrum

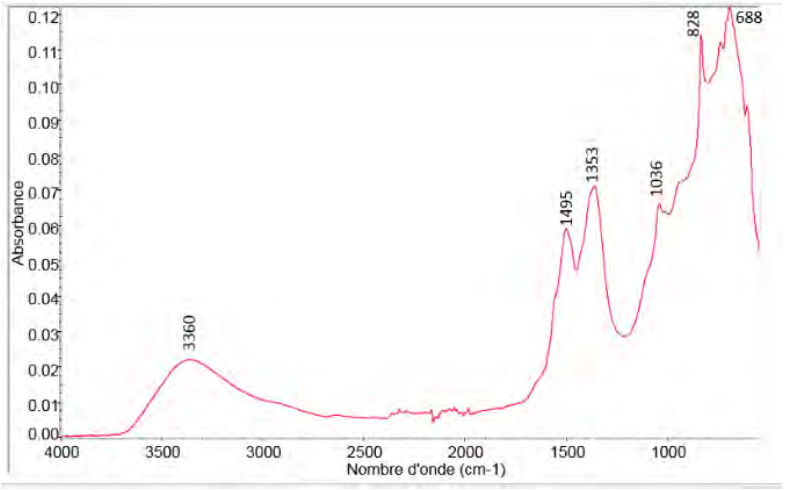

Figure 56- T0 after 6-months exposure (ZA1), ATR- FTIR spectrum

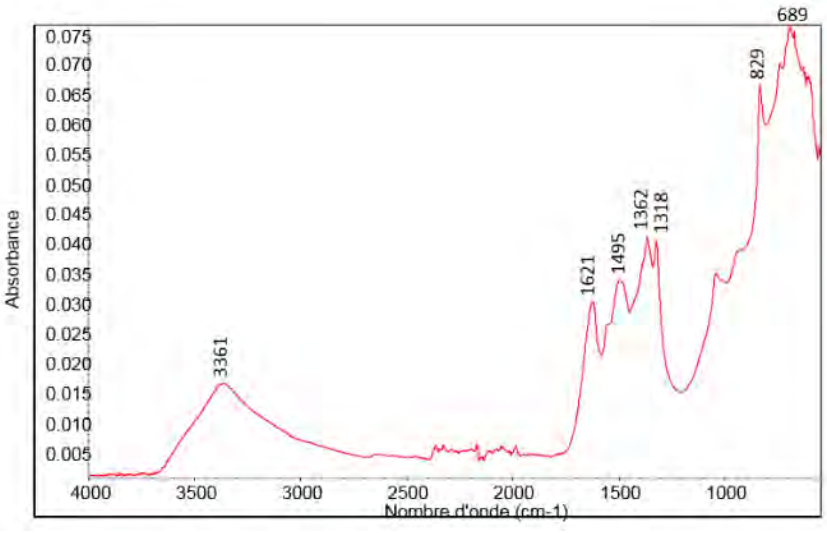

Figure 57 -T4, after biopatina treatment and exposure (ZA3), ATR- FTIR spectrum

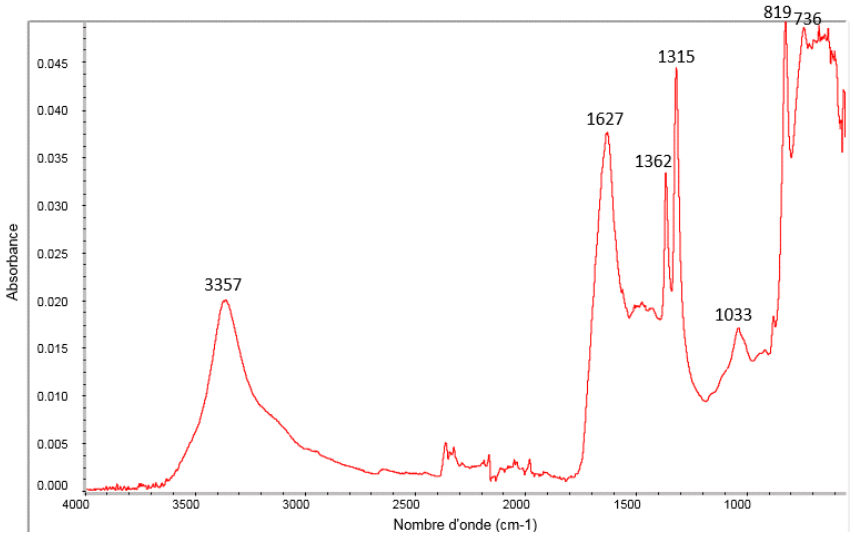

Figure 58- sample ZA13 after biopatina treatment and exposure (T4), ATR- FTIR spectrum

3-b.2.1.3. Bare copper alloy (C series)

Biopatina treatment

No noticeable difference was observed depending on whether the samples had been treated with biopatina or not previously except for some smaller stains which seem to have been induced by the contact with the gel. These stains remain on the surface although the metal was rinsed several times with water (Table 18). Thickness measurements show that no measurable oxide layer formed on the bare metal after biopatina treatment (Table 19). FTIR spectrum indicates the development of copper oxalates with characteristic peaks around 1622 and 1362 cm^{-1} (Figure 61).

The surface keeps a satin surface finish before and after exposure in all cases (with and without biopatina treatment). The colorimetric measurement indicates a slight decrease of lightness after biopatina treatment and an evolution on the green-red axe (towards red), Figures 59-60. This difference is slightly visible (delta E =5.75).

6-month exposure

The outdoor exposure generated in both cases the development of a dark brown-violet layer of corrosion products. This is confirmed for all samples treated and untreated by a much lower lightness value (Figure 59). Exposure induces for all samples – treated and untreated- a movement on both a* and b* axes towards green and blue (Figure 59).

The thickness of the corrosion layer formed after exposure is similar for both treated and untreated samples, the evolution of the thickness after 1, 3 and 6 months is also similar (Table 19). SEM imaging (SE) shows that the morphology of this layer is similar and masks progressively the parallel scratches on the surface (Table 18).

Both treated and untreated samples have similar spectra after 6-months exposure (Figures 62-63).Copper oxalates are not detected anymore on the biopatina treated samples. The peak around 600 cm^{-1} might be related to the presence of cuprite, copper(I) oxide Cu_2O (see Appendix 5: Reference data for analysis).

C	Before 6 months exposure	After treatment	After 6 months exposure
T0 **Reference** **(without biopatina treatment)**	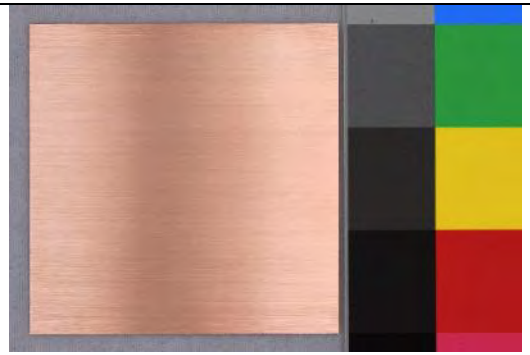 General view, sample C6	--------	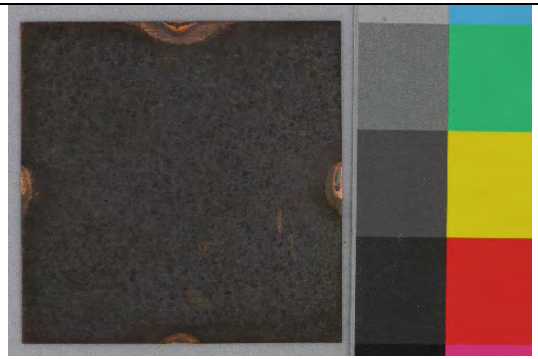 General view, sample C6
	 Sample C6, zone A, X96	--------	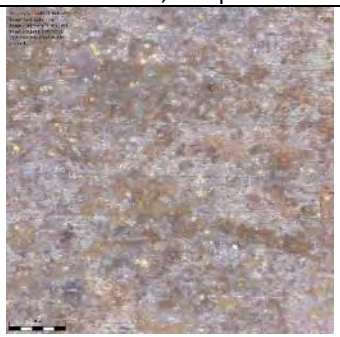 Sample C6, zone A, X96

	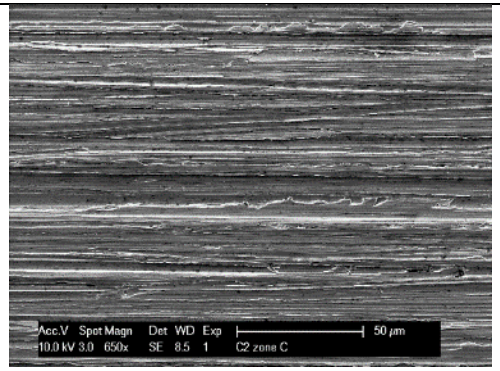 Sample C2, zone C, X650 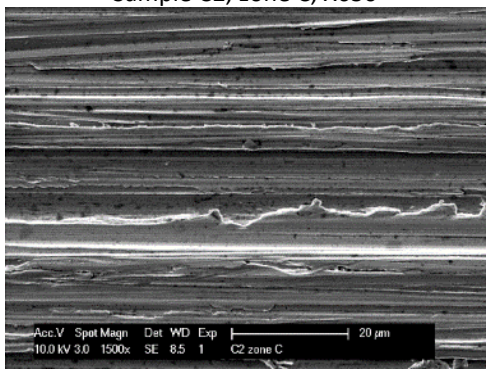 Sample C2, zone C, X1500	----------	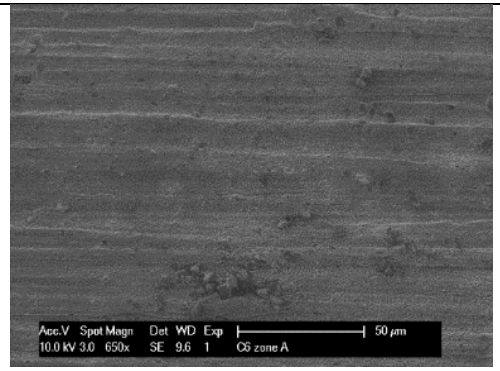 Sample C6, zone A, X650 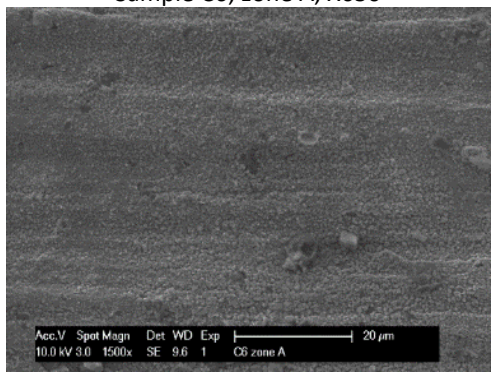 Sample C6, zone A, X1500
T4 **biopatina**	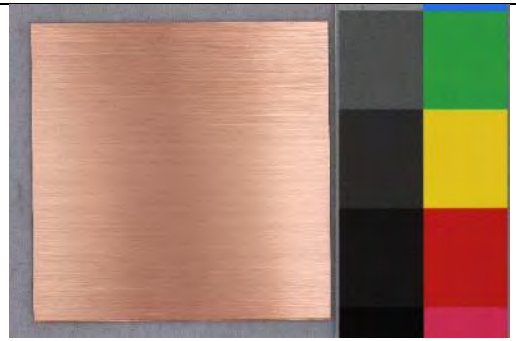 General view, sample 1	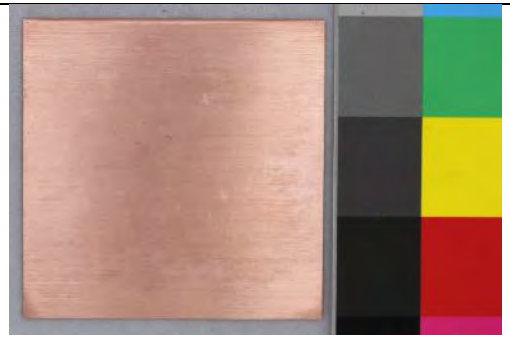 General view, sample 1	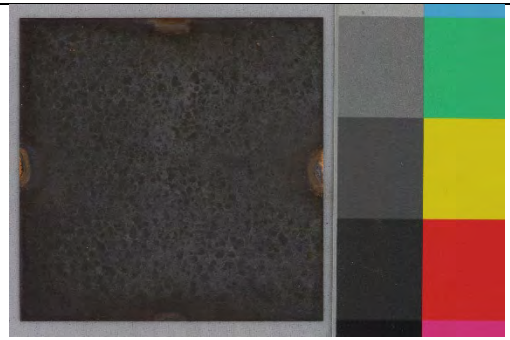 General view, sample 1

	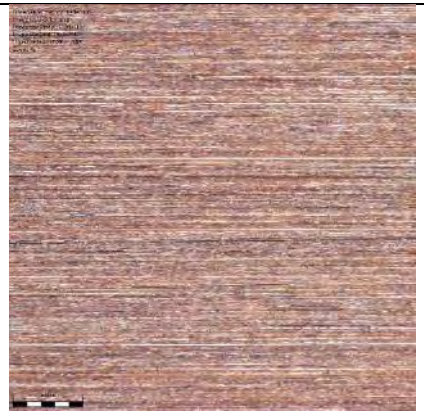 Sample C1, zone A, X96	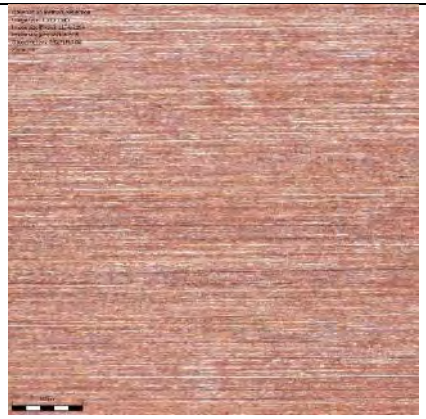 Sample C1, zone A, X96	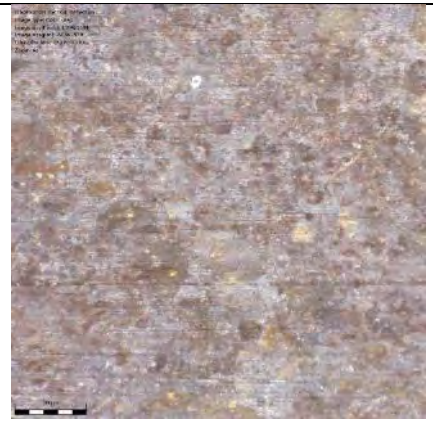 Sample C1, zone A, X96
	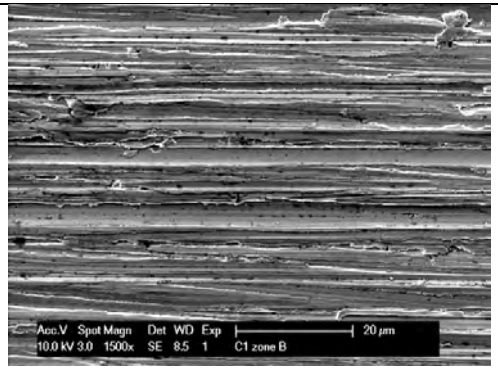 Sample C1, zone B, X1500	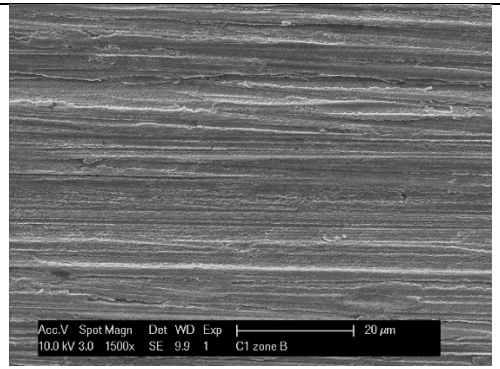 Sample C1, zone B, X1500 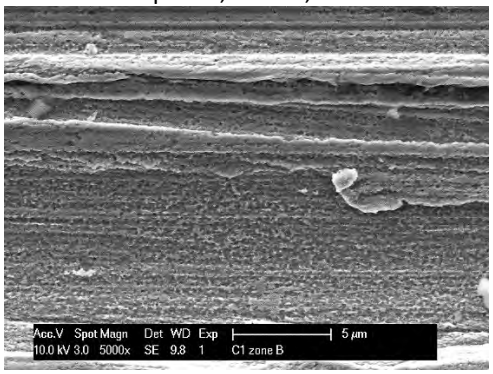 Sample C1, zone B, X5000	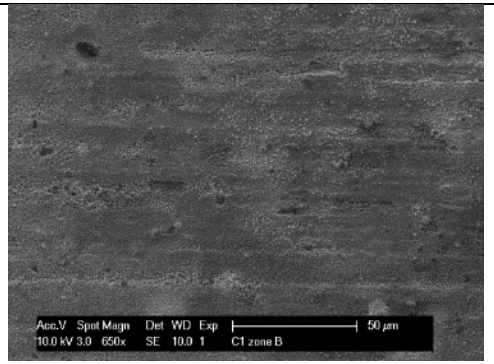 Sample C1, zone B, X650 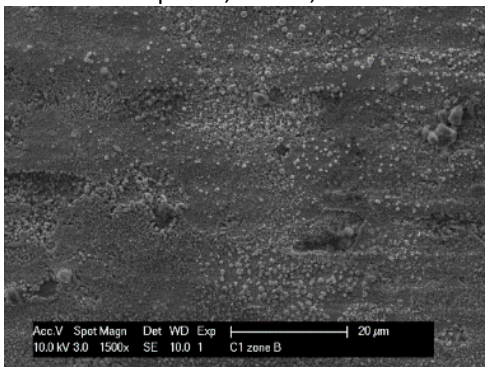 Sample C1, zone B, X1500

Table 18- Results of the visual examination on the bare copper samples (C)

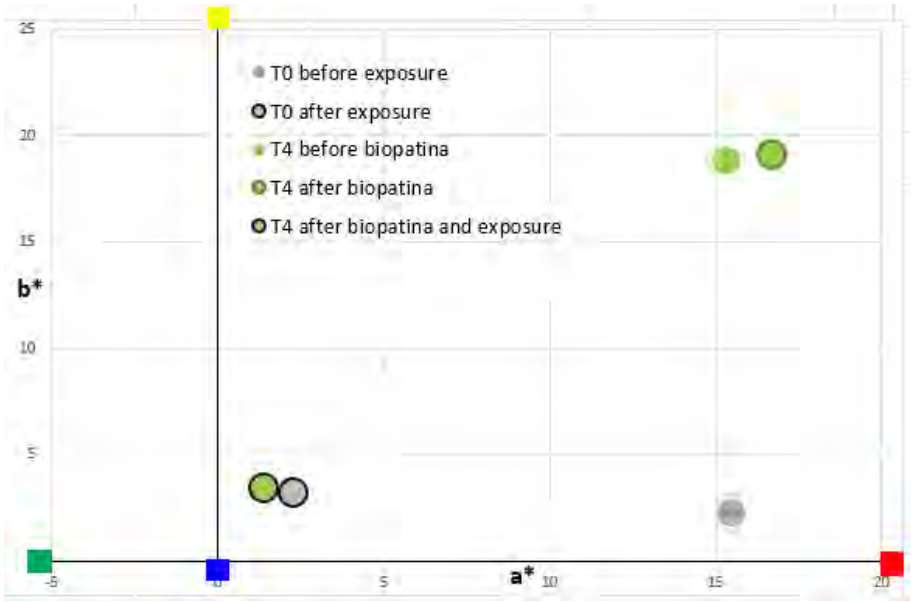

Figure 59- colorimetric measurements performed on bare copper sample (C)

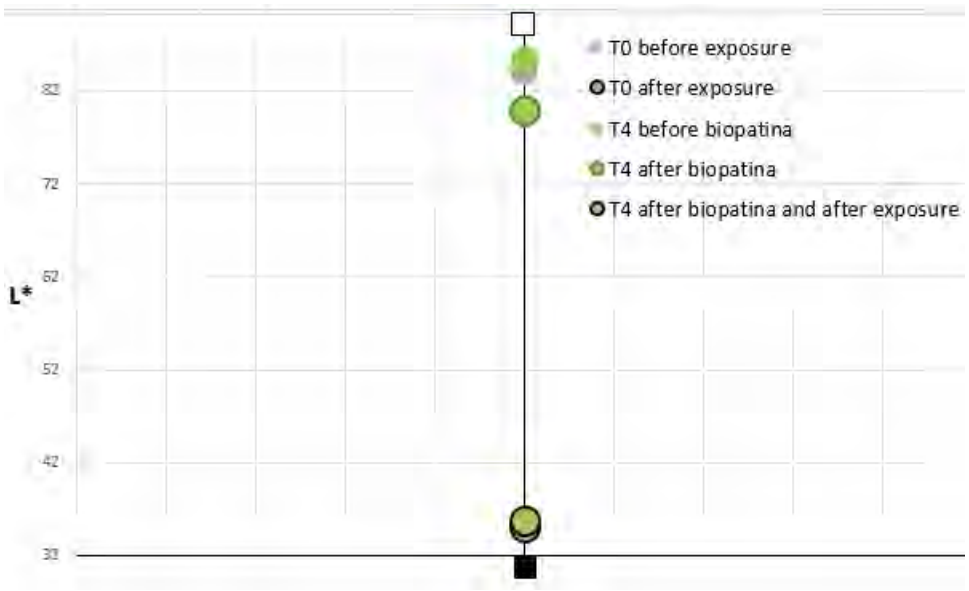

Figure 60- colorimetric measurements performed on bare copper sample (C)

C	Before exposure	After treatment	After 1 month	After 3 months	After 6 months
T0 (reference)	nm	nm	3.07	3.23	3.7
T4	nm	nm	3.07	12	3.9

Table 19- average thickness of the corrosion layer in µm on the bare copper samples (C)

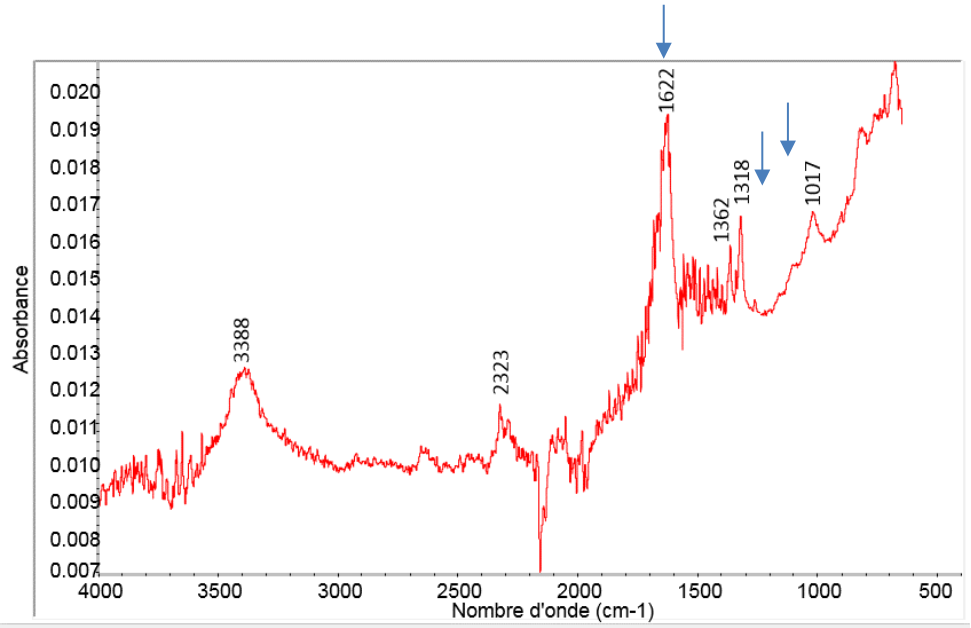

Figure 61- T4 after treatment and before exposure (C9), ATR- FTIR spectrum

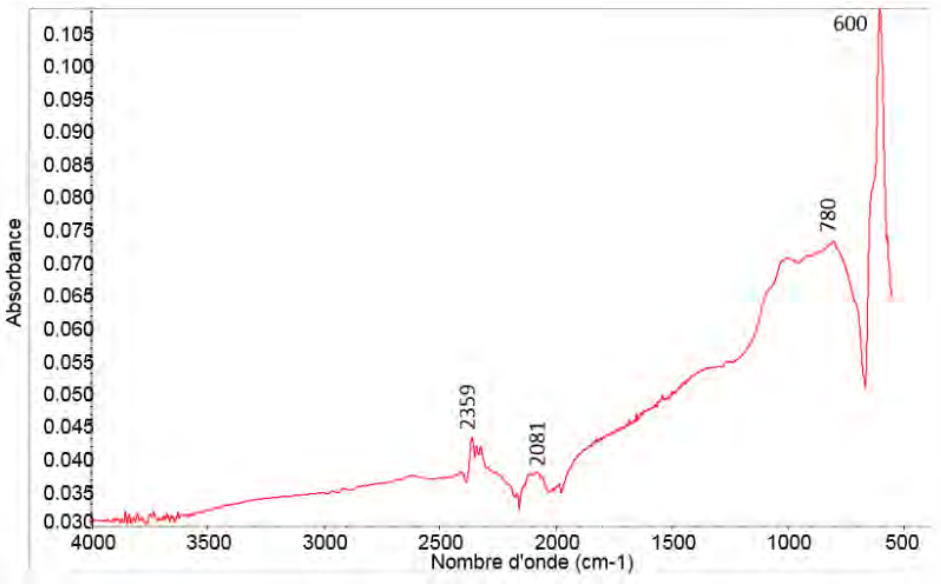

Figure 62- T4 after treatment and after exposure (C9), ATR- FTIR spectrum

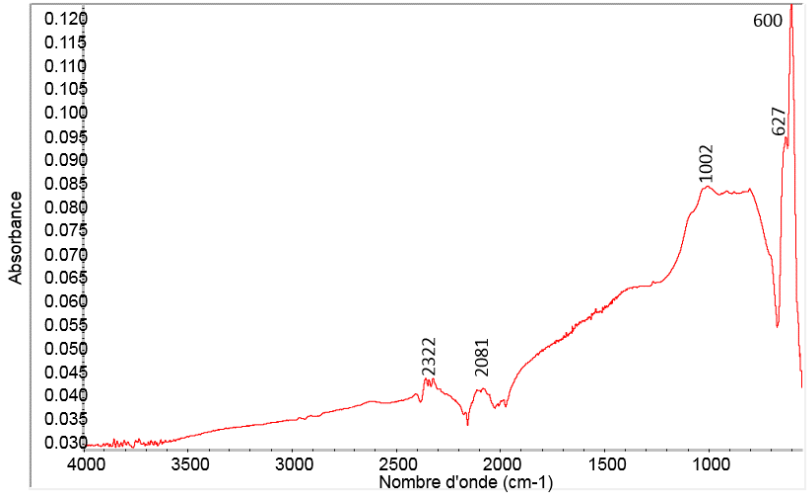

Figure 63- T0 after exposure (C6), ATR- FTIR spectrum

3-b.2.1.4. Ancient copper alloy (CA series)

Biopatina treatment

The samples which were treated with biopatina have a slightly different color in comparison to the untreated samples (Δ E =3.32) .The surface seems to be slightly greener, which is confirmed by colorimetric measurements (Figures 64-65).

SEM imaging (SE) shows that certain species form on the surface (probably copper oxalates), which are not present on the untreated reference samples. This is confirmed by FTIR analysis with characteristic peaks around 3380, 1622 and 1362 cm^{-1}, Figure 67. The biopatina treatment doesn't induce a growth of the corrosion layer (Table 21).

6-months exposure

The exposure induces on the untreated reference samples (T0) only a slight visual difference which is not perceptible for the human eye (Δ E= 0.9). Microscopical examination shows that small dark spots appear increasingly on the surface (Table 20). Colorimetric measurements confirm that the surface is slightly darker after exposure (Figure 65). The evolution of thickness is identical on the untreated and biopatina treated samples after 6-months exposure (Table 21).

The biopatina samples keep a higher Δ E (=7.62) in comparison to their appearance before treatment and outdoor exposure. The exposure induces visually the development of bright blue-green corrosion products. This is confirmed by the colorimetric measurements: the treated samples evolve towards green on the red-green axe (Figure 64).

FT-IR analysis performed on both treated and untreated samples shows similar results: the peaks at 3384, 3378, 1086, 776 and 727 cm^{-1} (Figure 68) might be due to the presence of brochantite $Cu_4SO_4(OH)_6$, a copper sulfate which is a characteristic corrosion product formed on weathered copper alloys.

Copper oxalate are not detected by FT-IR on the biopatina treated samples, but their characteristic morphology can be still observed on some zones with SEM imaging (Table 20, sample ZA5, zone A) after exposure.

CA	Before 6 months exposure	After treatment	After 6 months exposure
T0 Reference	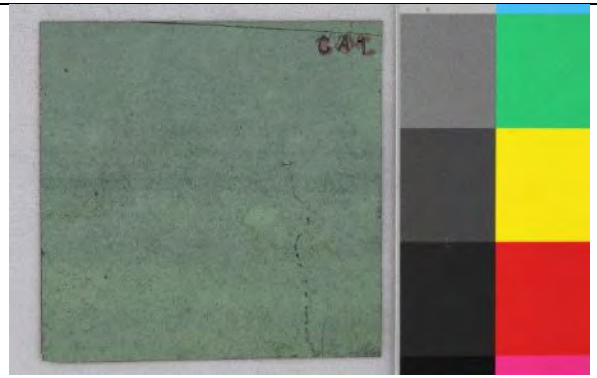 General view, Sample CA1	---	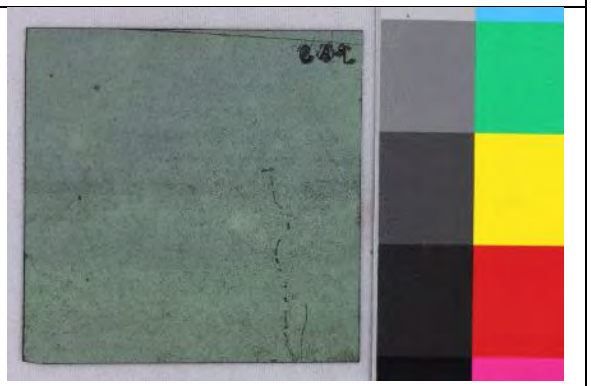 General view, Sample CA1
	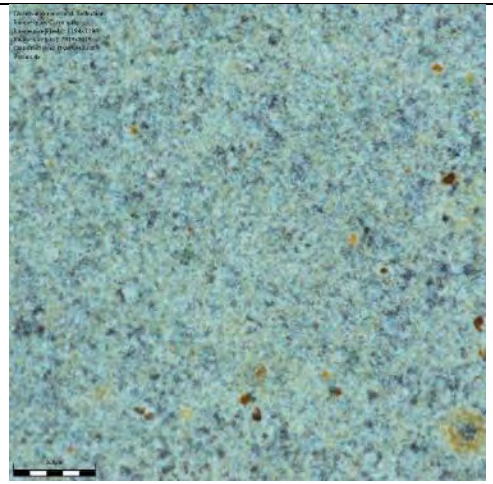 Sample CA1, zone B, X96	---	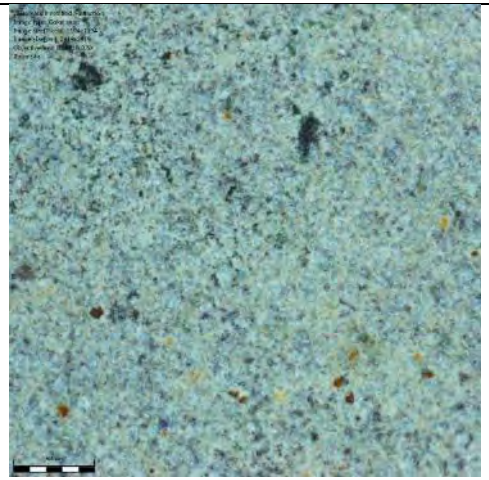 Sample CA1, zone B, X96

	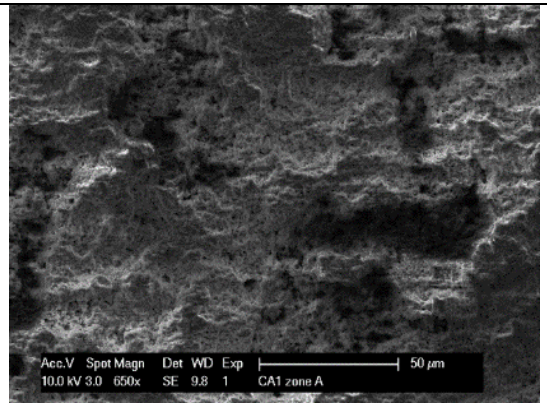 Sample CA1, zone A, X650 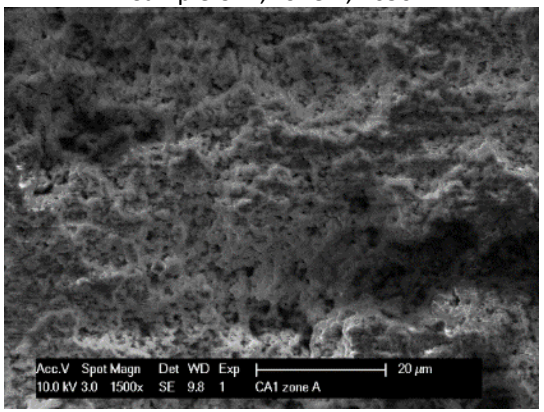 Sample CA1, zone A, X1500	----------	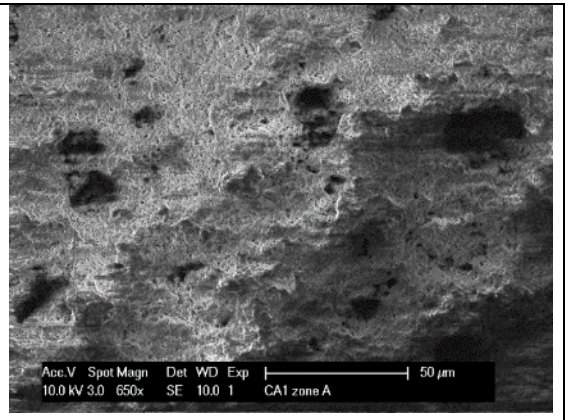 Sample CA1, zone A, X650 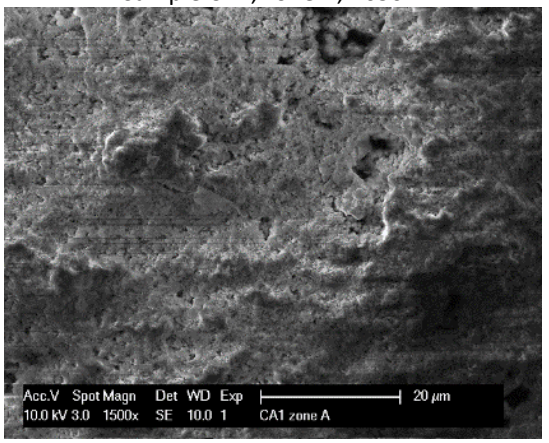 Sample CA1, zone A, X1500

T4 biopatina	----------	 General view, sample CA5	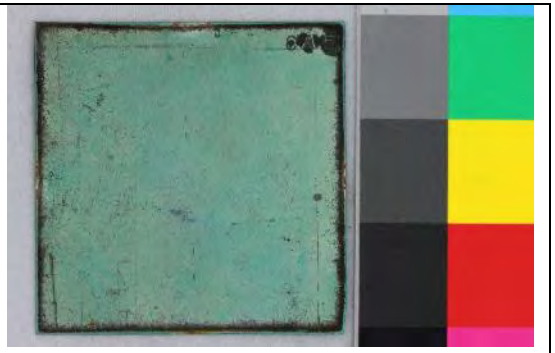 General view, sample CA5
	----------	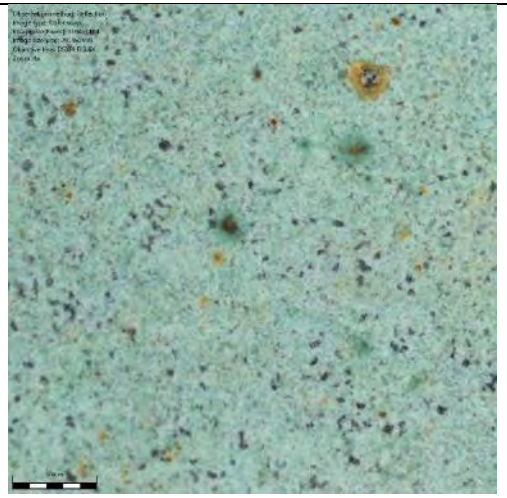 sample CA5, zone B, X96	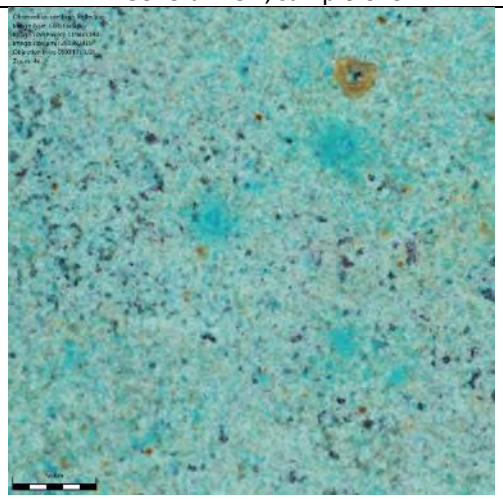 sample CA5, zone B, X96

	----------	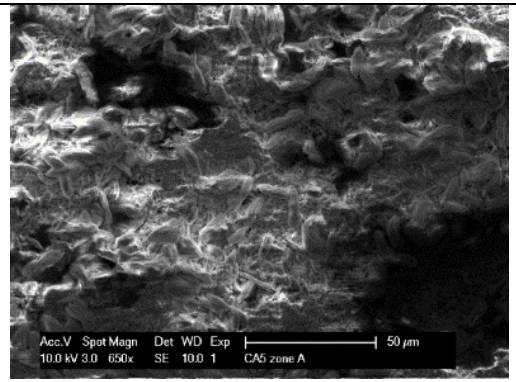 Sample CA5, zone A, X650 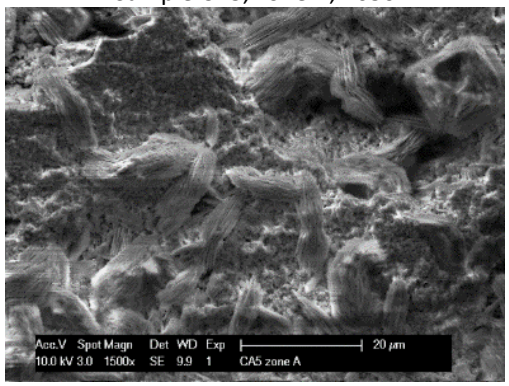 Sample CA5, zone A, X1500 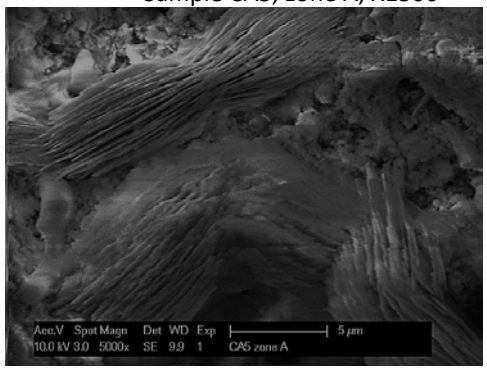 Sample CA5, zone A, X5000	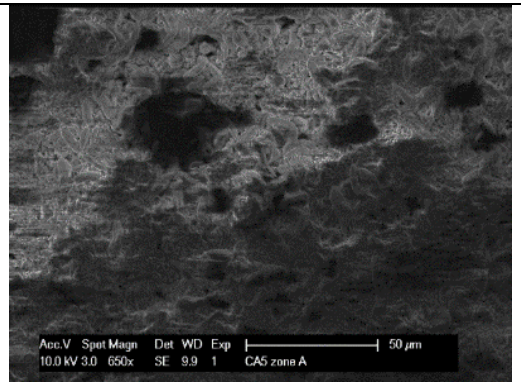 Sample CA5, zone A, X650 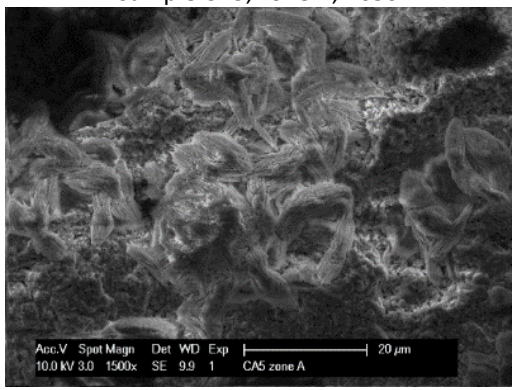 Sample CA5, zone A, X1500 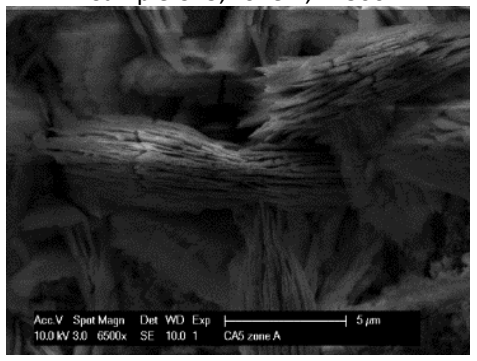 Sample CA5, zone A, X6500

Table 20- Results of the visual examination on the bare copper samples (CA)

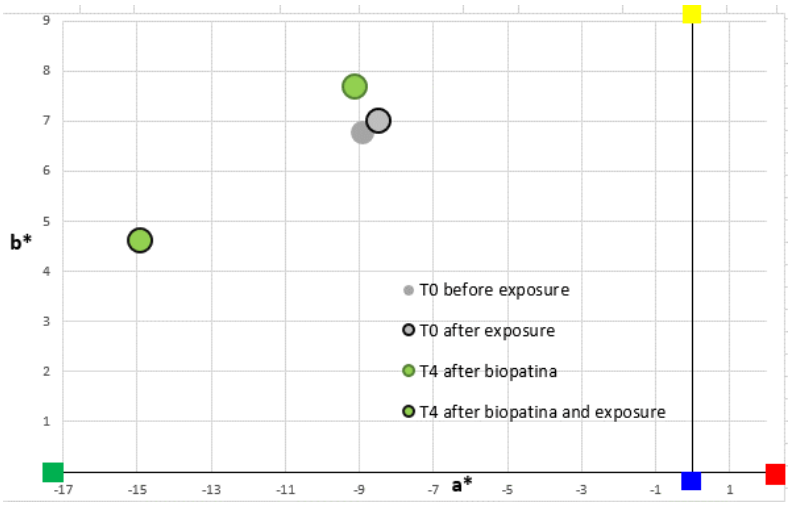

Figure 64 -colorimetric measurements performed on ancient copper samples (CA)

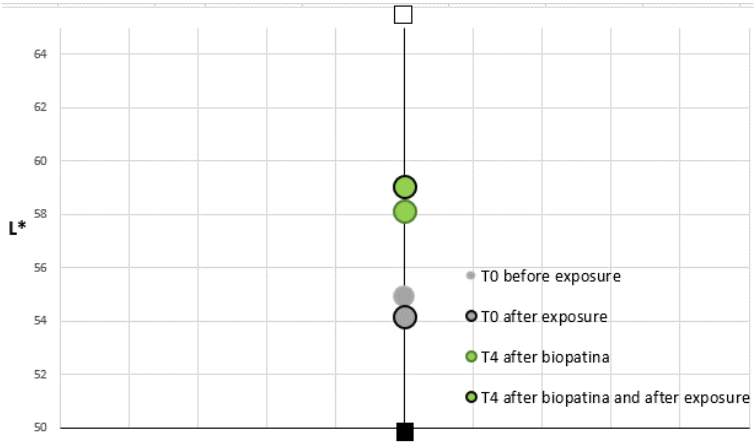

Figure 65- colorimetric measurements performed on ancient copper samples (CA)

CA	Before exposure	After treatment	After 1 month	After 3 months	After 6 months
T0 (reference)	33.45	----------	33.77	35.1	34.73
T4	32.95	33.65	37.13	35	35.6

Table 21 - average thickness of the corrosion layer in µm on the ancient copper samples (CA)

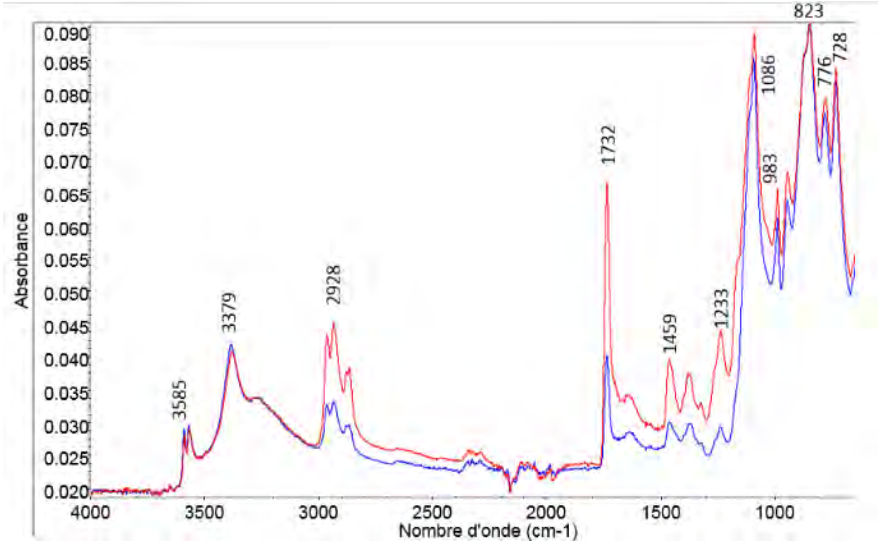

Figure 66- T0 before 6-months exposure (CA1 and CA2), ATR- FTIR spectra

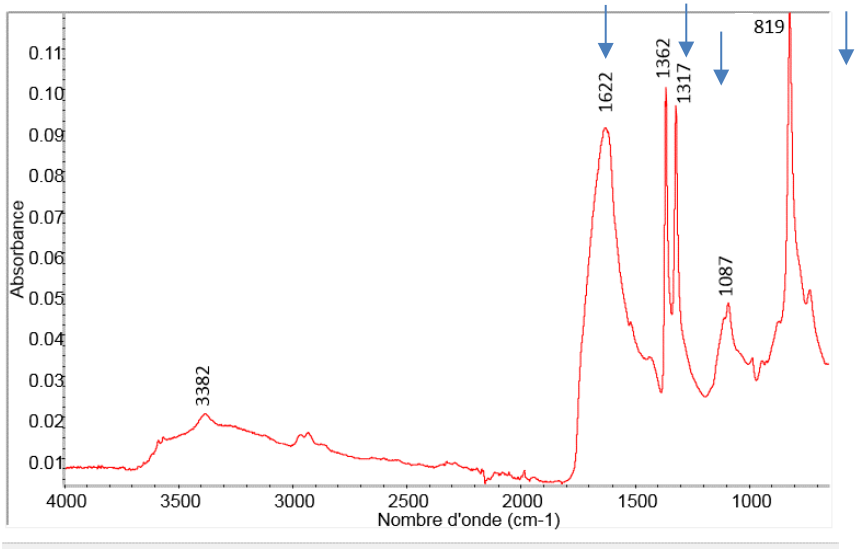

Figure 67-T4 after treatment and before exposure (CA3), ATR- FTIR spectrum: The arrows indicate characteristic absorbance bands of copper oxalates

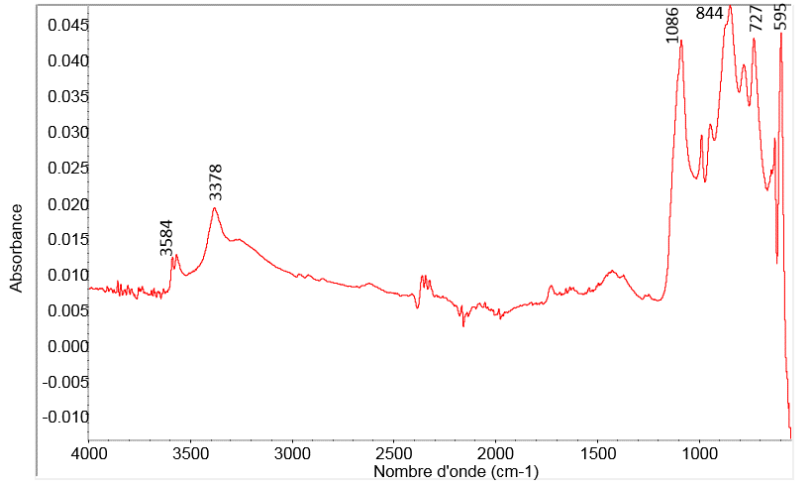

Figure 68 - T0 after 6-months exposure (CA1), ATR- FTIR spectra

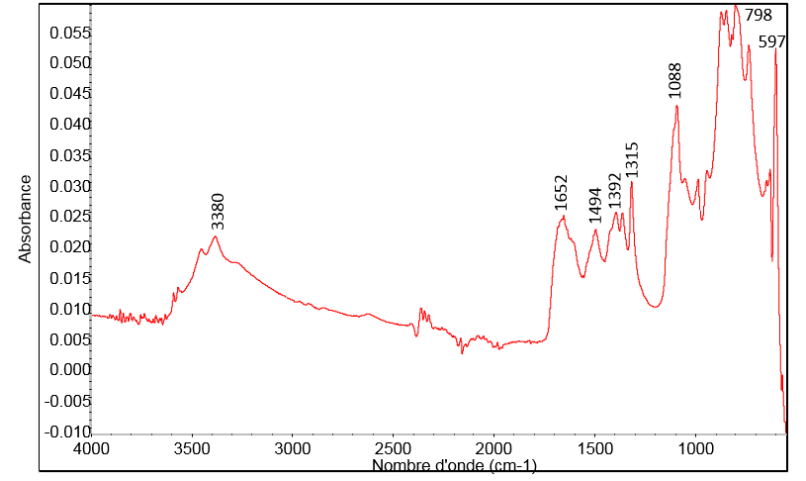

Figure 69- T4 after treatment and after exposure (CA3), ATR- FTIR

3-b.2.1.5. Non anodized aluminium (A series)

Biopatina treatment

No noticeable visual difference was observed depending on whether the samples had been treated with biopatina or not previously except for some smaller stains which seem to have been induced by the contact with the gel. These stains remain on the surface although the metal was rinsed several times with water. Thickness measurements show that a very thin layer of aluminium oxide probably formed after treatment (< 1µm). The colorimetric measurement indicates a slightly higher lightness after biopatina treatment, but a difference in color is only slightly perceptible (Δ E=3.06). SEM imaging doesn't show any change in surface morphology before and after treatment.

FTIR analysis shows that aluminum oxalates formed after biopatina treatment. Characteristic peaks are observed at 3381, 1622, 1362 cm^{-1} and 819 cm^{-1} (Figure 73).

6-months exposure

The surface keeps a matte surface finish before and after exposure in all cases (with and without biopatina treatment). Samples treated with biopatina evolve on the green-red axe towards green, whereas the exposure induces for all samples – treated and untreated- a movement on the yellow-blue axe (towards yellow), Figure 71. The overall color difference is low for both treated and untreated samples ((Δ E=2.78 /2.26)

6-month outdoor exposure generates in both cases also small dark spots (Figure 70). This is confirmed for all samples treated and untreated by a lower lightness value (Figure 72). As the anodized series AA wasn't affected at all by this phenomenon (the surface remained bright and shiny without any darker spots), this may indicate that localized chemical reactions took place in the case of the non-anodized aluminum.

The thickness of the aluminum oxide layer formed after exposure is similar for both treated and untreated samples (Table 22). FTIR spectra are identical after 6-months exposure for both treated and untreated samples (Figures 74-75). Aluminum oxalates on the biopatina treated samples are not identified (Figure 74). This might indicate that these products were superficial and were leached during outdoor exposure. The observed peaks couldn't be correlated with aluminum oxides or hydroxides (see Appendix 5: Reference data for analysis).

A	Before 6 months exposure	After treatment	After 6 months exposure
T0 series **Reference** **without biopatina treatment**	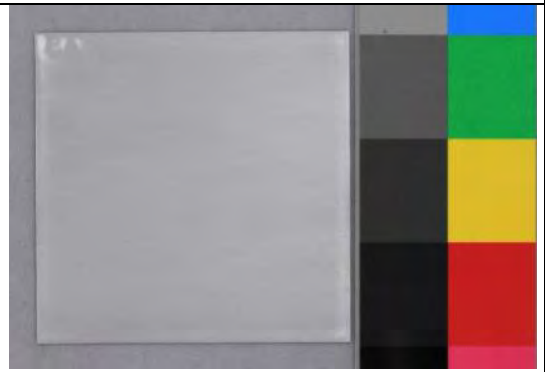 general view, sample A3	----------	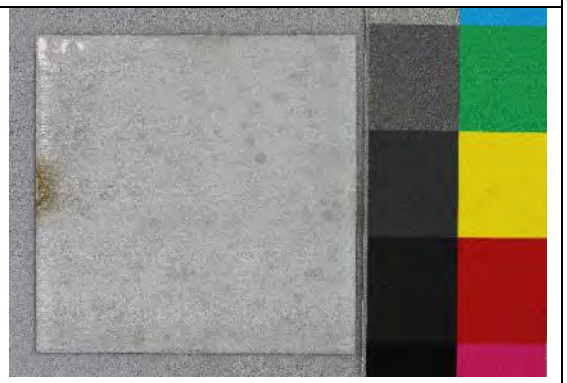 general view, sample A3
	 sample A3, zone D, X96	----------	 sample A3, zone D, X96
	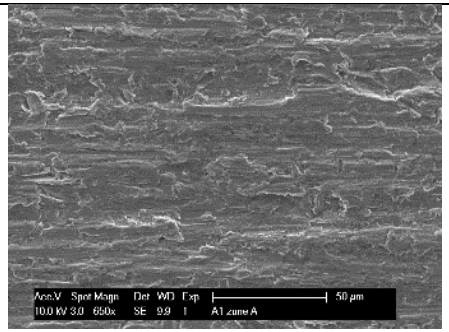 Sample A1, zone A, X650 (SE)	----------	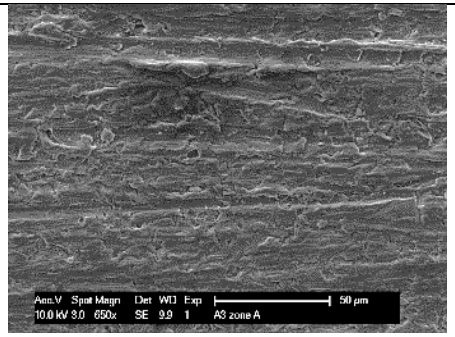 Sample A3, zone A, X650 (SE)
	Before 6 months exposure	**After treatment**	**After 6 months exposure**

T4 **biopatina**	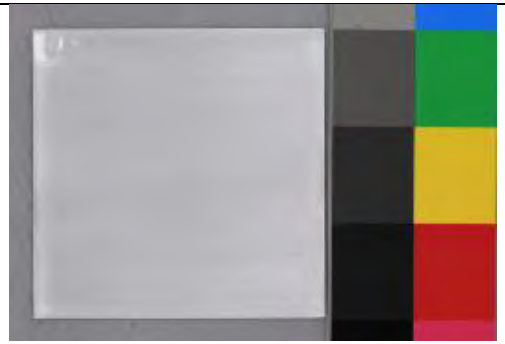 General view, Sample A5	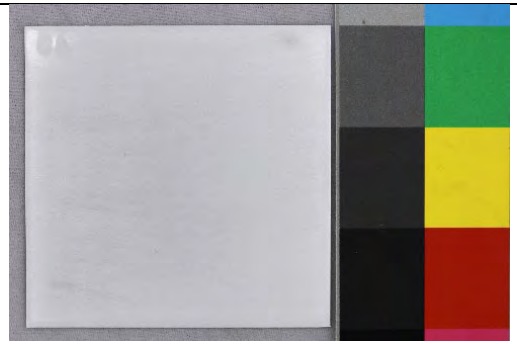 General view, Sample A5	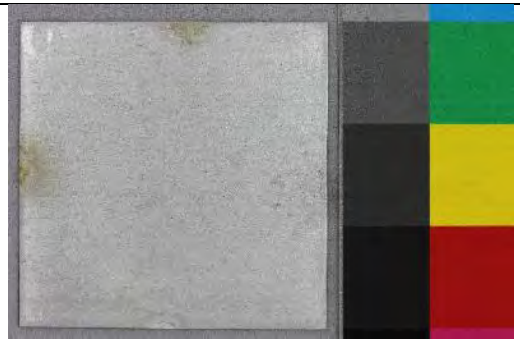 General view, Sample A5
	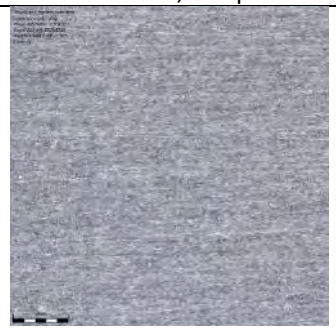 Sample A5, zone C, X96	 Sample A5, zone C, X96	 Sample A5, zone C, X96
	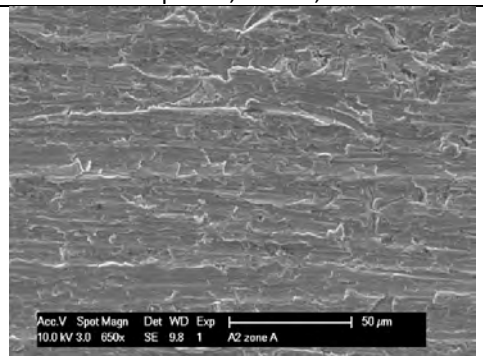 Sample A2, zone A, X650 (SE)	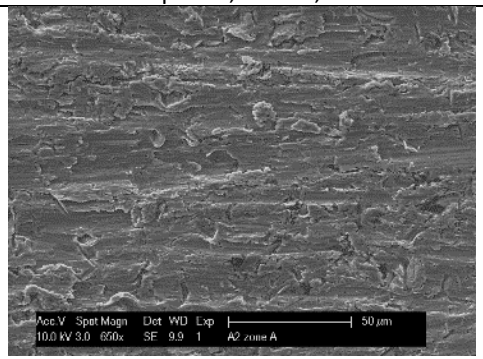 Sample A2, zone A, X650 (SE)	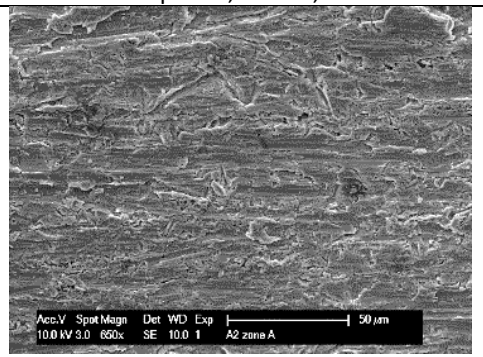 Sample A2, zone A, X650 (SE)

Figure 70 - Results of the visual examination on the bare aluminum samples (A)

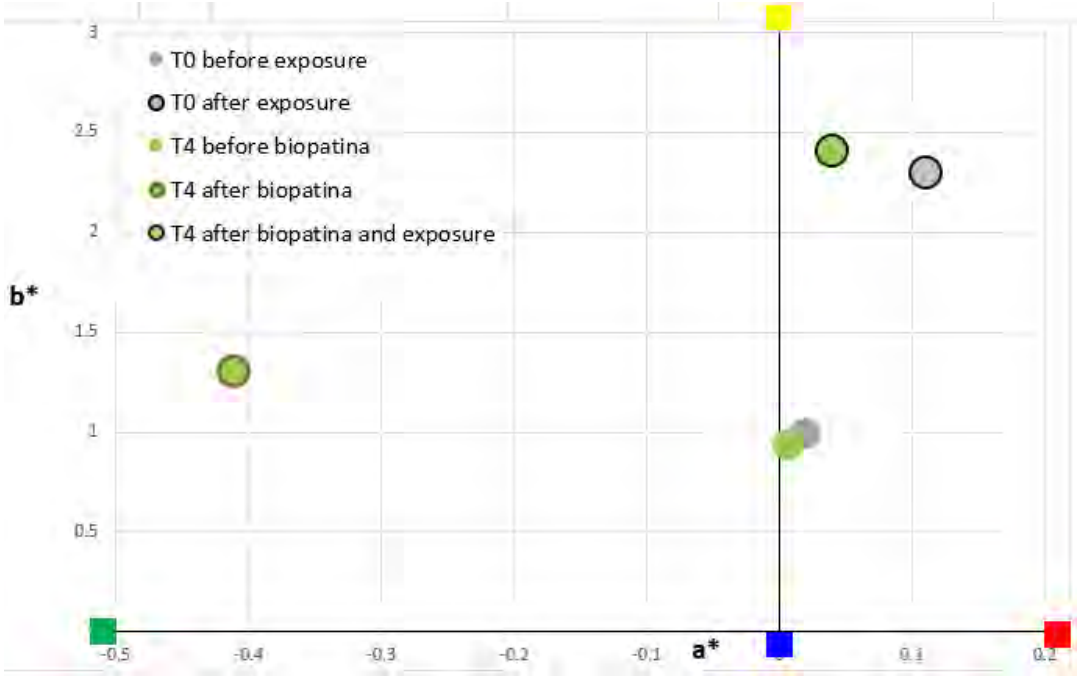

Figure 71- colorimetric measurements performed on the bare aluminum samples (A)

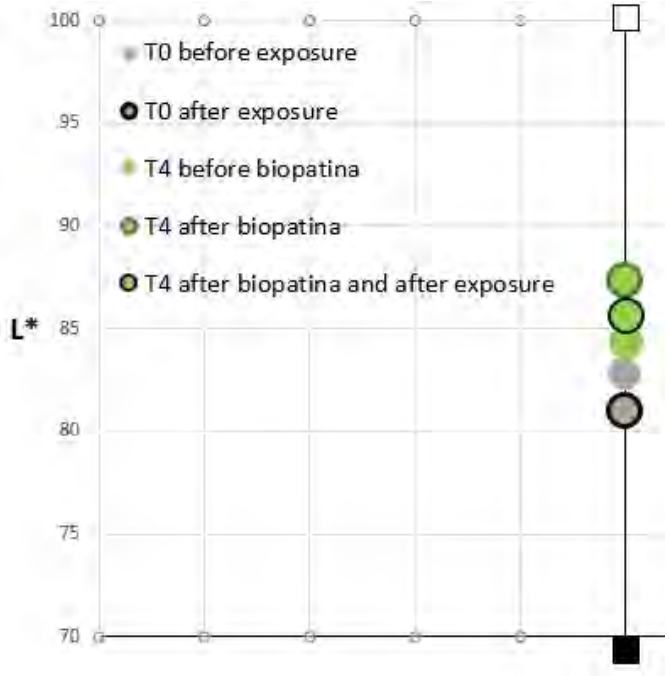

Figure 72- colorimetric measurements performed on the bare aluminum samples (A)

A	Before exposure	After treatment	After 1 month	After 3 months	After 6 months
T0 (reference)	nm	----------	1.6	3.7	2.1
T4	nm	0.05	1.8	2.73	2.17

Table 22 - average thickness of the corrosion layer in µm on the bare aluminum samples (A)

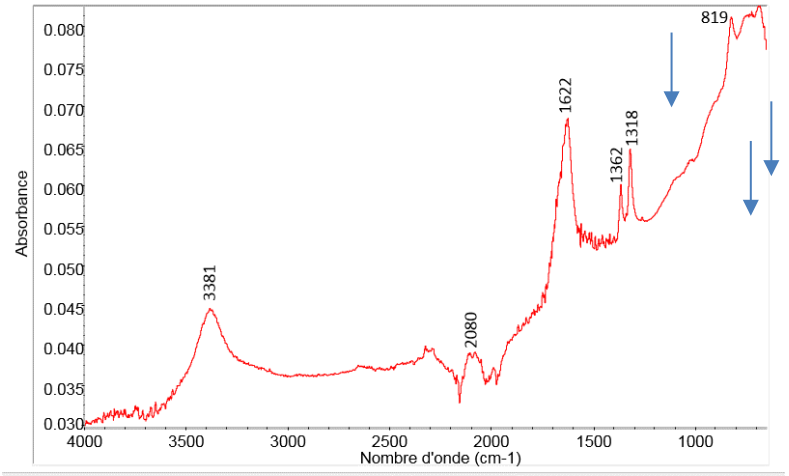

Figure 73- T4 after treatment and before exposure (A2), ATR- FTIR spectrum

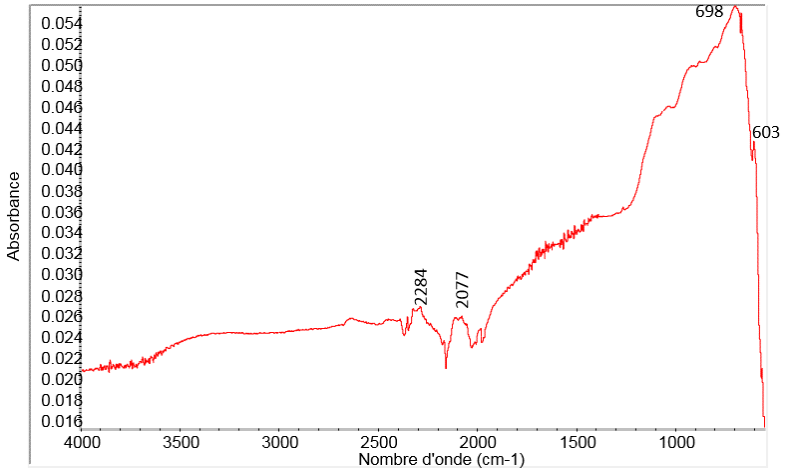

Figure 74- T4 after biopatina treatment and exposure (A2), ATR- FTIR spectrum

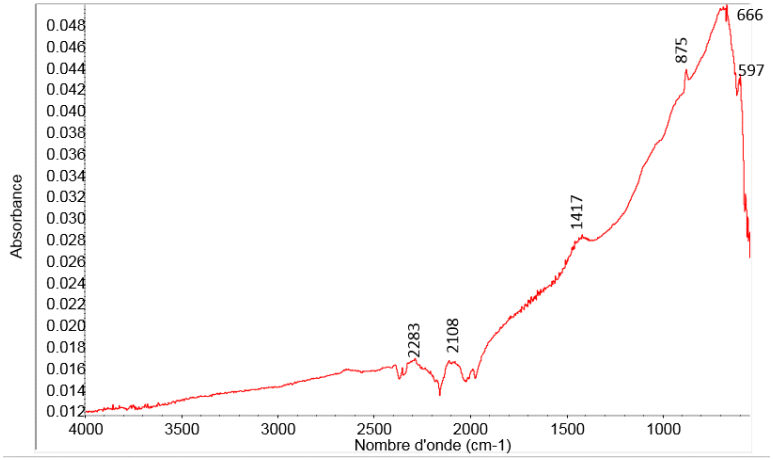

Figure 75 - T0, sample after exposure (A3), ATR- FTIR spectrum

3-b.2.1.6. Anodized aluminium (AA series)

After biopatina treatment

The surface composition was only analyzed with SEM-EDS before applying the biopatina. It shows that the metal was probably anodized with sulfuric acid.

Literature mentions that the chromic acid anodized surfaces contain more hydroxyls and water than the sulfuric acid anodized surfaces while the latter contain more alumina (Al_2O_3). These surfaces have a triplex structure composed mainly of hydrated and hydroxylated layers over an oxyhydroxylated layer which is over a hydrated alumina layer[14]. Colorimetric measurements show that the biopatina treatment induces a slightly darker appearance (Figure 77). They also indicate an evolution on the blue-yellow axe (towards yellow) and ΔE=0.51 (not perceptible color difference), Figure 75. The thickness of the isolating layer didn't change on all samples (Table 24).

SEM images show that the surface heterogeneities after treatment seem to be slightly leveled out, they are less visible (Table 23). The aluminum sample generates after biopatina treatment a peak around 3375 cm^{-1}, which could refer to aluminum oxide[15]. Peaks that can be characteristic of oxalates formation are clearly identified at 1627 and 1318 cm^{-1} (Figures 78-79). A broad peak around 1105 cm^{-1} can be attributed at sulfates or fosfates (atmospheric deposits).

After 6-months exposure

FTIR spectra are identical after 6-months exposure for both treated and untreated samples (Figure 80-Figure 81).

No noticeable visual difference was observed. In fact, ΔE is low for both untreated and treated samples after exposure (0.65 / 1.38). The thickness of the isolating layer didn't change on all samples (Table 24).

The biopatina treated samples get darker as the reference samples get slightly lighter. Colorimetric measurements indicate for all samples an evolution on the blue-yellow axe (towards yellow), Figure 76.

[14] Fondeur, Fernando & Koenig, Jack. (1993). FT-IR Characterization of the Surface of Aluminum as a Result of Chemical Treatment. The Journal of Adhesion. 40. 189-205. 10.1080/00218469308031284.

[15] Aluminum oxide has characteristic peaks around 3453 and 713 cm-1

AA	Before 6 months exposure	After treatment	After 6 months exposure
T0 **Reference** **Before /after exposure**	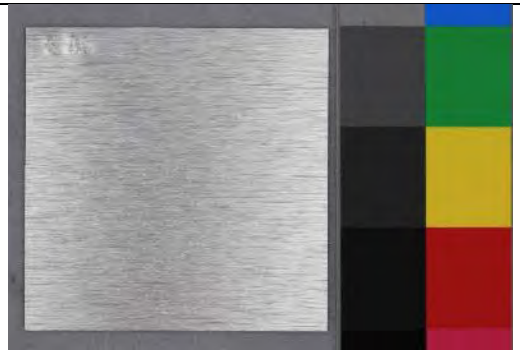 General view, sample AA3	----------	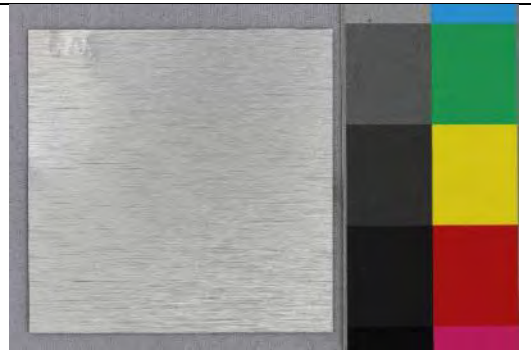 General view, sample AA3
	 Sample AA3, zone B, X96	----------	 Sample AA3, zone B, X96

	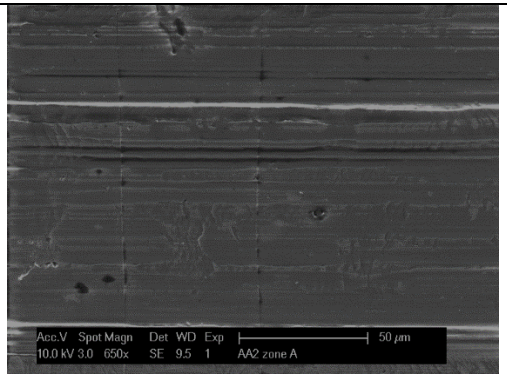 Sample AA2, zone A, X650 (SE)	----------	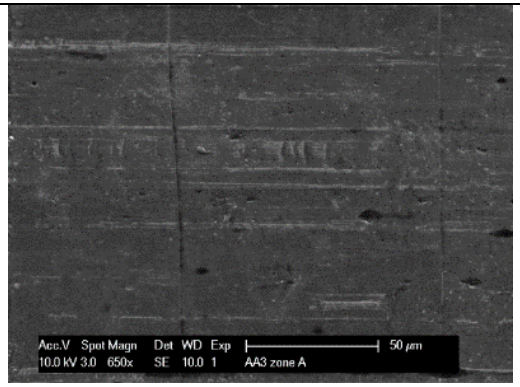 Sample AA2, zone A, X650 (SE)
T4 **biopatina**	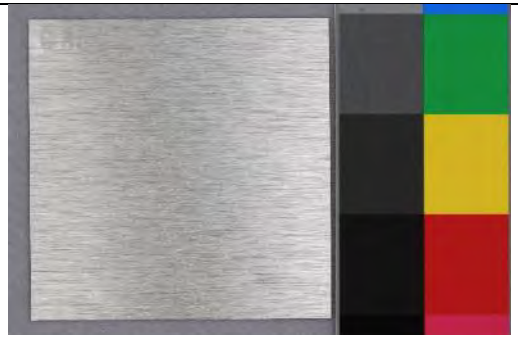 General view, sample AA7	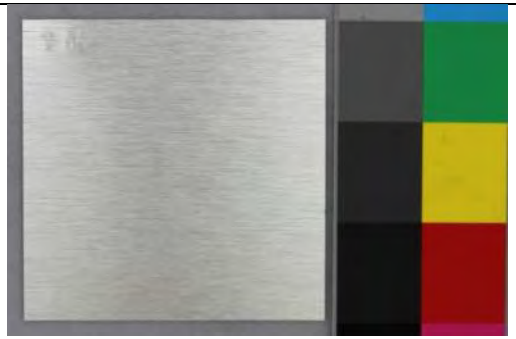 General view, sample AA7	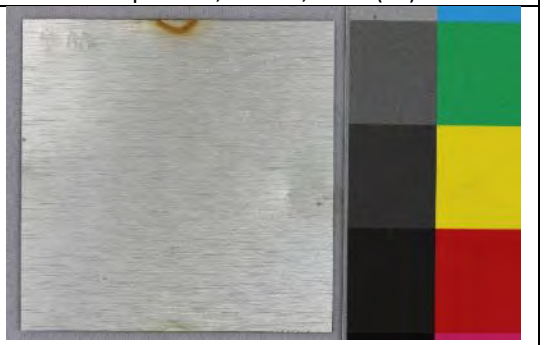 General view, sample AA7

	 Sample AA7, zone B, X96	 Sample AA7, zone B, X96	 Sample AA7, zone B, X96
	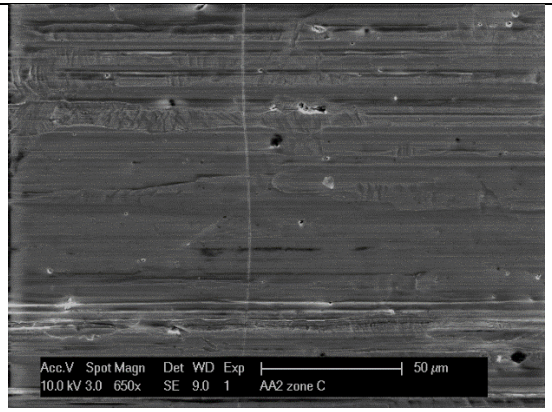 Sample AA2, zone C, X650	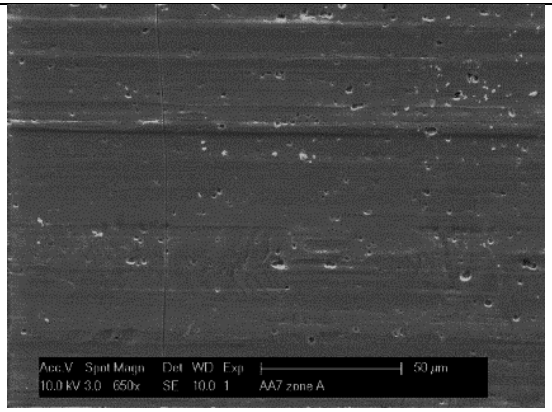 Sample AA7, zone A, X650	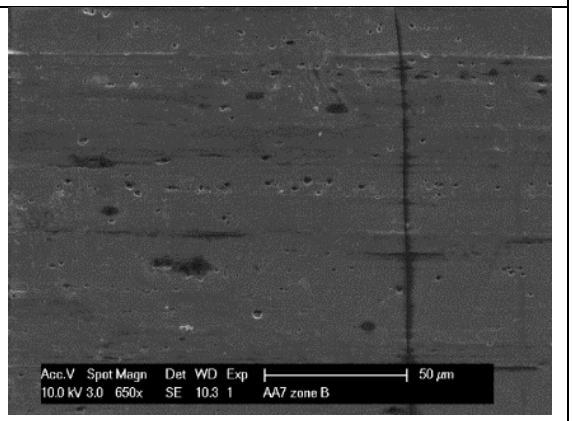 Sample AA7, zone B, X650

Table 23- Results of the visual examination on the anodized aluminum samples (AA)

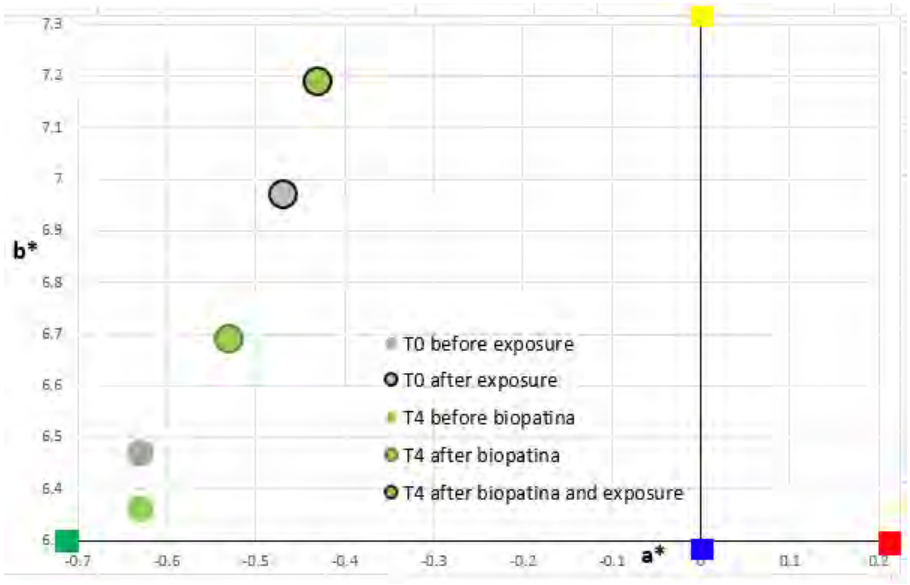

Figure 76- colorimetric measurements performed on the anodized aluminum samples (AA)

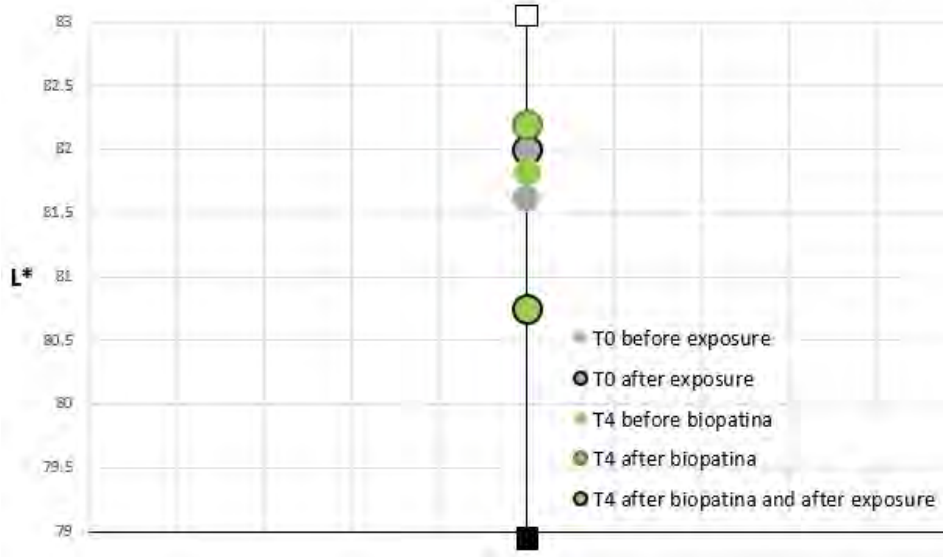

Figure 77- colorimetric measurements performed on the anodized aluminum samples (AA)

AA	Before exposure	After treatment	After 1 month	After 3 months	After 6 months
T0 (reference)	5.4	----------	6.57	8.6	8.2
T4		6.7	6.83	8.5	7.47

Table 24- average thickness of the corrosion layer in µm on the anodized aluminum samples (A)

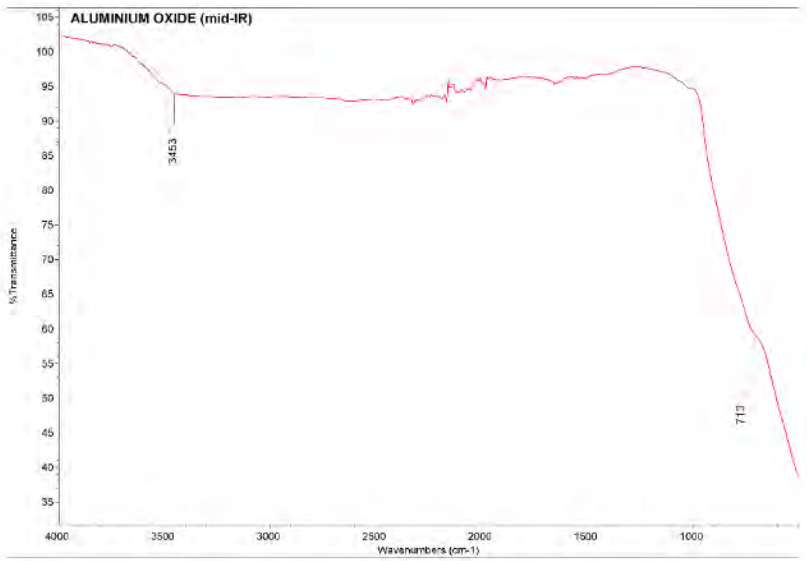

Figure 78 - reference ATR- FTIR spectrum for aluminium oxide[16]

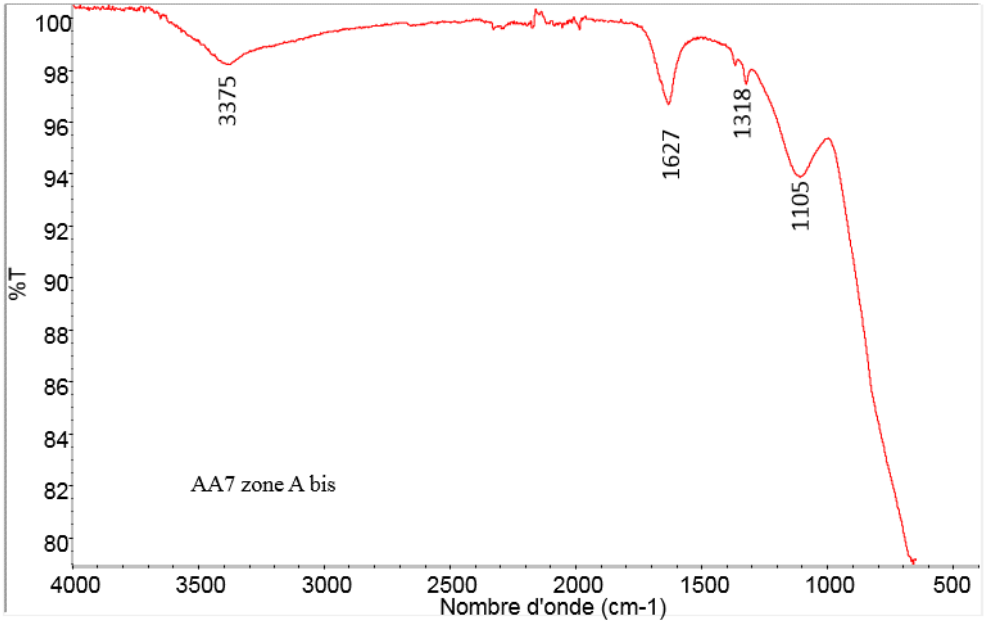

Figure 79 - T4 after biopatina treatment and before 6-months exposure (AA9), ATR- FTIR spectrum

[16] https://www.researchgate.net/publication/274433010_Re-Anodizing_Technique_as_a_Method_of_Investigation_of_Thermally_Activated_Defects_in_Anodic_Alumina_Films?_sg=A4RuaB6K0Jo-P7OCJr60dE_zPv2eDVRdjbsXONGaCsA1eAF5i3SQ4OSCa0vaQYPqhiUAplCEmw

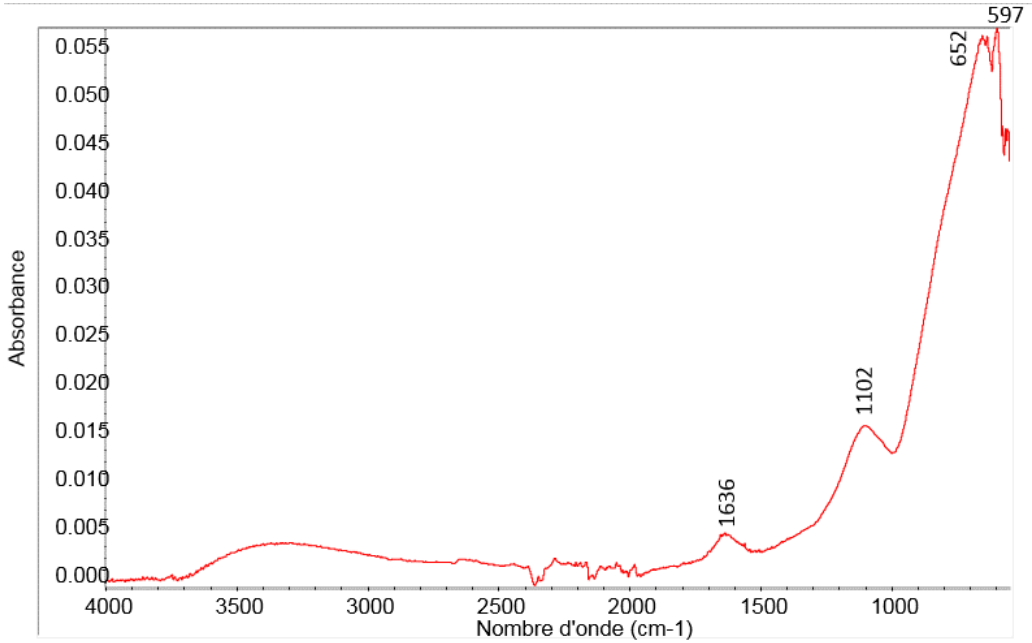

Figure 80 - T0 after 6-months exposure (AA3), ATR- FTIR spectrum

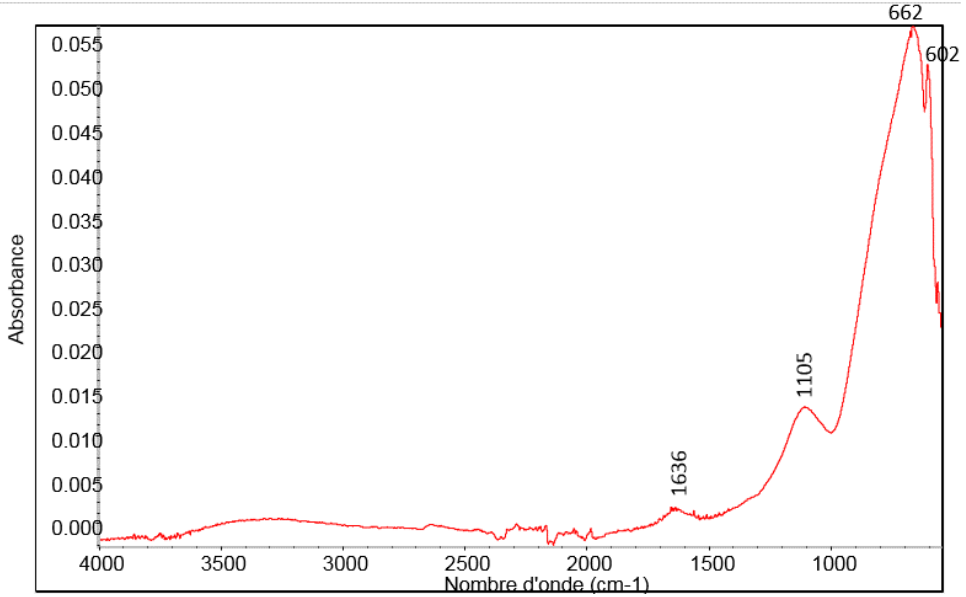

Figure 81 - T4 after biopatina treatment and 6-months exposure (AA9), ATR- FTIR spectra

3-b.2.2. Ferrous metals

3-b.2.2.1. bare iron alloy (S series)

biopatina treatment

The biopatina treatment induced the development of a heterogeneous bluish and brown product layer. This layer is about 20 µm thick (Table 26). Microscopic observation shows that poorly adherent orange corrosion products formed. They alternate with a very thin bluish oxide layer (circular spots), Table 25. On the latter, the underlying metal is still visible. The colorimetric measurements indicate an important decrease of lightness after biopatina treatment (Figure 83) and an evolution on the blue-yellow axe (towards yellow), Figure 82. The color difference is huge: delta E =35.49).

Raman spectroscopy shows that the treatment induces the development of lepidocrocite on the surface (1300, 642, 373, 243 cm^{-1}), Figures 86-87.

6-months exposure

On the biopatina treated samples outdoor exposure induces the development of a more homogenous brown orange corrosion product layer which covers entirely the surface (table 25). In comparison, the reference series without biopatina treatment is covered after a 6-months exposure by a heterogeneous corrosion layer, which doesn't cover the whole surface (Table 25). These observations can be correlated with the higher corrosion layer thickness of the biopatina samples (Table 26).

Exposure induces for all samples – treated and untreated- a movement on the green-red axe (towards red), Figures 82-85.

On all reference samples (T0) mainly lepidocrocite was detected by Raman spectroscopy (1303, 646, 525, 376, 248 cm^{-1}), Figure 89. In the case of the biopatina treated samples, lepidocrocite was also detected on all samples (peaks at 1302, 651, 526, 250 cm^{-1}) but associated to other species more stable species like goethite (peaks at 300, 386, 472, 553 cm^{-1}) in smaller amounts[17], Figure 88. Two less intense peaks at 996 and 687 cm^{-1} couldn't be identified.

[17] Sample S2 zone B has the most characteristic peaks, on other zones peaks are less intense, they are located in particular before 100 cm-1

S	Before 6 months exposure	After treatment	After 6 months exposure
T0 **Reference** **Before /after exposure**	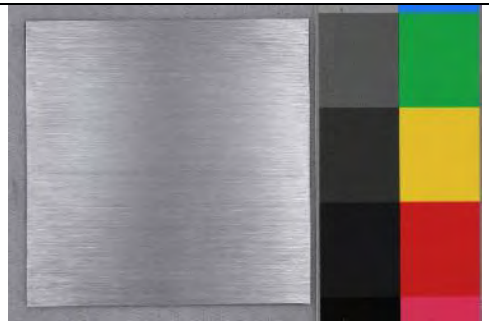 Sample S1, General view	----------	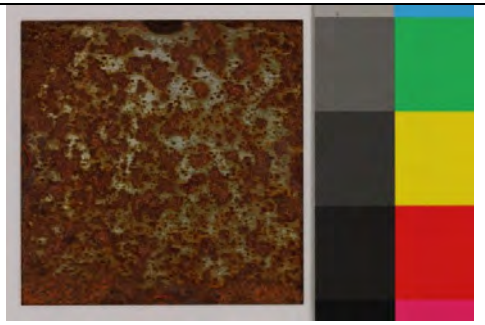 Sample S1, General view
	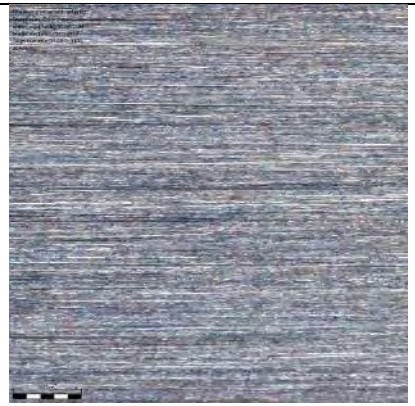 Sample S1, zone B, X96	----------	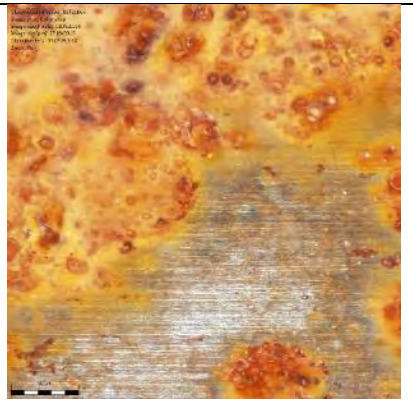 Sample S1, zone B, X96

	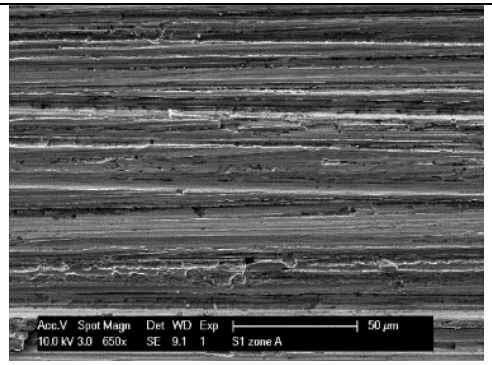 Sample S1, zone A, X650	----------	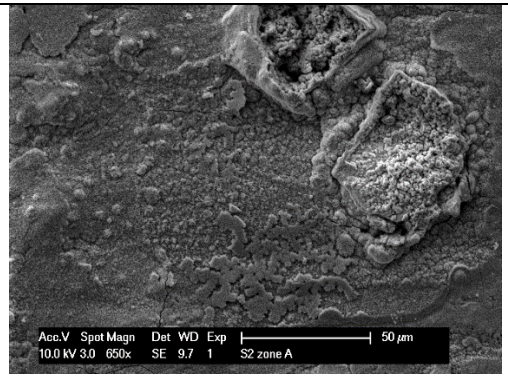 Sample S2, zone A, X650
T4 **biopatina**	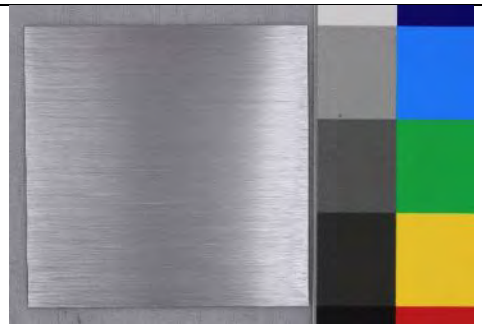 Sample S2, General view	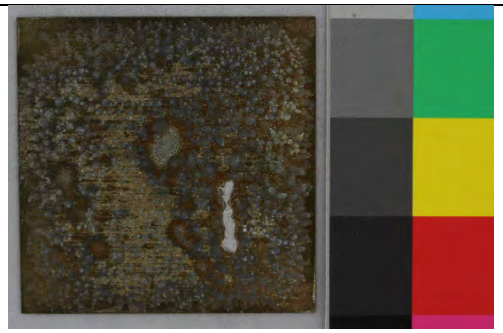 Sample S2, General view	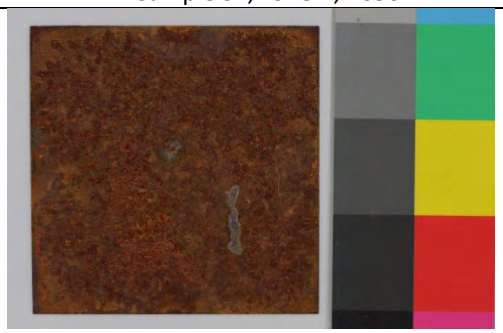 Sample S2, General view
	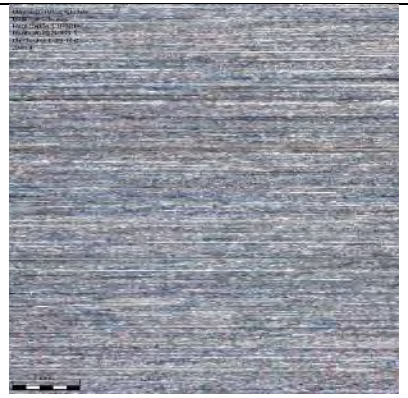 Sample S1, zone B, X96	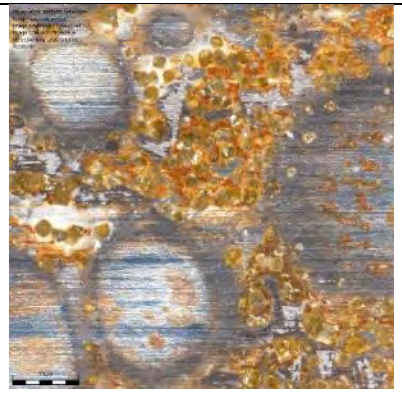 Sample S1, zone B, X96	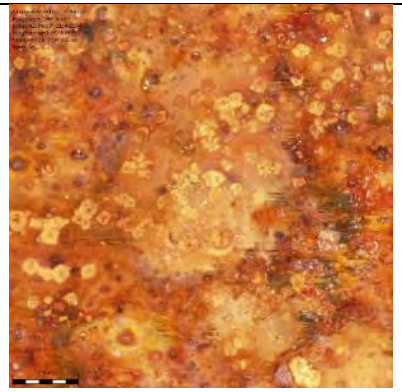 Sample S1, zone B, X96

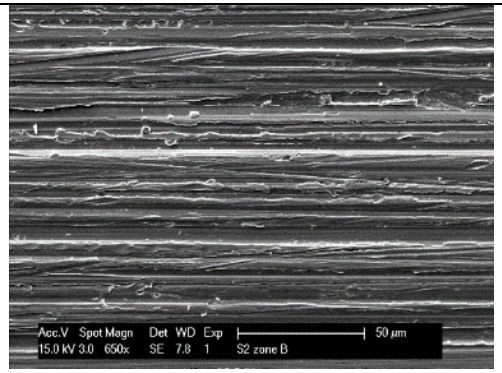

Sample S2, zone B, X650

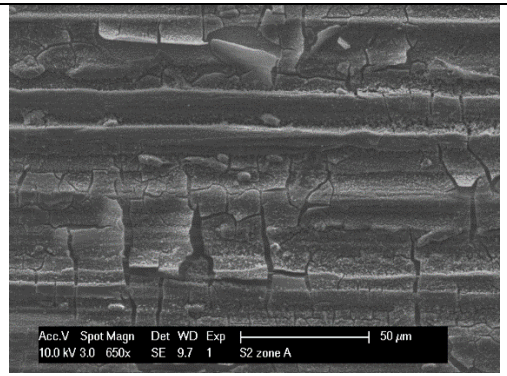

Sample S2, zone A, X650

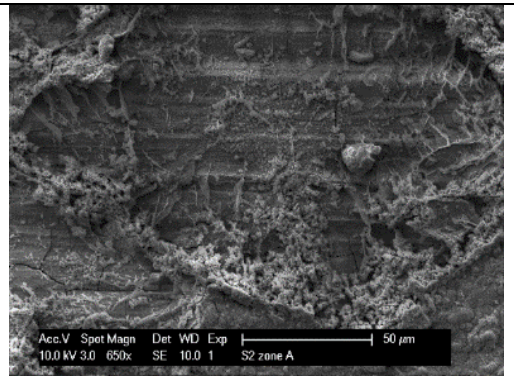

Sample S2, zone A, X650

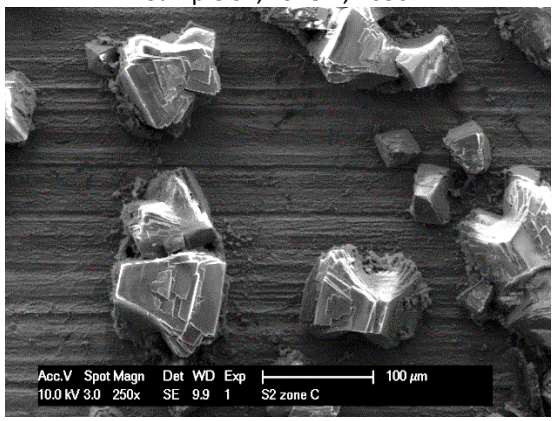

Sample S2, zone C, X250

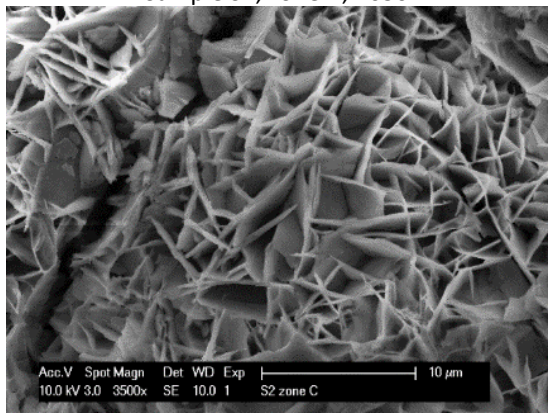

Sample S2, zone C, X3500

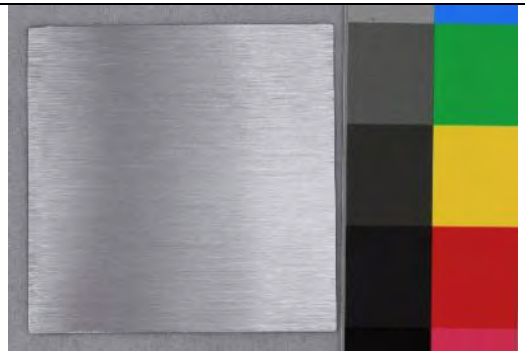

Sample S10, General view

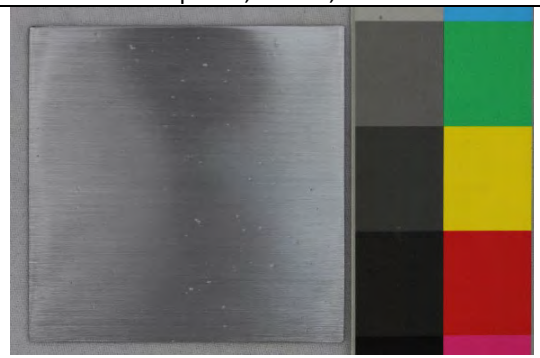

Sample S10, General view

	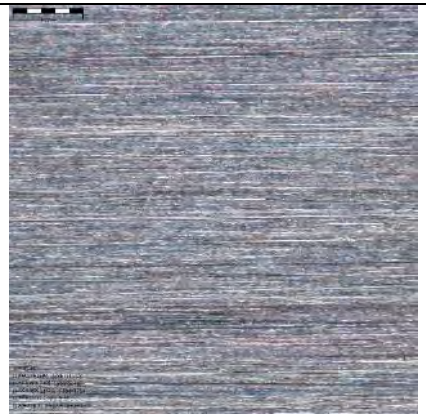 Sample S10, zone B, X96	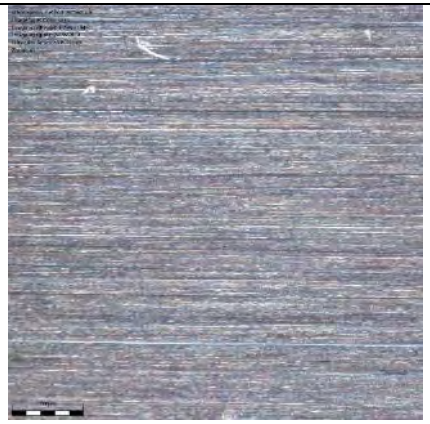 Sample S1, zone B, X96	 Sample S1, zone B, X96

Table 25 - Results of the visual examination on the bare steel samples (S)

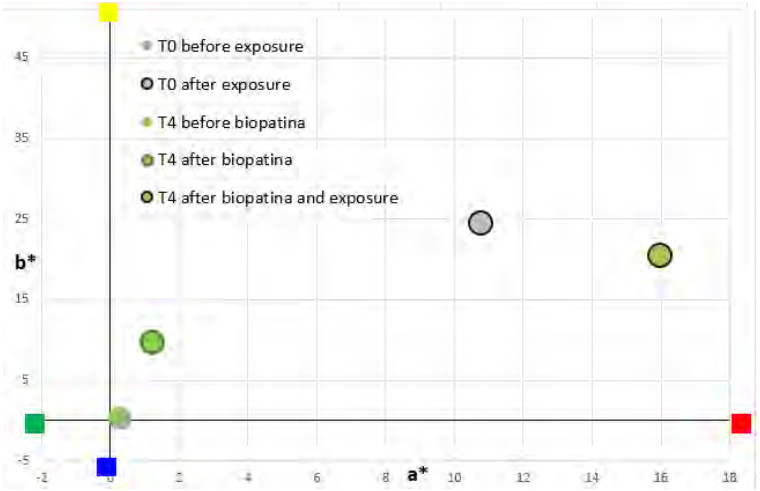

Figure 82 - colorimetric measurements performed on bare steel samples (S)

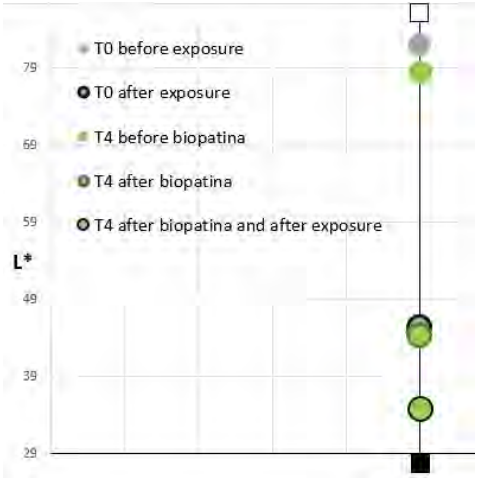

Figure 83 - colorimetric measurements performed on bare steel samples (S)

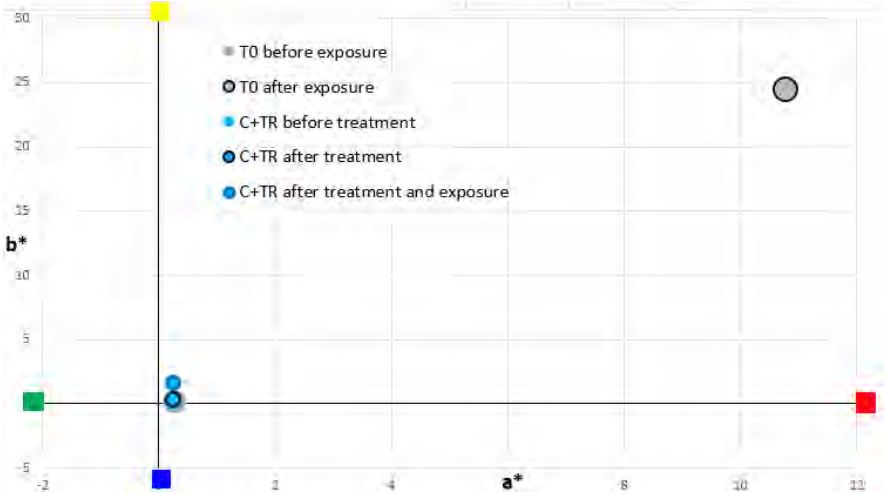

Figure 84 - colorimetric measurements performed on bare steel samples (S)

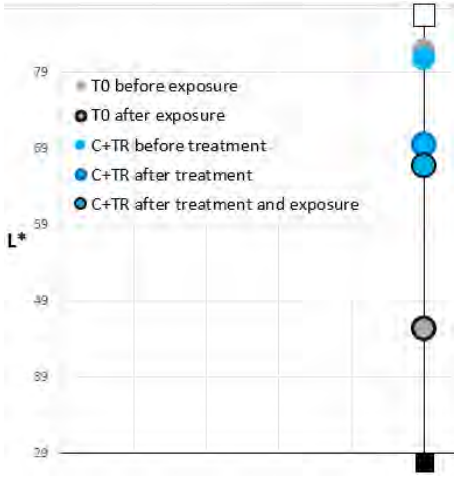

Figure 85- colorimetric measurements performed on bare steel samples (S)

S	Before exposure	After treatment	After 1 month	After 3 months	After 6 months
T0 (reference)	nm	----------	-0.63 (LOD)	-0.67(LOD)	2.47
T4	nm	19.75	21.53	8.9	6.8
C + TR Polyurethane coating	nm	18.27	18.93	17.2	17.57

Table 26- average thickness of the corrosion layer in µm on the bare steel samples (S)

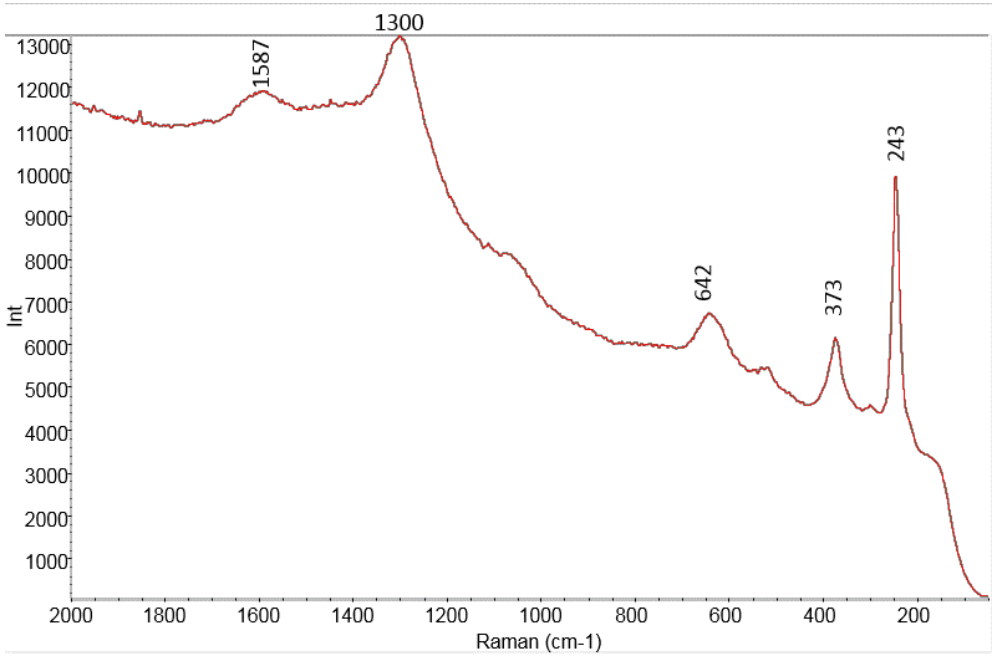

Figure 86 - T4 after biopatina treatment (sample S2), Raman spectrum

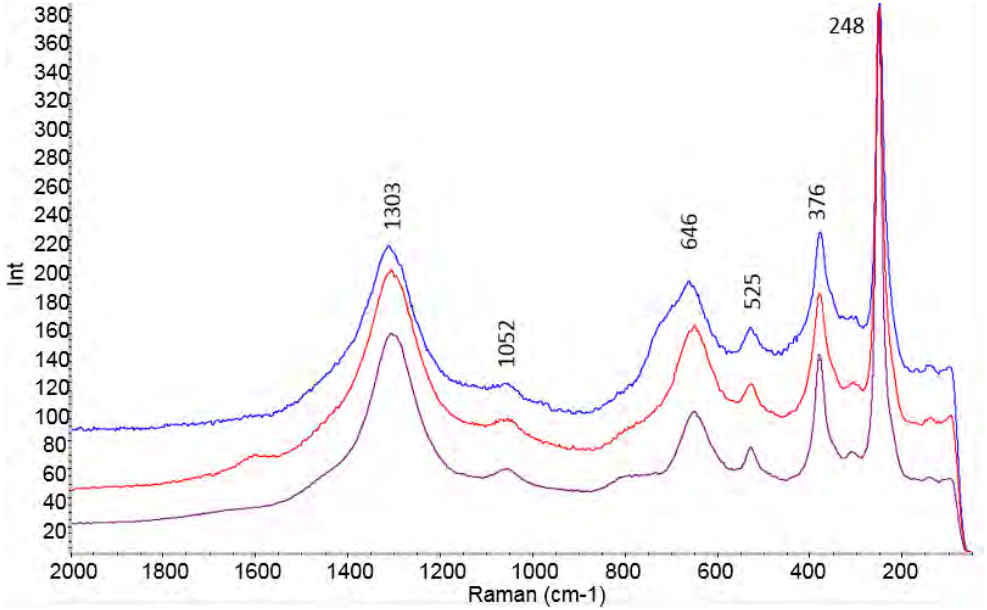

Figure 87 - T0 after 6-months exposure (sample S1 all zones), Raman spectra

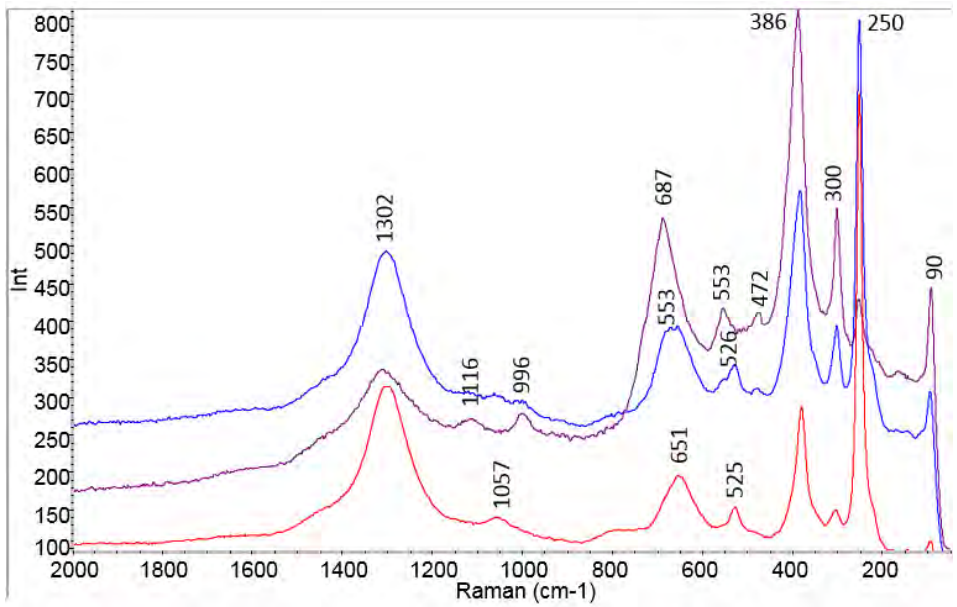

Figure 88 -T4, after biopatina treatment and exposure (sample S2 all zones), Raman spectra

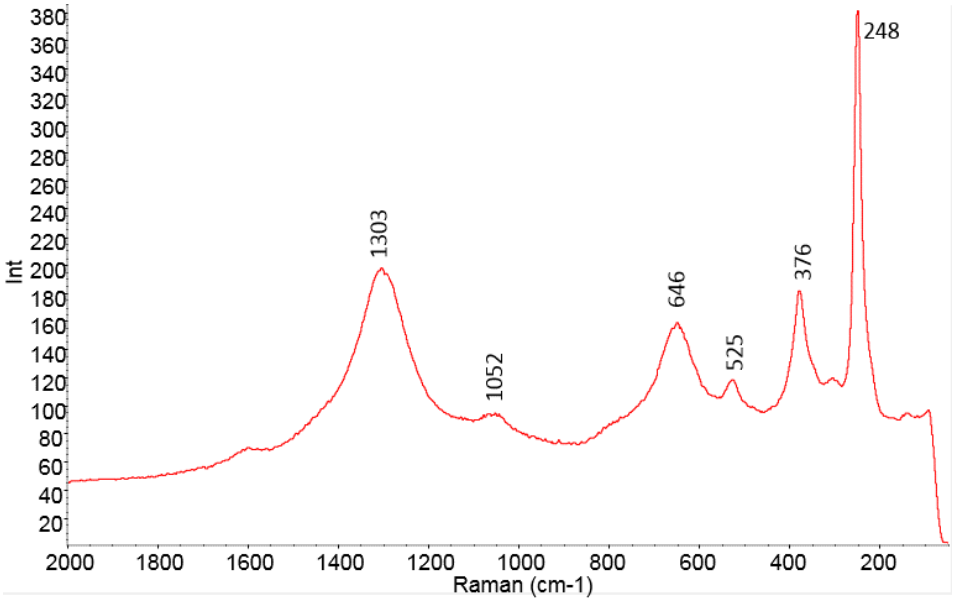

Figure 89 - T0, after exposure (sample S1), Raman spectrum

3-b.2.2.2. Self-weathering steel series (CS)

These samples are covered initially by a natural patina. On the reference samples (T0) characteristic peaks at 1313, 1049, 656, 525, 374, 245 cm^{-1} were detected by Raman spectroscopy, Figures 96-97. They indicate the presence of lepidocrocite, an iron oxyhydroxide γ-FeO(OH), which seems to be the predominant species in the superficial corrosion layers[18]. The peak at 481 cm^{-1} in one of the recorded spectra could refer to the presence of goethite α-FeO(OH), a less soluble corrosion product.

Biopatina and other treatment

The biopatina treatment induced a color modification. The samples look more homogenous and less reddish afterwards. The biopatina led to the growth of a thicker corrosion layer (Table 28). No specific products like iron oxalates were detected by Raman spectroscopy on the treated samples. The predominant species is lepidocrocite (Figure 99-101).

The two types of biopatina treatments (with and without cleaning before) induce a lower color difference (ΔE= 9.78 / 11.85), then the reference conservation treatment (ΔE=24.94).

Microscopic observation shows that isolated yellow-orange corrosion products formed as well as very small dark-bluish spots when the samples are treated with biopatina. A bigger amount of brownish-red corrosion products is also visible .The colorimetric measurements indicates a slight increase of lightness after treatment and an evolution on the green-red axe (towards red), Figure 90-91.

It's interesting to see that the cleaned series shows a difference in corrosion thickness depending on whether they have been treated with biopatina or coated with wax. Cleaning prior to biopatina seems to promote the development of a thicker layer (in comparison to non-cleaned samples treated with biopatina), Figure 30. This could be related to a different reactivity and composition of the superficial corrosion products.

6-months Exposure

The exposure induces for all samples – treated and untreated- a movement on the yellow-blue axe (towards blue), Figure 90-95. The average colorimetric values show that the surface tends to get darker by the biopatina treatment. The hugest difference before /after exposure can be seen for the series which were cleaned prior to biopatina treatment (ΔE= 18.69) and waxcoating (ΔE= 16.8). The untreated reference samples show only slight visual modification (ΔE= 4.88) as well as the biopatina treated samples (ΔE= 6.23).

SEM imaging (SE) doesn't show any noticeable differences between the different series (Table 27).

Thickness measurements don't indicate strong differences in corrosion layer growth for the different series (Table 28).

The composition of the untreated reference samples didn't evolve after 6-months exposure, Figure 98. The samples treated with biopatina (T4) show a similar composition (lepidocrocite: 1303, 656, 523, 377, 247 cm^{-1}), Figure 100.

In the case of the biopatina sample cleaned prior treatment (CS7), mainly lepidocrocite (detected peaks: 1306, 651, 528, 380, 302, 251 cm^{-1}, but also hematite (α-Fe_2O_3) was identified on one zone (zone A): characteristic peaks at 1318, 612, 411, 294 and 226 cm^{-1} were detected. The peak around 500 cm^{-1} might refer to goethite. The latter corrosion products are less soluble and chemically more stable then lepidocrocite (Figure 102). On the sample which was cleaned and coated with wax only lepidocrocite was detected: 1303, 650, 625, 377, 248 cm^{-1} (Figure 103).

[18] Cano H. et al., Characterization of corrosion products formed on Ni 2.4 wt%–Cu 0.5 wt%–Cr 0.5 wt% weathering steel exposed in marine atmospheres. In. Corrosion science 87, 2014, pp.438-451 / Aramendia et al, Portable Raman study on the conservation state of four CorTen steel-based sculptures by Eduardo Chillida impacted by urban atmospheres. In: Journal of Raman Spectroscopy, 43, John Wiley & Sons, Ltd, 2012, pp. 1111–1117

CS	Before 6 months exposure	After treatment	After 6 months exposure
T0 **Reference**	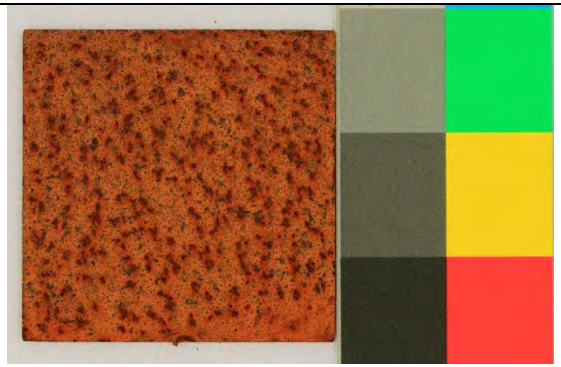 Sample CS1, General view	----------	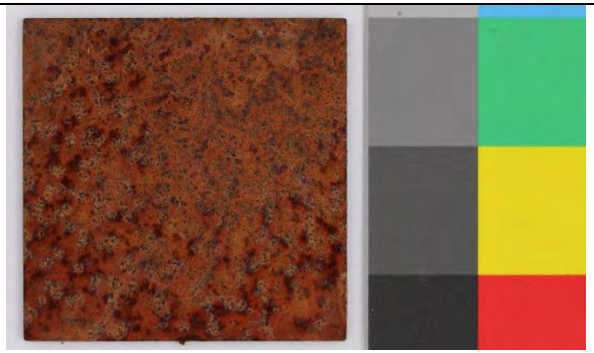 Sample CS1, General view
Before /after exposure	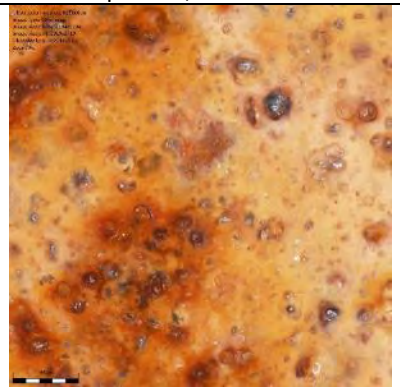 Sample CS1, zone B, X96	----------	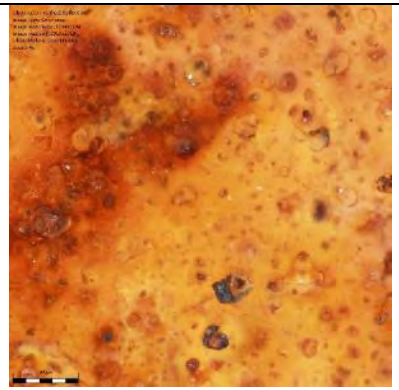 Sample CS1, zone B, X96

	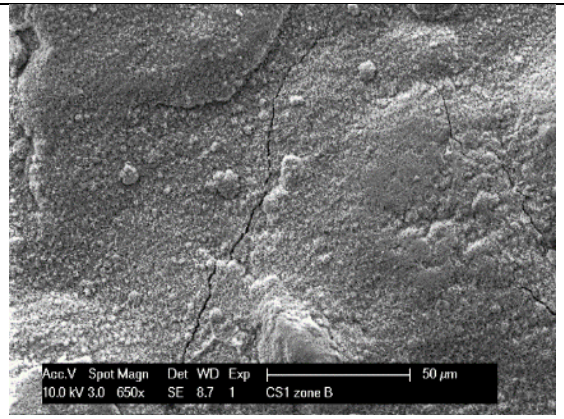 Sample CS1, zone B, X650	----------	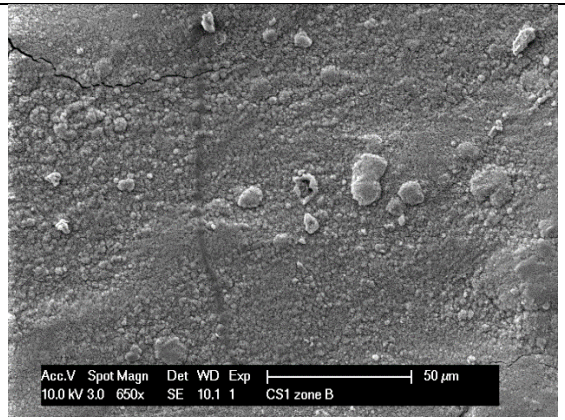 Sample CS1, zone B, X650
T4 **biopatina**	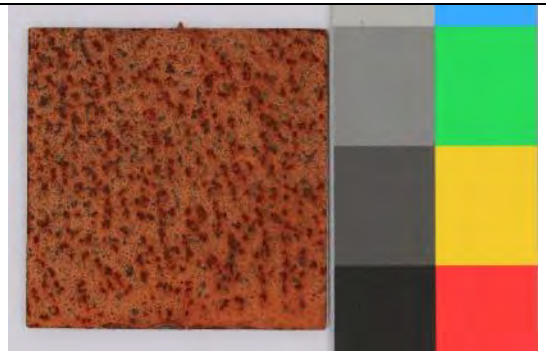 Sample CS2, General view	 Sample CS2, General view	 Sample CS2, General view
	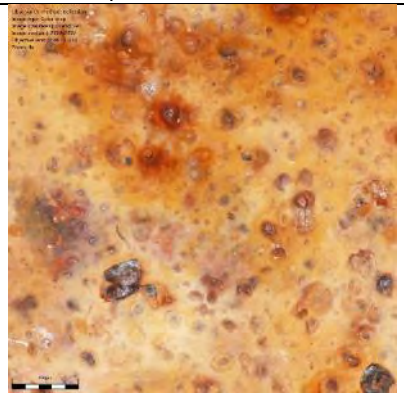 Sample CS2, zone B, X96	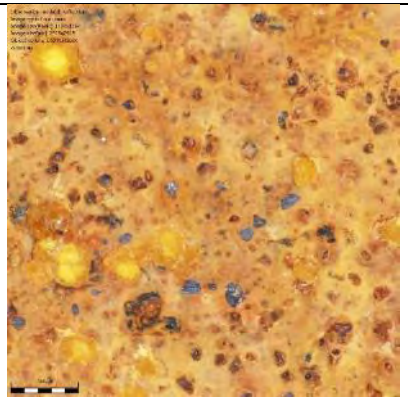 Sample CS2, zone B, X96	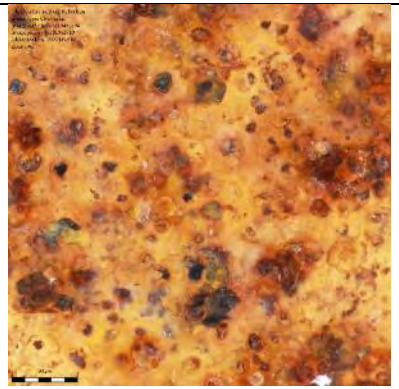 Sample CS2, zone B, X96

	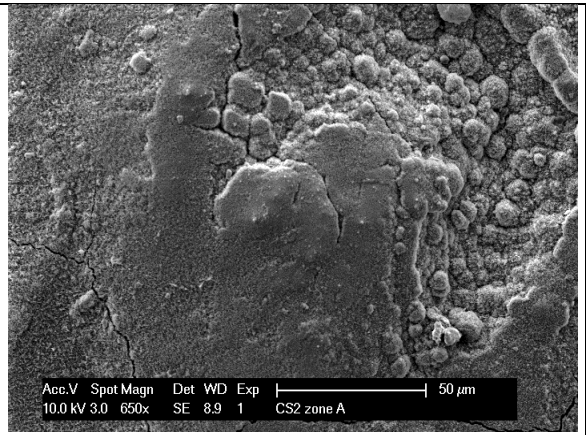 Sample CS2, zone A, X650	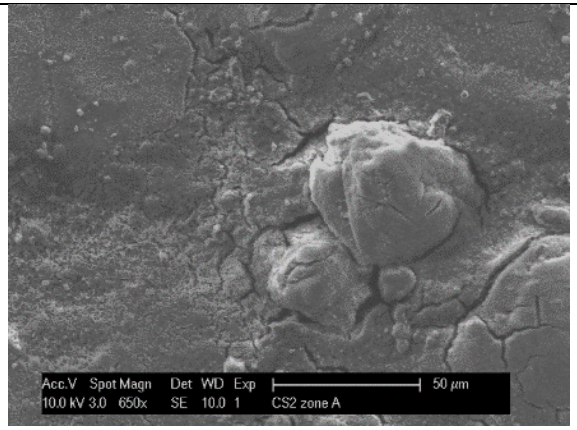 Sample CS2, zone A, X650	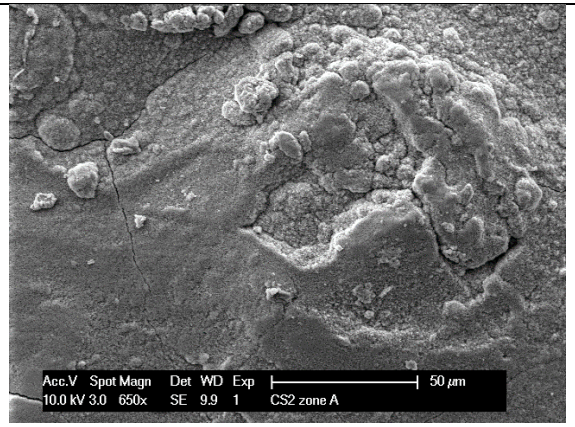 Sample CS2, zone A, X650
C+T4	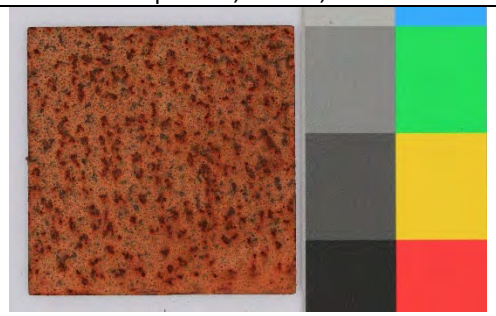 Sample CS7, General view	 Sample CS7, General view	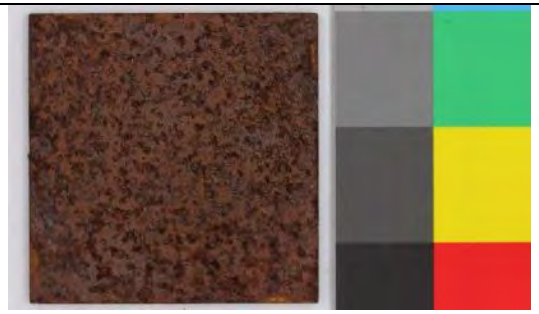 Sample CS7, General view
	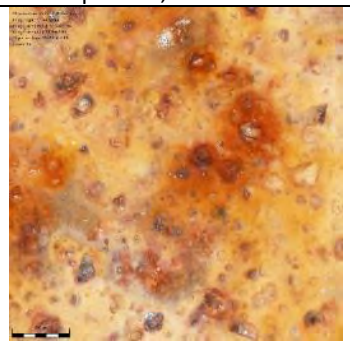 Sample CS7, zone B, X96	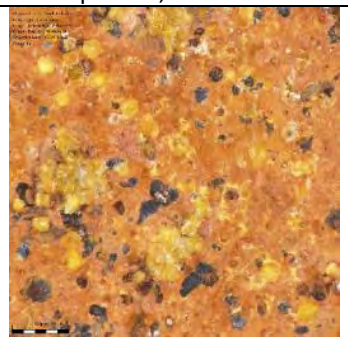 Sample CS7, zone B, X96	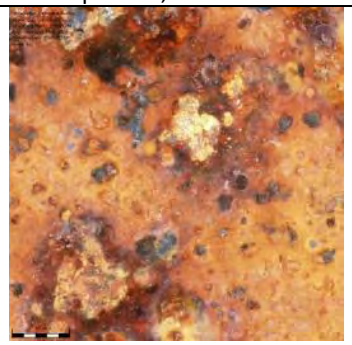 Sample CS7, zone B, X96

	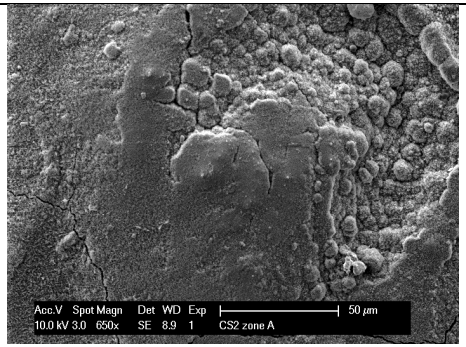 Sample CS2, zone A, X650	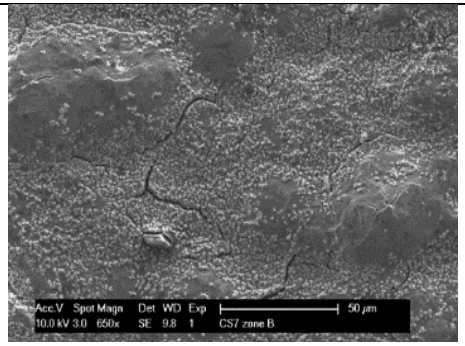 Sample CS7, zone B, X650	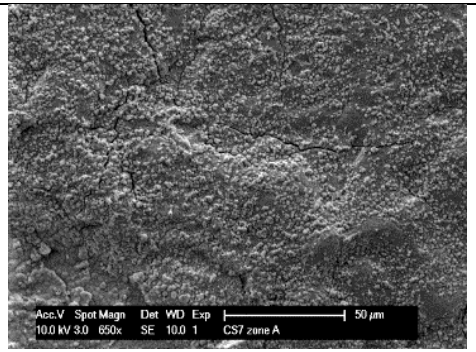 Sample CS7, zone A, X650
C+TR	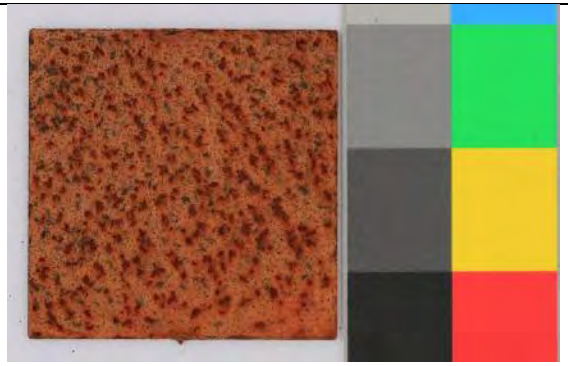 Sample CS6, General view	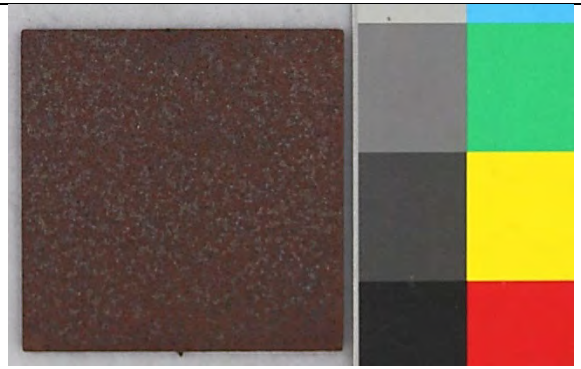 Sample CS6, General view	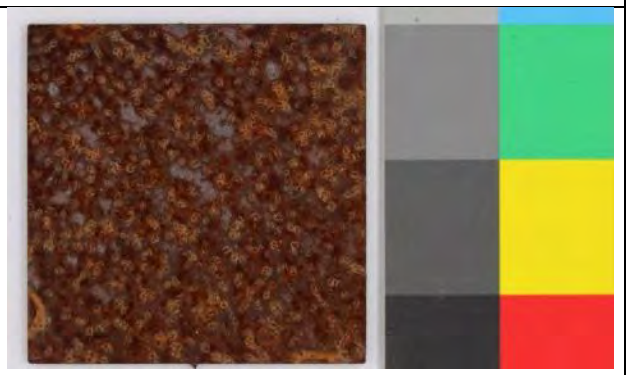 Sample CS6, General view

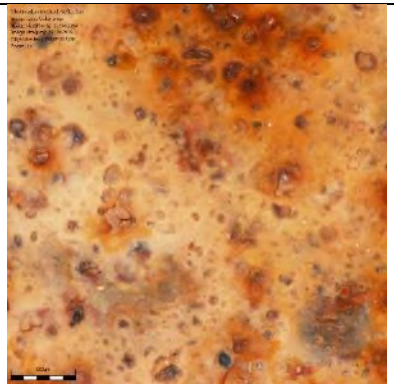 Sample CS6, zone B, X96	----------	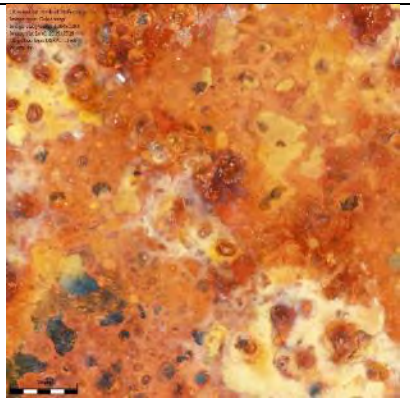 Sample CS6, zone B, X96
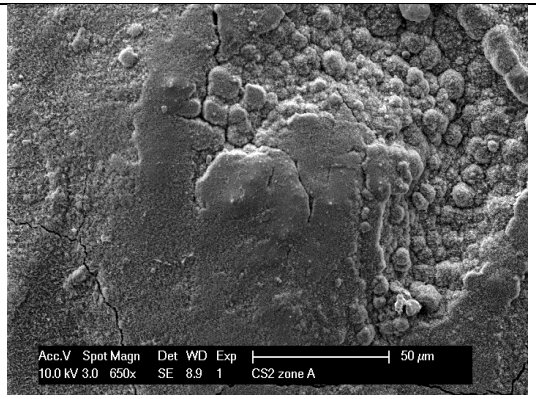 Sample CS6, zone A, X650	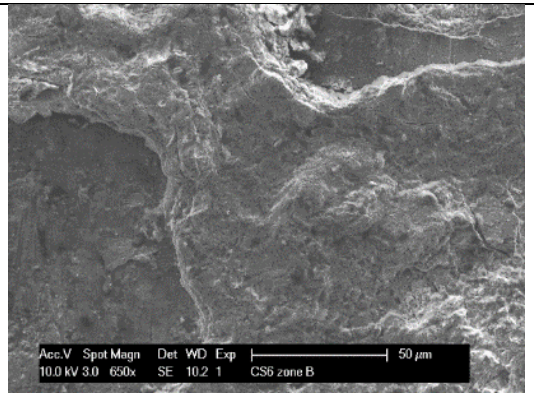 Sample CS6, zone B, X650	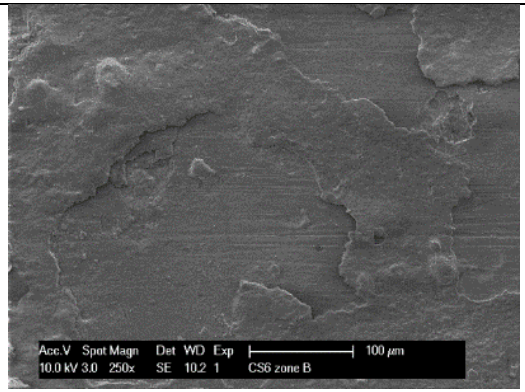 Sample CS6, zone B, X250

Table 27- Results of the visual examination on the self-weathering steel (CS)

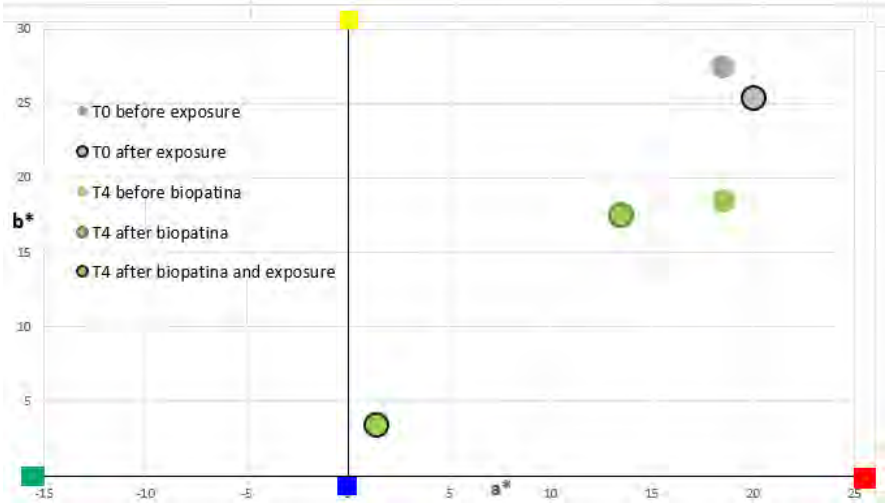

Figure 90 - colorimetric measurements performed on self-weathering steel samples (CS)

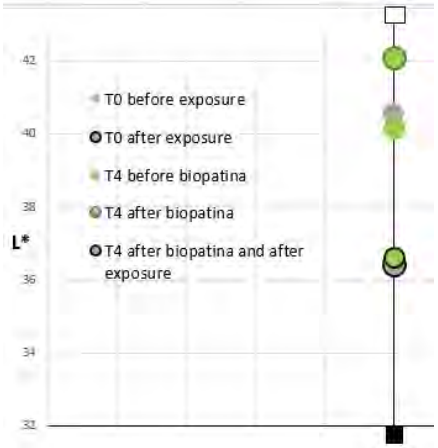

Figure 91- colorimetric measurements performed on self-weathering steel samples (CS)

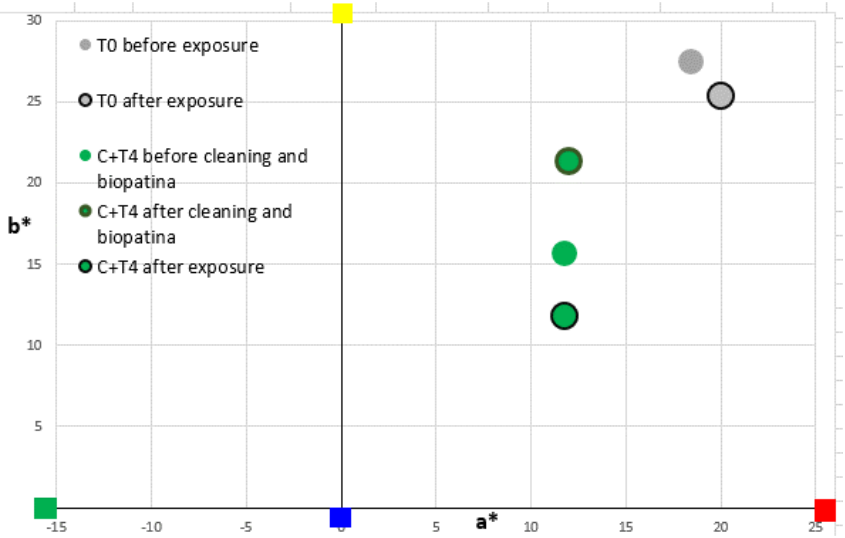

Figure 92- colorimetric measurements performed on self-weathering steel samples (CS)

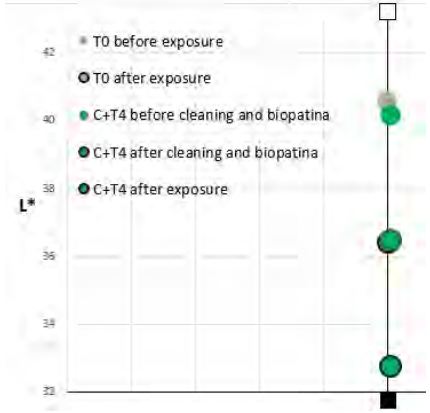

Figure 93- colorimetric measurements performed on self-weathering steel samples (CS)

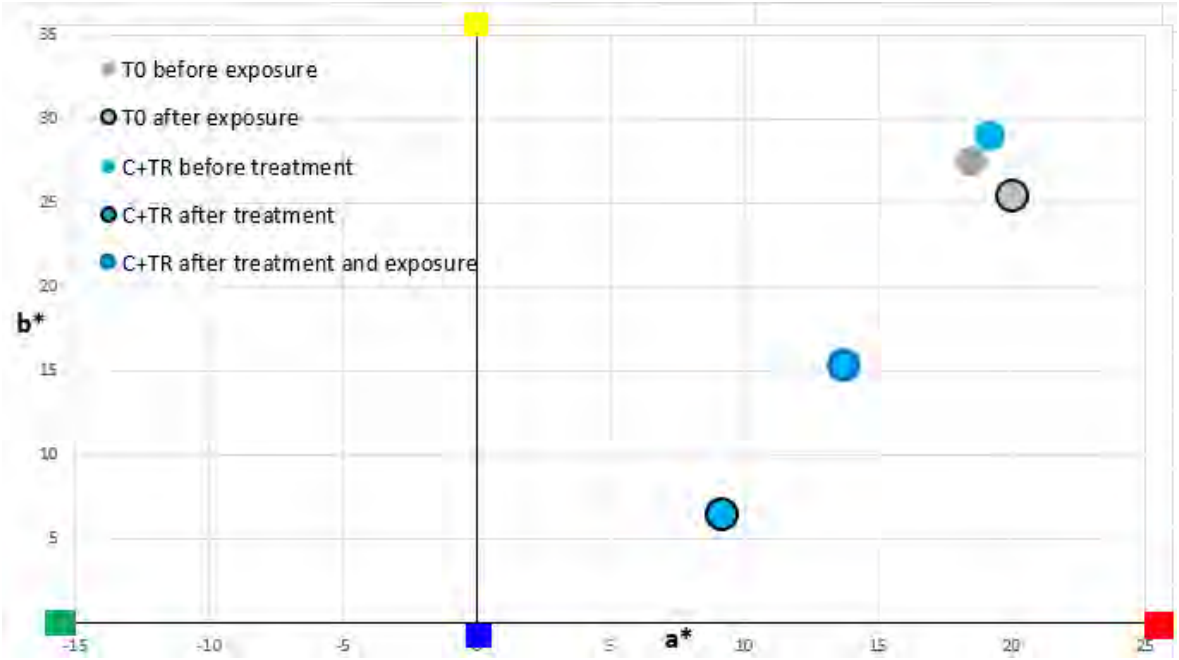

Figure 94 - colorimetric measurements performed on self-weathering steel samples (CS)

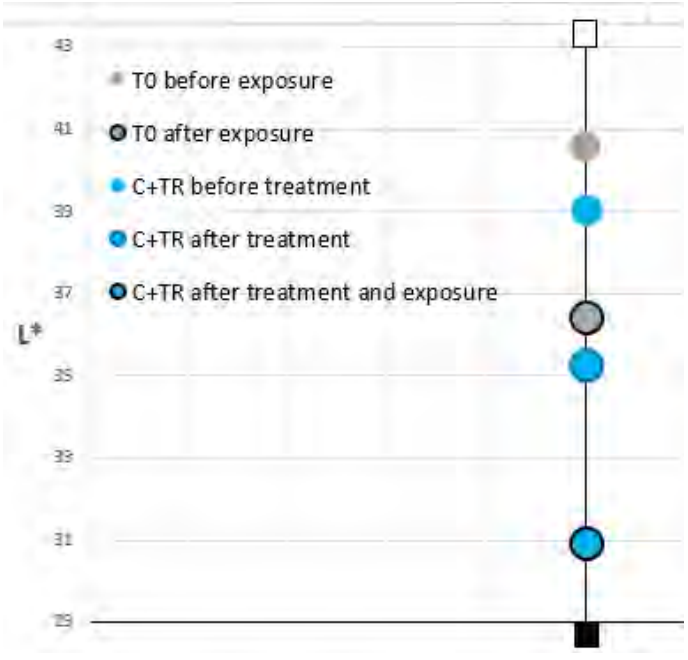

Figure 95 - colorimetric measurements performed on self-weathering steel samples (CS)

CS	Before exposure	After treatment	After 1 month	After 3 months	After 6 months
T0 (reference)	27.55	----------	21.6	34.87	29.97
T4		36.3	24.8	21.27	25.73
C+T4		40.5	21.8	19.2	24.67
C + TR		23.4	15.83	24.6	20.97

Table 28- average thickness of the corrosion layer in µm on the self-weathering steel samples (CS)

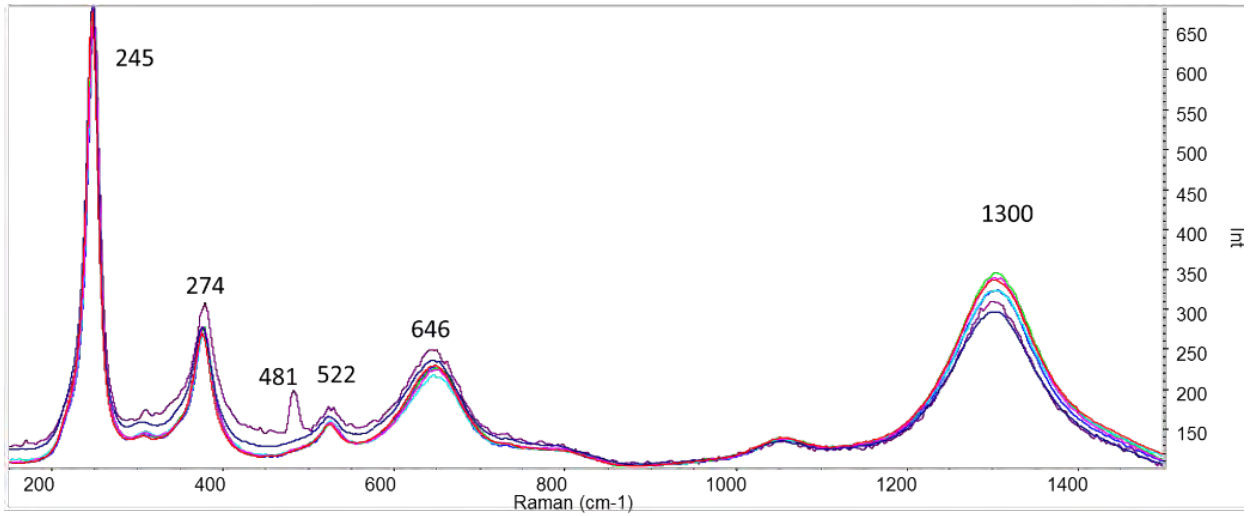

Figure 96 -Raman spectra obtained on all weathered steel samples

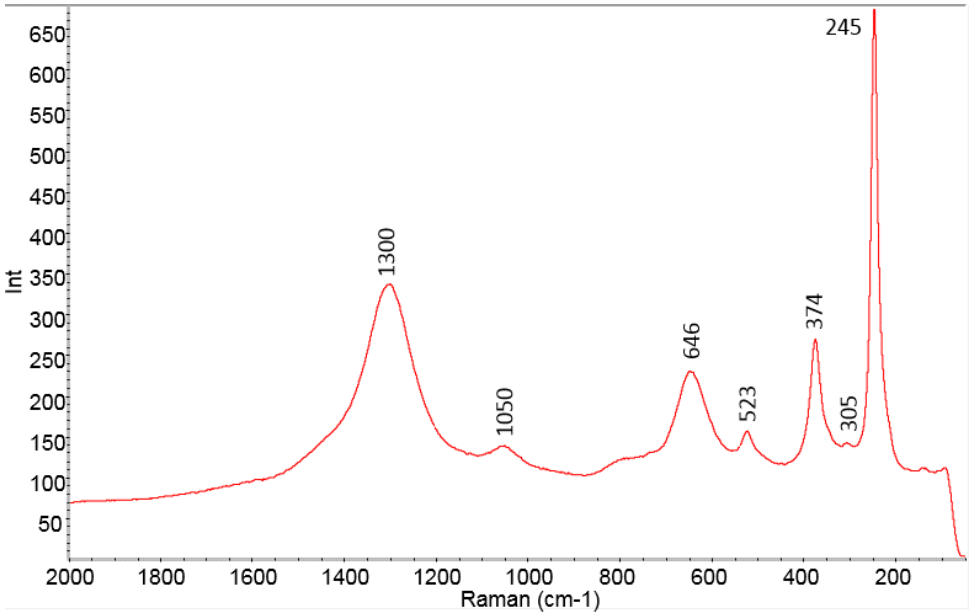

Figure 97 - T0 before exposure (sample CS1), Raman

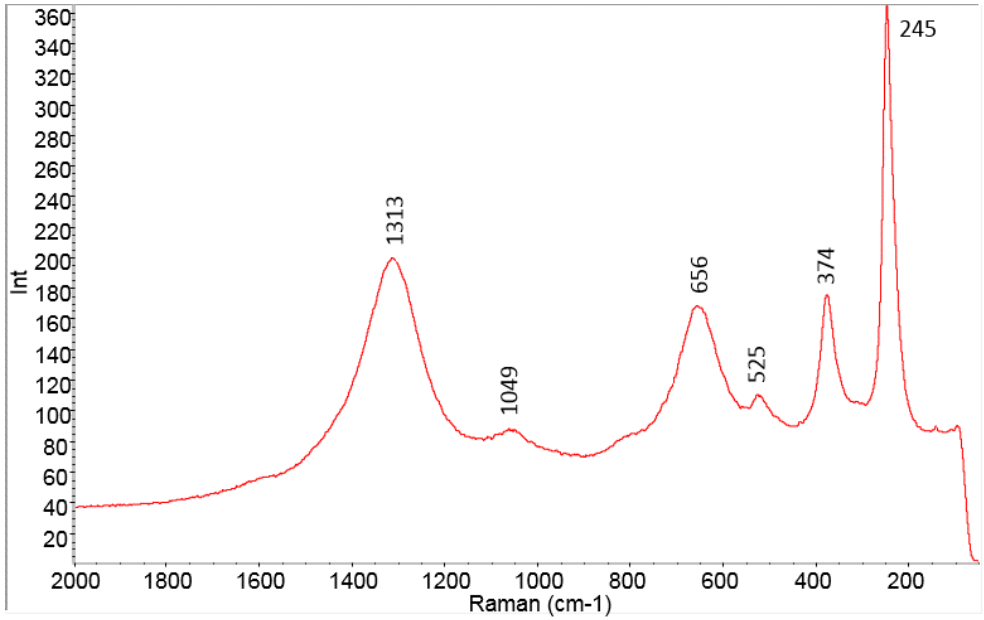

Figure 98 - T0 after exposure (sample CS1), Raman

Figure 99 - T4 after biopatina (sample CS2), Raman

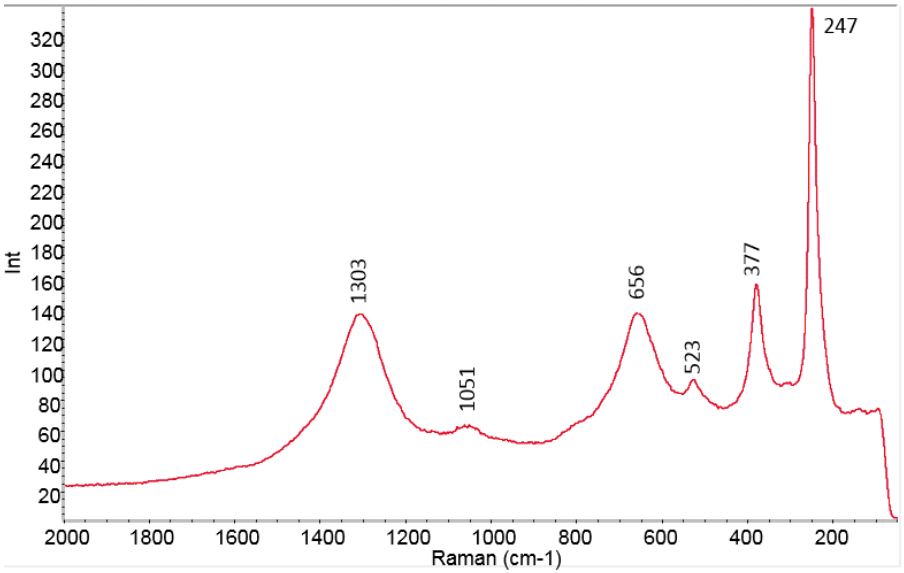

Figure 100 - T4 after biopatina and exposure (sample CS2), Raman

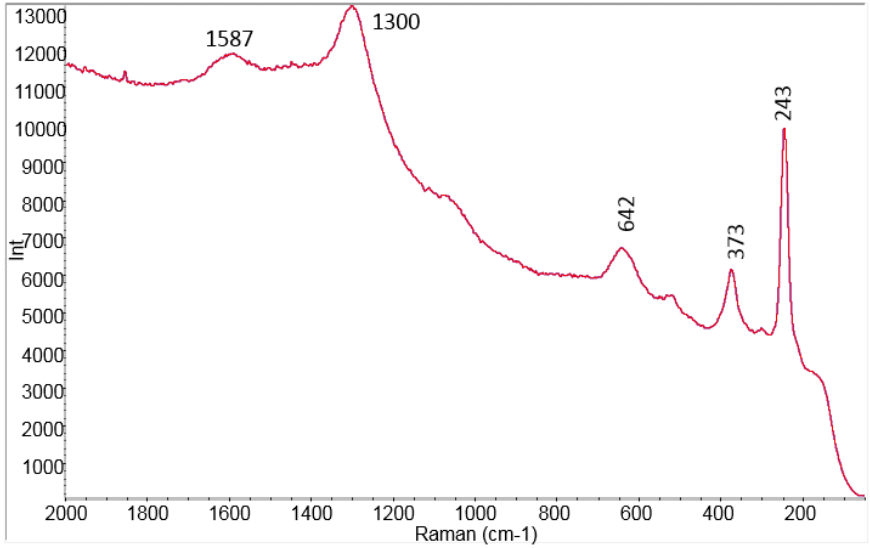

Figure 101 - T4 after cleaning and biopatina (sample CS7), Raman

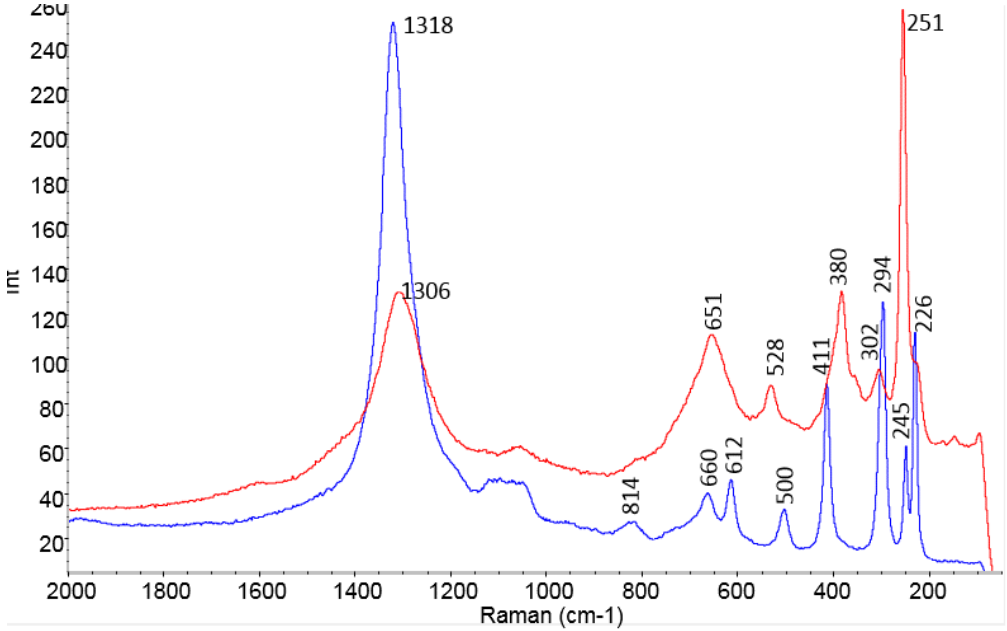

Figure 102 - C + T4 after biopatina and exposure (two zones on sample CS7), Raman

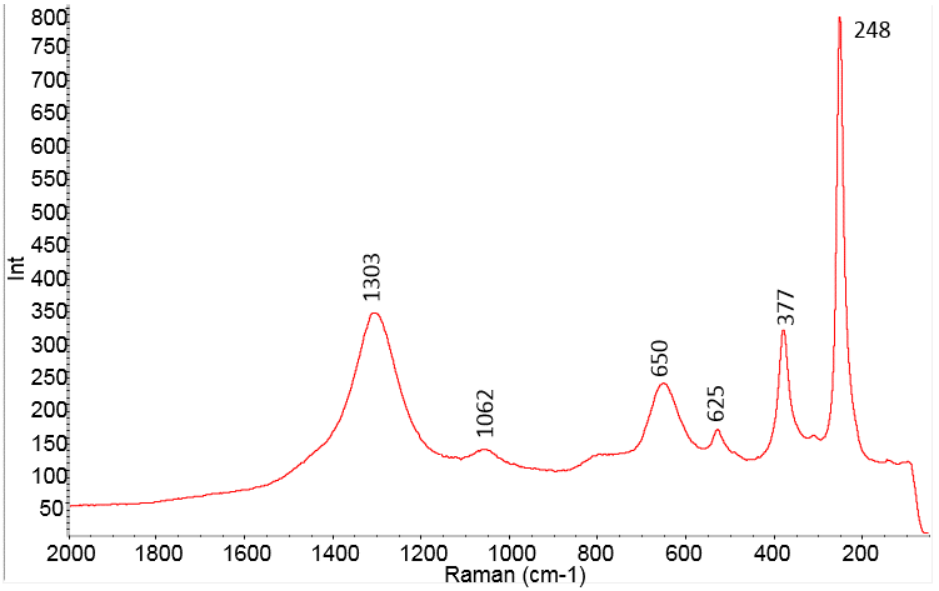

Figure 103 - C + TR after biopatina and exposure (sample CS6), Raman

3-b.2.2.3. Corroded steel (IMN series)

On reference samples, lepidocrocite was detected by Raman spectroscopy, as illustrated in Figures 110-111 where characteristic peaks at 246 cm^{-1}, 375 cm^{-1}, 640 cm^{-1}, 1302 cm^{-1} and 522 cm^{-1} are present. They can be attributed to γ-FeO(OH)[27]. Some spectra presented also a peak at 480 cm^{-1} that could correspond to goethite. The peak at 307 cm^{-1} could possibly indicate the presence of Akaganeite. This iron oxide appears in seaside environments when high amount of NaCl airborne is present.

Biopatina treatment

The biopatina treatment induces only slightly visible modifications. The layer thickness is not impacted by the treatment. Microscopic observation shows that the corrosion products are slightly more yellow than before (Table 29). The average colorimetric values indicate that the surface tends to get darker by the treatment (Figure 105). The colorimetric measurements indicates an increase of lightness after biopatina treatment and an evolution on the blue-yellow axe (towards yellow), Figure 104. This difference is slightly visible (Δ E= 4.55).

Specific products like iron oxalates were not detected after treatment by Raman spectroscopy (Figure 112), the peaks are characteristic of lepidocrocite: 1300, 642, 373, 243 cm^{-1}. The samples cleaned prior to biopatina with peaks at 1299, 650, 528, 380, 303 and 251 cm^{-1} also show a predominance of lepidocrocite.

Both extra series with cleaning prior to biopatina treatment and the reference conservation method (wax coating) induce higher color differences (Δ E= 16.01 /16.92), Figure 106-109.

New reddish corrosion spots can be seen on the reference samples after 6-months exposure, which can also be seen under the microscope. The biopatina samples (cleaned and non cleaned) look more homogenous after 6-months exposure under the microscope it can be seen that small dark corrosion spots formed. These two series (T4 and C+T4) show good results. They show only slight surface modification and new corrosion spots.

The C+T4 series show less new corrosion spots than the C+TR series which were coated with microcrystalline wax after cleaning (in particular the edges are less corroded), Table 29.

6-months exposure

The cleaned series (C+T4 and C+TR) evolve on the green-red axe towards green during the exposure. The color difference after 6-months exposure is more important for these two series (ΔE= 13.75/15.69). The biopatina treated sample also evolves towards green, but the color difference is low (ΔE=5.87).

In comparison, the only series which evolves slightly towards red and the lowest color difference (ΔE=2.41) is the reference series T0.

lepidocrocite was detected by Raman spectroscopy as the predominant species on all series including the reference conservation treatment (Figure 116):

The samples without any treatment (T0) show only lepidococite (1305, 645, 525, 377, 304, 248 cm^{-1}) after exposure and probably a small amount of akaganeite (at 304 cm^{-1}), Figure 110. The sample treated with biopatina (T4) shows peaks which can be related to lepidocrocite (1302, 650, 529, 379, 250 cm^{-1}), but also to akaganeite (302 cm^{-1}), Figures 113-114.

After exposure lepidocrocite is detected again on the samples which were cleaned prior to biopatina treatment (1301, 648, 528, 378, 306, 250 cm^{-1}), Figures 114-115.

The corrosion layer thickness is similar for the series which were cleaned before another treatment (biopatina or waxcoating) and similar for the series which were not cleaned (reference samples T0 and T4 biopatina samples (Table 30)

IMN	Before 6 months exposure	After treatment	After 6 months exposure
T0 **Reference**	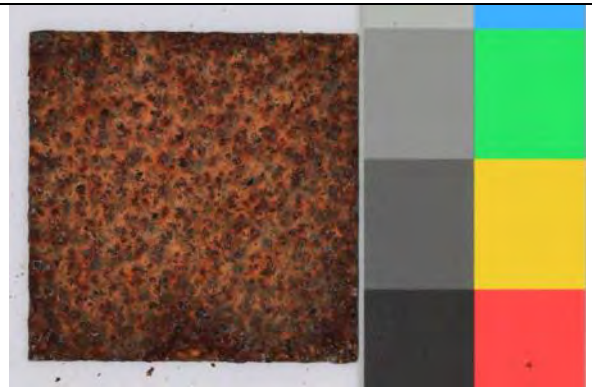 Sample IMN1, General view	----------	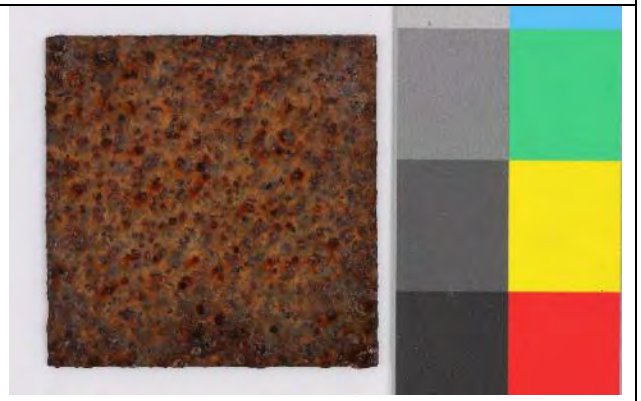 Sample IMN1, General view
Before /after exposure	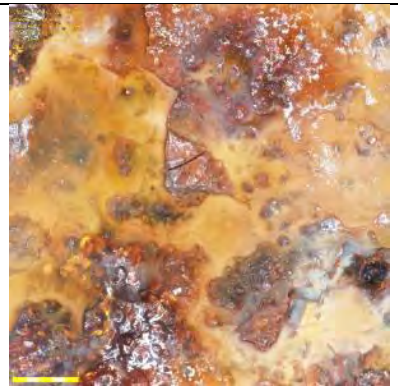 Sample IMN1, zone B, X96	----------	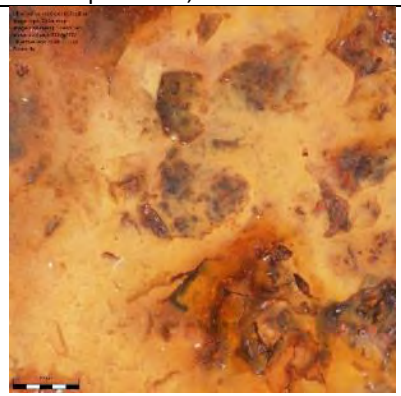 Sample IMN1, zone B, X96

	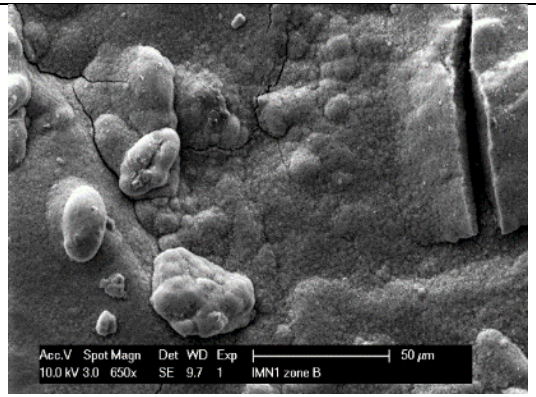 Sample IMN1, zone B, X650 (SE)	----------	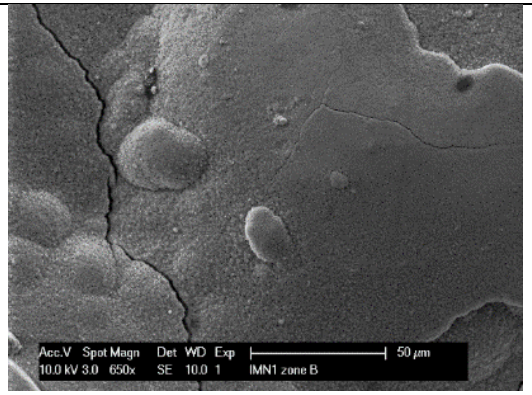 Sample IMN1, zone B, X650 (SE)
T4 biopatina	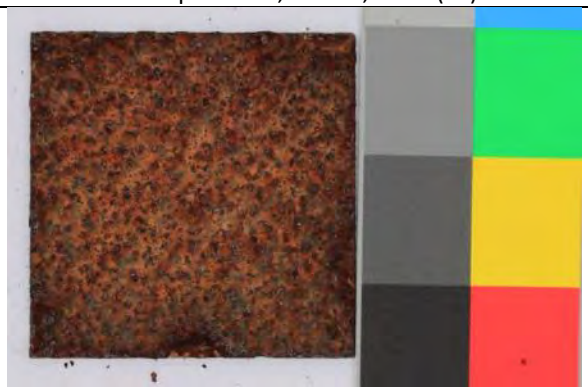 Sample IMN2, General view	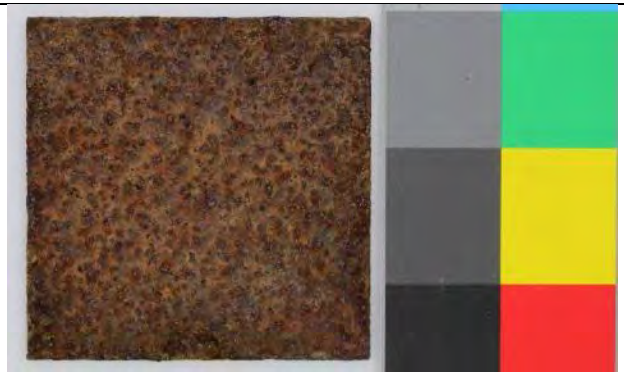 Sample IMN2, General view	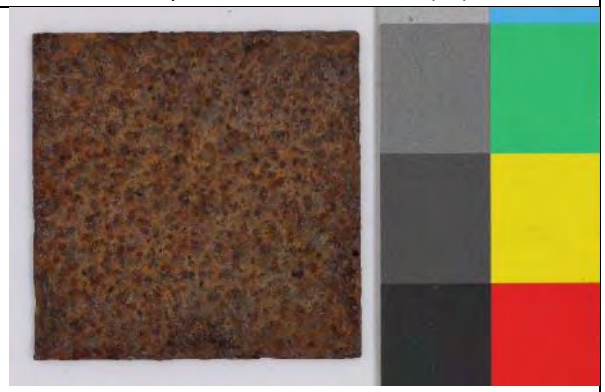 Sample IMN2, General view

Sample IMN2, zone B, X96

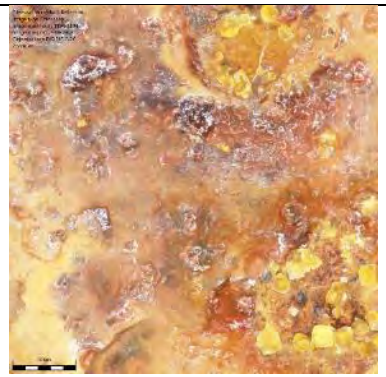

Sample IMN2, zone B, X96

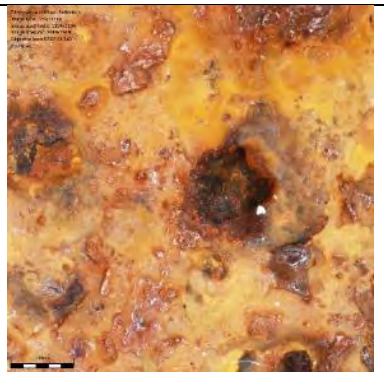

Sample IMN2, zone B, X96

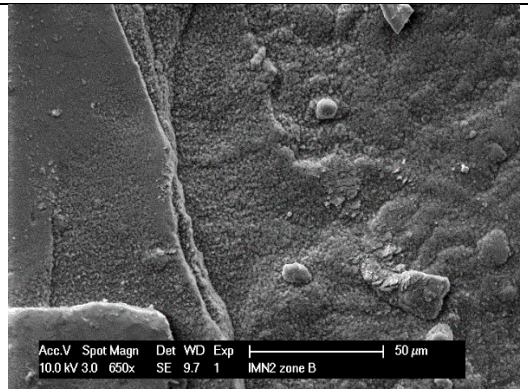

Sample IMN2, zone B, X650 (SE)

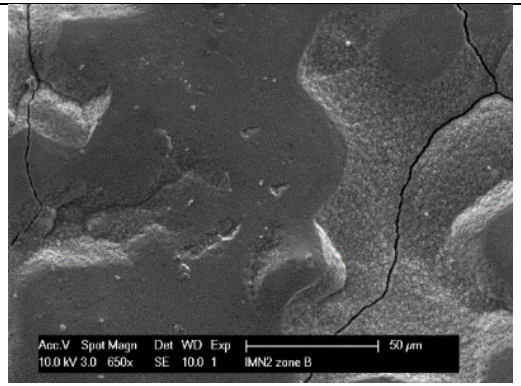

Sample IMN2, zone B, X650 (SE)

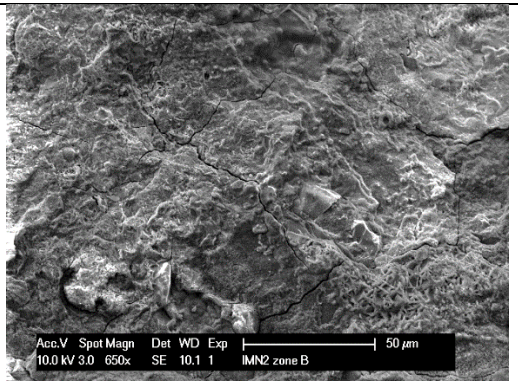

Sample IMN2, zone B, X650 (SE)

C+T4	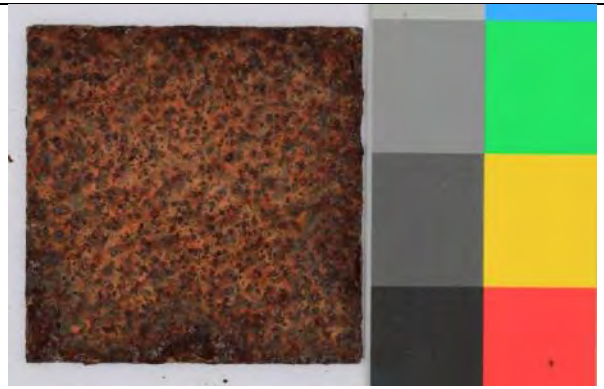 Sample IMN8, General view	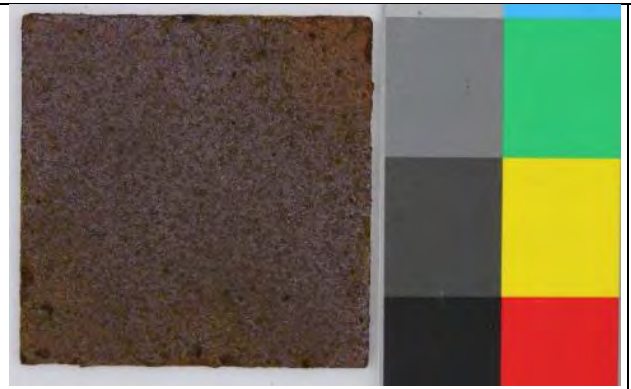 Sample IMN8, General view	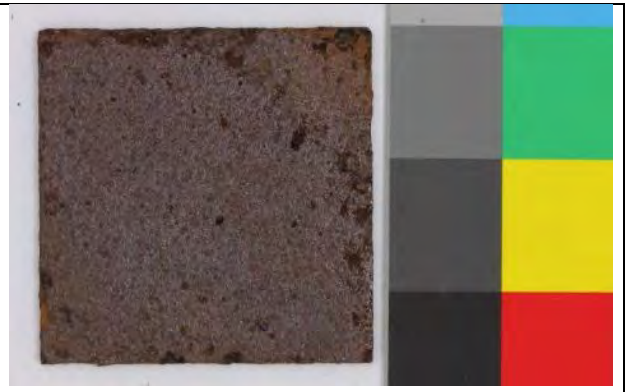 Sample IMN8, General view
	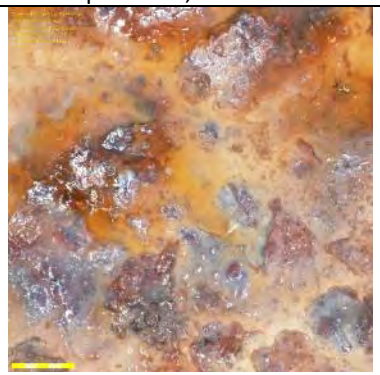 Sample IMN8, zone B, X96	 Sample IMN8, zone B, X96	 Sample IMN8, zone B, X96
	----------	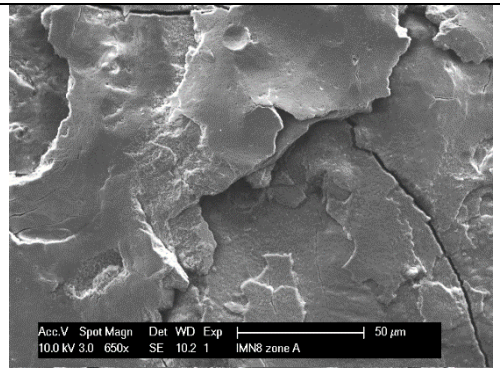 Sample IMN8, zone A, X650	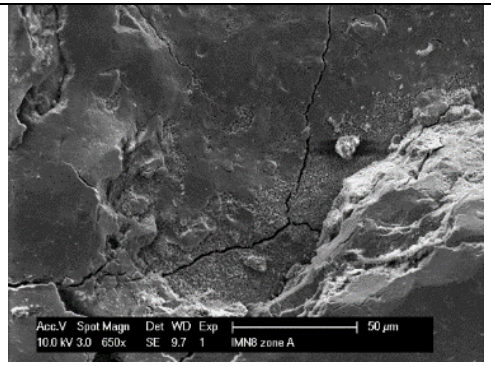 Sample IMN8, zone A, X650

		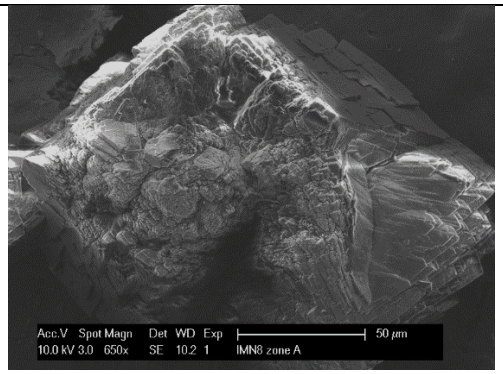 Sample IMN8, zone A, X650	
C+TR	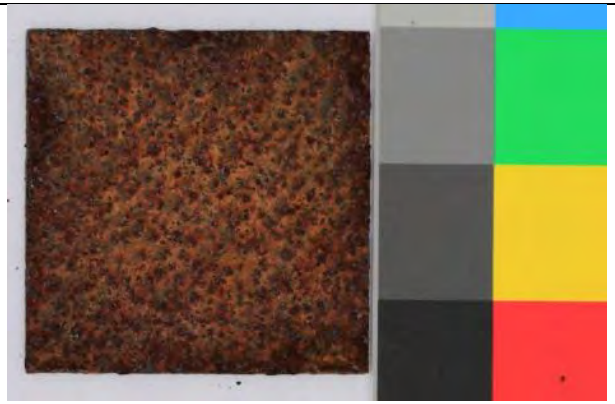 Sample IMN10, General view	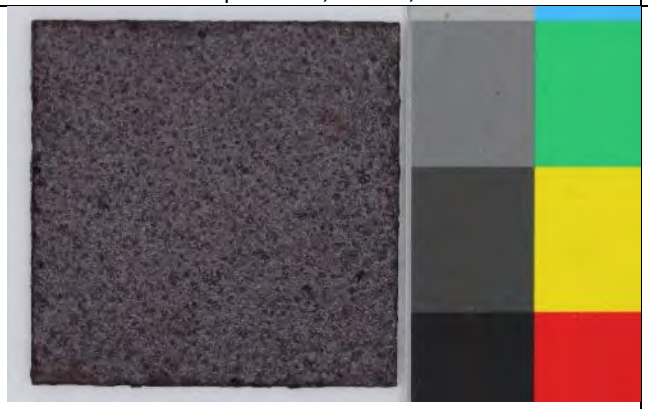 Sample IMN10, General view	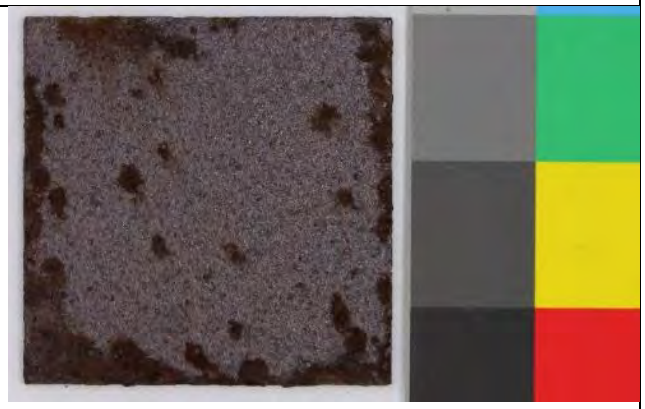 Sample IMN10, General view

	 Sample IMN10, zone B, X96	----------	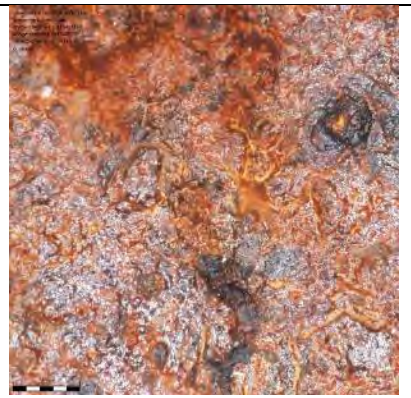 Sample IMN10, zone B, X96
	----------	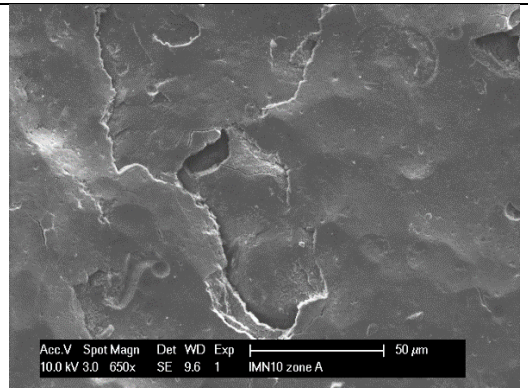 Sample IMN10, zone A, X650	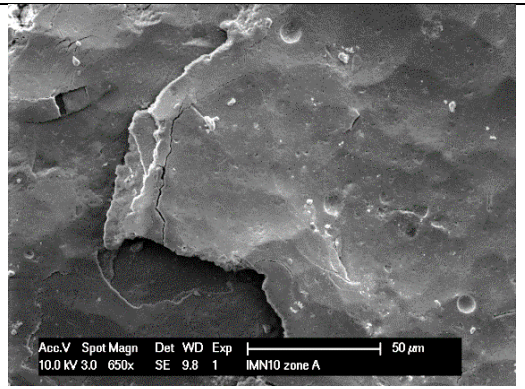 Sample IMN10, zone A, X650

Table 29- Results of the visual examination on corroded steel (IMN)

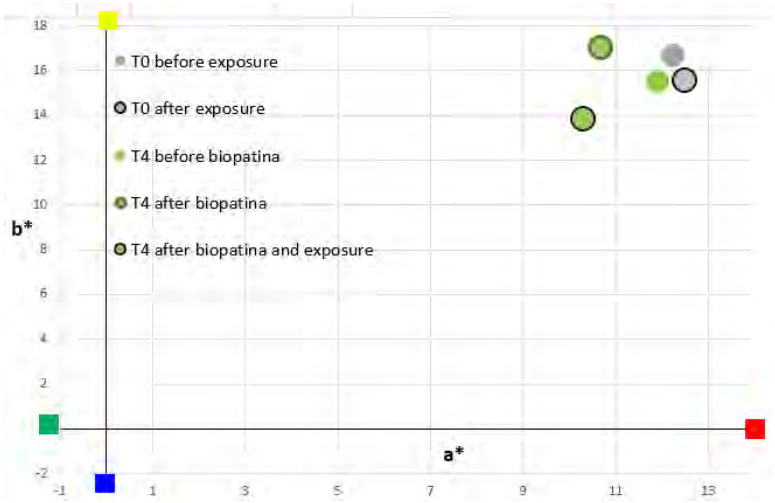

Figure 104- colorimetric measurements performed on corroded steel samples (IMN)

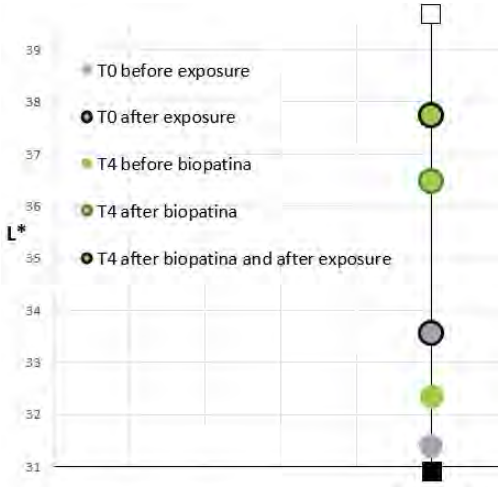

Figure 105- colorimetric measurements performed on corroded steel samples (IMN)

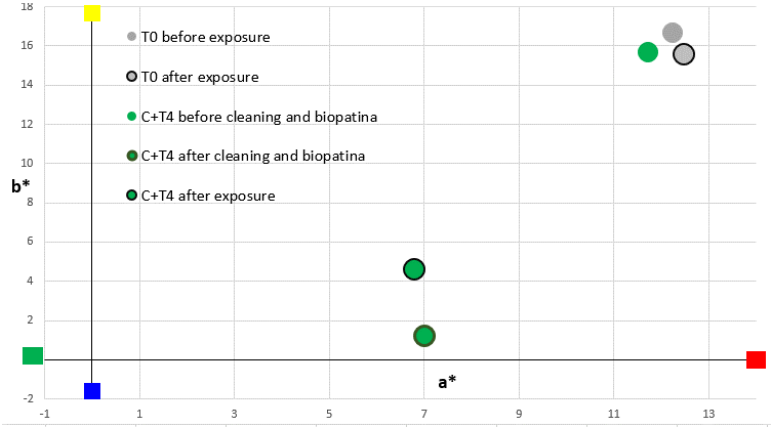

Figure 106 - colorimetric measurements performed on corroded steel samples (IMN)

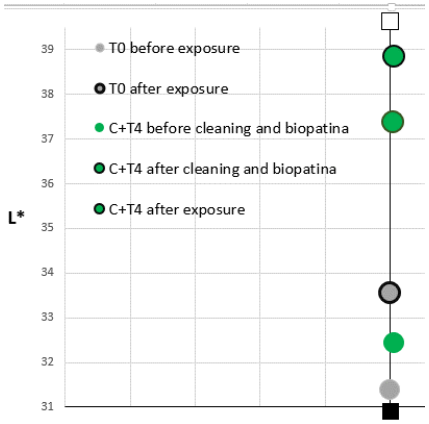

Figure 107- colorimetric measurements performed on corroded steel samples (IMN)

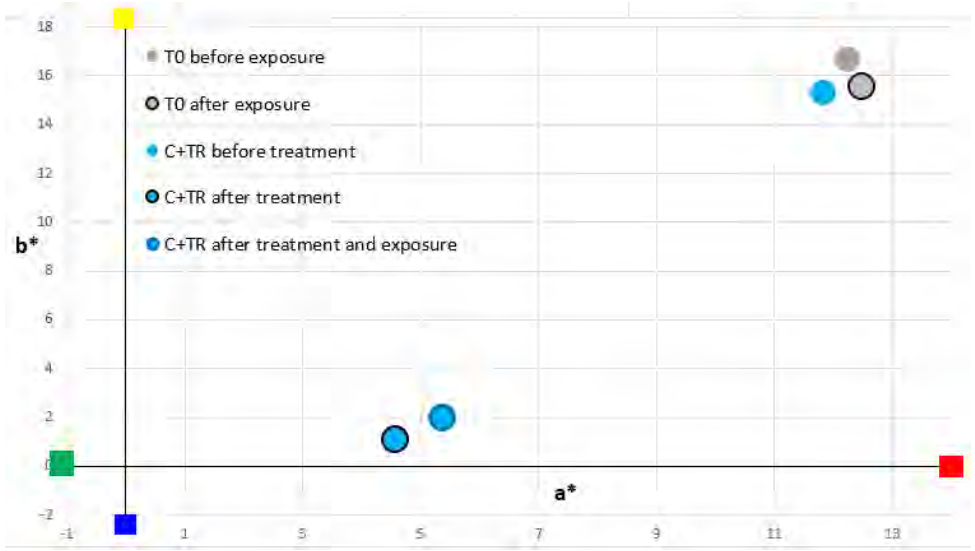

Figure 108 - colorimetric measurements performed on bare steel samples (IMN)

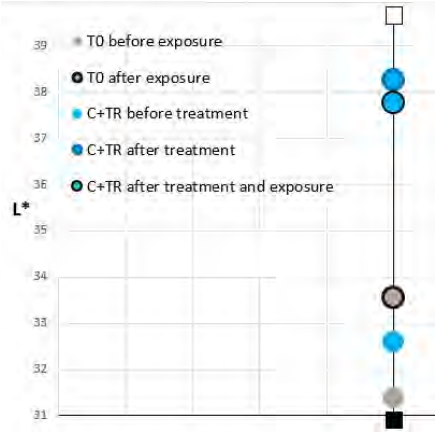

Figure 109 -colorimetric measurements performed on bare steel samples (IMN)

IMN	Before exposure	After treatment	After 1 month	After 3 months	After 6 months
T0 (reference)	88.1	----------	97.73	93.9	82.93
T4		89.5	95.57	97.57	86.37
C+T4		80.35	75.17	84.83	77.63
C + TR		72.65	70.73	76.4	78.83

Table 30 - average thickness of the corrosion layer in µm on the bare steel samples (IMN)

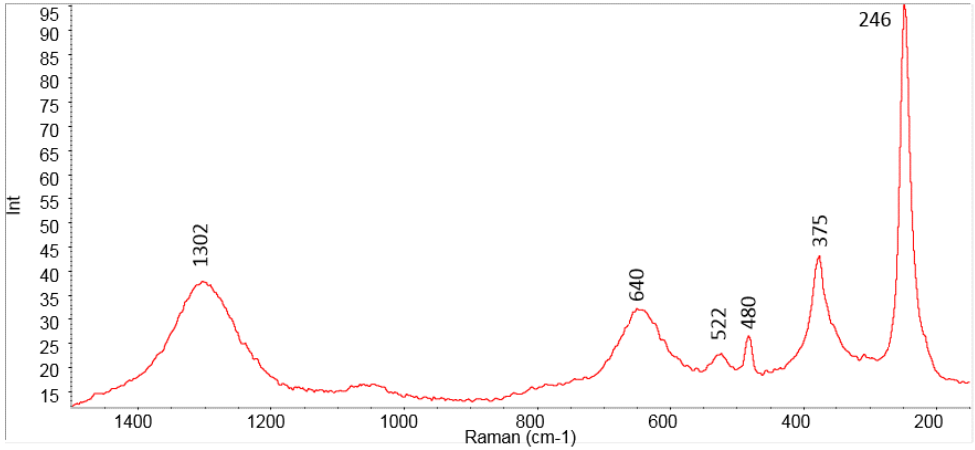

Figure 110 - T0 before exposure (sample IMN1), Raman spectrum

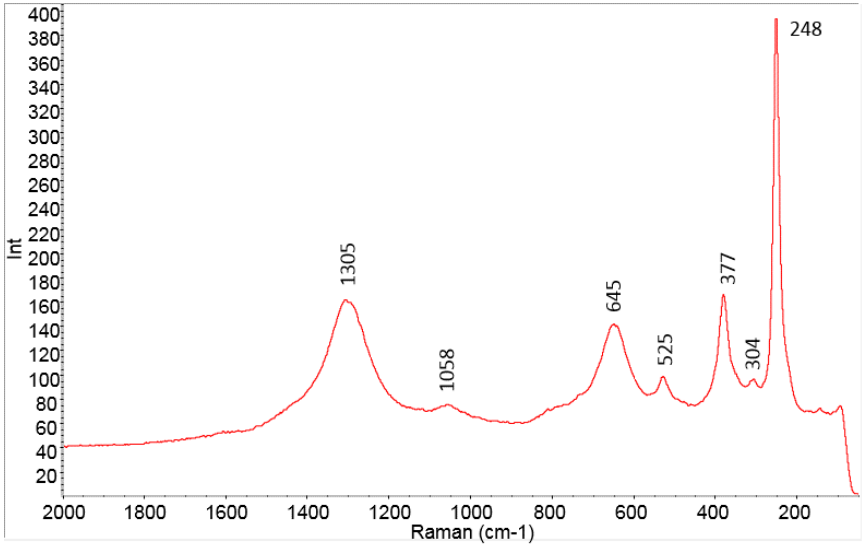

Figure 111 - T0 after exposure (sample IMN1), Raman spectrum

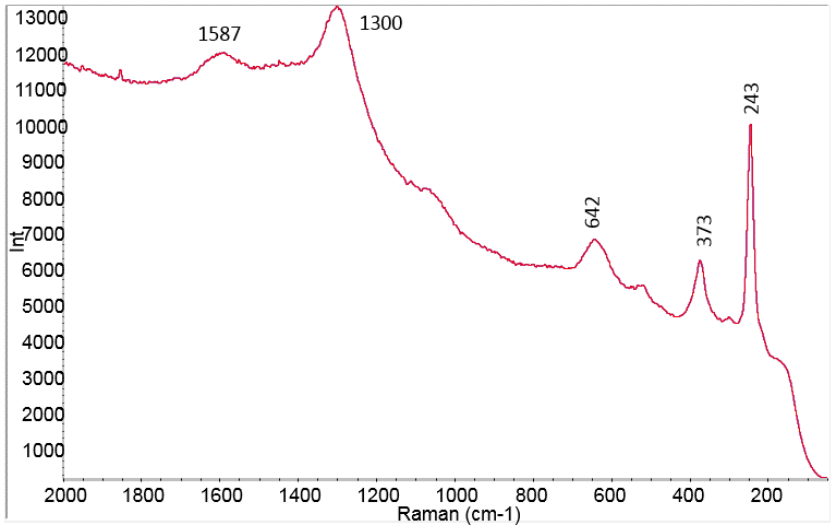

Figure 112 - T4 after biopatina (sample IMN2), Raman spectrum

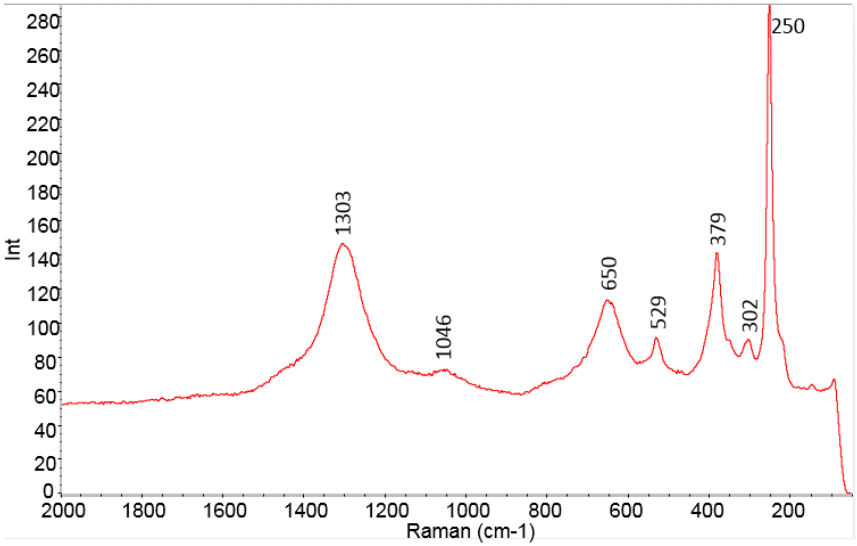

Figure 113 - T4 after biopatina and exposure (sample IMN2), Raman spectrum

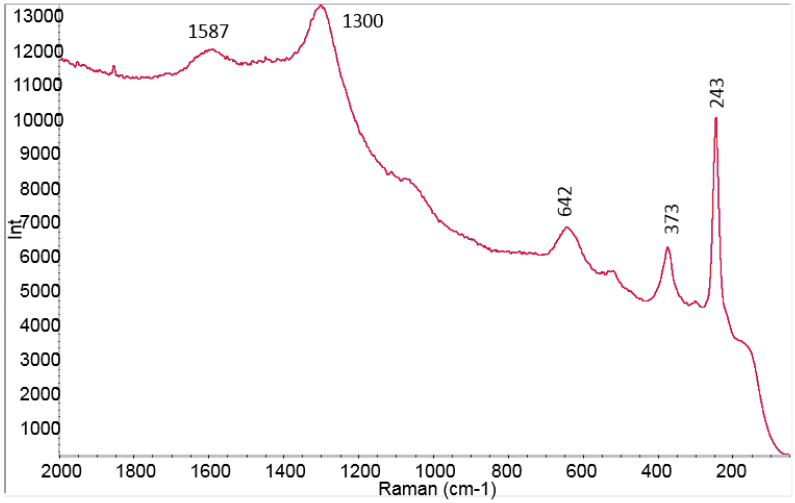

Figure 114 – C + T4 after biopatina (sample IMN8), Raman spectrum

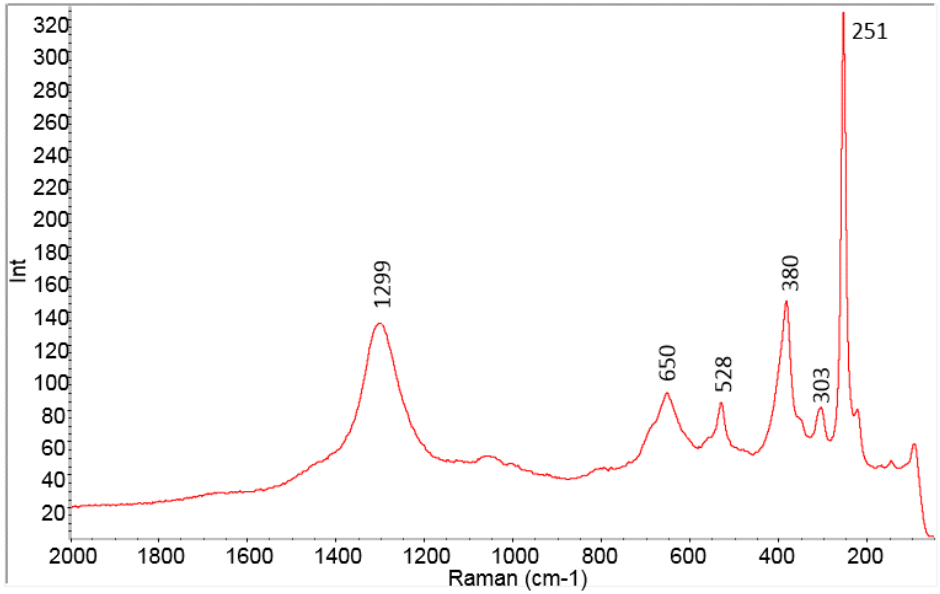

Figure 115 - C + T4 after exposure (sample IMN8), Raman spectrum

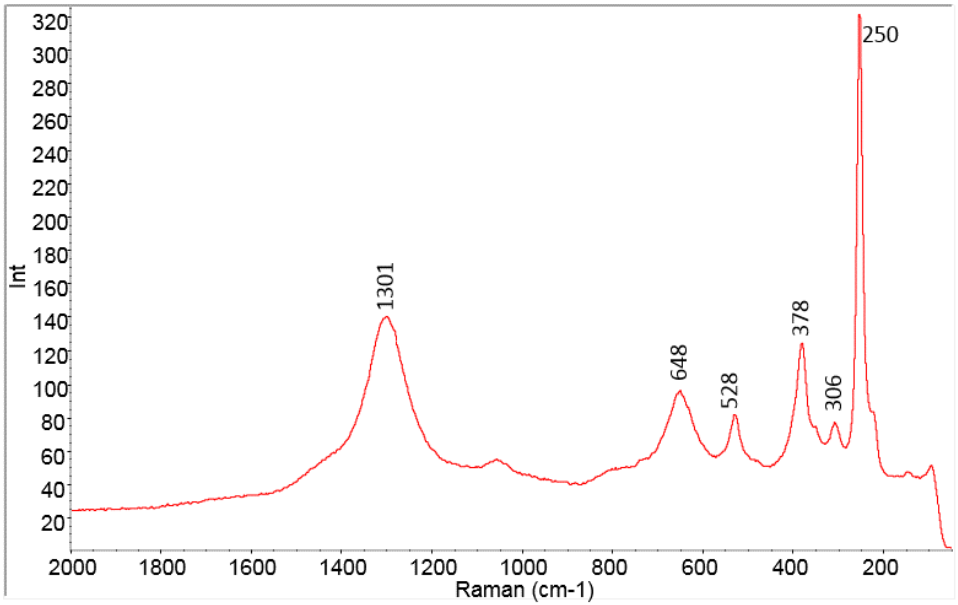

Figure 116 - C + TR after exposure (sample IMN10), Raman spectrum

3-c. Evaluation of the long-term behavior of treatments

In order to understand the long-term stability of the treatment, these tests were performed in the display environment of the case studies treated with biopatina treatment 3 years ago.

Lausanne, park La Légende

Statues analyses from the park Légende d'Automne in Lausanne, 3 years after the treatment. Colorimetric measures have been carried out on the statues and lecterns. The measures have been made on similar spots before and after treatment to compare the effect of the treatment (Figures 117-118).

Figure 117 : pictures of the lectern before (left) and 3 years after treatment (right)

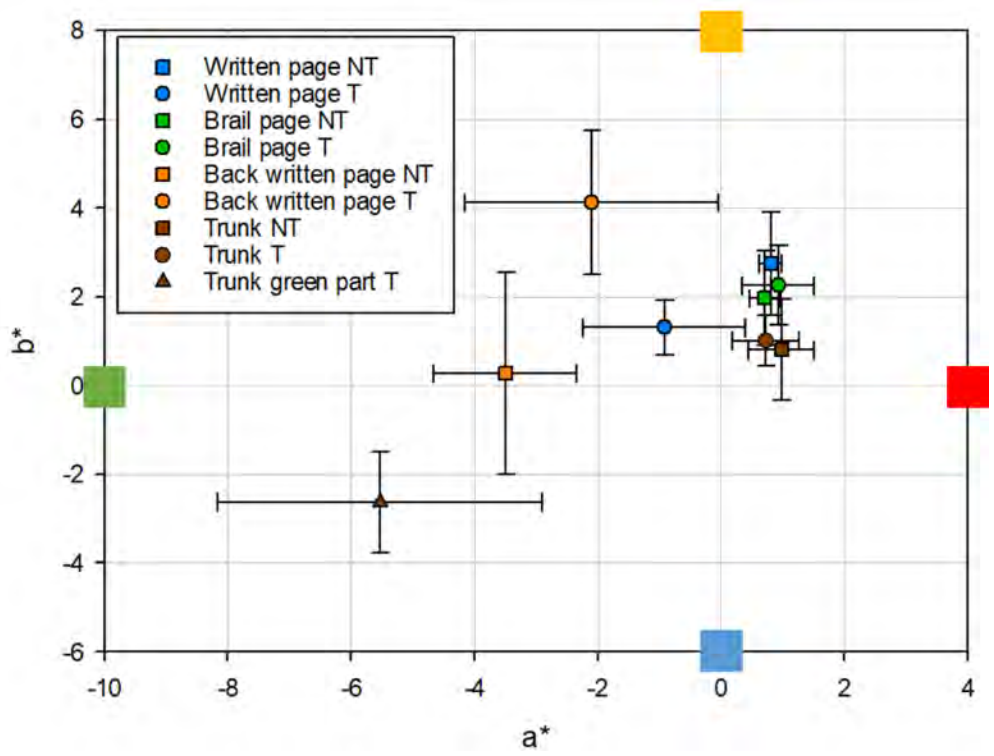

Figure 118 : colorimetric values of the lectern before and 3 years after treatment

We do not observe a difference before (NT) and after (T) treatment for the pages. The back of the book after treatment tends to a more brownish colour. However, we can observe that the green part of the trunk after treatment tends to a more blue-green colour.

Figure 119 : pictures of a treated (left) and an untreated (right) object

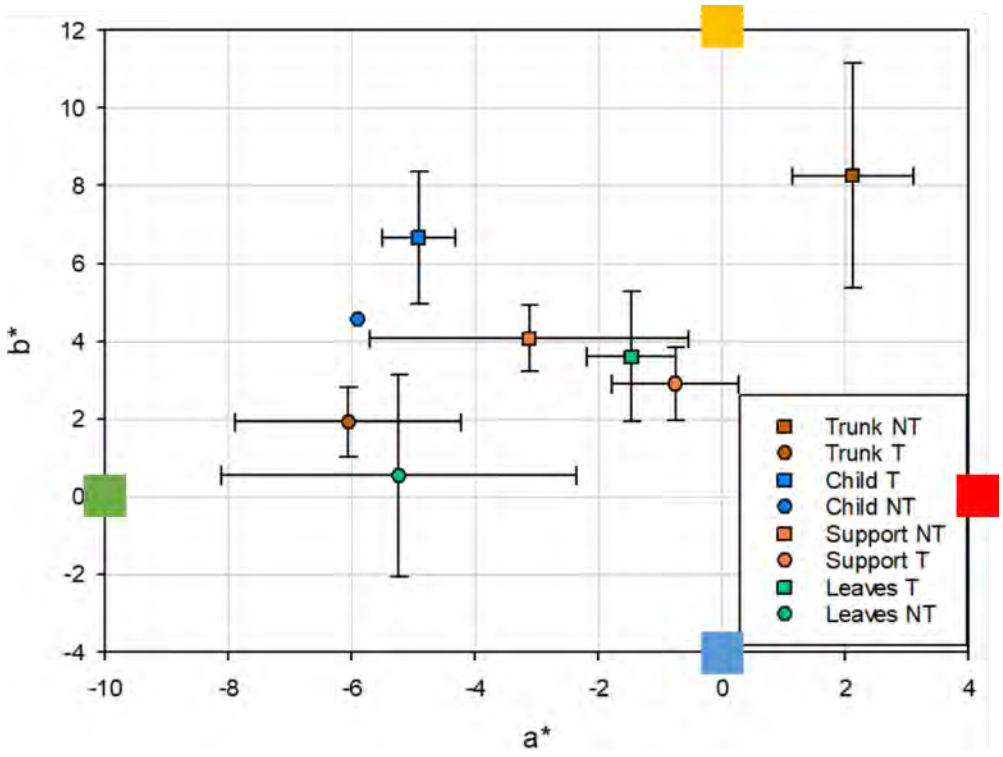

Figure 120 : colorimetric values of the objects before and after treatment

We observe here a larger range before and after treatment. More precisely, the tree trunk goes to a more blue-green stain after treatment, typical color characteristic of vert-de-gris forming in urban environment. The visual aspect of the children and the support do not change. On the opposite, the leaves go from blue to brown (Figure 119-120).

La Chaux-de-Fonds, Gallet park, does

Figure 121 : deer bronze object before (left) and 3 years after treatment (right)

Colorimetric measurements were carried out to evaluate the aesthetics and homogeneity of the treatment (Figures 121-122). Infrared analyses were also carried out, in-situ and in laboratory with samples (Figures 123-124).

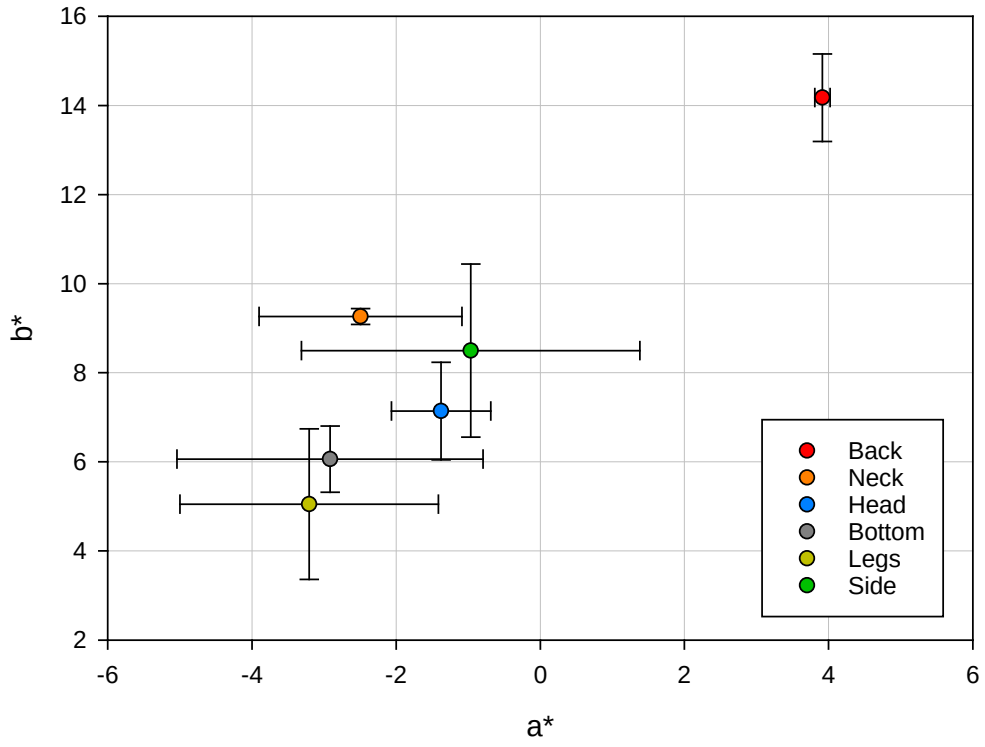

Figure 122 : colorimetric values of the deer before and 3 years after treatment

From a colorimetric point of view, we observe a* and b* values close to each other on the different zones measured, except for the back part. Indeed, this part is more touched by the public and so present less corrosion.

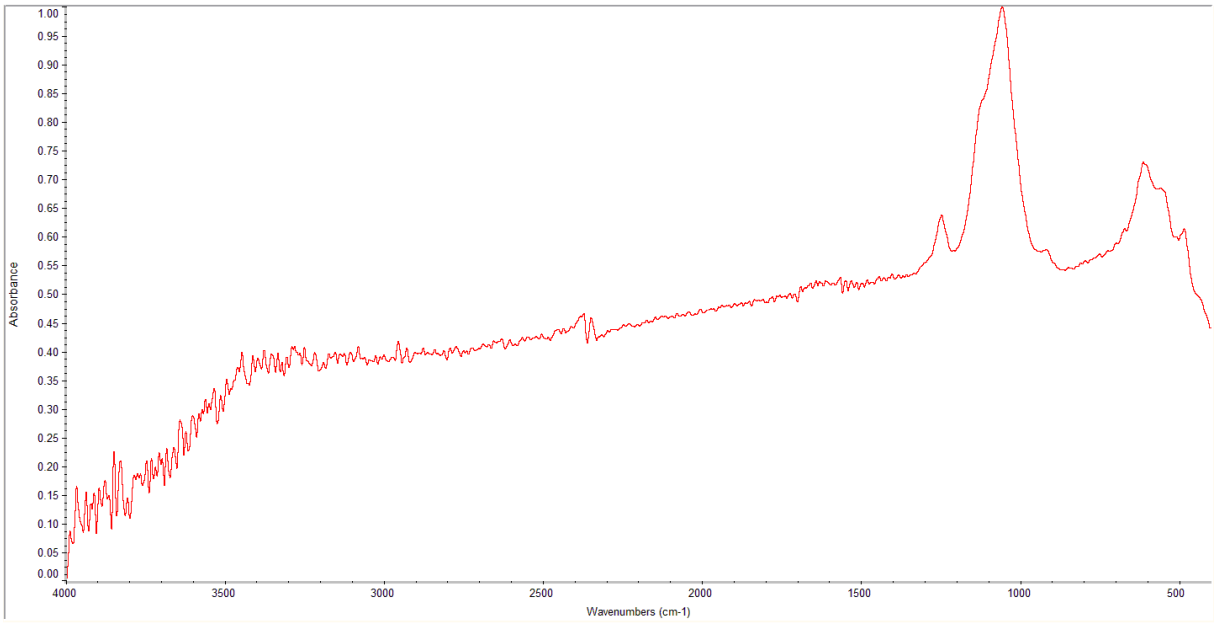

Figure 123 : contactless reflectance FTIR spectrum recorded in situ on the doe 3 years after treatment

The FTIR spectrum obtained in contactless external reflection showed vibrational bands that may be attributed to copper phosphates or to copper sulfates (1038, 1120 and 1240 cm^{-1}), Figure 123.

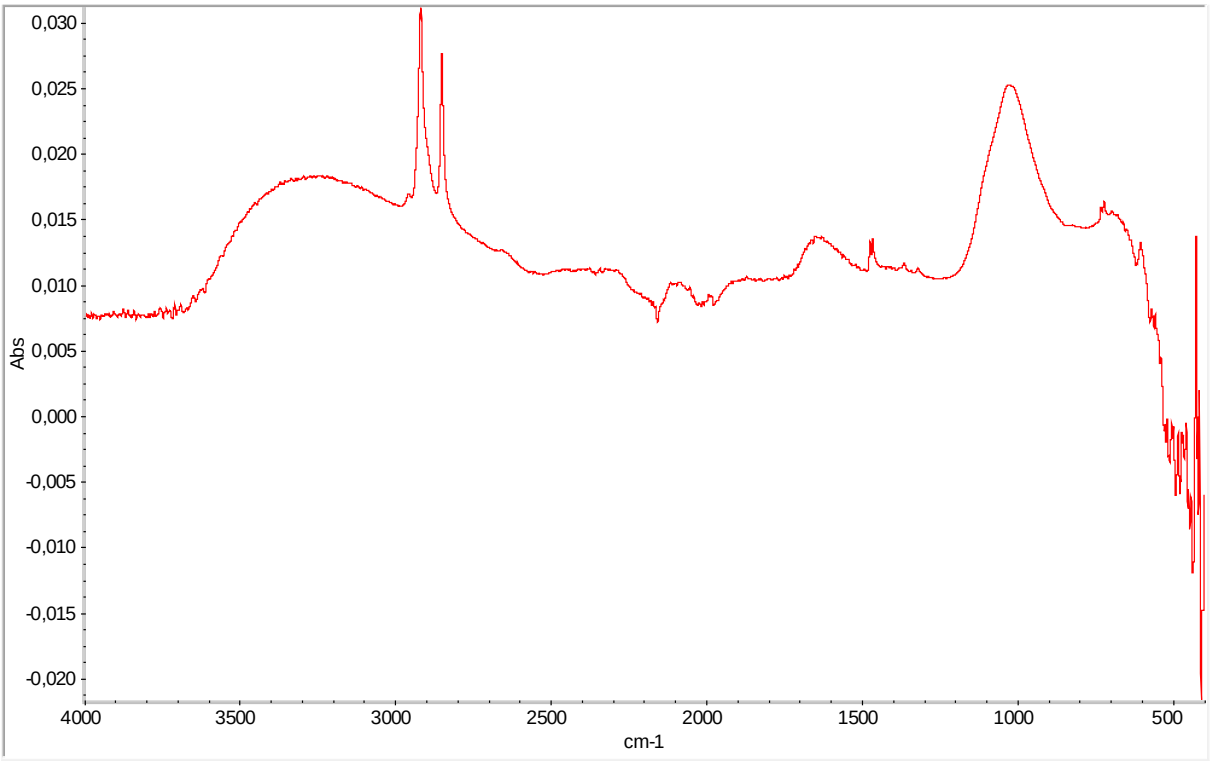

Figure 124 : ATR-FTIR spectrum recorded on the sample taken on the doe 3 years after treatment

Also on the sample taken and analysed by ATR-FTIR in the laboratory, Figure 124. The bands at 1318, 1364 and 1641 cm^{-1} show the presence of copper oxalates and some traces of wax applied as a sacrificial layer on top (1463 and 1475 cm^{-1}).

FINAL CONCLUSIONS

Regarding copper alloys, after 3 years treatment, copper oxalates are still present. The biopassivation represents therefore an excellent additive to organic coatings (shell-life of 2 years) to extend the duration of the preservation of outdoor bronze sculptures. The wax used as a top layer could be eventually reapplied.

Aside from the application on copper alloys, the test results are promising for zinc and iron alloys.

Indeed, In the case of selfweathering steel, the biopatina treatment might be an interesting alternative to usual conservation and maintainance practice for architectural parts in outdoor conditions. Tests show that the biopatina treatment leads to less color modification of the surface then the application of a traditional wax coating after cleaning.

The desired "rust effect" is preserved by biopatina. In terms of conservation, the results are encouraging: when comparing the sample series which was cleaned by soft micro airblasting (removal of less adherent superficial corrosion products with a soft abrasive) before treatments. In fact, more stable and less soluble compounds were detected after 6-months exposure only on the biopatina treated surfaces and not on the wax coated samples (mainly lepidocrocite was detected here). In the case of the biopatina samples, which were not cleaned prior to treatment, no particular difference in comparison to the reference series (no treatment =T0) was noticed in composition. For this reason an application of biopatina is recommended after preliminary cleaning of the selfweathering steel.

In the case of both bare and naturally corroded zinc surfaces, biopatina induces the formation of a more homogenous and less darker patina after 6-month exposure in comparison to untreated samples. Stable species like zinc oxalates are still detected after exposure together with hydrozincite, a stable corrosion product.

As biopatina shows good compatibility with both iron and zinc alloys, an application to degraded galvanized iron could be an appropriate way to extend the life-time of these type of surfaces. Tests which were also carried out on ancient damaged galvanized outdoor elements confirm the promising results obtained with the laboratory samples.

APPENDIXES

Appendix 1: Case study Bandstand, Gor du Vauseyon

Description and context

The bandstand is a construction typical of the nineteenth and early twentieth century (in the context of the development of cities and parks. In 1893, the bandstand is often a simple circular shelter in a public garden or a public square that can accommodate musicians for an outdoor concert. The bandstand is located in front of the Prussian house near the wheel of Gossliwil, at a place called Gor du Vauseyon, Neuchâtel.
It has an open octagonal structure. It is composed of a railing in the lower part and is surmounted by a canopy-shaped roof. The lower edge of the roof is adorned with a decorative frieze. The railing elements just like the decorative frieze seem to have been made of cast iron as well as the pillars probably. The repetitive elements of the frieze were molded by segment and then screwed on the rim of the roof (Figure 1a). The very structure of the roof is an assembly of rolled iron sheets (Figure 1b). A small stone staircase allows to climb in the kiosk. This bandstand comes from the rue de la Boine in Neuchâtel and was in the garden of Madame Gueissaz.

a b

Fig.1 : (a) Mounting of the railing in the lower part of the bandstand, (b) detailed view of the inner roof structure.

General observations and material analysis

Paint areas generally appear to be a very dark green blue color. Note that an entire area of the guardrails on either side of the entrance has a redder color at the volutes than the rest of the surface (Figure 3).
An area on the decorative roof frieze corresponds to a segment that appears to have undergone a bluish repainting test


Fig.2 : localisation of a blue painting test / Fig.3 : detailed view of the two different colors which can be observed on the railing

Methodology

The surfaces were characterized with the following methods in situ:

- The surfaces were first of all assessed visually and by digital USB microscopy (Dinolite®)

  XRF Analysis was performed using a Niton™ Thermoscientific XL3t GOLDD+ XRF Analyzer in a static modus (analyze time 45-45-90 sec., « general metals » option). Data collection and post-run processing were carried out using the Thermo Scientific™ Niton Data Transfer (NDT™) software.

The analysis does not make it possible to differentiate the ferrous alloys encountered (in particular the rolled elements and the molten products which should contain a higher carbon content). In addition, these analyzes also take into account the composition of the surface paint (Table 1). It is noted that lead is present in greater quantities on the protected parts (internal zone plate and sheltered roof transom), while the zones analyzed on the guardrail contain less lead and more iron.
The presence of iron in high proportion can be clearly linked to the presence of a ferrous substrate. The different percentages of lead observed could possibly be related to a larger amount of lead paint present on the parts that have not been directly leached by the rainwater and runoff at the roof level. A certain amount of titanium could be attributed to the presence of titaniferous pigments and not to a particular ferrous alloy, whereas the presence of aluminum and silicon is certainly attributable to contamination by the environment (atmospheric particles)

Localisation of the analysis spot	Pb	Fe	Ti	Al	Si
Railing 	17.6	70.2	1.7	2.3	4.4
Vertical pillar 	4.0	79.7	4.4	1.0	1.7
Horizontal roof pillar 	71.8	10.2	7.9	0.5	1.7
Internal side roof (sheet) 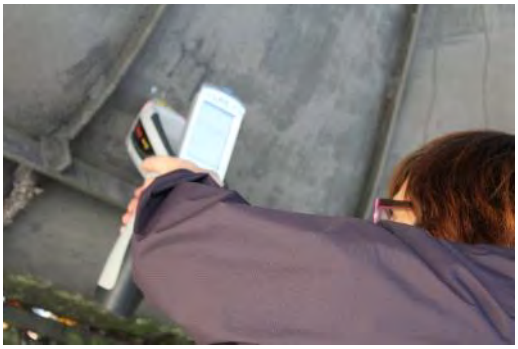	74.8	8.0	8.4	--	1.8

Table 1 : major and minor elements identified in the XRF analysis, expressed as atomic percentages.

Visuel examination of painting samples by microscopy

Four samples were taken and prepared in cross sections. The embedding was carried out with an epoxy resin of Araldite® type. Sampling was carried out on the various components of the kiosk: railing (Figure 4a and b), roof crossbar (Figure 4c) the roof plate (Figure 4d). As two different hues were observed at the railing level, two samples were taken from a brownish area and a darker area to compare the stratigraphy and constituent materials. The aim was to determine whether the difference in hue was related to a particular degradation of the paint or not, knowing that brown areas have a slightly more powdery appearance than other areas. The objective was also to better understand the delamination between the possible different layers of paint especially on the inside of the roof. The samples were observed under a binocular microscope and the cross

The study of the four cross sections makes it possible to affirm at first sight that the difference of color on the railing (more red-brown zone and darker and less altered green parts) is well linked to different paints. Indeed, sampling in a red-brown zone is the only one to have a superficial layer in which are red pigments. It should be noted that the sampling corresponds (n ° 1) is incomplete and that an underlying layer of minium could be observed visually in situ on the corresponding parts of the railing.

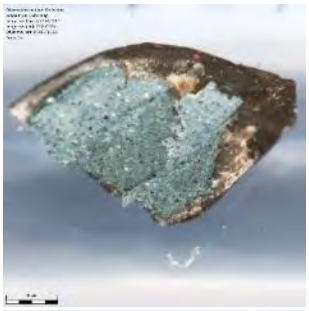

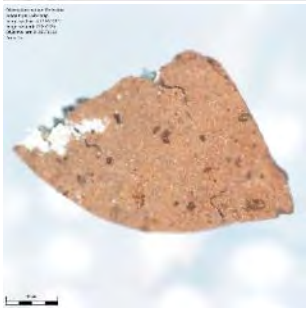

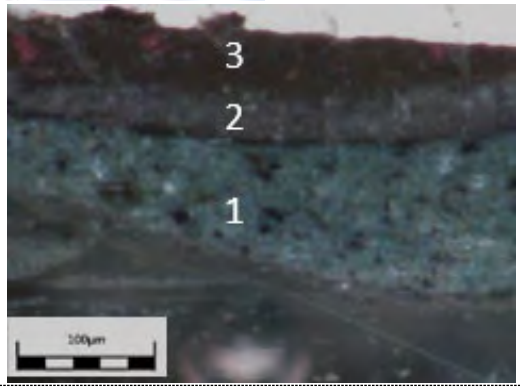

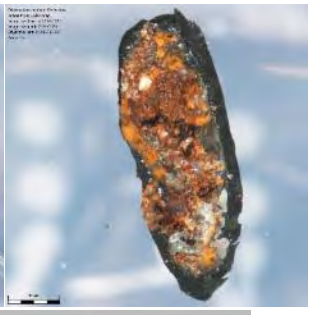

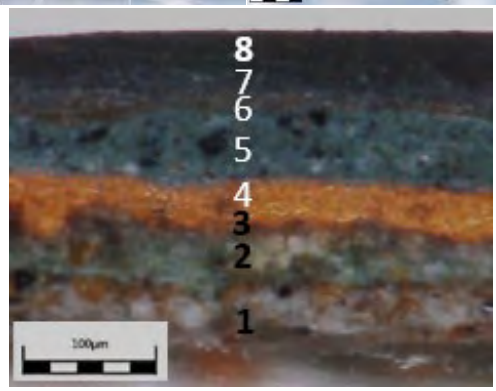

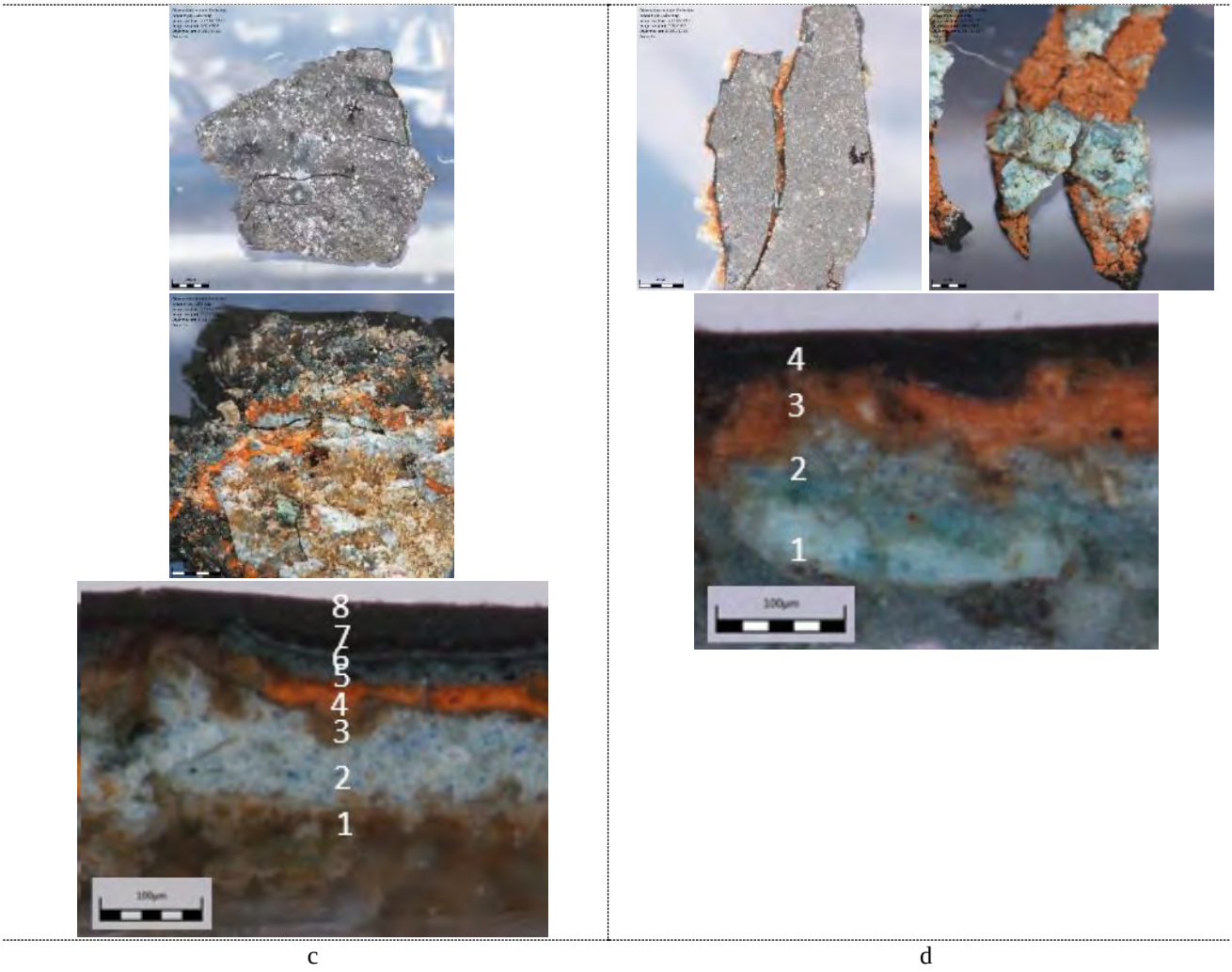

Fig.4 : samples, observations backside (left)-upper-side (right) and related cross-sections of a) volute of the railing (sample 1), b) pillar of the railing (sample 2), c) horizontal roofpillar (sample 3) et d) roof sheet (sample 4). Original enlargement of stereoscopic observations x121. Original enlargement of stereoscopic observations x361 (a-b-d) et x386 (c).

Elementary analysis of the painting samples

The cross sections of the paint samples 1, 2 and 3 were studied more precisely with scanning electron microscopy coupled with dispersive energy spectroscopy (SEM-EDS) (Table 3). The instrument used is a Philips XL30 scanning electron microscope, 10 mm working distance and 10^{-1}5 kV acceleration voltage. Carbon deposition was performed under vacuum to make the sample conductive. The imaging produced is in secondary electrons. Energy dispersive X-ray spectroscopy (EDS) analyzes make it possible to identify more precisely the elements present in the different layers of paints

As demonstrated during the in situ XRF analysis, lead is found, especially in the orange paint layer, which is usual for the anti-corrosion primer used for ferrous alloy paints. It is noted that the older layer (lying under the orange primer) mainly contains a certain

Amount of barium and strontium associated with the presence of sulfur (Figure 5). It

is also noted that the particle size of these older strata is larger than for the upper layer.

The deepest layer in contact with the iron support contains zinc and lead (lead and zinc oxides). It is also noted that only the most recent black layer (number 8) probably contains sulfur and barium, but also titanium, see Figure 5. In the deeper layer of Section 1 and 2, cobalt is also present .

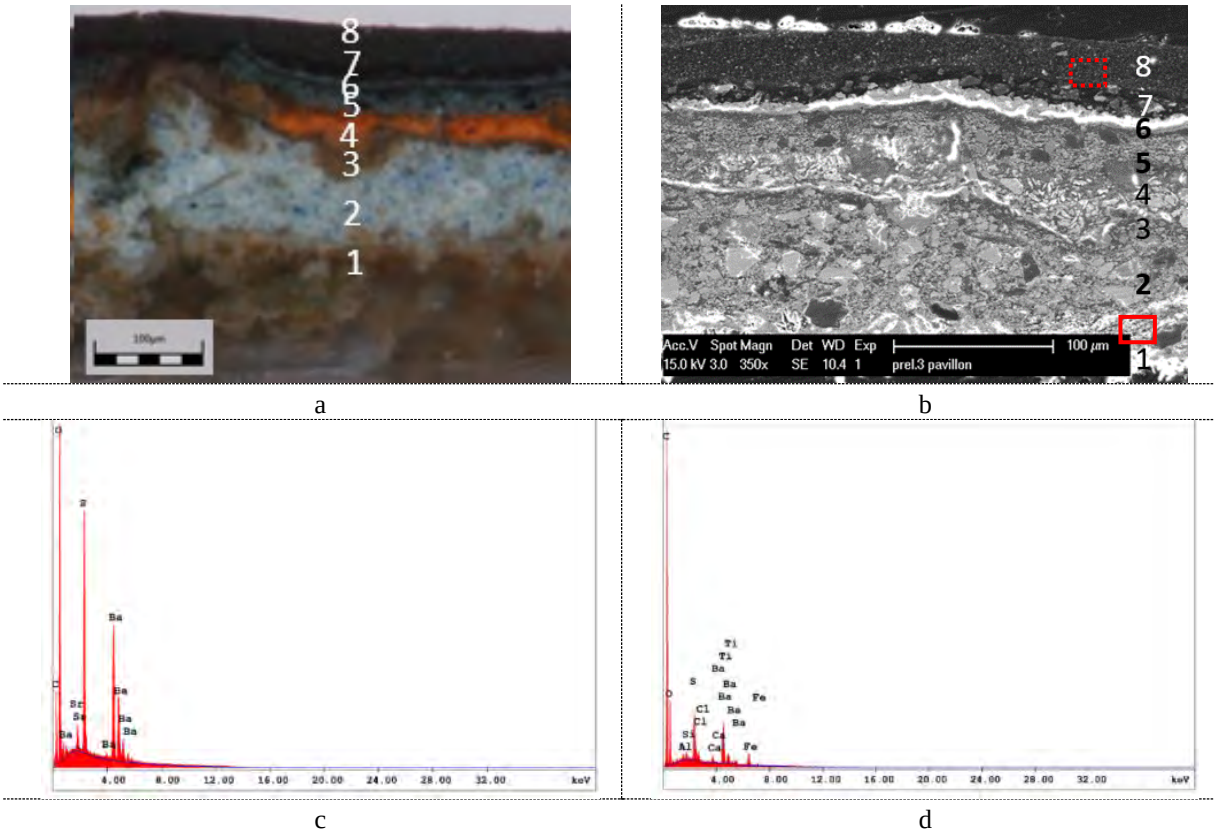

Fig. 5. Sample 3: a) cross-section, white-light microphotograph, original magnification x337, b) secondary electron image with localization of the EDS analysis zone of layer 2 (red rectangle) and layer 8 (rectangle discontinuous red), c) and d) corresponding EDS analysis spectra.

	Sample 1	**Sample 2**	**Sample 3**
layer	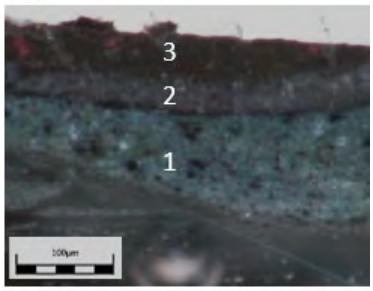	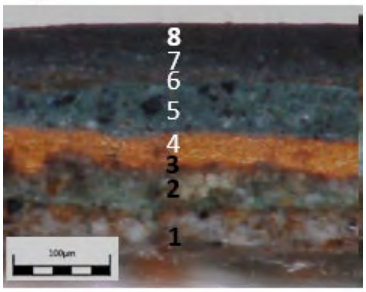	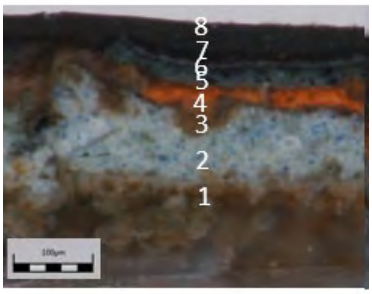
	railing	**Railing, pillar**	**roof**
8	-	-	**C, O** Fe, Ba, Ti *Cl, Ca, V, Co, Pb* *Dark grey layer*
7 *Red-brown layer*	**C, O** Pb Ba, *Al, Na, Si, Fe, Ca*	C, O, Al, Si *Pb, Ba, Fe, Na*	**C, O** Si *Pb, Ca*
6 *Thin grey layer*	**C, O** Pb *Cl, Si, Al*	**C, O** Si, Zn, Pb *Fe, Co, Mo?, Na*	**C, O** Pb *Zn, Ca*
Thin brownish layer (rust ?)	-	**C, O** Si, Fe , Pb, *S* *Ba, Co, Zn, Al, Cr, Ca*	-
5 *Grey-blue layer (white and black inclusions)*	**C, O, Pb** Co, Zn, Na, Fe, Ca, Si *Ba, Al*	**C, O** Al, Si, Pb, *Zn* *K, Ba, Fe, Co*	**C, O** Pb, Si, Fe, *Zn* *Al, Ba, Cr, Mn*
4 *Orange layer*	*Incomplete sample*	**C, Pb** *Na*	**C, O**, **Pb** *Ca*
3 *Intermediate rust layer*		*Not analyzed*	*Not analyzed*
2 *Blueish layer*		**C, O** S, Ba, Pb, Si *Na, Mg, Al, P, Fe, Co*	**C, O** Si, S, Pb, Sr, Ba *Na, Mg, Al, K, Ca, Cd*
1 *Light layer mixed with corrosion products*		**C, O** Pb, *Na* *Si, S, Ca, Ba, Fe, Co*	**C, O**, **Pb** Zn, Ca

Table 2 : Summary of the SEM-EDS interpretation performed on cross sections 1, 2 and 3. The major, secondary and trace elements are expressed in atomic %. Major element> 10%, secondary element> 1%, trace <1%. The double lines between strata 3-4 and 6-7 are an hypothesis concerning a possible renovation of the bandstand.

ATR-FTIR

Additional analyzes were performed by Fourier transform infrared spectroscopy on three cross sections (prel 1-3). The sections were placed directly under the objective of the infrared microscope and analyzed in attenuated total reflection mode (ATR). The spectra were acquired in a range of 4000-700 cm^{-1} using a Thermo Scientific Nicolet iN10MX microspectroscope connected to an ATR accessory equipped with a germanium crystal. The interpretation of the data obtained was performed using Thermo Scientific OmnicTM software. A total of 8 scans with a resolution of 4 cm^{-1} was conducted. The analyzes carried out on the first strata of sample 2 (Figures 6 and 7) point to the presence of a lead pigment in the layers of paint with the identification of basic lead carbonate.

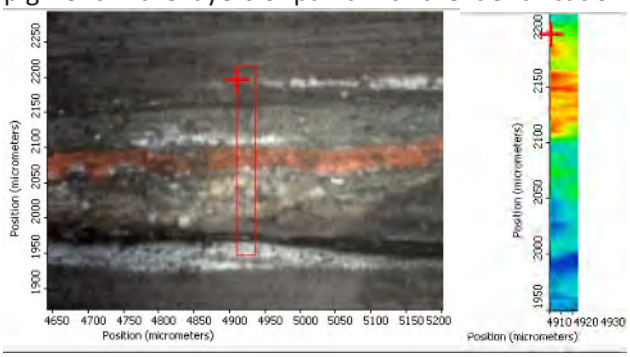

Fig.6. sample 2. : microscopic image of the cross-section showing with a red rectangle the mappingzone. Example of a false-color image which makes it possible to locate the presence of a lead pigment using the specific vibration at approximately 1400 cm^{-1} as (max-red intensity scale, min-blue).

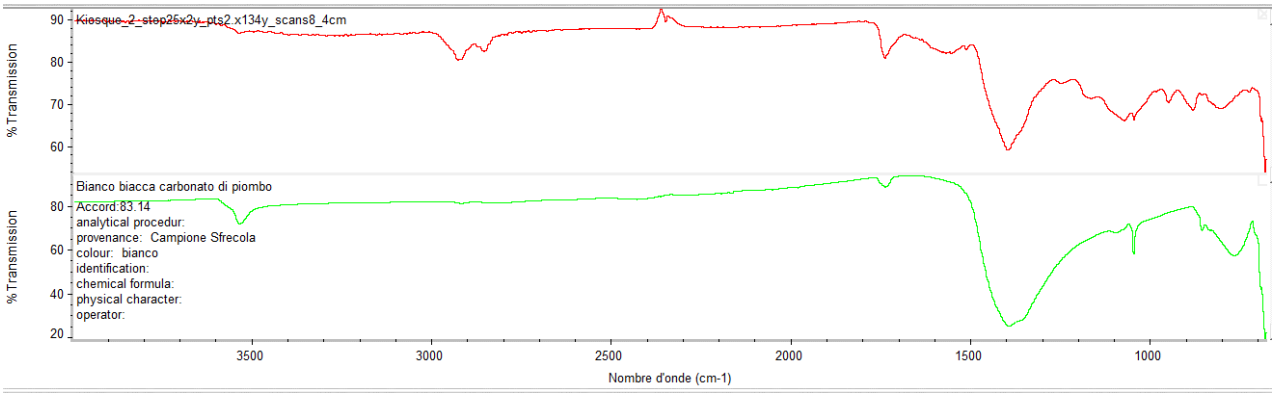

Fig.7. prel. 2 : spectrum extracted from the mapping (layer 5-8) and reference spectrum of lead white (below)

A spectrum was obtained from the same sample (No. 2), directly on the surface of the paint flake (outer layer 8, last repainted), see Figure 9.

For this sample, characteristic vibrations were obtained at 2850 and 2920 as well as at 1736, 1513, 1403, 1093, 777, 721 and 698 cm^{-1}. These absorbances can be attributed on the one hand to the presence of an organic binder probably oily (2850, 2920, 1736, 1093, 721), as well as to the presence of lead soaps, more specifically carboxylates, which include a peak characteristic around 1514 cm^{-1}. These are formed during the degradation of lead pigments (1403, 777, 698) in contact with an oily binder.

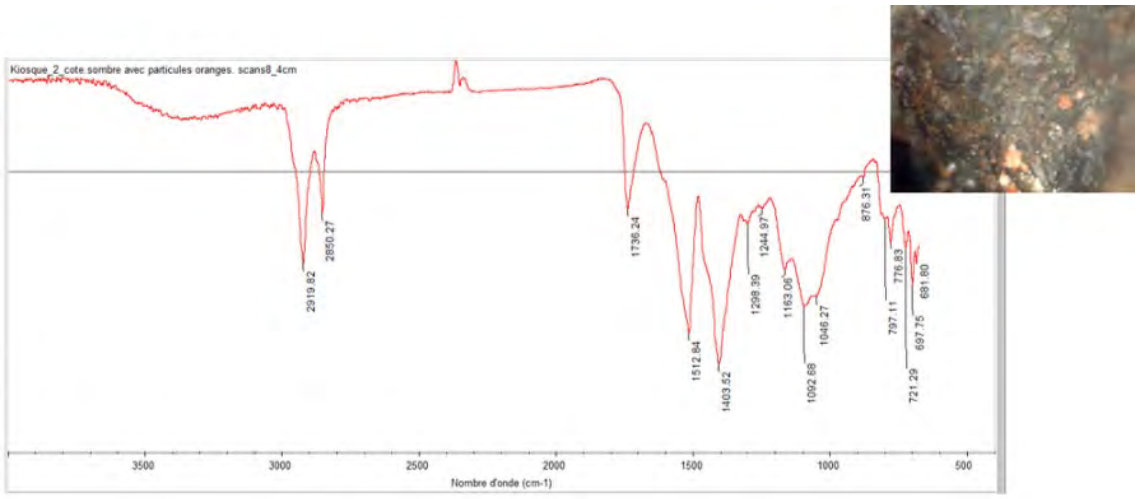

Fig.8. ATR-FTIR spectrum , surface of sample 2 (layer 8)

Analysis : conclusions

Exams and analyzes highlight at least two successive states of painting.

The earlier states of polychromy correspond to hues much more bright and clear bluish than the current finish. The difference in hue on the railing would be related to a local maintenance / repainting and not to a particular form of alteration of the paint. The opacifying fillers mainly used in paints are plumbers or correspond to sulphates of barium or strontium, clear pigments which gives a good opacity and is inexpensive.

The oldest layer in contact with the ferrous support (probably a primer) contains not only lead, but also zinc, the latter corresponds to a synthetic inorganic pigment based on zinc oxide (zinc white) which was used only from the second half of the nineteenth century in Europe. Also note the presence of cobalt in the oldest strata. Cobalt may have been used as a drying salt in the case of an oily binder or in the form of a blue pigment, which would corroborate with the color of the strata studied. The presence of a cadmium-based pigment (prel.3 stratum 2) indicates a repainting dating as early as the second half of the nineteenth century. The probable presence of a titanium oxide (a white opacifying pigment) can not be ruled out in the more recent stratum (prel 2, stratum 8). Titanium white was used from the beginning of the 20th century as a pigment in Europe. If necessary, a more in-depth study of the various pigments and binders present may be conducted.

State of condition

The actual surface state of the kiosk is very heterogeneous and it is noted that depending on the orientation and geometry of the constituent parts, the alterations are different or more or less developed (Table 4).

Type of degradation	image
A significant development of lichens (Biodetérioration) has been observed especially at the internal perforated parts of the decorative frieze of the roof.	
A large part of the roof sheets have suffered perforating corrosion, which causes water infiltration at the internal faces with rust flows	
Significant lifting of the painting associated with a development of ferrous corrosion is observed especially on the lower part of the railings.	
The dark paint on the inside of the roof has bleached, probably in contact with moisture. Delamination between the different layers of paint is also noticed.	
Parts exposed directly to bad weather and stagnant water are heavily rusted, the paint is no longer visible.	
The decorative frieze is in a particularly heterogeneous state, the surface presents different shades of colors generated by the iron oxides that have diffused into the paint, the leached areas and the biodeteriorated zones. Preferential corrosion has developed on the fastening systems	 

Table 3 :Summary of surface degradation phenomena

Conclusion/diagnosis

A number of successive repaints have been highlighted on the kiosk. The current shades are probably less bright and colorful than the older ones. The overall appearance is highly heterogeneous and unattractive due to alterations and various localized repaints.

Repainting without previous stripping could explain in particular the phenomena of paint delamination on the inner face of the roof. Without stripping to the substrate, the anti-corrosion effect is less effective and there may be incompatibility between newer and older layers (adhesion problem, mechanical stresses in the paint film related to a different composition layers). The finishing system is therefore defective.

The development of microorganisms at the level of the paint alters the latter in the long term and the applied paints no longer fulfill their role. In particular the perforating corrosion phenomena at the roof level pose an imminent conservation problem. In the long term, the sheets can lose their mechanical strength and be irretrievably lost. Repainting is highly recommended. The appropriate level of care should be determined before painting. The stripping will find a surface able to receive a painted protection. Consolidation and filling of perforations should be considered in order to avoid a greater loss of material at term.

Appendix 2: Case study Gossliwheel, Gor du Vauseyon

Surface characterization was carried out on the Gossliwil wheel and its conservation state assessed. The surfaces are entirely painted to protect the wheel from corrosion with a grey metallic layer. The original state of the surface (when in use) is not known and the historic layers have probably been stripped down. Two grey metallic painting layers were identified.

Methodology

The surfaces were characterized with the following methods in situ:

The surfaces were first of all assessed visually and by digital USB microscopy (Dinolite®)

XRF Analysis was performed using a Niton™ Thermoscientific XL3t GOLDD+ XRF Analyzer in a static modus (analyze time 45-45-90 sec., « general metals » option). Data collection and post-run processing were carried out using the Thermo Scientific™ Niton Data Transfer (NDT™) software.

In a second step, the painting layers were identified more precisely through samples collection. The sampling was done with a scalpel. The samples was observed under optical microscopy. Parts were embedded to produce cross-sections[19]. These cross-sections were characterized using the following methods:

The stratigraphy was examined with optical microscopy (Olympus micro LC).

The composition of the different painting layers was identified using Scanning Electron Microscopy coupled with Energy Dispersive X-Ray Spectroscopy (SEM-EDS). A Philips XL30 system at acceleration voltages of 10^{-1}5 kV and equipped with secondary and backscattered electrons detector was used. This system was coupled with an Oxford Instruments Energy Dispersive Spectroscopy (EDS) microprobe. A sputtering with carbon was carried out to obtain a conductive surface. Backscattered electrons images (BSE) *w*ere obtained and the elemental composition of the different layers was ascertained.

Four samples were taken. Only sample 3 (with a well preserved stratigraphy) was analyzed. Cross-sections were performed for sample 3 and 4 .

[19] An epoxy resin (Araldite®) was used

Localization of the sample	imaging
Sample 1: newer metal sheet (right side of the wheel), external painting layer	
Sample 2: newer metal sheet (right side of the wheel), external painting layer	
Sample 3: newer metal sheet (right side of the wheel) **Analyzed sample (FT-IR)**	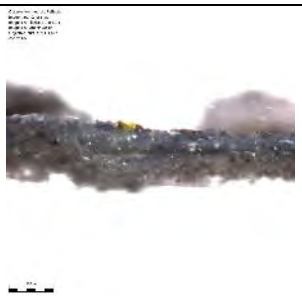 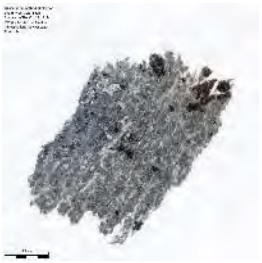 cross-section X434 / sample, external surface, X121
Sample 4: ancient metal sheet (left side of the wheel)	  cross-section X361 / sample, external surface, X121

Number and localization of samples

Results

XRF

XRF elementary analysis has been carried out on the three different parts of the wheel: iron sheet, supporting structure (spokes) and external wheel frame.

This technique doesn't allow to differentiate the iron alloys, in particular the laminated and casted products. Indeed, the latter should contain for example a higher carbon percentage but this light element is not detected by portable XRF instruments. Nevertheless, little amounts (less than 0,5%) of copper that could be linked to the iron alloy composition were observed. In fact, copper can be present in iron sheets as an alloy component to increase the corrosion resistance of the metal[20].

The analysis also gives information about the surface finishing. Aluminum was identified on the painted zones that were well preserved. Lower aluminum percentages were observed on the corroded areas and when this paint layer was removed. This lower percentage can be explained by the presence of residual aluminum-containing pigments and/or contamination by atmospheric deposits.

Barium, sulfur as well as zinc were also identified in lower concentrations. These elements can be linked to mineral filler in the paint layers. The presence of chlorine is probably due to surface contamination by atmospheric deposits.

Localization	Major elements (%)	Secondary elements (%)			Traces elements (%)						
Corroded sheet (zone of water stagnation)	Fe	Al	Si	Zn	Co	--	V	Ti	S	P	Cu
Corroded sheet after superficial cleaning (zone of water stagnation)	Fe	Al	Si	Zn	Co	--	V	Ti	S	P	Cu
Degraded painting (and metal corrosion)	Fe	Al	Si	Zn	Co	--	V	Ti	S	P	Cu
Metal sheet well preserved (superficial painting layer)	Fe	Al	Si	Zn	--	Mn	--	Ti	S	P	--
Sheet with paint losses	Fe	Al	Si	Zn	--	Mn	V	Ti	S	P	--
Painting well preserved (vertical wheel element)	**Fe**	Al	Si	Zn	Co	Mn	V	Ti	S	P	--
External strapping (painting well preserved)	**Fe**	Al	Si	Zn	Co	Mn	V	Ti	S	P	--

Major, secondary and trace elements detected

[20] http://notech.franceserv.com/materiau-acier.html

Microscopy

The examination of the cross-section indicates that two successive layers (fig. 27) were applied on the iron metallic substrate. The samples collected in an altered area shows that iron corrosion products are present inside the painting layer (red arrow, figure 28).

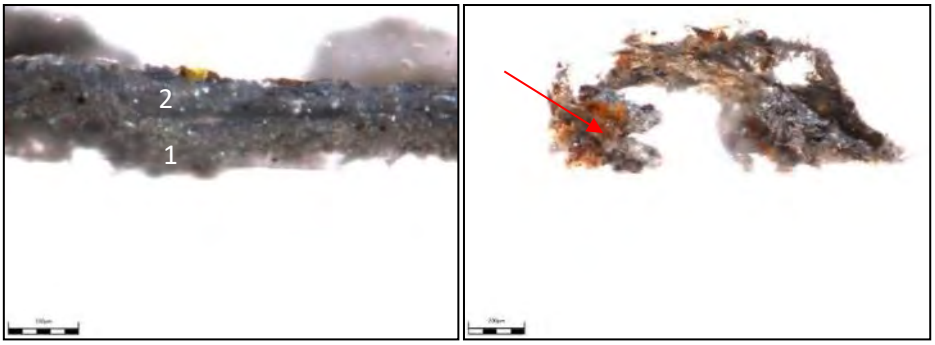

sample 3 (unaltered paint), magnification X434 / fig.28: sample 4 (altered area), magnification X169

SEM-EDS

BSE observations confirms the presence of two paint layers that have a poor adhesion on the metallic substrate as a void can be seen between the layers.
EDS analysis of the superficial layer (number 2) shows that the presence of zinc occurs at the time as sulfur and barium. For this reason, lithopone has likely been used as a pigment in this paint layer. This pigment is a mixture of barium sulfate and zinc sulfide, widely used as a white pigment powder as cheap material that provides good coverage.
On the contrary, zinc concentrations are not significant in the underneath layer (1). This layer seems to contain high percentages of C, O and Al. aluminum. Probably this paint layer is composed of pure metallic aluminum mixed with an organic binding medium that allow an easiest application of the paint on the metallic surface.. In fact, it is known that aluminum provides an inert barrier function as its electrochemical potential is lower than of an iron alloy.

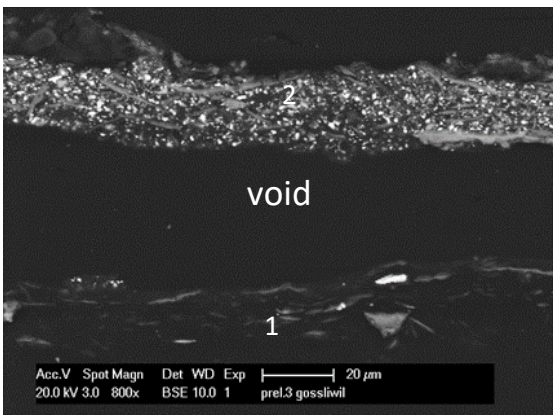

Sample 3 : cross-section, BSE Image with the area analyzed indicated by a red

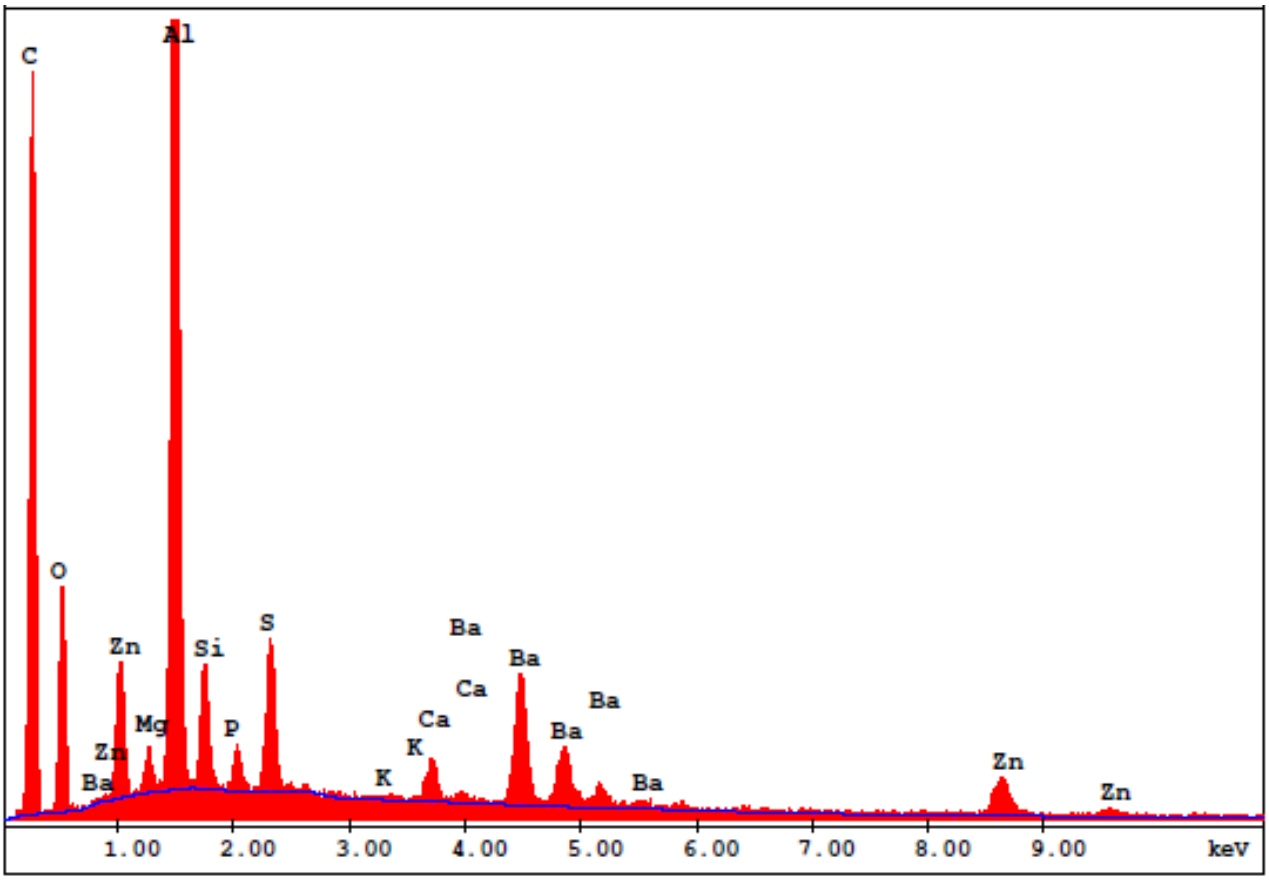

square related EDS spectrum

Conservation issues and diagnosis

Different conservation issues could be identified visually on the wheel:

The degradation of the paint (increased porosity, voids) led to the corrosion of the underlying iron alloy.

The wheel's geometry induces the presence of p sheltered areas and unsheltered areas that are directly exposed to rain and deposits (runoff areas). Rainwater can stagnate in the lower parts of the wheel and then infiltrates in between the iron sheets that are already partially perforated by corrosion. Differential aeration cells is developed next to the rivets and cause local corrosion phenomena.

Appendix 3: Case study absinthe dryer, Boveresse

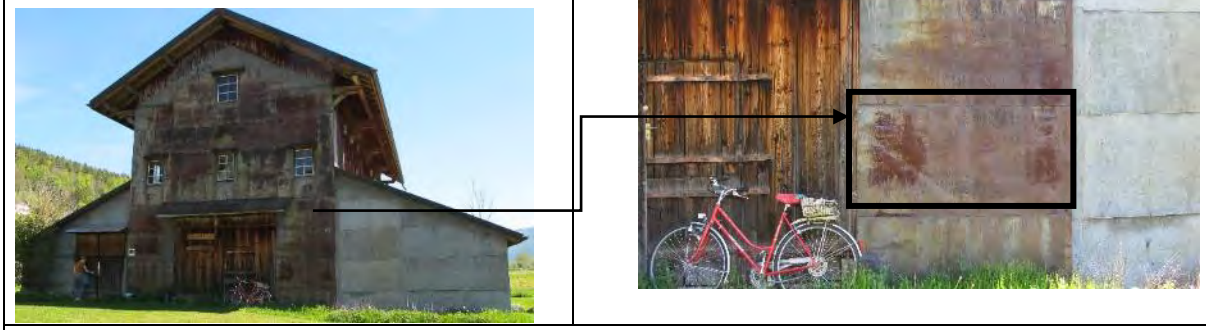

General view of the western frontside and localization of the test zone

Surface composition

The analysis confirm the presence of a galvanized iron alloy sheets which is heavily corroded (a majority of iron is detected on the surface. The presence of lead (as well as barium) could be due to the former presence of an anticorrosive paint (lead minium and barium sulfate) on the zinc layer. This residues are located on the middle part of the west facade, where a slightly opaque orange-colored powdery layer is visible. The latter has a similar appearance if compared to the paint used for the panel above the entrance

Localisation of the analyzed spot		**Major elements >10 % at**	**Minor elements**	**Trace elements (<0.1 % at)**
Western front side Galavanized iron plate	Zone 1 smooth greenish zone 	**Pb**	Fe, Sb, P, S, Al	Sn, Mn, Ca, Cl, Ba, Si
	Zone 2 painting 	**Pb**	Ca, Fe	Sb, Sn, Mn, Ba
	Zone 3 zone corroded iron 	**Pb**	Sb, As, Fe	Zn, Ni
	Zone 4 painting 	**Pb**	Fe, Sb, Al, Si, P, S	Zn, Sn, Ca, Cl

Major, minor and trace elements detected during XRF analysis on a metal sheet of the frontside, expressed as atomic percentage (%at).

Application of the biopatina gel, western side of the absinthe dryer

Degraded setting after storm

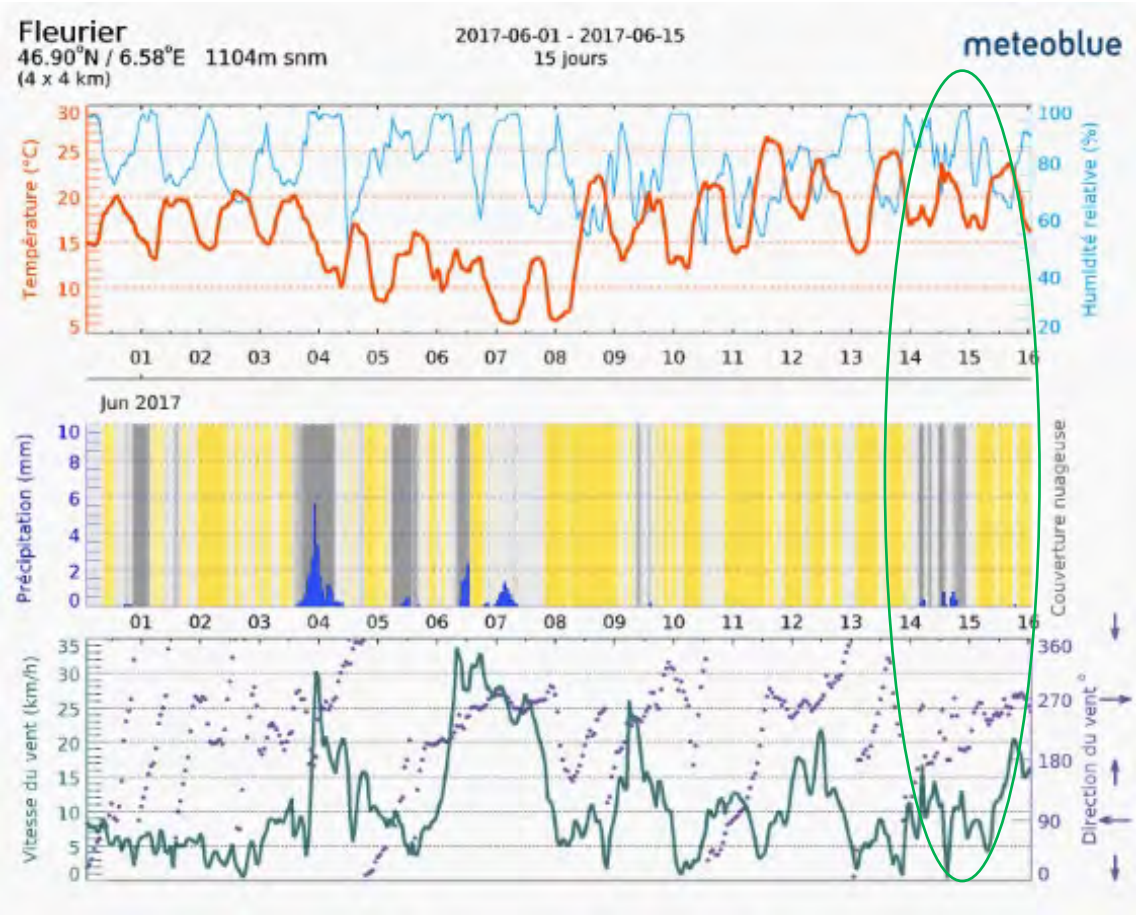

Climatic condition during the test period in the vicinity of the absinthe dryer

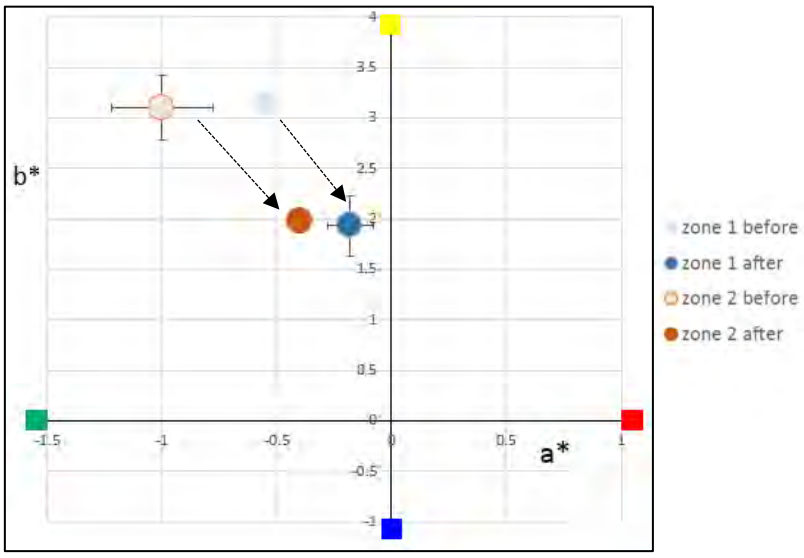

Colorimetric measurements obtained on the northern side of the dryer before and after biopatina

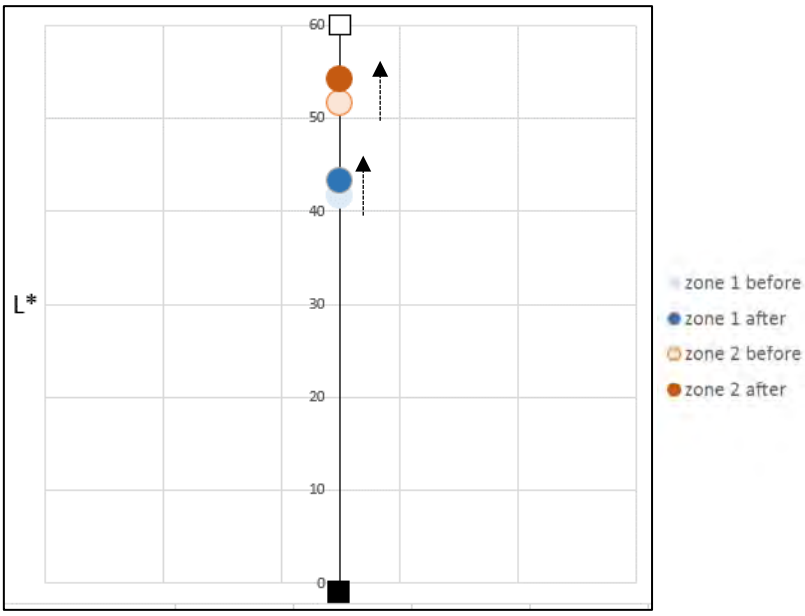

Colorimetric measurements obtained on the northern side of the dryer before and after biopatina

BEFORE AND AFTER TREATMENT: AVERAGE VALUES AND STANDARD DEVIATION										
sample	L*(D65)			a*(D65)			b*(D65)			gloss component
zone 1 BEFORE	41.72	±	2	-0.55	±	0.01	3.16	±	0.06	SCI
zone 2 BEFORE	51.67	±	3.38	-1.00	±	0.22	3.10	±	0.32	
zone 1 AFTER	43.25	±	0.81	-0.18	±	0.10	1.93	±	0.30	
zone 2 AFTER	54.14	±	2.67	-0.4	±	0.04	1.98	±	0.11	

Colorimetric measurements : Average values and standard-deviation

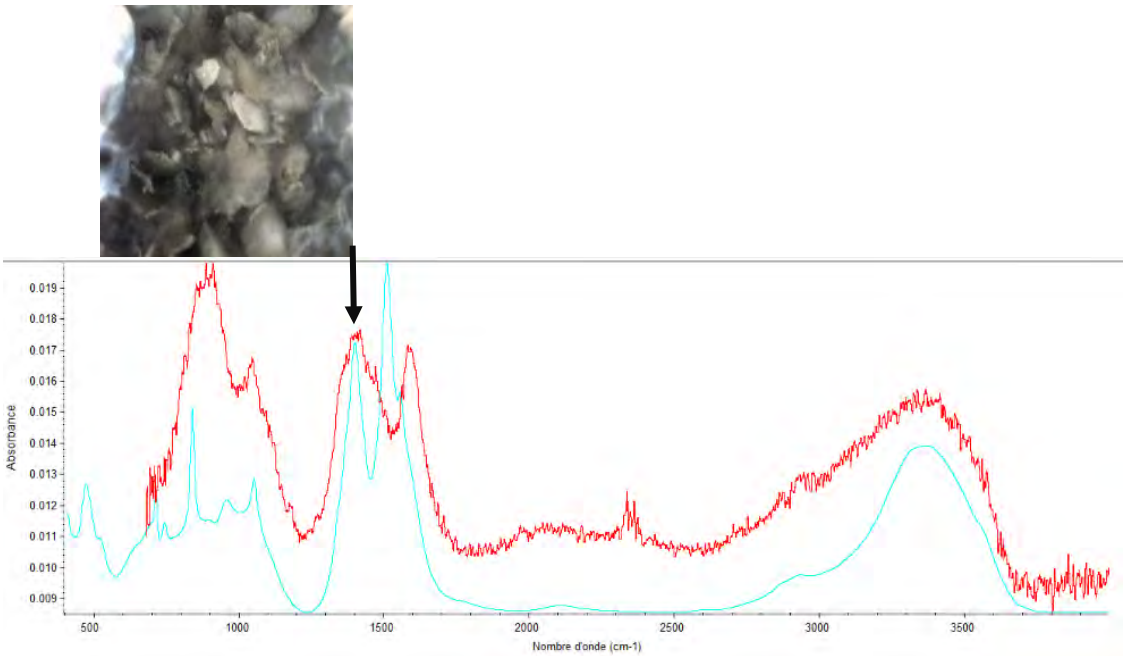

image and ATR-FTIR spectra obtained on a sample after biopatina treatment on the northern side of the dryer (red) and reference spectrum for hydrozincite (blue).

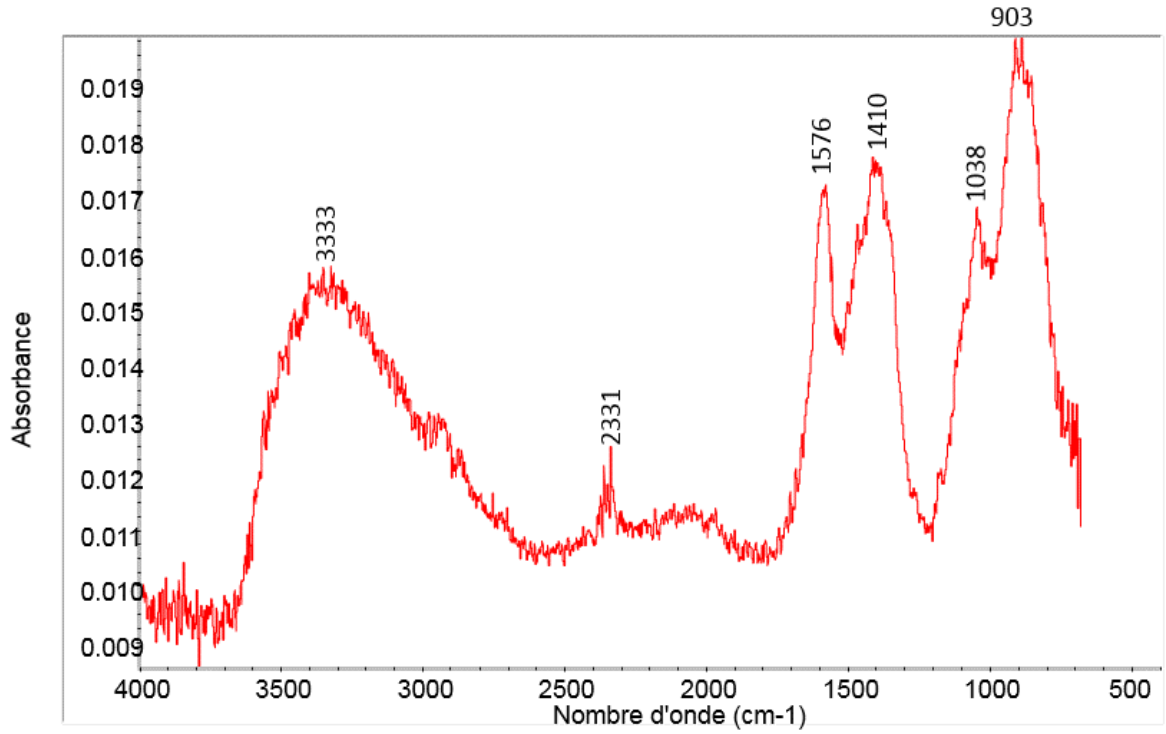

ATR-FTIR spectra obtained on a sample after biopatina treatment on the northern side of the dryer

Appendix 4: Case study Farelhaus, Biel

General view of the roof ledge located on the north-west side and localization of the test zone

General view of the test zone

Setting on the roof ledge

Destruction of the setting due to bad weather

Surface composition, roof ledge

The results obtained on the roof ledge covered by an aluminum sheet indicate the presence of an aluminum alloy containing a small amount of manganese and iron (see table below). This could be related to an Al-Mn-Fe alloy. The presence of Si could also indicate an Al- Mn-Fe-Si alloy, but a contamination of the surface by silicates (atmospheric deposits) is possible as the Si content seems much lower on zone 5 of the roof ledge. Zone 5 is the only aluminum surface analyzed that was already cleaned using an abrasive method.

Al-Mn-Fe-Si can be found in the following grades: 1XXX series and some alloys of the 8XXX series (e.g. 8111 and 8006) as well as 3XXX (e.g. 3003)[21]. 3003 and 3105 grades containing mainly a certain amount of Mn (0.3^{-1}.5 %), iron and silicon are typically used in architecture.

Localisation of the analyzed spot		**Major elements >10 % at**	**Minor elements**	**Trace elements (<0.1 % at)**
Roof ledge made of aluminium sheets	**Zone 1** 	**Al**	Fe, Mn, Si, P, S	Zn, Cu, Cr, Ti, K Cl
	Zone 2  Dark line	**Al**	Fe, Mn, Si, P, S	Ca, Zn, Cu, Cr, Ti, K, Cl
	Zone 3  Protected zone located next to the edge	**Al**	Fe, Mn, Si, S, Cl, P, Ca, Zn	K, Ti, Cr, Cu, Zn,
	Zone 4  Roof edge (street side)	**Al**	Fe, Mn, Si, P, S	Zn, Cu, Ti, K, Cl
	Zone 5  Cleaned area (street side)	**Al**	Fe, Mn, Si, S	Zn, Cu, Cr, P, Cl

Major, minor and trace elements detected during XRF analysis on roof ledge, expressed as atomic percentage (%at).

[21] Nikolay A. Belov, Dmitry G. Eskin, Andrey A. Aksenov, Multicomponent Phase Diagrams: Applications for Commercial Aluminum Alloys, 1st ed., Amsterdam ; Boston : Elsevier, 2005, 413p.

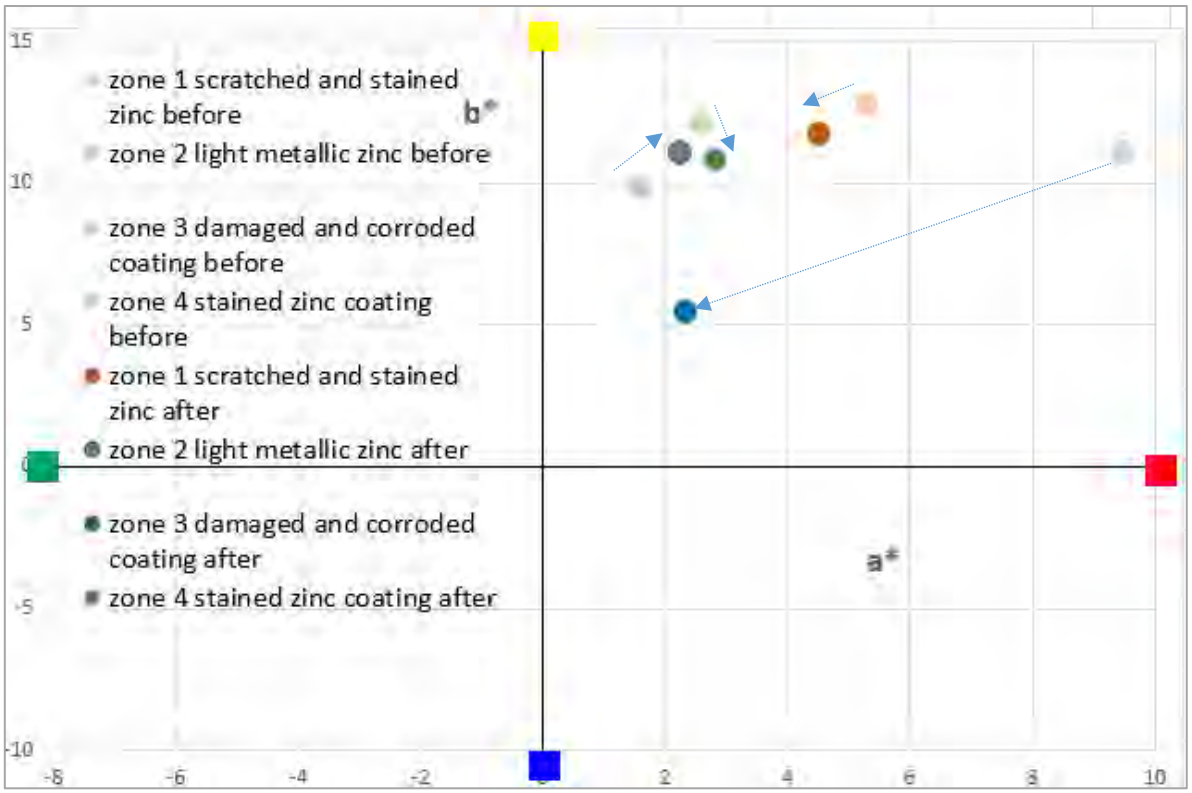

Results of the colorimetric results performed on the zinc coated iron sheet of the bench before and after biopatina treatment . Each point represents the averaged value of the measurements recorded on one zone.

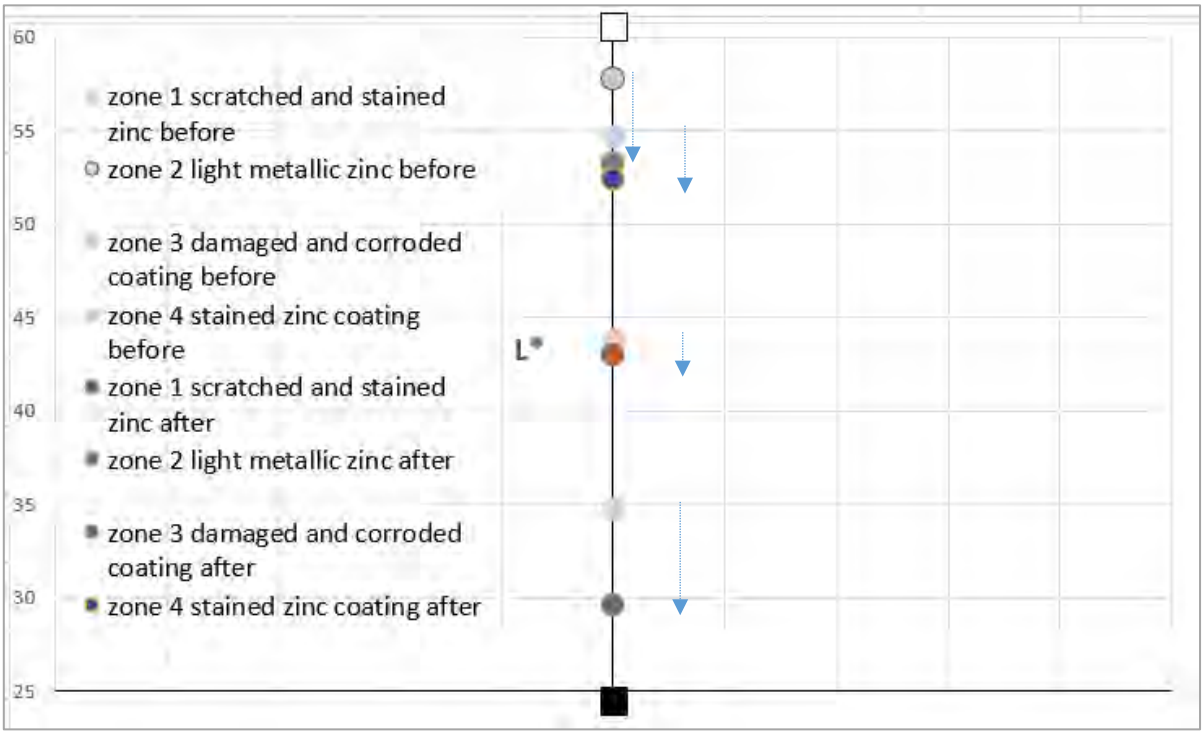

Results of the colorimetric results performed on the zinc coated iron sheet of the bench before and after biopatina treatment . Each point represents the averaged value of the measurements recorded on one zone.

AVERAGE VALUES AND STANDARD DEVIATION										
sample	L*(D65)			a*(D65)			b*(D65)			gloss component
zone 1 before	43.83	±	0.32	5.32	±	0.15	12.72	±	0.45	
zone 1 after	43.00	±	0.29	4.55	±	0.12	11.65	±	0.25	
zone 2 before	57.81	±	1.85	1.59	±	0.28	9.84	±	1.02	
zone 2 after	53.30	±	2.25	2.27	±	0.57	11.02	±	0.84	SCI
zone 3 before	34.80	±	0.12	9.51	±	0.21	11.05	±	0.20	
zone 3 after	29.59	±	0.55	2.35	±	0.22	5.40	±	0.23	
zone 4 before	54.70	±	0.88	2.59	±	0.55	12.09	±	0.58	
zone 4 after	52.42	±	0.97	2.85	±	0.07	10.77	±	0.41	

Colorimetric measurements ; Average values and standard deviation

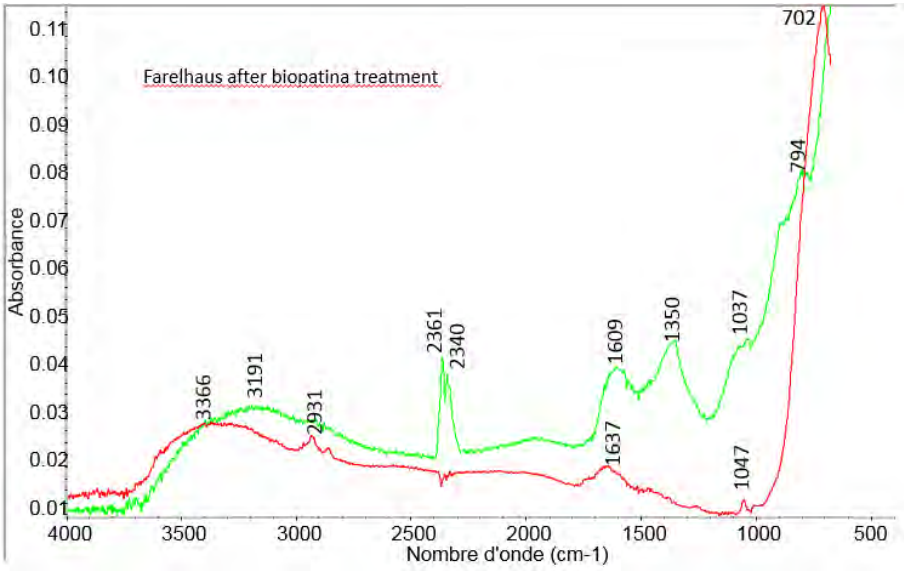

FTIR analysis on a corrosion sample after treatment

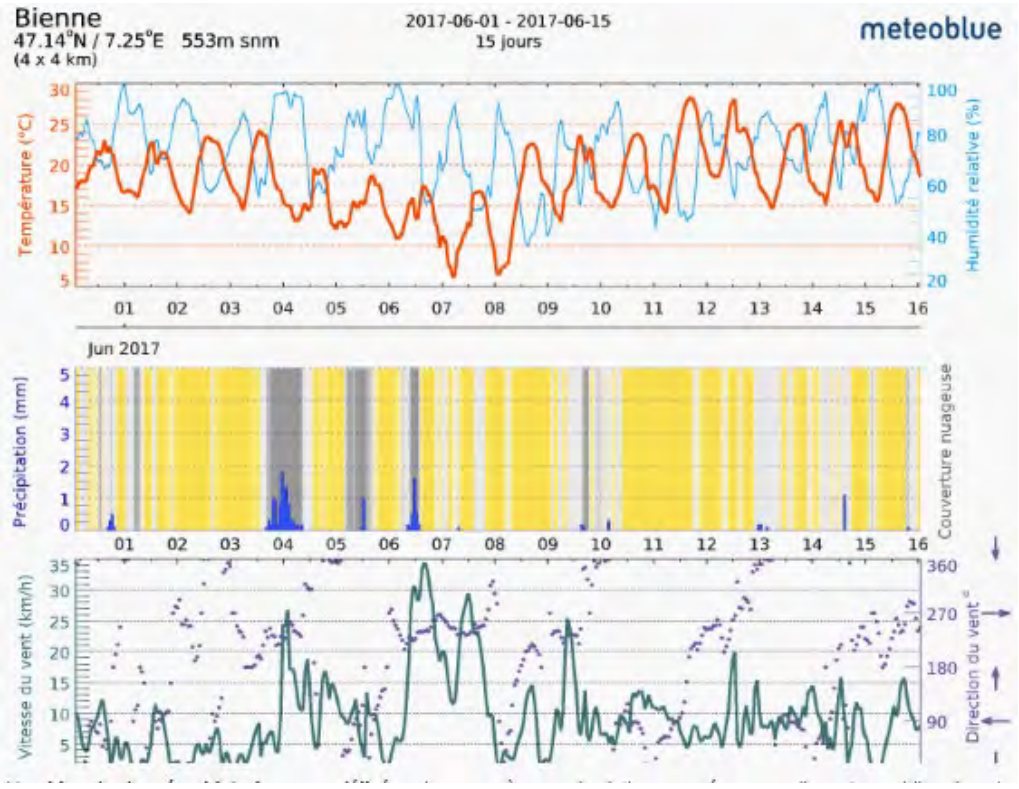

Climatic condition during the test period in the vicinity of the Farelhaus

Appendix 5: Reference data for analysis

ZINC COMPOUNDS

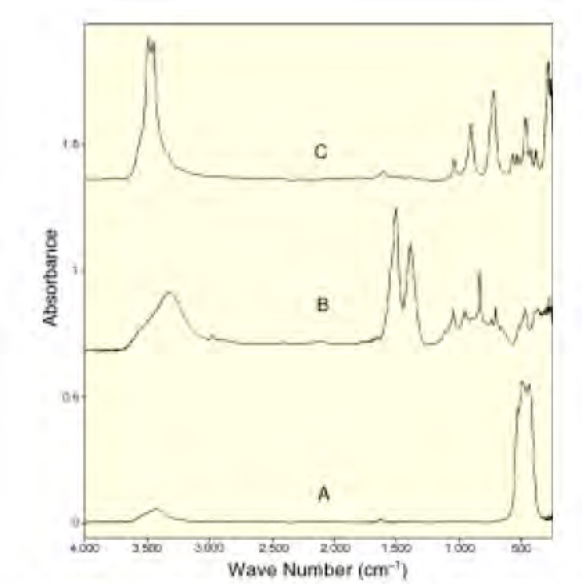

IR spectra of reference compounds A) zinc oxide, B) hydrozincite and C) simonkolleite

Reference: F. Zhu, D. Persson, D. Thierry, and C. Taxen*, Formation of Corrosion Products on Open and Confined Zinc Surfaces Exposed to Periodic Wet/Dry Conditions. In. NACE International, corrosion, December 2000, pp.1256^{-1}265

Comment: Spectra of three reference compounds (namely zincoxide, hydrozincite, and simonkolleite) are shown in Figure 6. The different reference compounds have characteristic absorption bands at different positions. The absorption seen in the 350-cm–1 to 600-cm–1 region of the zinc oxide spectrum corresponds to the zinc-oxygen bond. Hydrozincite has strong bands at 1,380 cm–1 and 1,510 cm–1, corresponding to the asymmetric stretching vibrations of the carbonate ion. Other modes attributable to carbonate are present at 1,040 cm–1 (the symmetric stretch), 830 cm–1, 735 cm–1, and 675 cm–1. The sharp bands associated with O-H stretching around 3,400 cm–1 are characteristic of simonkolleite, and bands at 895 cm–1 and 700 cm–1 arise from hydroxide deformations.

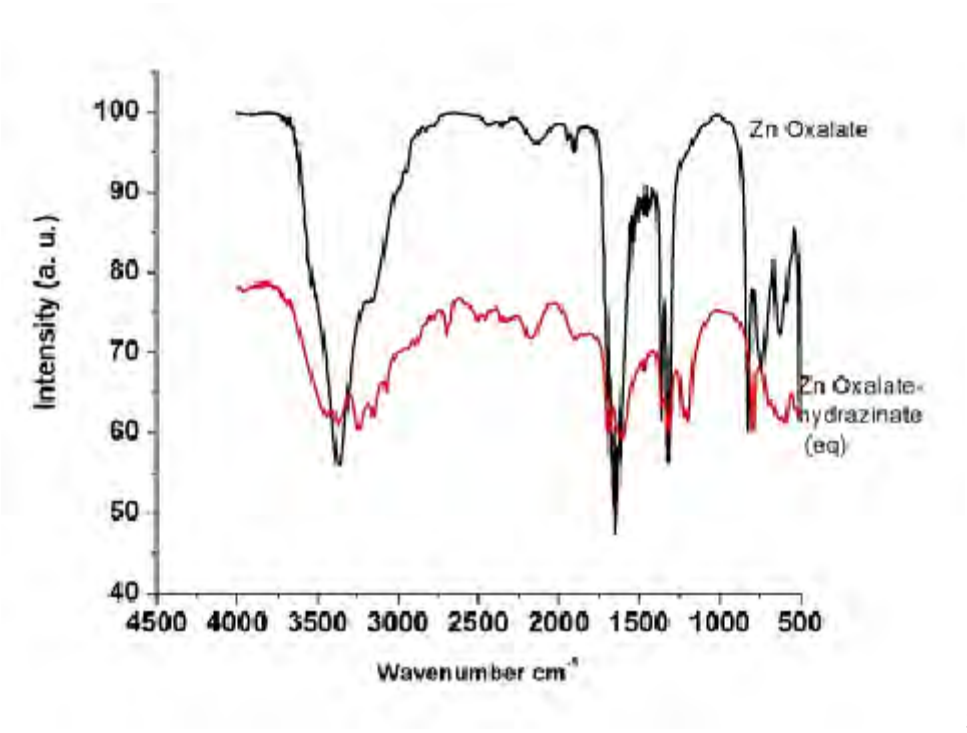

$

Borker, Vrinda & Karmali, Rajashri & Rane, Koyar. (2014). Comparison of degradation of methylene blue dye by ZnO, N doped ZnO and iron ore rejects. European Chemical Bulletin. 3. 520-529.

ALUMINUM COMPOUNDS

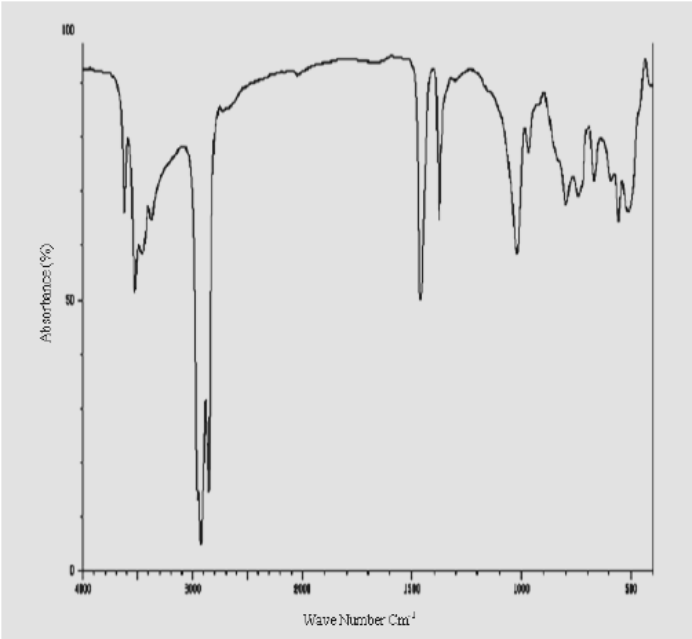

FT-IR spectrum of aluminum hydroxide

Reference: International, Chemistry & Bhatti, Muhammad Pervaiz & Mehmood, Komal & A. Raza, Muhammad & Rasheed, Ayub & Ahmad, Shakeel & Adnan, Ahmad & Iqbal, Munawar. (2015). Extraction and applications of aluminum hydroxide from bauxite for commercial consumption. Chemistry International. 1. $99^{-1}02$.

Comment: stretching frequencies for hydroxyl group were observed at 3632 $^{-1}$ $^{-1}$ cm and 942 cm^{-1} , respectively.

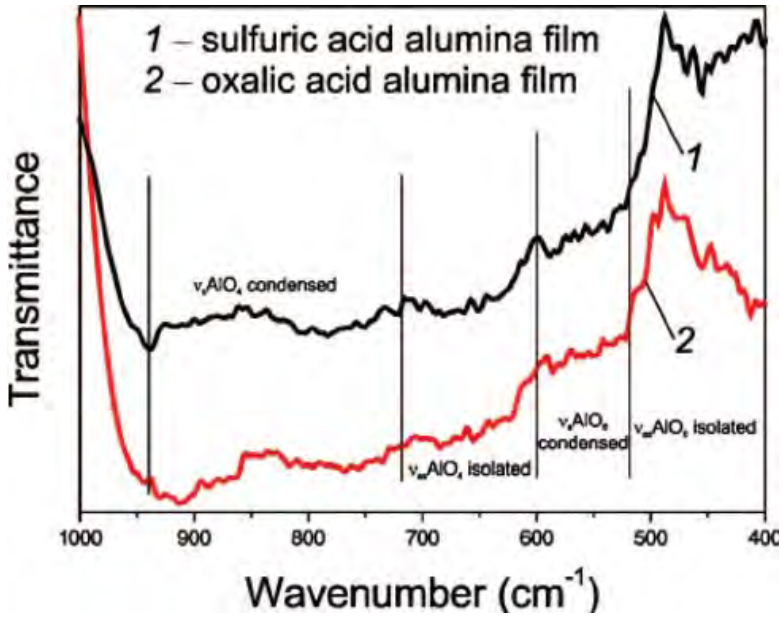

FT-IR spectra of sulfuric alumina and oxalic alumina films

Reference: Fernando Fondeur & J. L. Koenig (2006) FT-IR Characterization of the Surface of Aluminum as a Result of Chemical Treatment, The Journal of Adhesion, 40:2-4, 189-205, DOI: 10.1080/00218469308031284

COPPER COMPOUNDS

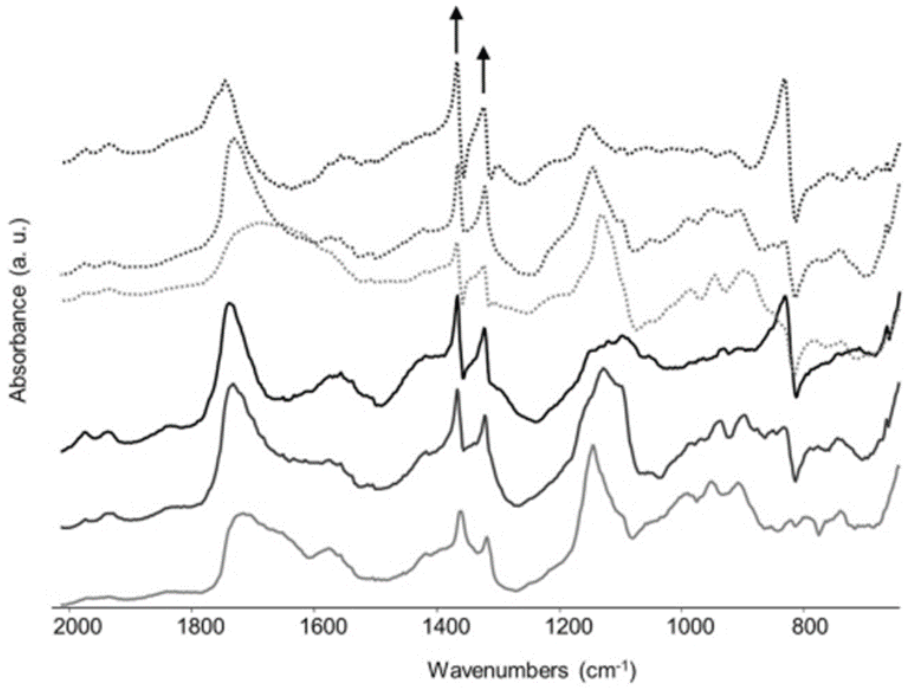

reference : Joseph Edith, Cario Sylvie, Simon Anaële, Wörle Marie, Mazzeo Rocco, Junier Pilar, Job Daniel, Protection of Metal Artifacts with the Formation of Metal–Oxalates Complexes by Beauveria bassiana, Frontiers in Microbiology, vol. 2, 2012

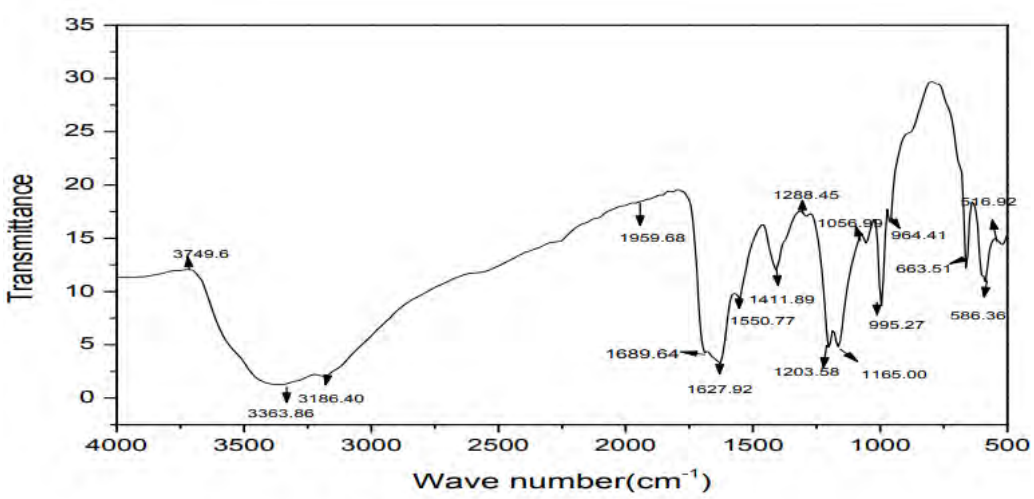

Fig. 3 FTIR spectrum of CuS

Reference : S.Umasankari , R.Anitha, SYNTHESIZE AND CHARACTERIZATION OF COPPER SULFIDE (CuS) NANOPARTICLE USING PRECIPITATION METHOD. In: International Journal of Advanced technology in Engineering and Science, Vol. No5, Issue No 02, February 2017

Interactive IRUG Spectrum

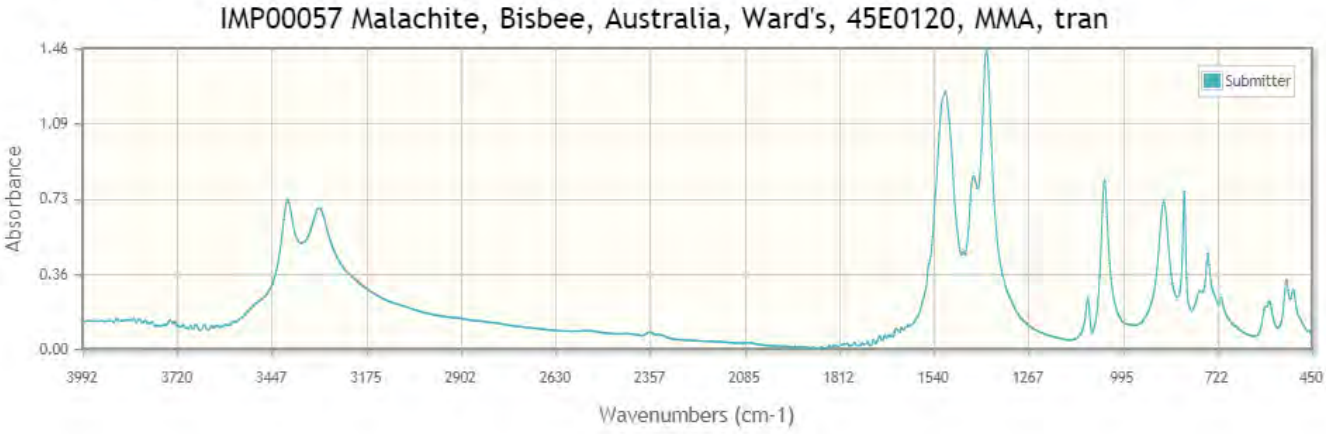

Interactive IRUG Spectrum

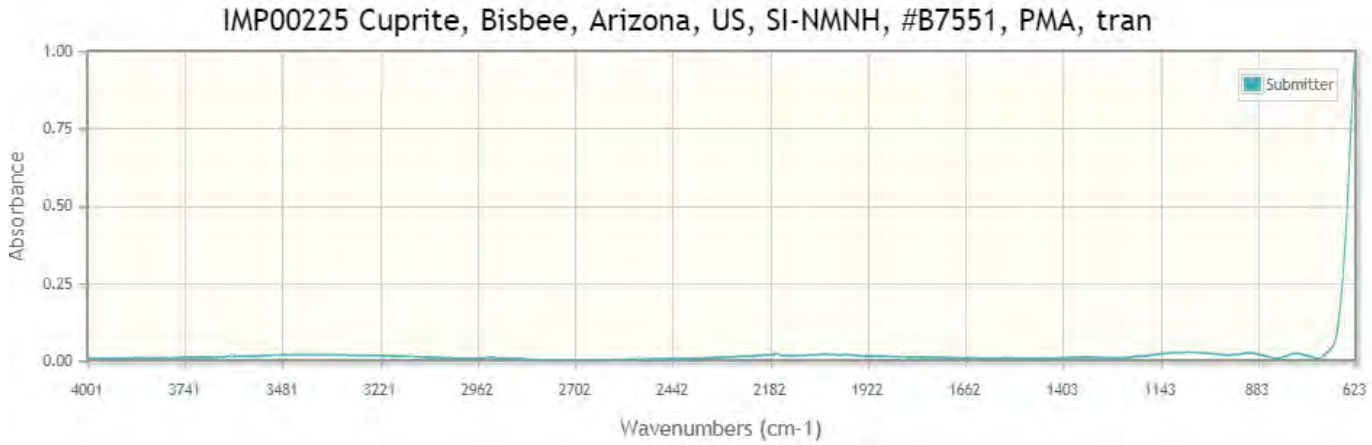

Interactive IRUG Spectrum

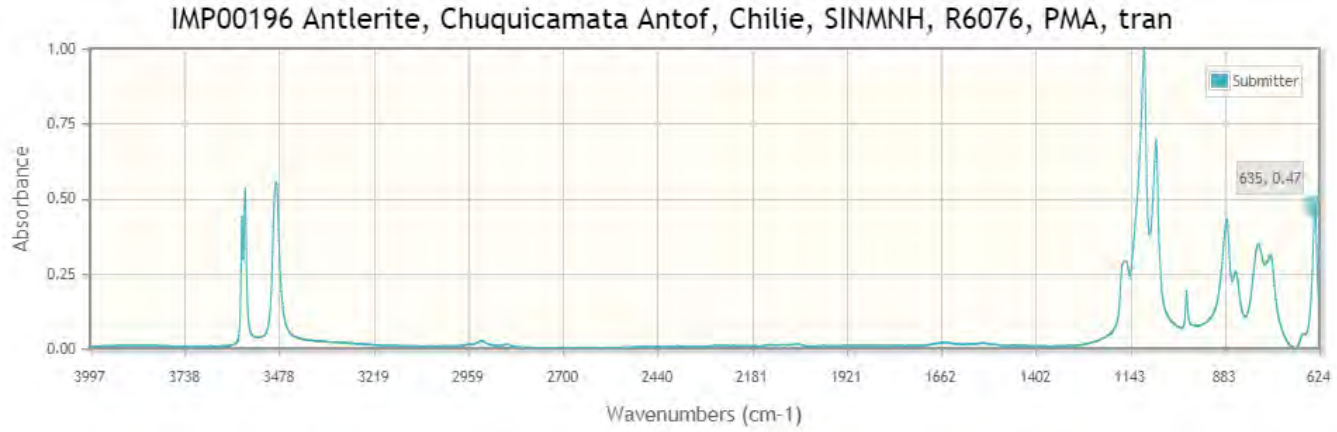

Interactive IRUG Spectrum

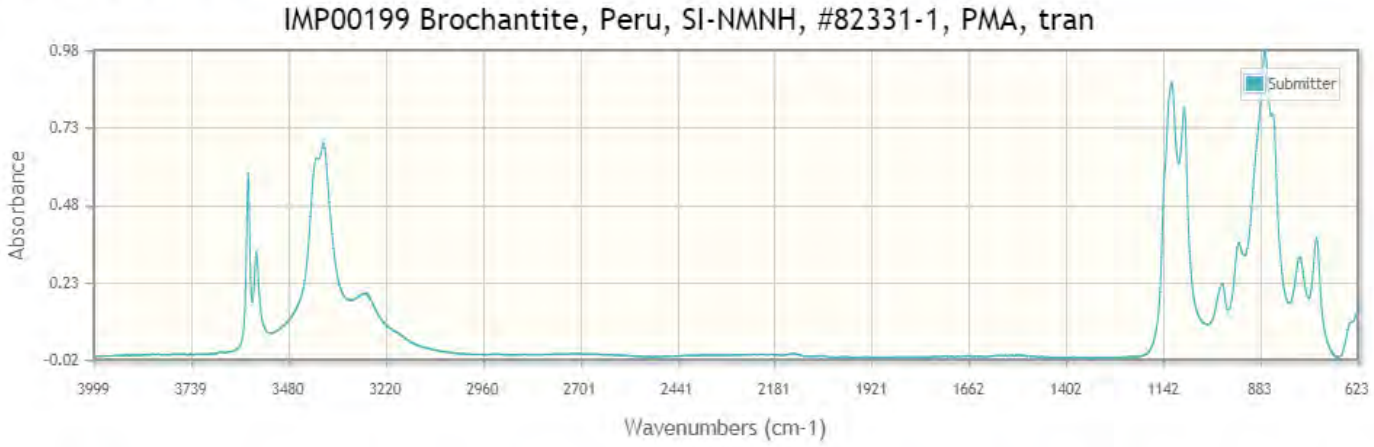

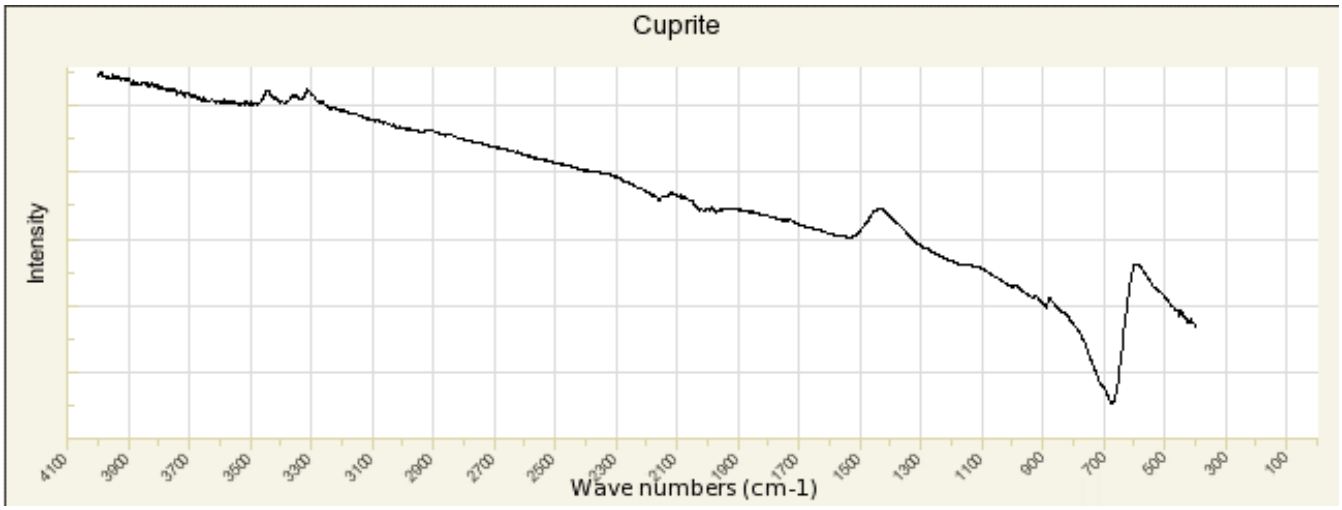

Reference: http://rruff.info/Cuprite/R050384

IRON COMPOUNDS

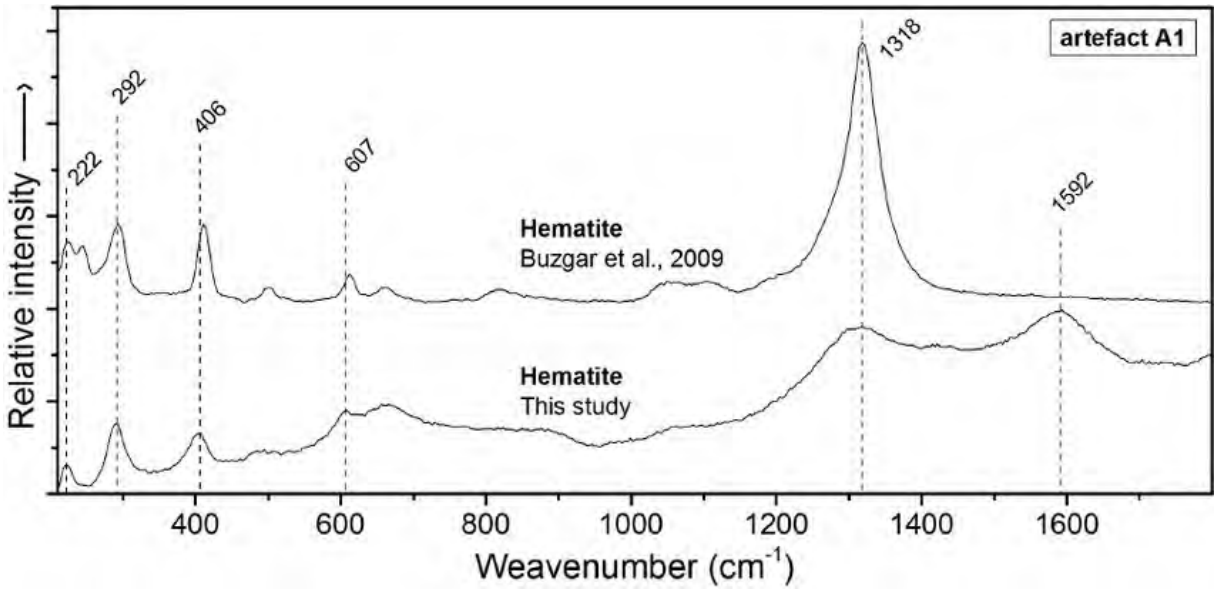

Reference: Buzgar, Nicolae & Apopei, Andrei & Diaconu, V & Buzatu, Andrei. (2013). The composition and source of the raw material of two stone axes of Late Bronze Age from Neamț County (Romania) - A Raman study. Analele științifice ale Universității "Al. I. Cuza" din Iași, Seria Geologie. 59. 5-22.

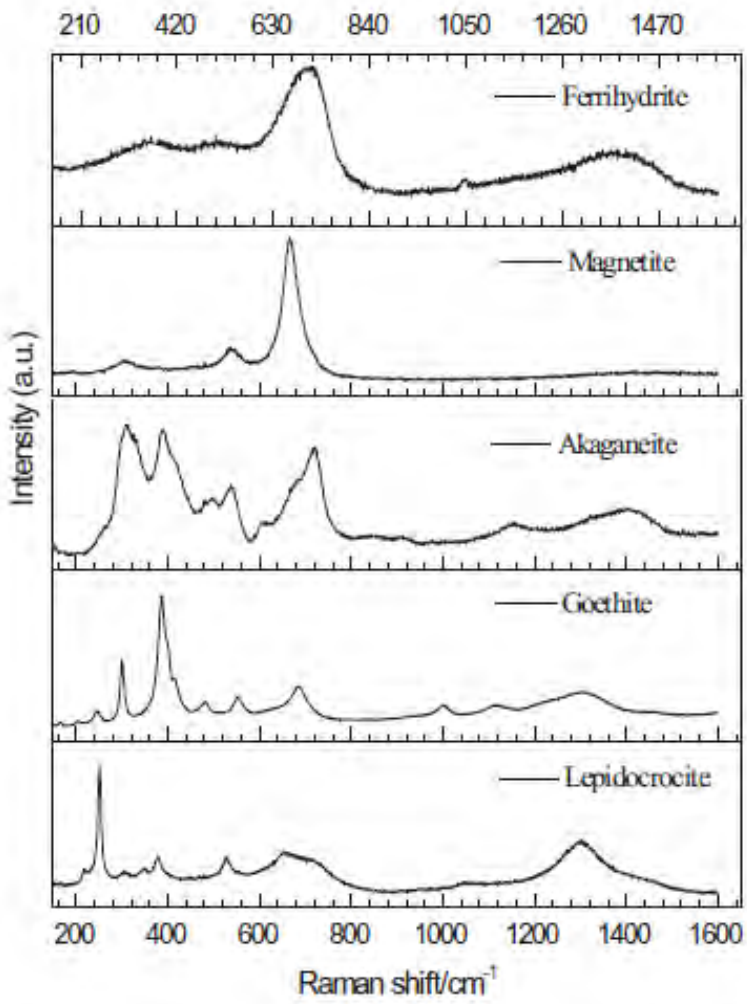

Fig. 2. Reference spectra for pure phases obtained at 532 nm, 80 μW [27].

Reference: Heidis Cano, Delphine Neff, Manuel Morcillo, Philippe Dillmann, Iván Diaz, Daniel de la Fuente, Characterization of corrosion products formed on Ni 2.4 wt%–Cu 0.5 wt%–Cr 0.5 wt% weathering steel exposed in marine atmospheres. In: Corrosion Science 87 (2014) 438–451

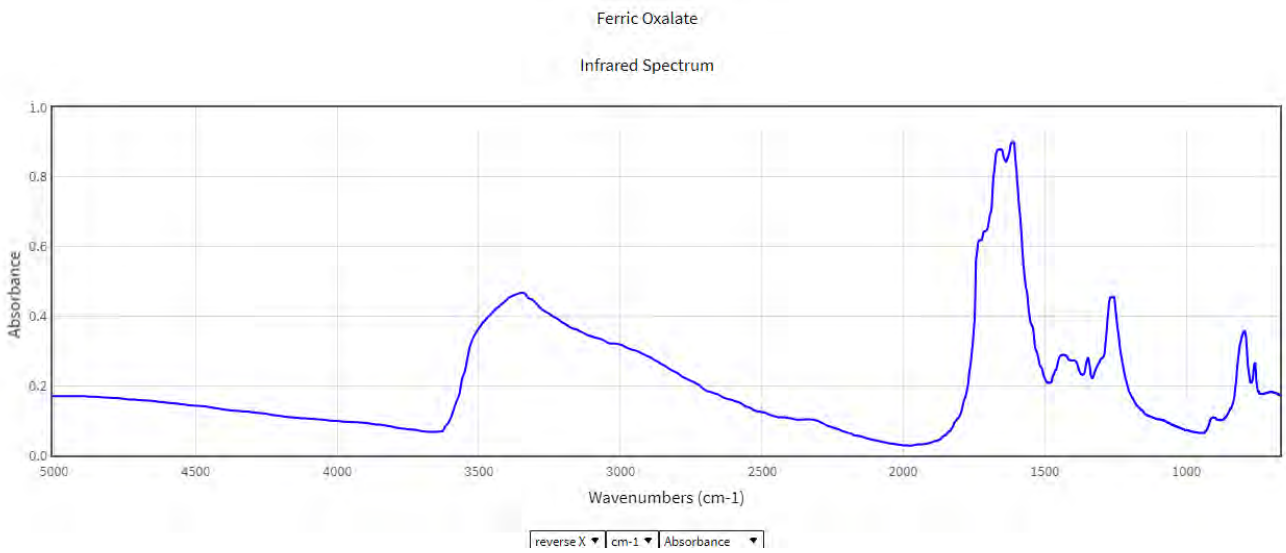

Reference: https://webbook.nist.gov/cgi/inchi?ID=B6000084&Mask=80

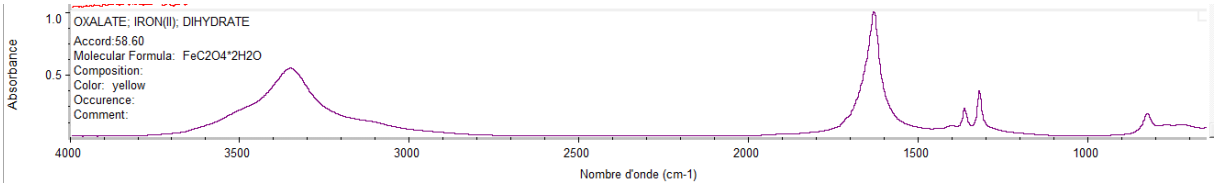

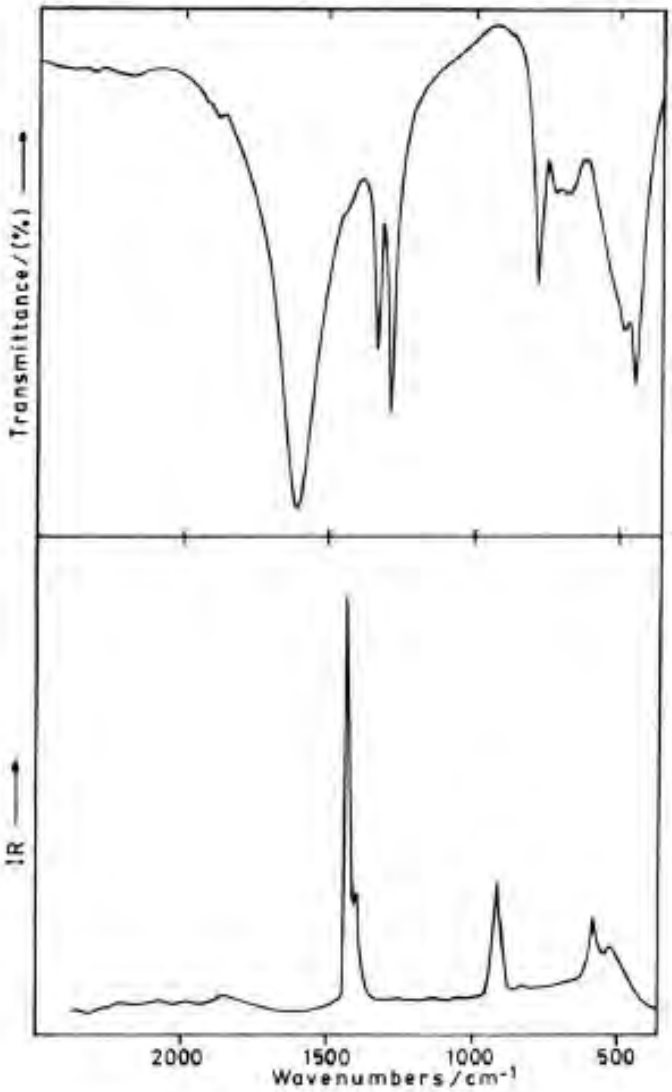

Figure 2. FT-Infrared (above) and Raman spectra (below) of α-$Fe(C_2O_4)\cdot 2H_2O$ in the spectral range between 2000 and 400 cm^{-1}.

Reference: Maria C. D'Antonio et al., Spectroscopic investigations of iron(II) and iron(III) oxalates.In: J. Braz. Chem. Soc. vol.20 no.3 São Paulo 2009

Appendix 6: colorimetric measurements- average values and standard deviation

AVERAGE VALUES AND STANDARD DEVIATION										
sample		L*(D65)			a*(D65)			b*(D65)		
A	T0 before exposure	82.81	±	1.07	0.02	±	0.01	0.99	±	0.1
	T0 after exposure	80.97	±	1.4	0.11	±	0.03	2.3	±	0.2
	T4 before biopatina	84.29	±	1.45	0.007	±	0.02	0.94	±	0.1
	T4 after biopatina	87.3	±	1.15	-0.41	±	0.49	1.3	±	0.1
	T4 after exposure	85.65	±	1.39	0.04	±	0.04	2.41	±	1.3
AA	T0 before exposure	81.61	±	0.04	-0.63	±	0	6.47	±	0
	T0 after exposure	82	±	1.05	-0.47	±	0.05	6.96	±	0.2
	T4 before biopatina	81.82	±	0.11	-0.63	±	0.008	6.36	±	0
	T4 after biopatina	82.19	±	0.03	-0.53	±	0.008	6.69	±	0
	T4 after exposure	80.74	±	2.17	-0.43	±	0.04	7.19	±	0.4
C	T0 before exposure	84.12	±	2.95	15.46	±	0.17	18.96	±	0.3
	T0 after exposure	34.97	±	0.66	2.28	±	1.9	3.23	±	1.7
	T4 before biopatina	85.43	±	2.68	15.33	±	0.14	18.82	±	0.1
	T4 after biopatina	79.85	±	1.94	16.66	±	0.22	19.12	±	0.2
	T4 after exposure	35.78	±	0.95	1.39	±	1.12	3.41	±	2.1
CA	T0 before exposure	54.91	±	0.6	-8.9	±	0.35	6.78	±	1.2
	T0 after exposure	54.15	±	0.91	-8.48	±	0.35	7.02	±	1.3
	T4 before biopatina	nm	±	nm	nm	±	nm	nm	±	nm
	T4 after biopatina	58.09	±	1.88	-9.12	±	0.69	7.71	±	1.4
	T4 after exposure	59.04	±	1.69	-14.93	±	0.28	4.62	±	1
CS	T0 before exposure	40.55	±	0.68	18.45	±	0.27	27.51	±	0.5
	T0 after exposure	36.42	±	1.51	20	±	2.26	25.42	±	3.5
	T4 before biopatina	40.15	±	0.68	18.51	±	0.46	18.51	±	0.5
	T4 after biopatina	42.07	±	0.45	11.11	±	0.58	27.56	±	0.8
	T4 after exposure	36.6	±	2.42	13.49	±	1.96	17.52	±	3.1
	C+TR before cons treatment	39.05	±	0.07	19.18	±	0.53	28.97	±	8.1
	C+TR after cons treatement	35.26	±	0.1	9.14	±	0.3	6.46	±	0.2
	C+TR after exposure	30.9	±	1.48	13.76	±	0.73	15.31	±	1.6
	before cleaning and biopatina	40.16	±	0.32	18.47	±	0.64	27.64	±	0.8
	after cleaning and biopatina	36.46	±	3.71	11.98	±	0.48	21.33	±	0.5
	after exposure	32.75	±	1.69	11.76	±	1.14	11.85	±	1.8

IMN	T0 before exposure	31.38	±	0.49	12.23	±	0.74	16.66	±	0.9
	T0 after exposure	33.53	±	2.22	12.48	±	1.15	15.6	±	2.3
	T4 before biopatina	32.34	±	0.28	11.9	±	0.5	15.52	±	0.6
	T4 after biopatina	36.46	±	0.96	10.68	±	0.87	17.01	±	2.7
	T4 after exposure	37.73	±	1.24	10.28	±	1.01	13.85	±	1.9
	C+TR before cons treatment	32.6	±	0.87	11.82	±	0.49	15.31	±	0.8
	C+TR after cons treatement	38.27	±	0.59	4.56	±	0.14	1.12	±	0.1
	C+TR after exposure	37.78	±	1	5.38	±	0.47	1.97	±	0.6
	C+T4 before cleaning and biopatin	32.45	±	1	11.72	±	0.38	15.7	±	0.8
	C+T4 after cleaning and biopatina	37.38	±	0.69	7.01	±	0.2	1.21	±	0.5
	C+T4 after exposure	38.87	±	0.54	6.78	±	0.76	4.59	±	1
S	T0 before exposure	81.93	±	0.37	0.27	±	0.01	0.22	±	0
	T0 after exposure	45.29	±	3.44	10.77	±	2.07	24.46	±	1.6
	T4 before biopatina	78.46	±	3.2	0.21	±	0.07	0.49	±	0.1
	T4 after biopatina	44.2	±	1.15	1.22	±	1	9.7	±	1.3
	T4 after exposure	34.87	±	0.86	15.97	±	0.92	20.53	±	0.6
	C+TR before cons treatment	80.81	±	1.74	0.24	±	0.06	0.31	±	0.1
	C+TR after cons treatement	69.5	±	1	0.24	±	0.02	0.4	±	0.1
	C+TR after exposure	66.82	±	3.82	0.26	±	0.06	1.58	±	0.6
Z	T0 before exposure	91.63	±	0.77	-1.5	±	0.03	-1.39	±	0.1
	T0 after exposure	63.2	±	2.48	-1.35	±	0.19	1.79	±	1.5
	T4 before exposure	90.81	±	1.3	-1.5	±	0.03	-1.13	±	0.3
	T4 after biopatina	77.24	±	0.74	-1.97	±	0.1	0.28	±	0.3
	T4 after exposure	69.03	±	2.93	-1.95	±	0.12	0.84	±	0.4
ZA	T0 before exposure	51.97	±	0.53	-1.36	±	0.09	0.05	±	0
	T0 after exposure	49.56	±	0.4	-1.58	±	0.03	1.51	±	0.3
	T4 before exposure	51.93	±	0.3	-1.38	±	0.1	2.32	±	0.2
	T4 after biopatina	70.48	±	1.27	-1.49	±	0.06	1.14	±	0.3
	T4 after exposure	61.13	±	0.64	-1.94	±	0.08	-0.14	±	1.3

Appendix 7: colorimetric measurements- ΔE

Δ E BEFORE AND AFTER TREATMENT	
A	3.06
AA	0.50
C	5.74
CA	3.32
CS	11.85
CS	24.94
CS	9.78
IMN	4.55
IMN	16.92
IMN	16.01
S	35.49
S	11.31
Z	13.65
ZA	18.59

Δ E BEFORE TREATMENT AND AFTER EXPOSURE	
A	2.26
A	2.78
AA	0.65
AA	1.38
C	53.26
C	53.82
CA	0.9
CA	7.62
CS	4.88
CS	6.23
CS	16.8
CS	18.69
IMN	5.87
IMN	15.69
IMN	13.75
IMN	2.41
S	50.5
S	14.05
S	44.05
Z	28.61
Z	21.87
ZA	2.83
ZA	9.54